Evolution of Topography in Glaciated Mountain Ranges

by
Simon H. Brocklehurst

B.A. (Hons) Natural Sciences (Geological Sciences)
Queens' College, University of Cambridge, 1997

SUBMITTED TO THE DEPARTMENT OF EARTH, ATMOSPHERIC AND PLANETARY SCIENCES IN PARTIAL FULFILLMENT OF THE REQUIREMENTS FOR THE DEGREE OF

DOCTOR OF PHILOSOPHY
AT THE
MASSACHUSETTS INSTITUTE OF TECHNOLOGY

SEPTEMBER 2002

Signature of Author: _____
Department of Earth, Atmospheric and Planetary Sciences
August 26th, 2002

Certified by: _____
Kelin X Whipple
Thesis Supervisor

Accepted by: _____
Ronald G. Prinn
Department Head

Top. Fluvial-glacial transition in Shepherd Creek, eastern Sierra Nevada, California. Middle left: Trimlines, Birch Creek, eastern Sierra Nevada. Middle right: Old surface below University Peak, eastern Sierra Nevada. Bottom left: Khumbu Glacier, Nepal Himalaya (photograph by Karen Viskupic). Bottom right: Mt Cook, Southern Alps, New Zealand (photograph by Kelin Whipple).

Evolution of topography in glaciated mountain ranges

by

Simon H. Brocklehurst

Submitted to the Department of Earth, Atmospheric, and Planetary Sciences on August 26th, 2002 in Partial Fulfillment of the Requirements for the Degree of Doctor of Philosophy in Geology

ABSTRACT

This thesis examines the response of alpine landscapes to the onset of glaciation. The basic approach is to compare fluvial and glacial landscapes, since it is the change from the former to the latter that accompanies climatic cooling. This allows a detailed evaluation of hypotheses relating climate change to tectonic processes in glaciated mountain belts. Fieldwork was carried out in the eastern Sierra Nevada, California, and the Sangre de Cristo Range, Colorado, alongside digital elevation model analyses in the western US, the Southern Alps of New Zealand, and the Himalaya of northwestern Pakistan.

The evidence presented here suggests that the so-called "chicken-and-egg" hypothesis is overstated in its appeal to glacial erosion as a major source of relief production and subsequent peak uplift. Glaciers in the eastern Sierra Nevada and the western Sangre de Cristos have redistributed relief, but have produced only modest relief by enlarging drainage basins at the expense of low-relief topography. Glaciers have lowered valley floors and ridgelines by similar amounts, limiting the amount of "missing mass" that can be generated, and causing a decrease in drainage basin relief.

The principal response of glaciated landscapes to rapid rock uplift is the development of towering cirque headwalls. This represents considerable relief production, but is not caused by glacial erosion alone. Large valley glaciers can maintain their low gradient regardless of uplift rate, which supports the "glacial buzzsaw" hypothesis. However, the inability of glaciers to erode steep hillslopes as rapidly can cause mean elevations to rise.

Cosmogenic isotope dating is used to show that (i) where plucking is active, the last major glaciation removed sufficient material to reset the cosmogenic clock; and (ii) former glacial valley floors now stranded near the crest of the Sierra Nevada are at varying stages of abandonment, suggesting a cycle of drainage reorganisation and relief inversion due to glacial erosion similar to that observed in river networks.

Glaciated landscapes are quite distinct from their fluvial counterparts in both landforms and processes. Given the scarcity of purely fluvial, active mountain ranges, it is essential that glacial erosion be considered amongst the processes sculpting active orogenic belts.

Thesis Supervisor: Kelin X Whipple
Title: Associate Professor of Earth, Atmospheric and Planetary Sciences

Biographical Notes

I was born on December 16th, 1975, in Islington, London, and moved to Bishop's Stortford, Hertfordshire shortly thereafter. I attended Thorley Hill JMI School and The Bishop's Stortford High School, where I took Physics, Chemistry, Mathematics, Further Mathematics and German at A-Level. I then studied Natural Sciences at Queens' College, University of Cambridge, where I took Geology, Physics, Chemistry, Mathematics and Ecology before choosing to focus on Geological Sciences. For my undergraduate mapping project I examined the Palaeozoic sediments of the Cantabrian Mountains, near Crèmenes, northern Spain, supervised by Dr Tim Holland.

I came to the USA in August, 1997, to study for a PhD in glacial geomorphology at MIT. I have been a teaching assistant for Professor Kelin Whipple on three occasions, for Geologic Image Interpretation (twice), and Surface Processes and Landscape Evolution. The remainder of my financial support has come from a NASA Earth System Science Graduate Fellowship and research assistantships funded by NSF and NASA.

I move on from MIT to a position as a Research Associate (Visiting Fellow) at the Cooperative Institute for Research in Environmental Sciences and the Department of Geological Sciences, University of Colorado at Boulder.

Acknowledgements

Firstly, I would like to thank my advisor, Kelin Whipple, for taking a chance on the potential student at the other end of an email exchange, and since then being a constant source of inspiration, enthusiasm, and support. His dedication to his students is quite remarkable, even if it seems at times that he is coming up with too many potential research ideas.

I am very grateful to Darryl Granger, from the PRIME Lab at Purdue University, for his patience, guidance and hospitality in giving me a thorough education in the techniques behind cosmogenic isotope dating, and for agreeing to sit on my thesis committee. I also greatly appreciate the input that I received from the other members of my thesis committee, Clark Burchfiel, Brad Hager, and David Mohrig, and Maureen Raymo, who was a valuable member of my general examination committee.

I was extremely fortunate to spend a semester at the Quaternary Research Center at the University of Washington, where Bernard Hallet was a very accommodating host. I also benefited greatly from the expertise of Steve Porter, Charlie Raymond, David Montgomery, Sean Willett, Alan Gillespie and Ed Waddington on the faculty at the UW, and from stimulating discussions with students and postdocs there, including Alison Anders, Ginny Catania, Karen Gran, Sara Mitchell, Yann Merrand, Felix Ng, Gerard Roe, and Drew Stolar. I have also been encouraged by interactions with a number of scientists from other institutions, including Richard Alley, Bob Anderson, Chris Beaumont and Kelly MacGregor.

I want to thank the principle characters who encouraged me on this route. David Hows at The Bishop's Stortford High School inspired me to push the boundaries of my scientific curiosity, even though this ultimately led me away from my initial interest in physics. Mark Anderson, somewhat jokingly, predicted that my future would lie at MIT. Numerous other members of staff also encouraged me to continue to seek new challenges. Roger Baker, Neil Collie, Simon Lloyd, Daniel Plunkett, Alex Stiles and Mark Thurgood have helped me keep in touch with events back home. James Jackson, at Queens' College, University of Cambridge, opened my eyes to the exciting field of geology. Tjeerd van Andel, David Pyle, Tim Holland, Paul Wilson, Ros Rickaby and Ian McCave were also sources of encouragement at various stages during my time in the Department of Earth Sciences at Cambridge. Amongst my fellow Cambridge students, I have enjoyed comparing postgraduate experiences with Jenny Brett, Sarah Colclough, Mary Goldsworthy, David Barnett and Jonathan Blower.

My experience at MIT would not have been the same without my fellow graduate students. I am very proud to have been associated with my contemporaries in the Geology and Geochemistry PhD program, Julie Baldwin, Marin Clark, Lindy Elkins Tanton, Karen Viskupic and Sinan Akciz. I am particularly glad that I happened to arrive at MIT at the same time as Sinan, fellow European, and football (soccer) fan. My path was made much smoother (and more entertaining) by following a year behind Noah Snyder, the first student on the Whipple program, and also by Eric Kirby, a later convert.

Ben Crosby, Joel Johnson, Will Ouimet, and Cam Wobus have since added valuable new perspectives to the group. I have enjoyed the company of a varied cast of officemates, including Nancy Harris, Kathy Keefe, Frank Dudas, Blair Schoene and Mark Schmitz. I could fill a sizeable portion of this thesis thanking specific people for specific things. Suffice it to say that I feel very fortunate that my time at MIT coincided at least in part with Amy Draut, Anke Friedrich, Nicole Gasparini, Kristen Jellison, Jenny Matzel, Kirsten Nicolaysen, Kate Ruhl, Lindsay Schoenbohm, Mark Behn, Daniel Collins, Matt Dawson, Homero Flores-Cervantes, José Hurtado, Stephen Lancaster, Greg Lawson, Bill Lyons, Jeff Niemann, Steve Parman, Jeff Parsons, Frederik Simons, Steve Singletary, Patrick Stoller, Chris Studnicki-Gizbert, John Thurmond, Jim Van Orman, and Arthur White, amongst many others. Sinan and Lindsay have been supportive and entertaining housemates.

Finally, I would like to thank my family, for understanding why I thought about coming to the US for graduate school in the first place, and for encouraging and supporting me ever since.

Contents

Chapter 1

Introduction

Motivation

This thesis was motivated by the growing recognition of the crucial role played by glacial erosion in proposed linkages between climate change, surface processes and tectonics (e.g., Brozovic et al., 1997; Molnar and England, 1990; Raymo and Ruddiman, 1992; Whipple et al., 1999). One of the major changes associated with the late Cenozoic is the development of glaciers in mountain ranges previously sculpted by rivers and hillslope processes only. This thesis is concerned with taking a closer, quantitative look at glaciated landscapes, principally in comparison with their fluvial counterparts, in the context of how glaciers have altered the relief structure of the landscape and thus affected the tectonic response to erosion. This allows a more rigorous appraisal of hypotheses relating glacial erosion and tectonic processes, and suggests guidelines for evaluating new landscape evolution models that incorporate glacial erosion (e.g., Braun et al., 1999; MacGregor et al., 2000; Merrand and Hallet, 2000). In addition, this study explores novel applications of recently available high quality digital elevation models (DEMs), fast computers, and cosmogenic isotope dating techniques.

Recent interest in the relief structure of mountain belts was stimulated by Molnar and England's (1990) explanation for the apparent worldwide uplift of mountain ranges in the late Cenozoic. Their comments came in response to suggestions that climate change might have been driven by the tectonic uplift of the Himalaya and Tibet, and the mountains of the western U.S. (Raymo, 1991; Raymo and Ruddiman, 1992; Raymo et al., 1988). Molnar and England proposed that the sedimentary records suggesting apparently synchronous mountain uplift around the globe in the late Cenozoic could instead reflect enhanced erosion driven by a stormier, cooler climate (Zhang et al., 2001). If this were accompanied by relief production, the isostatic response to this relief production would cause peak elevations to rise. However, Small and Anderson (1998) outlined how relief production driven by glacial erosion in the Wind River Range has been insufficient to drive major peak uplift, and Whipple et al. (1999) described how, on theoretical grounds, the transition from fluvial to glacial erosion in most settings is unlikely to generate sufficient relief to cause the scales of peak uplift envisioned by Molnar and England. One of the primary goals of this thesis was to investigate further the relief structure of glaciated mountain ranges, to test the validity of the so-called "chicken-and-egg" hypothesis, by

determining whether the conclusions reached by Small and Anderson (1998) are more generally applicable, and whether field evidence supports the theoretical arguments of Whipple et al. (1999).

A second motivating factor was the study by Brozovic et al. (1997) of the hypsometry (frequency distribution of elevations) of the region around Nanga Parbat, Pakistan. They discovered that glaciated landscapes here look essentially the same regardless of uplift rate. The so-called "glacial buzzsaw hypothesis" proposes that the majority of the landscape, regardless of tectonics, is limited to an elevation closely tied to the snowline, and thus that the glacial erosion is the major influence on landscape form. That glaciers can erode as fast as the most rapid tectonic uplift rates with no change in mean elevation suggests that glaciers do not steepen in response to rapid uplift. This contrasts with fluvial landscapes, where significant steepening, and consequent rise in mean topography, appears to be required to erode at a faster rate (e.g., Howard et al., 1994; Tucker and Whipple, in press). Meanwhile it has not been established convincingly whether glaciers in general can erode faster than rivers (e.g., Hallet et al., 1996; Hicks et al., 1990; Koppes and Hallet, 2002). Hence further goals of this thesis are: (i) to evaluate what information about the relative rates of fluvial and glacial erosion can be gleaned from careful examination of glaciated landscapes; (ii) to carry out a more detailed evaluation of the response of glaciated landscapes to rapid rock uplift, to evaluate the so-called "glacial buzzsaw" hypothesis; and (iii) to examine how processes other than uplift affect the hypsometry of glaciated landscapes.

Given the extra complexity associated with incorporating glacial erosion into a landscape evolution model, most authors have attempted to study the evolution of glaciated mountain ranges with models that incorporate only hillslope and/or fluvial process rules (e.g., Beaumont et al., 1996; Koons, 1995; Willett, 1999). However, initial attempts at building landscape evolution models that incorporate glacial erosion have been made (e.g., Braun et al., 1999; MacGregor et al., 2000; Merrand and Hallet, 2000). In order to evaluate this new generation of models it is essential that we develop a more detailed quantitative understanding of the landforms produced by glacial erosion in a variety of tectonic settings.

Finally, this study afforded the opportunity to explore a pair of applications of cosmogenic isotope dating techniques in glaciated landscapes. The first was an evaluation of the suggestion by Briner and Swanson (1998) that inheritance might be an issue in attempting to use

cosmogenic isotopes to date the retreat of glaciers since the last glaciation (or alternatively in attempting to use independently determined deglaciation ages to constrain the production rates of cosmogenic isotopes). Inheritance here refers to the presence of cosmogenic isotopes that were produced prior to, and not eroded during, the most recent glaciation. Inheritance (more cosmogenically-produced isotopes than expected) results in anomalously old calculated ages. Cosmogenic isotopes were also used to test the hypothesis that enigmatic "old surfaces" at the crest of the Sierra Nevada and other mountain ranges are of varying ages, and represent former glacial valley floors at various stages of being isolated by drainage reorganisation and relief inversion. These processes of drainage capture and relief inversion are similar to processes that happen in fluvial landscapes.

Background

There are many potential influences on glacier dynamics and glacial erosion (Benn and Evans, 1998; Sugden and John, 1976). The mass balance of glaciers reflects both precipitation and temperature, so that glaciers in warmer, wetter coastal regions may well be larger than their cooler, drier inland counterparts despite the difference in temperature. This in turn will affect ice discharge and velocity. In temperate regions (where, by definition, the ice is at the pressure melting point) the presence of water will lubricate the glacier bed and allow much faster sliding rates than in colder regions, where ice is frozen to the bed. In general, glacial erosion rates are thought to scale with ice velocity (e.g., Harbor, 1992). However, the role of basal water may well be more complicated, since glacial erosion by quarrying (plucking of blocks from the glacier bed) requires water pressure fluctuations to fracture the bedrock (Alley et al., 1999; Hallet, 1996; Hooke, 1991). This is more readily achieved when the basal drainage network is poorly connected.

There are numerous feedback mechanisms that may importantly influence patterns and rates of glacial erosion and landscape modification. Since the atmospheric temperature distribution is dependent on elevation, as a glacier incises its valley floor it will move into a region of warmer temperatures, where faster melting rates may well cause the glacier to shrink (e.g., MacGregor et al., 2000; Oerlemans, 1984). In contrast, as valley walls increase in height, they will act to shade and cool the glacier below, having a positive influence on mass balance. Debris cover upon the glacier will also act to insulate it from warmer air temperatures, and again

have a positive influence on mass balance (e.g., Clark et al., 1994). The degree of landscape modification will be affected by both glacier size and residence time (e.g., Porter, 1989). Both larger glaciers and glaciers that are present for longer periods of time during climatic fluctuations will modify the landscape more significantly

Bedrock lithology will affect the development of glaciated landscapes, as rock strength is a major influence on the development of the hillslopes surrounding the glacier, and thus on valley cross-sectional form (Augustinus, 1992, 1995; Harbor, 1995). Quarrying/plucking will be easier when the bedrock is already fractured. Erosion by abrasion will be easier in more poorly consolidated bedrock. However, while 'tools' assist in abrasion, too much fine material at the bed of the glacier will serve to protect the bed (Hallet, 1979).

Given the many feedbacks listed above, and uncertainties in the current understanding of the controls on glacial erosion rates, the response of glaciers to tectonic uplift is less clear. By analogy with rivers, it is likely that glaciated landscapes in areas of more rapid rock uplift may well look different from their counterparts in areas of less rapid uplift, although initial efforts to evaluate this suggest that glaciated landscapes are generally unaffected by variations in rock uplift rate (Brozovic et al., 1997).

In light of these various influences on the development of glaciated landscapes, this study was designed to isolate individual influences on the development of glaciated landscapes whilst maintaining as many other factors as possible uniform across the region of interest.

Design

The first stage of the research was to carefully select field areas with drainage basins showing a range of degrees of glacial modification within a region of uniform climate, tectonics and lithology, to allow a direct, quantitative comparison of the topographic effects of glaciation. The chosen field areas were the eastern Sierra Nevada, above Owens Valley, California, and the northern Sangre de Cristo Range, Colorado. Analyses of longitudinal profiles, hypsometry, and relief distributions were carried out using USGS 30m digital elevation models (DEMs). In addition to a direct comparison between different basins showing varying degrees of glacial modification, the local presence of basins essentially unmodified by glaciers allows the local calibration of a fluvial erosion model to compare the current glacial topography of other basins with a model of how the same basin would look now had glaciation not occurred. A program of

fieldwork was designed to test three hypotheses: firstly, that glacial relief production scales with ice thickness (Whipple et al., 1999); secondly, that inheritance from prior interglacials may be a problem in using cosmogenic isotopes to date glacier retreat after the last glaciation (Briner and Swanson, 1998); and thirdly, that glaciers are responsible for headwall erosion, drainage reorganisation and relief inversion, resulting in former glacial valley floors now lying at ridgetops. The second hypothesis also serves as a coarse test of the hypothesis that glacial incision below the mean Quaternary equilibrium line altitude is comparatively minor in small, alpine basins. The equilibrium line altitude (ELA) refers to the elevation on a glacier's surface that separates the region of net annual accumulation above from the region of net annual ablation below, i.e., it represents the point of zero net balance. The mean Quaternary ELA is an ELA determined for a representative mean Quaternary climate, as determined from oxygen isotope records, and typically lies midway between modern, interglacial conditions and last glacial maximum (LGM) conditions (Porter, 1989). Given the popularity of hypsometry as a tool for analysing glaciated landscapes (e.g., Brozovic et al., 1997; Kirkbride and Matthews, 1997; Montgomery et al., 2001), this portion of the study was extended to other ranges of the western US and to the Ben Ohau Range, New Zealand, to fully explore the application of this tool. Thus characterising glacial topography in the absence of rapid tectonic uplift, the study moved on to a pair of tectonically active regions, the northwestern Himalaya of Pakistan and the Southern Alps of New Zealand, to directly address interactions between glacial erosion and tectonic uplift, as exhibited in these modern glaciated landscapes.

Outline of Chapters 2-9

Chapter 2 introduces the majority of the DEM analysis techniques that were employed, along with illustrating their application in the eastern Sierra Nevada. This includes demonstration of a new ridgeline-related "sub-ridgeline" relief calculation method, along with more traditional quantitative landscape analyses, to compare fluvial and glacial landscapes. A novel application of fluvial landscape evolution models is used to evaluate how the landscape looks now compared with how it might have looked now had glaciers never developed in this region. To summarise the conclusions, glaciers have incised little more than rivers below the long-term mean equilibrium line altitude (ELA), but have incised noticeably more rapidly at high elevations, above the mean Quaternary ELA (Porter, 1989). However, the glaciers have also brought down

ridgelines, so that, although glaciers redistribute relief, there is no net generation of relief unless the glaciers have produced relief by headward extension of the valley network into a pre-existing undissected, high-elevation plateau. It is demonstrated that headwall erosion has been active in the Sierra Nevada, although this still has not produced the scales of relief production appealed to by Molnar & England (1990).

Chapter 3 describes fieldwork undertaken in both the Sierra Nevada and the Sangre de Cristo Range of southern Colorado as a test of the hypothesis proposed by Whipple et al. (1999) that relief production in glaciated landscapes scales with ice thickness. This included mapping trimlines and moraines of the last glacial maximum (LGM) to deduce ice extent, and then using some simple calculations to reconstruct LGM glaciers and determine likely ice thicknesses, to compare with estimates of hanging valley and sub-ridgeline relief. Field observations also show that structure and lithology play a much more important role in the development of glaciated landscapes among the Palaeozoic sediments of the Sangre de Cristos than in the more homogeneous granites of the Sierra Nevada. Chapter 4 contains a more thorough development of the application of a fluvial landscape evolution model to compare likely modern nonglacial topography with observed glacial topography. The approach contrasts with the work of Mathes (1930), who viewed the higher portions landscape as being modified from below following pulses of uplift. By contrast this approach presents evidence that the major recent landscape modification has occurred at higher elevations. The technique is extended to basins in the western Sangre de Cristo Range as a direct comparison with the Sierra Nevada case described in Chapter 2, and also to larger basins on both sides of the Sierra Nevada. This reveals a distinct difference between the smaller, steeper glaciated basins described before and the larger glaciated basins. In the smaller basins glaciers have done little to incise below the mean ELA, merely widening the valley floor to produce a U-shaped valley cross-section. In the larger basins the glaciers have apparently modified the longitudinal profile of the basin far below the mean Quaternary ELA, introducing many more steps. These steps are seen in both the Sierra Nevada and the Sangre de Cristos, and so do not merely reflect the weathering of granites in the Sierra Nevada (Wahrhaftig, 1965). The landform prior to glaciation is an important influence on the subsequent landscape evolution. Possible causes for this include the marked increase in accumulation area in larger basins allowing glaciers to extend to lower elevations, the possibility of subglacial drainage network development depending on slope, ice dynamics in general

responding to the valley floor gradient, and the taller hillslopes associated with thicker ice and greater relief resulting in greater shading of the glacier below. Furthermore, this major distinction is something that should be captured by glacial landscape evolution models.

Chapter 5 summarises the results of a cosmogenic isotope study carried out in the eastern Sierra Nevada to test the hypothesis suggested by Briner and Swanson (1998) that inheritance could be a problem in using cosmogenic dating techniques on bedrock surfaces to date glacier retreat. The smaller basins of the eastern Sierra Nevada represented a good choice of field site for this test because the modelling studies described in Chapters 2 and 4 suggested that glacial erosion below the mean Quaternary ELA is minimal, mostly in the form of valley widening rather than downcutting, and abundant, glacially polished bedrock is exposed in at least some of the drainage basins. Thus the sample sites selected were those that were most likely to record inheritance. The cosmogenic isotope dates support previous, independent estimates of the timing of deglaciation in the eastern Sierra Nevada, obtained principally from lake cores, i.e., there was no suggestion of inheritance. This shows that valley incision during the Last Glacial Maximum advance was at least ~2m, and thus that inheritance is not a major issue in temperate alpine glaciated landscapes. However, this does not discount quite modest rates of incision during the glaciation.

Chapter 6 describes a second application of cosmogenic isotope dating, testing a hypothesis for the longer-term evolution of glaciated mountain belts as a cycle of drainage reorganisation and relief inversion. It is suggested that, over time, glaciated basins can enlarge at the expense of their neighbours, beheading valleys and isolating high, low relief, former valley floors. These low relief surfaces are eroded more slowly than the surrounding landscape and eventually find themselves on the ridgelines (relief inversion), detached from the valley floors below. Samples of demonstrably erratic boulders from a pair of enigmatic 'old surfaces' at the crest of the Sierra Nevada were collected to determine minimum ages for these surfaces. The calculated ages support field observations suggesting the two surfaces were quite different in age, and thus the abandonment of these surfaces is an ongoing process.

Chapter 7 focuses on the use of hypsometry as a tool of landscape analysis. As hypsometry sees ever greater use in both fluvial and glacial landscapes, as an apparent indicator of steady state, dominant erosion process, landscape 'age', or regional erosion rate, it seemed pertinent to conduct a careful study of what hypsometry can indicate about glaciated landscapes

in the absence of gradients in tectonic activity. Two different variants on hypsometry, a frequency distribution of elevations and the hypsometric curve, were determined for a range of drainage basins in the western US and the Ben Ohau Range of New Zealand (Kirkbride and Matthews, 1997). There is a recognisable pattern to the variation in hypsometry of individual basins between non-glaciated basins and those demonstrating a range of degrees of glaciation. Furthermore, the position of the ELA within the basin relief can have a major impact on the hypsometry. The hypsometry of large regions can mask the variability of individual drainage basins, and the sequence of landscapes caused by lowering of the ELA is comparable to the traditional view of 'maturing' fluvial landscapes (Strahler, 1952).

Chapter 8 takes some of the approaches used in the Sierra Nevada (Chapter 2) to directly address glacial response to tectonic uplift (Brozovic et al., 1997), in a rather different manner than employed by those authors. Brozovic et al. (1997) found very similar hypsometry and slope-elevation distributions for different regions experiencing widely differing tectonic uplift rates around Nanga Parbat, Pakistan. They concluded that since the landscapes were essentially identical, the glaciers were able to keep pace with some of the fastest uplift rates on earth without steepening. This is critical because rivers and debris flows are capable of eroding at rates equal to the highest uplift rates, but they must steepen to do so, increasing both relief and mean elevation as a consequence. This idea was tested in two field areas, the Southern Alps of New Zealand, and the northwestern Himalaya, Pakistan, as studied by Brozovic et al. (1997). While smaller glaciers steepen slightly in response to rapid tectonic uplift, the change is slight, and larger glaciers do not steepen at all. In essence the "glacial buzzsaw" hypothesis described by Brozovic et al. (1997) is accurate; glaciers can erode the valley floor at rates comparable to tectonic uplift rates without steepening. However, the giant hillslopes that develop once they become too steep to maintain permanent snow are of crucial importance. These hillslopes then evidently cannot be eroded at the same rate as the valley floor, and are capable of growing to several kilometres high, forming a significant component of peak elevation, and having a potentially major impact on atmospheric dynamics, orographic precipitation, and avalanche hazard. It is not clear whether these hillslopes are continuing to grow or have reached equilibrium, although ultimately their height should be limited (Schmidt and Montgomery, 1995).

Finally, the Conclusion (Chapter 9) brings together the various themes explored during the thesis to summarise what has been learned in the context of the initial motivation behind the work, and to suggest some avenues of further research. The evidence presented in this thesis does not support the idea of glacial erosion being responsible for peak uplift to the extent that Molnar and England (1990) appeal to. Glaciers are only associated with modest relief production, except in areas with rapid rock uplift, in which case it is this rock uplift causing steep, tall headwalls that glaciers cannot erode that causes high peaks. The relief generated by glaciers maintaining a shallow slope is a secondary effect. The glacial buzzsaw hypothesis (Brozovic et al., 1997) apparently applies to regions where rock uplift rates are slow, but where rock uplift rates are more rapid, may only apply in regions of localised uplift. The peaks that penetrate the "snowline envelope" are potentially important features of glaciated landscapes.

Future work should focus on the hillslopes in glaciated mountain belts, to examine their role in headwall erosion and drainage reorganisation (Chapters 2 and 6), and their apparent response to rapid tectonic uplift rates (Chapter 8). One major idea that is only hinted at in Chapter 4 is the suggestion that the condition of the landscape prior to glaciation plays a major role, i.e., large, low gradient fluvial basins will evolve quite differently from smaller, steeper basins. This notion needs to be developed further, in particular the various hypotheses for the cause of this distinction need to be tested. This work has also highlighted the essential landscape details that glacial landscape evolution models should produce, namely significant downward cutting at high elevations at the same time as minor incision lower in the basin (at least in the case of smaller, steeper alpine basins), headward erosion in certain settings, and inability to erode steep headwalls in certain settings. Interest in climate change on both short and long timescales makes it essential that the development of these models continues.

With the exception of the Introduction and the Conclusion, all of the chapters in this thesis have been designed for publication. As such there is a modest amount of overlap and repetition amongst the chapters to enable each to stand alone. Chapter 2 is reprinted from *Geomorphology*, vol. 42, S.H. Brocklehurst and K.X. Whipple, *Glacial erosion and relief production in the Eastern Sierra Nevada*, pp. 1-24, Copyright (2002), with permission from Elsevier Science.. Chapters 3-8 have been prepared for submission to *Geological Society of America Bulletin*, *Geomorphology*, *Geology*, *Geology*, *Earth Surface Processes and Landforms*, and *Geological Society of America Bulletin*, respectively.

References

Alley, R. B., Strasser, J. C., Lawson, D. E., Evenson, E. B., and Larson, G. J., 1999, Glaciological and geological implications of basal-ice accretion in overdeepenings, *in* Mickelson, D. M., and Attig, J. W., eds., Glacial Processes Past and Present: Geological Society of America Special Paper: Boulder, Colorado, Geological Society of America, p. 1-9.

Augustinus, P. C., 1992, The Influence of Rock Mass Strength on Glacial Valley Cross-Profile Morphometry: A Case Study from the Southern Alps, New Zealand: Earth Surface Processes and Landforms, v. 17, p. 39-51.

-, 1995, Glacial valley cross-profile development: the influence of in-situ rock stress and rock mass strength, with examples from the Southern Alps, New Zealand: Geomorphology, v. 14, p. 87-97.

Beaumont, C., Kamp, P. J. J., Hamilton, J., and Fullsack, P., 1996, The continental collision zone, South Island, New Zealand: Comparison of geodynamical models and observations: Journal of Geophysical Research, v. 101, no. B2, p. 3333-3359.

Benn, D. I., and Evans, D. J. A., 1998, Glaciers and Glaciation: London, Arnold, 734 p.

Braun, J., Zwartz, D., and Tomkin, J. H., 1999, A new surface-processes model combining glacial and fluvial erosion: Annals of Glaciology, v. 28, p. 282-290.

Briner, J. P., and Swanson, T. W., 1998, Using inherited cosmogenic 36Cl to constrain glacial erosion rates of the Cordilleran ice sheet: Ge ology, v. 26, p. 3-6.

Brozovic, N., Burbank, D. W., and Meigs, A. J., 1997, Climatic Limits on Landscape Development in the Northwestern Himalaya: Science, v. 276, p. 571-574.

Clark, D. H., Clark, M. M., and Gillespie, A. R., 1994, Debris-Covered Glaciers in the Sierra Nevada, California, and their Implications for Snowline Reconstructions: Quaternary Research, v. 41, p. 139-153.

Hallet, B., 1979, A Theoretical Model of Glacial Abrasion: Journal of Glaciology, v. 23, no. 89, p. 39-50.

-, 1996, Glacial quarrying: a simple theoretical model: Annals of Glaciology, v. 22, p. 1-8.

Hallet, B., Hunter, L., and Bogen, J., 1996, Rates of erosion and sediment evacuation by glaciers: A review of field data and their implications: Global and Planetary Change, v. 12, p. 213-235.

Harbor, J., 1995, Development of glacial-valley cross sections under conditions of spatially variable resistance to erosion: Geomorphology, v. 14, no. 2, p. 99-107.

Harbor, J. M., 1992, Numerical modeling of the development of U-shaped valleys by glacial erosion: Geological Society of America Bulletin, v. 104, p. 1364-1375.

Hicks, D. M., McSaveney, M. J., and Chinn, T. J. H., 1990, Sedimentation in proglacial Ivory Lake, Southern Alps, New Zealand: Arctic Alpine Research, v. 22, p. 26-42.

Hooke, R. L., 1991, Positive feedbacks associated with erosion of glacial cirques and overdeepenings: Geological Society of America Bulletin, v. 103, p. 1104-1108.

Howard, A. D., Dietrich, W. E., and Seidl, M. A., 1994, Modeling fluvial erosion on regional to continental scales: Journal of Geophysical Research, v. 99, p. 13971-13986.

Kirkbride, M., and Matthews, D., 1997, The Role of Fluvial and Glacial Erosion in Landscape Evolution: The Ben Ohau Range, New Zealand: Earth Surface Processes and Landforms, v. 22, p. 317-327.

Koons, P. O., 1995, Modeling the Topographic Evolution of Collisional Belts: Annual Review of Earth and Planetary Sciences, v. 23, p. 375-408.

Koppes, M. N., and Hallet, B., 2002, Influence of rapid glacial retreat on the rate of erosion by tidewater glaciers: Geology, v. 30, no. 1, p. 47-50.

MacGregor, K. R., Anderson, R. S., Anderson, S. P., and Waddington, E. D., 2000, Numerical Simulations of Glacial Valley Longitudinal Profile Evolution: Geology, v. 28, no. 11, p. 1031-1034.

Mathes, F. E., 1930, Geologic History of the Yosemite Valley, USGS Professional Paper.

Merrand, Y., and Hallet, B., 2000, A physically based numerical model of orogen-scale glacial erosion: Importance of subglacial hydrology and basal stress regime: GSA Abstracts with Programs, v. 32, no. 7, p. A329.

Molnar, P., and England, P., 1990, Late Cenozoic uplift of mountain ranges and global climate change: chicken or egg?: Nature, v. 346, p. 29-34.

Montgomery, D. R., Balco, G., and Willett, S. D., 2001, Climate, tectonics and the morphology of the Andes: Geology, v. 29, no. 7, p. 579-582.

Oerlemans, J., 1984, Numerical Experiments on Large-scale Glacial Erosion: Zeitschrift fuer Gletscherkunde und Glazialgeologie, v. 20, p. 107-126.

Porter, S. C., 1989, Some Geological Implications of Average Quaternary Glacial Conditions: Quaternary Research, v. 32, p. 245-261.

Raymo, M. E., 1991, Geochemical evidence supporting T. C. Chamberlin's theory of glaciation: Geology, v. 19, p. 344-347.

Raymo, M. E., and Ruddiman, W. F., 1992, Tectonic forcing of late Cenozoic climate: Nature, v. 359, p. 117-122.

Raymo, M. E., Ruddiman, W. F., and Froelich, P. N., 1988, Influence of late Cenozoic mountain building on ocean geochemical cycles: Geology, v. 16, p. 649-653.

Schmidt, K. M., and Montgomery, D. R., 1995, Limits to Relief: Science, v. 270, p. 617-620.

Small, E. E., and Anderson, R. S., 1998, Pleistocene relief production in Laramide mountain ranges, western United States: Geology, v. 26, p. 123-126.

Strahler, A. N., 1952, Hypsometric (area-altitude) analysis of erosional topography: Geological Society of America Bulletin, v. 63, p. 1117-1141.

Sugden, D. E., and John, B. S., 1976, Glaciers and Landscape: London, Arnold, 376 p.

Tucker, G. E., and Whipple, K. X., in press, Topographic Outcomes Predicted by Stream Erosion Models: Sensitivity Analysis and Intermodel Comparison: Journal of Geophysical Research.

Wahrhaftig, C., 1965, Stepped topography of the Southern Sierra Nevada, California: Geological Society of America Bulletin, v. 76, p. 1165-1190.

Whipple, K. X., Kirby, E., and Brocklehurst, S. H., 1999, Geomorphic limits to climate-induced increases in topographic relief: Nature, v. 401, p. 39-43.

Willett, S. D., 1999, Orogeny and orography: The effects of erosion on the structure of mountain belts: Journal of Geophysical Research, v. 104, no. B12, p. 28957-28981.

Zhang, P., Molnar, P., and Downs, W. R., 2001, Increased sedimentation rates and grain sizes 2-4 Myr ago due to the influence of climate change on erosion rates: Nature, v. 410.

Chapter 2

ELSEVIER

Geomorphology 42 (2002) 1–24

GEOMORPHOLOGY

www.elsevier.com/locate/geomorph

Glacial erosion and relief production in the Eastern Sierra Nevada, California

Simon H. Brocklehurst *, Kelin X. Whipple

Department of Earth, Atmospheric and Planetary Sciences, Massachusetts Institute of Technology, Cambridge, MA 02139-4307, USA

Received 22 May 2000; received in revised form 8 March 2001; accepted 9 March 2001

Abstract

The proposal that climate change can drive the uplift of mountain summits hinges on the requirement that glacial erosion significantly enhances the relief of a previously fluvially sculpted mountain range. We have tested this hypothesis through a systematic investigation of neighbouring glaciated and nonglaciated drainage basins on the eastern side of the Sierra Nevada, CA. We present a simple, objective method for investigating the relief structure of a drainage basin, which shows noticeable differences in the spatial distribution of relief between nonglaciated and glaciated basins. Glaciated basins on the eastern side of the Sierra Nevada have only ~80 m greater mean geophysical relief than nonglaciated basins. This "extra" relief, though, is attributable principally to the larger size of the glaciated basins, as geophysical relief generally increases with basin size. The glaciers on this side of the range were only responsible for relief production if they substantially increased headward erosion rates into low relief topography, such as an elevated plateau, and thus enlarged previously fluvial basins. We carried out a preliminary morphometric analysis to elucidate the importance of this effect and found that the glaciers of the eastern Sierra Nevada may have eroded headward at considerably faster rates than rivers, but only when they were not obstructed from doing so by either competing larger glaciers in adjacent valleys or transfluent ice at the head of the basin. Our results also suggest that, in temperate regions, alpine glaciers are capable of eroding downward at faster rates than rivers above the equilibrium line altitude (ELA). Although we can rule out significant peak uplift in response to local relief production, in the special case of the Sierra Nevada the concentration of mass removal above the ELA could have contributed to flexural uplift at the edge of a tilting block.

Keywords: Glacial erosion; Relief; Landscape evolution

1. Introduction

The evolution of topography in a mountain range results from a complex interaction between tectonic forces, climatically driven erosion, and the geodynamic response to erosion. To understand the role of late Cenozoic climatic cooling in this system, it is necessary to evaluate the impact of glacial erosion on topography. How does landscape form evolve during glaciation of a previously fluvially sculpted landscape?

Modern topography documents that glaciated landscapes have a distinctive form, exhibiting cirques, arêtes, horns, hanging valleys, truncated spurs,

* Corresponding author. Fax: +1-617-252-1800.
E-mail address: shb@mit.edu (S.H. Brocklehurst).

0169-555X/02/$ - see front matter
PII: S0169-555X(01)00069-1

and U-shaped flat-bottomed troughs (Fig. 1) (e.g., Sugden and John, 1976). The change in "missing mass," or "geophysical relief" (Small and Anderson, 1998), governs the local isostatic response to erosion. Net removal of mass, if concentrated geographically, will affect far-field flexural uplift (Small and Anderson, 1995). Geophysical relief can increase (and thus induce isostatic uplift) either if the erosion of summits and ridgelines is slower than mean erosion rates (i.e., valleys are growing deeper and/or wider; Fig. 2) or if incising drainage basins are enlarged at the expense of low relief topography. Does the development of the distinctive glaciated landscape result in a major change in relief structure? Small and Anderson (1995) proposed that a significant component of the late Cenozoic rock uplift in the Sierra Nevada was driven by the lithospheric response to coupled erosion of the Sierra Nevada and deposition in the adjacent Central Valley. Did climate change and development of glaciers in the Sierra Nevada contribute to this effect?

Landscape evolution models are being used increasingly to investigate linkages between surface and geodynamic processes, but cannot yet answer these questions. Most models treat only fluvial erosion and hillslope processes (e.g., Koons, 1989; Beaumont et al., 1992; Tucker and Slingerland, 1994, 1997). Furthermore, while much work has been focused on small-scale observations of glacial erosion processes (e.g., Boulton, 1974; Hallet, 1996), we do not have a good, quantitative understanding of the mesoscale effects of glacial erosion. Preliminary efforts at modelling mesoscale glacial erosion are currently underway (e.g., Braun et al., 1999; MacGregor et al., 2000; Merrand and Hallet, 2000; Tomkin and Braun, 2000).

The idea that mountain building processes and climate change are strongly coupled was first suggested by Chamberlin (1899). Raymo and Ruddiman (1992) built on his ideas, proposing that the tectonic uplift of mountain belts and elevated plateaux results in enhanced chemical erosion rates (drawing down atmospheric CO_2), an increase in albedo, and significant changes in atmospheric circulation. These three effects would combine to cause global cooling. The implication is that tectonic processes are the primary control on mountain range elevations. Wager (1933), on the other hand, suggested that an isostatic response to erosion at the edge of the Tibetan Plateau could explain the elevations of the Himalayas. Molnar and England (1990) further suggested that the transition to an icehouse climate state, driven by a non-tectonic mechanism, causes significant glacial erosion and relief production. The authors envisioned a positive

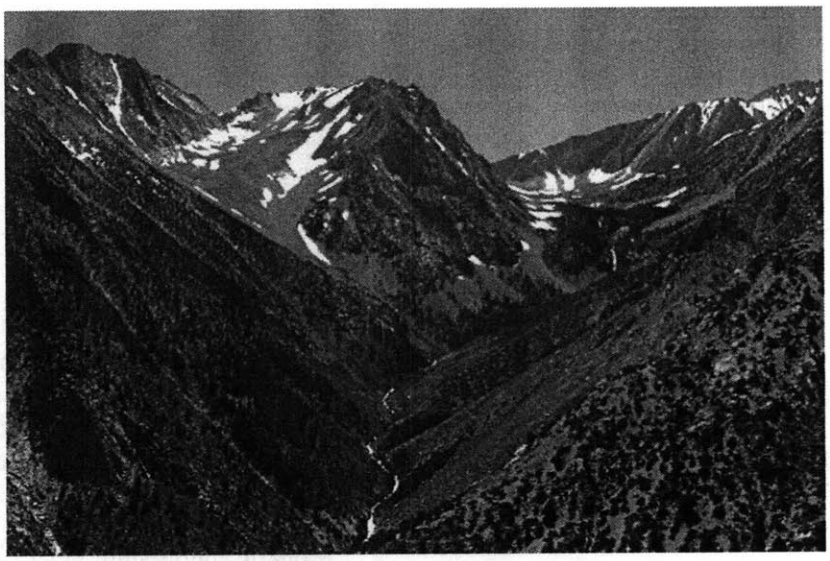

Fig. 1. View looking west up Shepherd Creek, showing fluvial reach downstream of a heavily glaciated upper valley, with a notable hanging valley on the south side, below Mount Williamson (far left). Notice the flatter valley floors in the glacial sections.

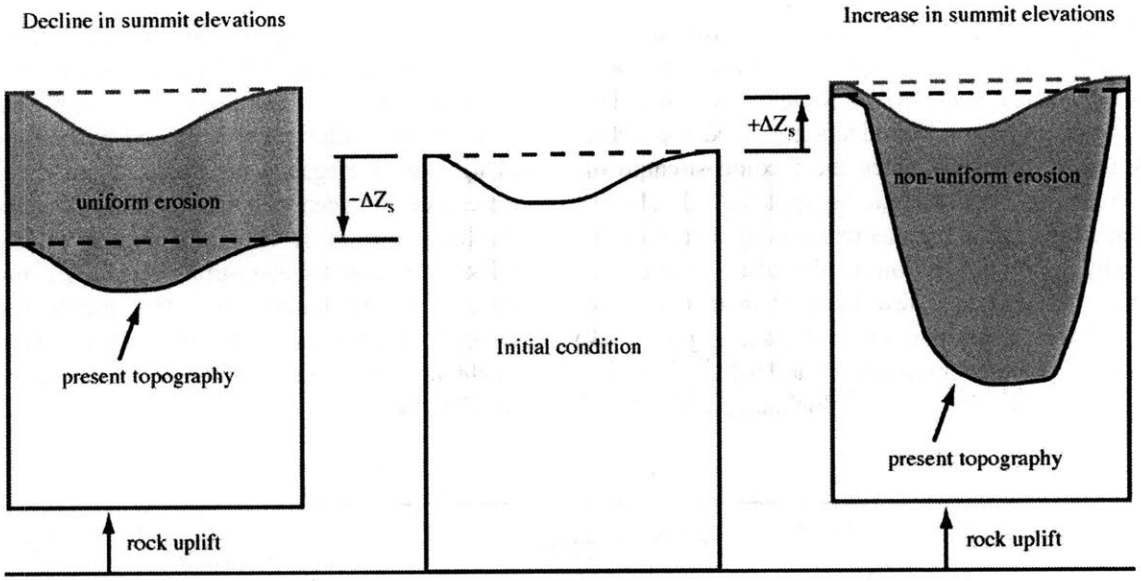

Fig. 2. Two cases of mountain erosion. Centre panel represents initial condition. The geophysical relief is the mean elevation difference between a smooth surface connecting the highest points in the landscape [dashed line—current (black) and prior (grey)] and the topography. When erosion (shaded area) is spatially uniform (left panel), there is no change in geophysical relief, and the sum of erosionally driven rock uplift and summit erosion results in lower summit elevations ($-\Delta Z_s$). When erosion is spatially variable (right panel), there is a notable increase in geophysical relief, and changes in summit elevation are positive ($+\Delta Z_s$) because rock uplift is greater than summit erosion. Rock uplift is the same in each case because average erosion, which drives rock uplift, is equal (shaded areas are the same size) (after Small and Anderson, 1998).

feedback between valley glacier erosion and rising summit and ridge elevations whereby the increased peak elevations resulting from isostatic adjustment enhance the mass balance of glaciers, increasing valley erosion and producing additional increases in elevation. Thus, peak uplift attributed to tectonic processes by earlier workers could instead be a result of relief production and subsequent isostatic peak uplift.

The limiting case of the isostatic response to fluvial incision of an initial plateau surface can account for 20–30% of peak uplift (Gilchrist et al., 1994; Montgomery, 1994), but this number decreases dramatically (~5%) if a realistic flexural strength for the lithosphere is considered (Montgomery, 1994). The more general case of enhanced fluvial erosion in a narrow fluvially sculpted mountain belt was examined by Whipple et al. (1999), who concluded that in almost all nonglacial landscapes an increase in the erosivity of the fluvial system would lead to a reduction in both trunk stream and tributary relief. Furthermore, such a change in climate cannot significantly increase the hillslope component of relief in a tectonically active orogen.

Turning to the glacial system, a first-order, unresolved question is whether glaciers can erode faster than bedrock streams. Hicks et al. (1990) used sediment yields in the Southern Alps of New Zealand to challenge the long-held view that glaciers are the more effective erosive agents. Hallet et al. (1996) used a global dataset to argue that glaciers are capable of eroding at significantly faster rates than rivers. Hallet et al. (2000) recently reduced the highest glacial erosion rate estimates from Alaska to ~10–60 mm/year, but these still exceed fluvial erosion rates. Brozović et al. (1997) suggested that their topographic analyses from the northwestern Himalaya showed that glacial erosion rates at high elevations can match the highest tectonic uplift rates, limiting regional-scale elevations to some distance above the equilibrium line altitude (ELA).

If glaciers are more efficient erosive agents, are they able to produce relief? Small and Anderson

(1998) demonstrated that differential erosion rates occurred between the summit flats and valley floors in the glaciated Wind River Range, Wyoming, but that the resulting relief production yielded negligible peak uplift, especially when the flexural strength of the crust was considered. Whipple et al. (1999) presented the following theoretical argument illustrating why relief production in the glacial system is probably limited to a few hundred metres in most cases. Extra relief due to ice-buttressing of rock slopes or the development of a U-shaped valley cross-section depends on ice thickness, while relief due to hanging valleys depends on the difference in ice thickness between tributaries and the trunk stream. MacGregor et al.'s (2000) modelling study confirmed that hanging valley relief is caused by both ponding of tributary ice against the trunk stream ice and the difference between tributary and trunk stream ice discharge. In most temperate alpine settings, ice thicknesses and tributary-trunk stream ice thickness differences are limited to a few hundred metres. Exceptional glaciers in the Swiss Alps or Himalayas might have reached a kilometre in thickness during the Pleistocene.

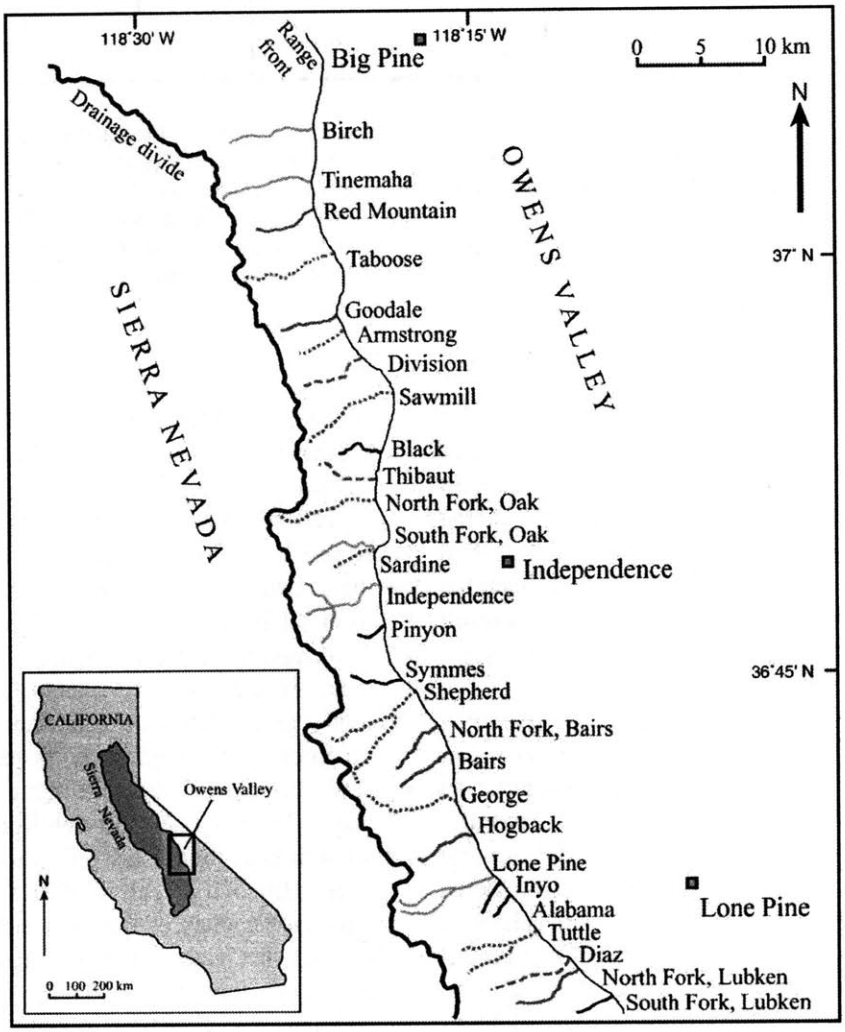

Fig. 3. Study site on the eastern side of the Sierra Nevada, California, highlighted on the inset map. Our five categories of basin, based on the degree of glaciation at the Last Glacial Maximum, are illustrated as follows: nonglaciated (black), minor glaciation (medium grey, dashed), moderate glaciation (medium grey, solid), significant glaciation (medium grey, dotted), and full glaciation (light grey).

Given that climate change and glacial erosion have variously been proposed to raise, have negligible effect on, or lower peak elevations, while probably increasing relief, but by an undetermined amount, clarification of the effect of glacial erosion on the landscape is clearly needed. Two critical questions are (i) how does glacial erosion impact range crest elevations? and (ii) how does glacial erosion impact the relief structure of the landscape?

The aim of this study was to address these questions through a careful comparison of nonglaciated and glaciated topography. A study of the eastern Sierra Nevada, between the towns of Lone Pine and Big Pine (Fig. 3), was undertaken (i) to determine whether glacial erosion has a significant impact on range crest elevations, (ii) to quantify the impact of glaciation on geophysical relief, and (iii) to assess whether glacial erosion has made an important contribution to erosional unloading (Small and Anderson, 1995). In this study area, adjacent drainage basins encompass the full spectrum from those that were completely unglaciated to those that were fully occupied by glacial ice during the Last Glacial Maximum (LGM). (While we realise that all of our drainage basins have experienced climatic cooling events ("glaciations"), we use the term glaciation to refer to the development of a glacier within a given drainage basin.) This allowed a direct comparison of the topography and relief structure between the two endmember cases, no glaciation and full glaciation, while the range of extents of glaciation permitted us to look at intermediate cases. Thus, we could effect a systematic evaluation of the consequences of glacial erosion on a previously fluvially sculpted mountain range in a temperate region without dramatic tectonic activity. In the current absence of glacial ice from the study area, the landforms produced by glaciation are exposed and readily analysed.

The core component of this study was the development of a novel and simple approach to calculate relief on a basin-wide scale, using the freely available US Geological Survey (USGS) 30-m resolution digital elevation models (DEMs). We compared the relief in glaciated and nonglaciated drainage basins and used the nonglaciated basins to constrain a fluvial erosion model. The model was used to estimate nonglacial topography both (i) along the longitudinal profile and (ii) for the basin as a whole, to suggest how the glaciated basins might look now had ice never occupied these basins.

2. Field site

We studied 28 individual drainage basins (Fig. 3) that have experienced similar tectonic and climatic histories. Present-day tectonic activity is dominated by strike-slip motion on the Owens Valley Fault farther to the east, although the range front normal fault may still be active, contributing to minor uplift rates (~ 0.2 mm/year; Gillespie, 1982). On a regional scale, this section of the Sierra Nevada comprises homogeneous Cretaceous granodiorites and quartz monzonites (Moore, 1963, 1981; Bateman, 1965). Triassic, Jurassic, and Paleozoic metamorphic rocks are minor components. Hence, major topographic differences between the drainage basins can be attributed principally to different glaciation histories. This region has seen a number of previous glacial studies (e.g., Gillespie, 1982; Burbank, 1991; Clark et al., 1994; Clark and Gillespie, 1997). However, this is the first quantitative analysis of the mesoscale impact of glacial erosion in this area.

A flow routing routine in ArcInfo was used to extract the drainage network structures of each of the basins from USGS 30-m DEMs (Table 1). The downstream extent of each drainage basin was taken to coincide with the range front, so as to exclude the alluvial fan regime and allow reasonable and consistent comparison between basins. The drainages were divided into five categories on the basis of the degree of glaciation experienced at the LGM: none, minor, moderate, significant, and full. We used LGM ice extents from aerial photograph interpretation, field observations, and previous mapping (e.g., Gillespie, 1982) as a proxy for relative ice extent throughout the Quaternary, although we appreciate that these do not represent the average ice extents during the Quaternary (Porter, 1989). "Full glaciation" symbolises LGM glaciers extending to the range front, while minor, moderate, and significant glaciers extended $\sim 1/4$, $\sim 1/2$, and $\sim 3/4$ of the length of the drainage basin, respectively. The three middle categories were also considered collectively as "partial glaciation."

Table 1
Summary of topographic characteristics

Basin	Degree of glaciation	Length (km)	Headwall elevation (m)	Drainage area (km^2)	Longitudinal profile			Basin-wide		
					θ	$\ln(k_s)$ (fixed θ)	S_r (A_r=10^6 m^2)	θ	$\ln(k_s)$ (fixed θ)	S_r (A_r=10^6 m^2)
Alabama	None	4.31	3738	3.15	0.32±0.07	3.38±1.60	0.378	0.23±0.04	2.88±0.48	0.413
Black	None	5.47	3564	6.88	0.20±0.07	3.49±1.67	0.389	0.19±0.06	2.76±0.73	0.368
Inyo	None	3.98	3901	2.93	0.37±0.06	3.41±1.59	0.391	0.27±0.06	2.87±0.80	0.409
Pinyon	None	7.37	3753	12.6	0.19±0.06	3.41±1.72	0.337	0.23±0.04	2.76±0.54	0.363
South Fork, Lubken	None	3.43	3194	3.41	0.45±0.08	3.34±1.57	0.357	0.38±0.07	2.67±0.83	0.313
Symmes	None	6.54	3963	11.8	0.37±0.05	3.32±1.68	0.374	0.29±0.03	2.72±0.36	0.352
Diaz	Minor	8.67	4092	11.4	−0.01±0.05	3.38±1.73	0.251	0.17±0.07	2.52±0.91	0.281
Division	Minor	6.39	3747	12.8	0.04±0.05	3.44±1.71	0.299	0.08±0.07	2.41±0.87	0.258
Thibaut	Minor	7.88	3826	8.74	0.00±0.07	3.40±1.67	0.303	0.24±0.06	2.62±0.86	0.318
Bairs	Moderate	6.94	3944	7.71	0.13±0.05	3.33±1.67	0.313	0.18±0.04	2.69±0.53	0.339
Goodale	Moderate	13.27	4034	20.8	0.12±0.06	3.55±1.76	0.333	0.07±0.05	2.64±0.62	0.316
Hogback	Moderate	5.76	3955	12.4	0.14±0.07	3.47±1.69	0.352	0.26±0.07	2.66±0.96	0.331
North Fork, Bairs	Moderate	8.44	4330	10.0	0.20±0.05	3.36±1.68	0.336	0.22±0.04	2.69±0.60	0.339
North Fork, Lubken	Moderate	7.54	3854	10.1	0.19±0.07	3.43±1.71	0.345	0.20±0.04	2.65±0.59	0.322
Red Mountain	Moderate	8.13	4064	16.9	0.05±0.05	3.36±1.74	0.261	0.15±0.05	2.55±0.73	0.286
Armstrong	Significant	6.72	3616	8.17	0.08±0.07	3.29±1.72	0.267	0.13±0.06	2.23±0.78	0.215
George	Significant	11.37	4105	24.9	0.16±0.04	3.45±1.80	0.297	0.15±0.03	2.66±0.38	0.314
North Fork, Oak	Significant	10.41	4016	20.9	0.13±0.05	3.39±1.80	0.267	0.14±0.04	2.49±0.62	0.261
Sardine	Significant	5.63	3835	5.16	−0.10±0.07	3.46±1.67	0.302	0.05±0.09	2.57±1.23	0.321
Sawmill	Significant	12.02	3968	19.6	0.00±0.05	3.48±1.80	0.232	0.20±0.08	2.19±1.15	0.202
Shepherd	Significant	16.38	3988	36.0	0.08±0.05	3.33±1.80	0.233	0.24±0.03	2.54±0.39	0.285
Taboose	Significant	10.67	3846	19.1	0.07±0.06	3.42±1.81	0.243	0.20±0.04	2.67±0.48	0.331
Tuttle	Significant	9.25	4096	21.6	0.08±0.06	3.33±1.77	0.242	0.21±0.02	2.71±0.28	0.343
Birch	Full	8.82	4036	13.4	0.09±0.05	3.34±1.77	0.251	0.23±0.06	2.40±0.86	0.250
Independence	Full	12.03	3955	30.4	0.13±0.05	3.43±1.78	0.293	0.20±0.07	2.26±0.98	0.213
Lone Pine	Full	10.86	4226	31.6	0.07±0.06	3.49±1.82	0.261	0.14±0.07	2.42±0.93	0.243
South Fork, Oak	Full	6.76	3951	10.0	−0.03±0.06	3.35±1.74	0.230	0.14±0.10	2.35±1.34	0.243
Tinemaha	Full	8.72	4064	14.9	0.01±0.05	3.47±1.77	0.252	0.09±0.05	2.56±0.65	0.293
Means	None	5.18	3686	6.79	0.315±0.114	3.38±1.62	0.371	0.273±0.077	2.77±0.66	0.370
	Partial[a]	9.15	3960	15.7	0.080±0.093	3.40±1.76	0.287	0.169±0.080	*2.56±0.77*	0.298
	Minor	*7.65*	*3888*	*11.0*	*0.012±0.048*	*3.41±1.74*	*0.284*	*0.163±0.089*	*2.54±0.90*	*0.286*
	Moderate	*8.35*	*4030*	*13.0*	*0.138±0.090*	*3.40±1.73*	*0.323*	*0.179±0.077*	*2.64±0.68*	*0.322*
	Significant	*10.31*	*3934*	*19.4*	*0.062±0.094*	*3.39±1.79*	*0.260*	*0.163±0.078*	*2.50±0.77*	*0.284*
	Full	9.44	4046	20.1	0.079±0.081	3.37±1.82	0.258	0.160±0.085	2.38±0.99	0.249

[a] Figures for the three subdivisions of the 'Partial Glaciation' category are shown in italics.

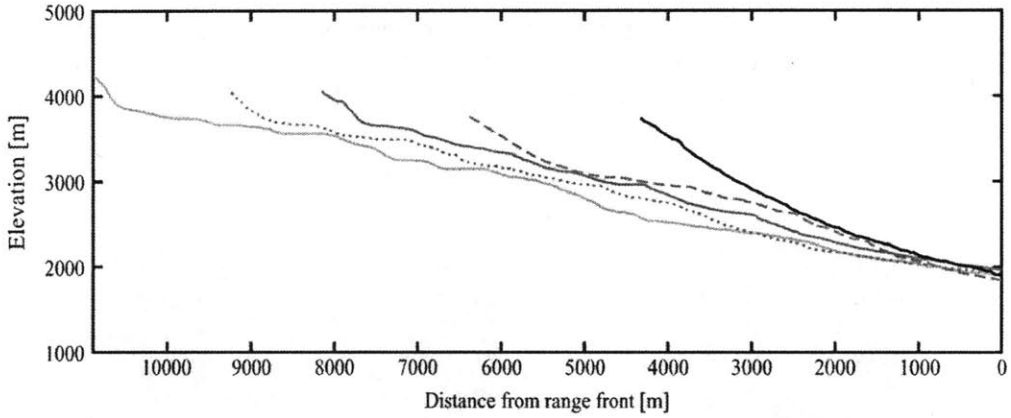

Fig. 4. Longitudinal profiles from Alabama Creek (nonglaciated, black), Division Creek (minor glaciation, medium grey, dashed), Red Mountain Creek (moderate glaciation, medium grey, solid), Tuttle Creek (significant glaciation, medium grey, dotted) and Lone Pine Creek (full glaciation, light grey). "Alabama Creek" is the name given to an unnamed creek that drains towards the Alabama Hills.

Some representative examples of longitudinal profiles taken from the five different categories of basin are shown in Fig. 4. The longitudinal profiles of the fluvial basins look much like those seen in other entirely unglaciated ranges (e.g., the Appalachians of Virginia and Maryland (Hack, 1957; Leopold et al., 1964), the King Range, northern California (Snyder et al., 2000)). Partial glaciation is typified by a flatter section in the upper reaches of the profile, while the lower parts retain the shape of a bedrock stream. Full glaciation yields stepped profiles with long, shallow sections separated by steeper steps, but the lower parts again resemble bedrock stream profiles.

3. Sub-ridgeline relief distribution

3.1. Method

Measurement of "relief" is a notoriously difficult problem, because in any landscape relief varies with the scale over which it is measured. Accordingly, many alternative definitions of relief are available.

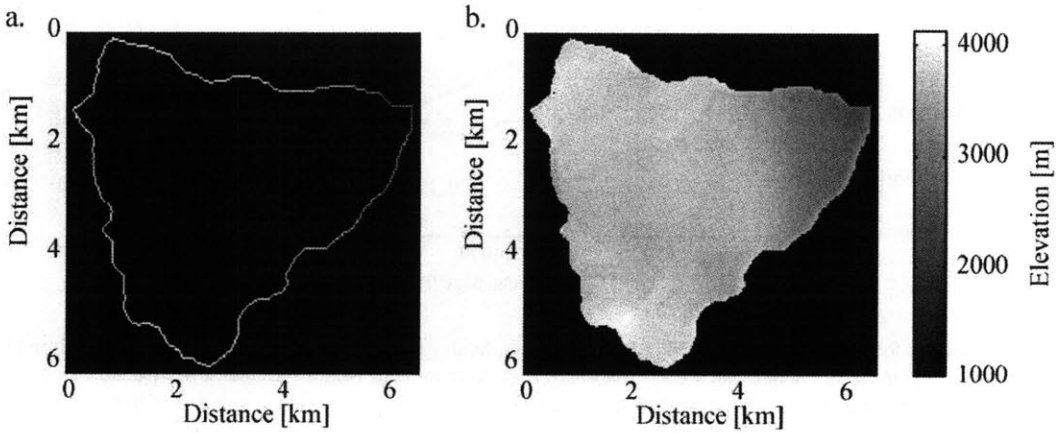

Fig. 5. Illustration of the "sub-ridgeline relief" method for Independence Creek. (a) Isolated ridgelines around the basin. (b) Interpolated smooth surface between these ridgelines.

At any given point, one can stand on the valley floor, pick a point on the ridgeline above, and call this difference in elevation the "relief." Relief can also be defined on the basis of differences in elevation between two points along a channel (the trunk stream or tributary relief, as appropriate), on a hillside (the hillslope relief) (e.g., Whipple et al., 1999), in an arbitrary direction (Weissel et al., 1994),

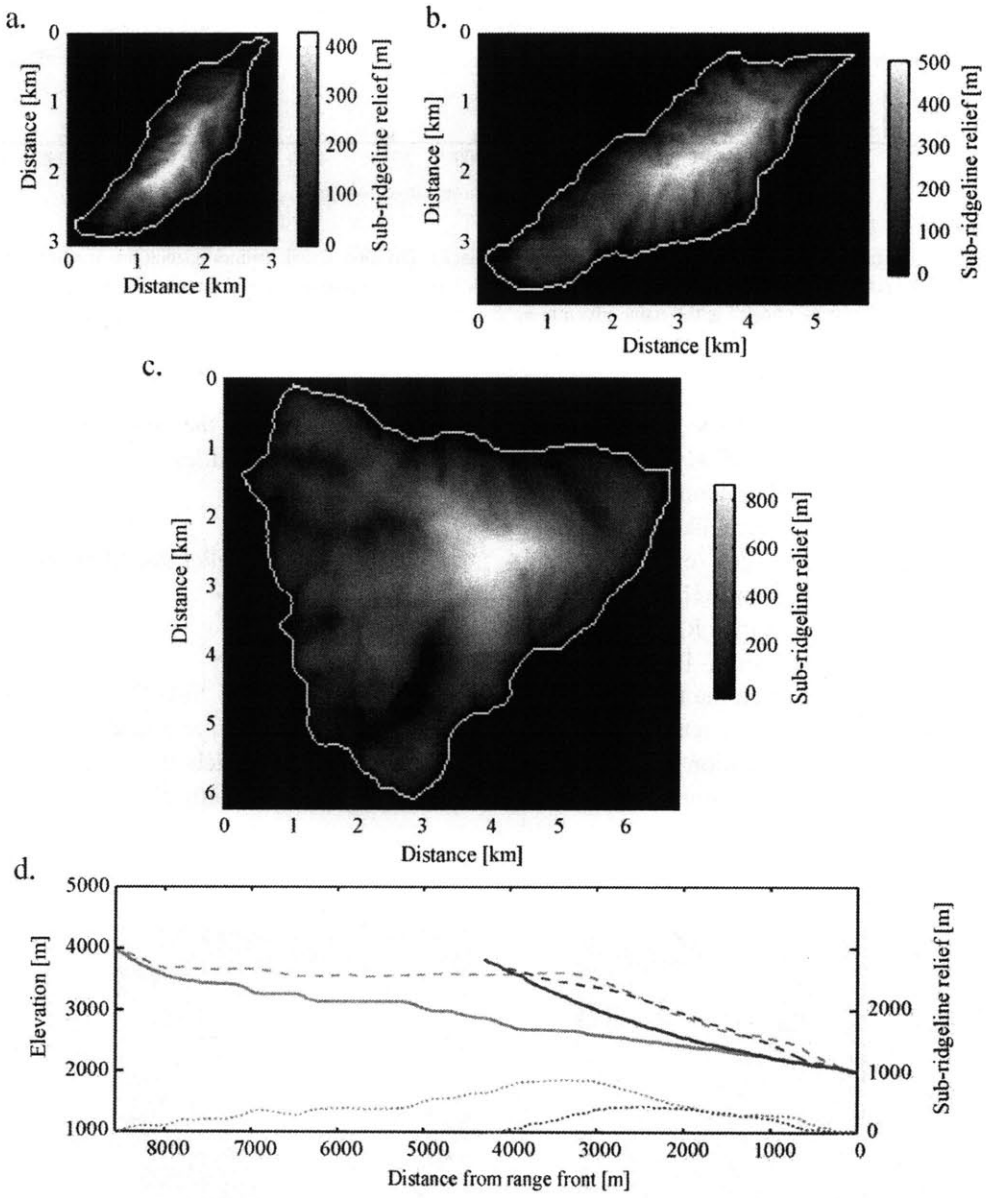

Fig. 6. Relief distribution for non-, partially, and fully glaciated valleys. In all cases, the basin outlet is on the right (east), and the scale is the same. (a) Relief distribution for the nonglaciated case, Alabama Creek, in map view. Notice the "bullseye" pattern of relief, greatest in the centre of the basin. (b) Relief distribution for the partially glaciated case, Bairs Creek, in map view. "Fingers" of high relief propagate upstream from high relief core. (c) Relief distribution for the fully glaciated case, Independence Creek, in map view. The high relief core shifts away from the range front in comparison with Alabama Creek. (d) Relief distribution along the longitudinal profiles of Alabama (dark grey) and Independence (light grey) Creeks. Solid lines are DEM topography, dashed lines are the sub-ridgeline interpolated surface along the longitudinal profile, and dotted lines are sub-ridgeline relief. Notice the flat ridgelines in the upper part of Independence Creek.

or within an arbitrary box (Ahnert, 1984). We define explicitly the nature of the "relief" that is relevant to our argument. For the purposes of a possible geodynamic response to erosion, the relevant measure is the geophysical relief (Small and Anderson, 1998). The geophysical relief is given by the volume of material "missing" below peaks and ridges divided by the surface area. These authors demonstrated that, if remnants of the pre-erosion surface are preserved, one can estimate not only the present relief but also the total amount and distribution of erosion. We have devised a similar, more general mathematical approach to measuring the modern geophysical relief structure to give a robust, objective, quantitative measure of the spatial distribution of relief (Brocklehurst and Whipple, 1999).

The first step in our method is to isolate the ridgelines outlining a given drainage basin (Fig. 5a). A cubic spline surface is then interpolated between these. The triangle-based cubic interpolation was found to be more satisfactory than either a triangle-based linear interpolation or a nearest-neighbour interpolation because it produces (i) a smooth surface and (ii) a surface that is continuous across the whole of the basin rather than producing a break down the centre line of the basin. We test whether any peaks or ridges within the basin protrude above this surface and repeat the interpolation with the surface also passing over these high points, to avoid underestimating the relief within the basin. This gives us a smooth reference datum (Fig. 5b) from which we subtract the current topography to give the spatial distribution of what we call "sub-ridgeline" relief (Fig. 6), i.e., the relief structure. In the absence of preserved remnants around the basin, we do not suggest that our interpolated surface represents the land surface at any time in the past, so we cannot equate our calculated sub-ridgeline relief with an amount of erosion. However, we can still compare the relief structures of different basins. Finally, we calculate the geophysical relief for each basin as the sub-ridgeline relief per unit area.

The isostatic response to relief production depends primarily on the isostatic response function, i (Gilchrist et al., 1994):

$$i = \rho_c/\rho_m \quad (1)$$

where ρ_c is the density of material eroded from the top of the crust, and ρ_m is the density of the mantle at the depth of compensation. The value of i gives the amount of isostatic uplift per unit depth of dissection and is generally slightly less than the mean geophysical relief (~ 0.82 for typical crustal and mantle densities).

3.2. Results and interpretations

Our analyses revealed an apparent trend in the dependence of sub-ridgeline relief distribution on the degree of glaciation. Nonglaciated valleys exhibit a "bullseye" pattern of relief, greatest at the centre of the basin (Fig. 6a). Progressively greater glaciation first causes a propagation of high relief "fingers" up the valleys from the high relief core (Fig. 6b) and then an enlargement of this core (Fig. 6c). Fig. 6d illustrates the sub-ridgeline relief along the trunk streams of a nonglaciated and a glaciated basin along with the current longitudinal profiles and the elevations of our interpolated surfaces along these profiles. The maximum relief in the glaciated basin, Independence Creek, is greater than that in the nonglaciated basin, Alabama Creek, and is located farther from the range front. Geophysical relief in valleys experiencing minor, moderate, significant, and full glaciation is on average $\sim$17-m less, $\sim$28-, $\sim$60-, and $\sim$81-m greater than that in nonglaciated basins, respectively (Fig. 7). An increase in geophysical relief of $\sim$81 m would generate only $\sim$66 m of uplift in the extreme case of pure isostatic response to incision. This number would be reduced considerably for a realistic elastic thickness. Moreover, the apparent increase in relief with degree of glaciation could reflect principally the larger size of the glaciated basins. Accordingly, Fig. 7 also illustrates the geophysical relief in GOLEM fluvial simulations for each basin (see below), which in most cases is comparable with the geophysical relief from the DEM. We also undertook a series of simulations varying the size of a drainage basin of fixed shape. We used the shape, drainage network, and number of pixels (from the 30 m DEM) of Symmes Creek, but varied the pixel size between 10 and 55 m to generate the range of basin areas shown by the smooth curve on Fig. 7. This curve clearly demonstrates a trend of increasing geophysical relief with increasing drainage area, similar in magnitude to that seen comparing fluvial and glaciated basins.

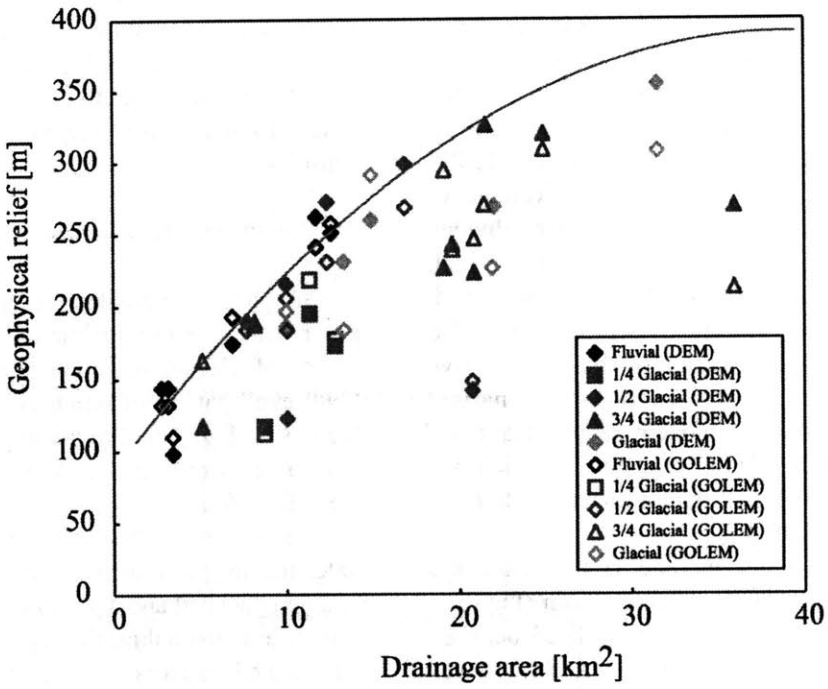

Fig. 7. Geophysical relief plotted against drainage area for current topography (DEM) and simulated topography (GOLEM), as explained in the text. The solid line represents simulating different-sized basins with the drainage pattern and basin shape of Symmes Creek (see text for explanation).

The interpolated surfaces used to define sub-ridgeline relief suggest that the ridgelines surrounding the glaciated basins are relatively flat for a significant proportion of the upper part of each basin (Fig. 6d). This is supported by the uniformity of headwall elevations, independent of basin size (Table 1). These observations can be interpreted as reflecting either prominent headward glacial erosion into a plateau surface, or significant lowering of hillslopes and ridgelines farther from the range front in response to downward cutting by the glaciers in the upper reaches of the glaciated basins. Simulations of nonglacial topography described below were used to evaluate the relative importance of these two possibilities.

4. Simulated nonglaciated topography

We simulated expected fluvial topography to address two questions: (i) how has glaciation changed the form of the landscape (and thus contributed to either isostatic or flexural uplift)? and (ii) are the observed differences in mean geophysical relief between the basins in the Sierra Nevada due purely to differences in drainage basin size (as suggested above)? Our approach was to use slope–drainage area analysis of the nonglaciated basins to constrain a model for bedrock channel erosion. This model was then employed with the drainage patterns of the glaciated basins to simulate the hypothetical modern forms of the basins should they never have been occupied by ice.

We focused first on the longitudinal profile because it is an important component of the relief structure (Whipple et al., 1999) and readily simulated. We used the error-weighted mean concavity and steepness from nonglaciated basins in concert with the present glacially influenced drainage structure to simulate a fluvial longitudinal profile for each glacially modified basin. As a simple indicator of likely changes to the longitudinal profile due to glaciation, we compared the current longitudinal profiles of glaciated basins with our simulations of expected present-day fluvial longitudinal profiles. We later suggest that this method can also be used as a tool to predict relative

headwall erosion rates. Moving to two-dimensional simulations allowed us to separate the effect of basin size from the effect of glaciation in the development of relief (Fig. 7). These simulations of expected fluvial topography, constrained by the drainage pattern and shape of a glaciated basin, also allowed us to address the question "what would the Sierra Nevada look like now if it had not been glaciated?" This was a question that we were unable to resolve on the basis of field studies alone, because insufficient evidence of the prior landform remains.

4.1. Slope–area analysis

Our simulations are based on the observed power–law relationship between slope and drainage area in fluvial topography (e.g., Flint, 1974), and thus require prior analysis of the slope–area data for the nonglaciated basins within the study area. Flint (1974) characterised fluvial topography in terms of two parameters: the concavity index, θ, and the steepness index, k_s:

$$S = k_s A^{-\theta}. \quad (2)$$

We employed linear regression of the logarithms of local channel gradient, S, and drainage area, A, to determine the concavity and steepness in all of the basins. For the glaciated basins, this was purely for the purpose of comparison rather than to suggest a mechanistic interpretation of slope–area data for glacial erosion. The power–law relationship (Eq. (2)) is commonly observed in many fluvial systems (Flint, 1974; Tarboton et al., 1991; Montgomery and Foufoula-Georgiou, 1993; Willgoose, 1994; Snyder et al., 2000), and under the special conditions of steady state (erosion rate equal to uplift rate at all points) the concavity and steepness can be related to the parameters of the bedrock channel erosion model (e.g., Whipple and Tucker, 1999). The error-weighted mean concavities and steepnesses for the nonglaciated basins were employed in our subsequent fluvial simulations to generate topography with the same fundamental characteristics. Since we merely sought to reproduce similar topography, we did not need to assume that either the current fluvial topography or the simulated topography represent steady state conditions. The only assumption necessary is that the observed slope–area relationship for the nonglaciated basins (area ~ 10 km^2) can be extrapolated to the greater drainage area of the glaciated basins (~ 30 km^2). Previous studies have demonstrated such a power–law relationship over larger ranges of drainage area (e.g., Tarboton et al., 1991; Whipple and Tucker, 1999).

The concavity and steepness were determined using two different sets of slope–area data: data along the trunk stream only, and data from the entire drainage basin. Restricting the analysis to the longitudinal profile of the trunk stream avoids complications due to errors in computing tributary flow paths across gently sloping terrain on ridges and valley floors and reduces scatter due to intra-basin variations. The stair-step nature of the DEM-derived nonglacial longitudinal profiles produces considerable scatter in slope–area data, but can be attributed to artefacts of DEM resolution and pit-filling routines. Smoothing of these data was achieved by calculating slopes on interpolated 10-m elevation contour intervals (Snyder et al., 2000). The same routine was employed with the glacial profiles, although glacial valleys naturally exhibit flat reaches, overdeepenings, and adverse slopes. The basin as a whole is the domain used by most previous workers (Tarboton et al., 1991; Montgomery and Foufoula-Georgiou, 1993; Willgoose, 1994; Tucker and Bras, 1998). For both analyses, we excluded the hillslopes above the channel heads from the regression, because the slope–area relation (Eq. (2)) is only applicable to the bedrock channel sections of the basin. We chose a critical drainage area for channel initiation of 10^5 m^2, because it was at this area that there was a break in slope–area scaling in the majority of the basins, also discussed by Montgomery and Foufoula-Georgiou (1993) and Snyder et al. (2000). The slope distribution below this critical drainage area threshold gives representative slopes for the hillslope regions. By choosing the downstream extent of our basins to lie at the range front, we avoided areas with significant alluviation of the trunk stream and thus did not need to impose an upper limit on the drainage area considered in the regression analysis (see discussion in Snyder et al., 2000).

Nonglaciated basins are characterised by longitudinal profile concavities (θ) with an error-weighted mean of 0.32 ± 0.11 (1σ) (Table 1). This figure

plunges dramatically to a mean of 0.08±0.09 for partially glaciated basins and 0.07±0.08 for fully glaciated basins. All of the glaciated basins have concavities that are significantly different from the nonglacial basins, but there is little variation between the four different categories of glacial extent. Clearly, one effect of glaciation is to reduce the overall concavity of the longitudinal profile. At drainage areas below the break in the slope–area relationship ($A<10^5$ m^2), the slopes cluster around 40°, so we take this as the maximum permitted hillslope angle in our subsequent simulations (see below).

Given the intimate relationship between concavity and steepness (derived from regression slope and intercept, respectively), we followed two different methods to determine meaningful measures of steepness. To obtain a representative k_s for the nonglaciated basins for our subsequent modelling, we fixed the concavity at the error-weighted mean nonglaciated value and repeated the regressions for this subset of the basins (Snyder et al., 2000). To gain an indication of the errors on our determination of k_s, we also determined k_s with the concavity fixed at the mean concavity plus and minus the 1σ error. For a concavity of 0.32, the mean value of k_s for the nonglaciated basins is 30 ($\theta+1\sigma$: 149; $\theta-1\sigma$: 5.9). The errors in k_s are not symmetrical as the steepness is the exponential of the intercept, which does have symmetrical errors. Where concavity varies considerably, the method employed by Snyder et al. (2000) is not ideal, so for the dataset as a whole we followed the technique suggested by Sklar and Dietrich (1998). Normalising by a representative area (A_r) in the centre of the range of drainage area data gives a representative slope, S_r, which expresses the relative steepness of the profile:

$$S = S_r(A/A_r)^{-\theta} \quad (3)$$

In our case A_r was 10^6 m^2. Fig. 8 shows that S_r is not independent of concavity. The less concave, glaciated basins tend to also have lower representative slopes S_r, as suggested by Fig. 4. In other words, the glaciated basins are fundamentally less steep than their nonglaciated counterparts.

The basin-wide concavities average 0.27±0.08 (1σ) for nonglaciated basins, 0.17±0.08 for partially glaciated basins, and 0.16±0.08 for fully glaciated basins (Table 1). Again, the subcategorisation of the

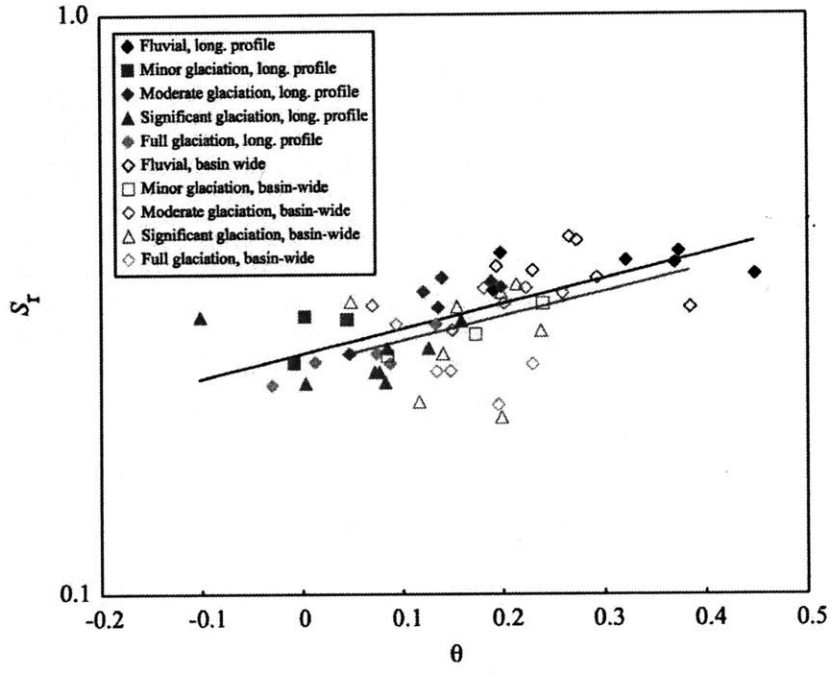

Fig. 8. Steepness index, S_r, plotted on a log scale against concavity, θ, for both longitudinal profile and basin-wide data. The dark grey line is the best fit exponential for the longitudinal profile data, the pale grey line the best fit for the basin-wide data.

partially glaciated basins reveals little. A basin-wide concavity set at 0.27 yields a mean k_s in the non-glaciated basins of 16 ($\theta+1\sigma$: 31; $\theta-1\sigma$: 8.3). In terms of steepness, the basin-wide data show a near identical pattern to that of the longitudinal profile data, with shallower representative slopes in the less concave glaciated basins (Fig. 8).

The longitudinal profile concavity is noticeably lower than the basin-wide concavity in the glaciated basins because of the low slopes in the upper reaches of the main channel in the glacial system, corresponding to the floors of cirques and overdeepenings. These low slopes act to decrease the concavity of the trunk stream profile as defined by the slope of the best-fit line in log slope–log area space. When the whole basin is considered, steeper slopes at low drainage areas in tributaries (especially near the range front) act against a decline in concavity. Such distinctive low slopes high in the glaciated drainage basins are also clearly demonstrated in the hypsometry and slope–elevation distributions of the eastern Sierra Nevada (Brocklehurst and Whipple, 1999, 2000). In the nonglacial basins, the longitudinal profile and basin-wide concavities are the same within error.

4.2. One-dimensional simulated topography

4.2.1. Methods

The one-dimensional simulations were obtained by integrating the slope–area relation established for nonglaciated basins along the longitudinal profiles of the glaciated basins. We also analysed the non-glaciated basins to verify that we could reproduce a close approximation to the current topography using the mean values reported above. The concavity and steepness indices came from the longitudinal profile-restricted data (see above), with a maximum permitted hillslope angle at the channel head of 40°, also from our slope–area analyses. Simply integrating the observed relationship requires no assumptions about steady state for either the current nonglacial topography or our simulated fluvial topography. We fixed the outlet elevation at its current elevation, reasoning that the glacial system has had very little opportunity to modify this elevation by either erosion (very short ice residence time in this region even for the fully glaciated cases) or by deposition (the vast majority of sediment continues downstream to the alluvial fans and beyond). We obtained an indication of the accuracy of our simulated profiles by employing the mean concavity with the 1σ error either added or subtracted and the correspondingly adjusted steepnesses, as described above (dashed lines on Fig. 9).

4.2.2. Results and interpretations

In our simple one-dimensional simulations, we were able to accurately reproduce a typical nonglaciated profile using the error-weighted mean and associated steepness (e.g., Alabama Creek, Fig. 9a). The mean concavity and steepness produced a more representative profile than either the upper- or lower-bound concavities with their corresponding steepnesses. We found that the glaciated basins fell into two categories. For some of the glaciated basins, we generated a very close match between the simulated profile and the present profile lower in the basin, but with considerable deviation in the upper part of the basin where the simulated profile lay at a much higher elevation (e.g., Birch Creek, Fig. 9b). In the remaining cases, the simulated fluvial profile lay significantly below the present topographic profile in the middle reaches (e.g., Tinemaha Creek, Fig. 9c). These "undercutting" profiles were found independently of the degree of glaciation.

Our interpretation of the deviation between simulated and observed topography in the upper part of non-undercutting glaciated basins is that considerable downcutting is required here to evolve from a typical nonglaciated profile to the currently observed glaciated profiles. Had the glaciers not developed and eroded a significant "extra" amount of material, the observed fluvial profiles would currently have a profile similar to our simulations. Thus, we suggest that at higher elevations in the Sierra Nevada glaciers erode faster than streams. The good agreement lower in the basin may be due to the short residence time of glaciers in this part of the basin, even in the fully glaciated cases (Porter, 1989), or might indicate that glacial erosion in the ablation zone of these glaciers was either inefficient or dominated by subglacial water.

One could interpret the undercutting profiles (Fig. 9c) as representing lower erosion rates in this part of the glacial system than would have occurred in the fluvial system. Alternatively, locally resistant bedrock

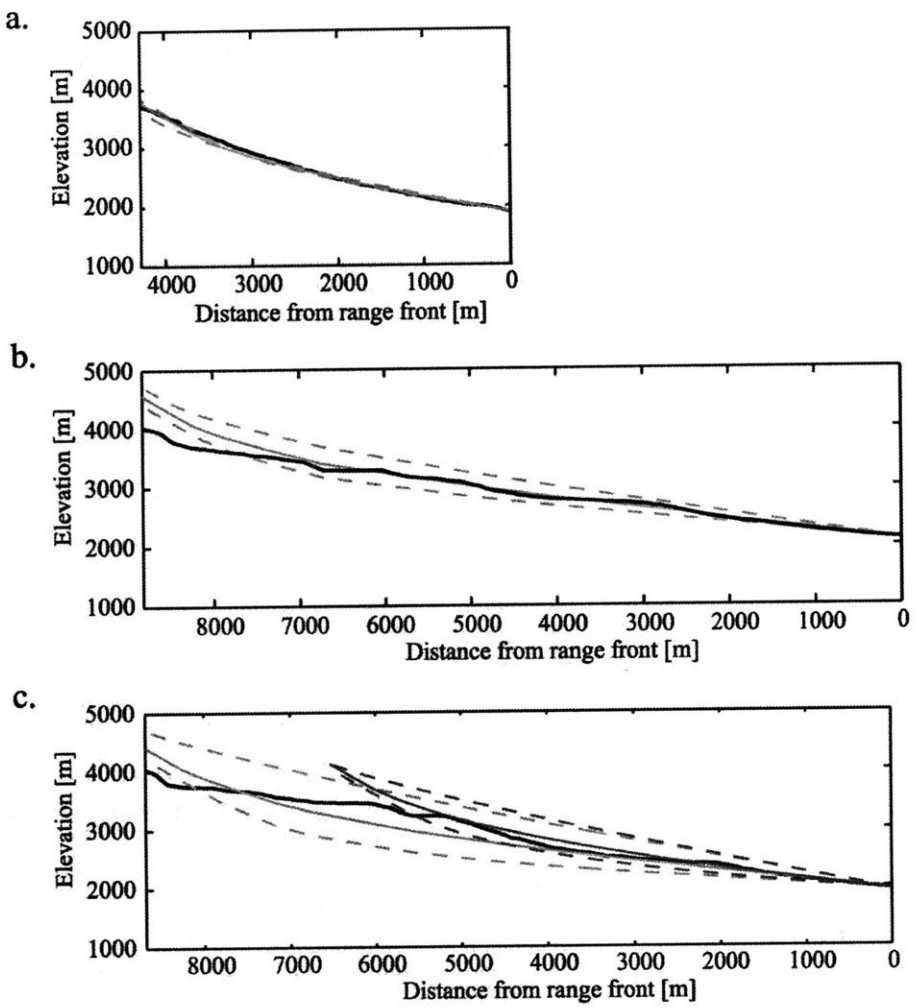

Fig. 9. (a) One-dimensional simulated profiles for Alabama Creek, a nonglaciated basin. The black line is the longitudinal profile extracted from the DEM, the pale grey, solid line is the simulated longitudinal profile, and the pale grey, dashed lines are the simulated longitudinal profiles varying concavity and steepness in concert by $\pm 1\sigma$. (b) Birch Creek. Key as for Alabama Creek. (c) Tinemaha Creek. Key as for Alabama Creek, plus the dark grey, solid line is the shortened, simulated longitudinal profile (see text), and the dark grey, dashed lines are the shortened, simulated longitudinal profiles, varying concavity and steepness by $\pm 1\sigma$.

might be responsible for the observed undercutting (observed profile not eroding as much as our simulation predicts). However, we note that in each case, shortening the simulated profile from the divide (upstream end) places it more in line with the observed topographic profile in the lower reaches of the basin. Hence, our preferred interpretation is that "undercutting" is a consequence of faster (horizontal) headwall erosion rates in the glacial system (as discussed below). That is, if glaciation had not occurred, some of the drainages on the eastern side of the Sierra Nevada would now be shorter.

4.3. Two-dimensional simulated topography (GOLEM)

4.3.1. Methods

We employed the nonglaciated basin-wide error-weighted mean concavity and steepness statistics as the principle inputs to the Geologic–Orogenic Landscape Evolution Model (GOLEM, described in detail by Tucker and Slingerland, 1994, 1997) to simulate most likely present-day fluvial landforms. GOLEM simulates basin evolution under the action of tectonic uplift, weathering processes, hillslope transport, and

bedrock channel erosion and sediment transport. While this set of processes is not exhaustive, it incorporates the most important landscape-forming processes in basins that are dominated by physical rather than chemical erosion. Bedrock-channel erosion follows a shear-stress derived power–law relationship. We prescribed the basin outline and initial drainage pattern to be the same as for the current topography in order to allow meaningful comparison between the simulated and current topography. Our two-dimensional simulations have not addressed the possibility of headwall erosion directly. The model was run until it reached a steady-state condition, but this was done solely to reproduce the slope–area

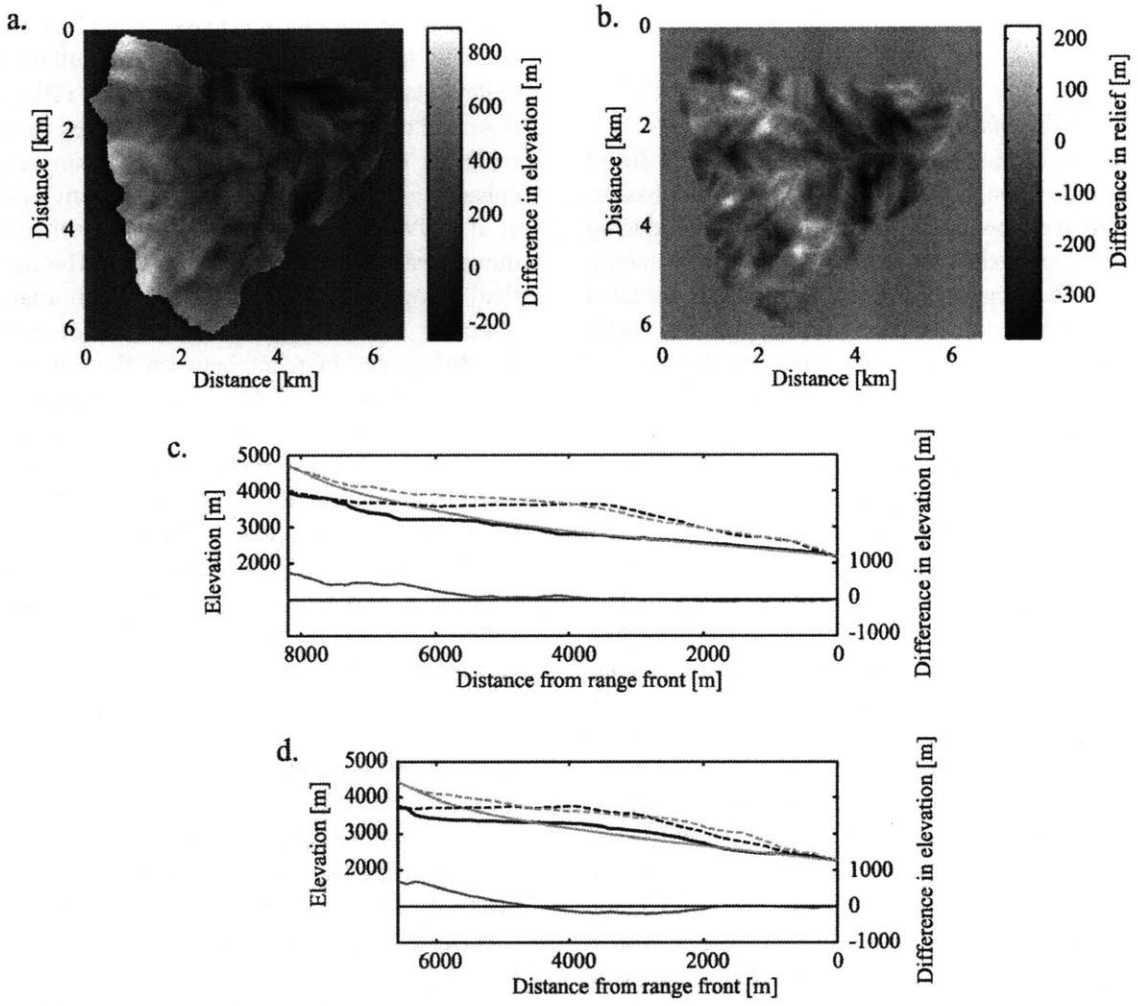

Fig. 10. Two-dimensional simulations of Independence Creek and South Fork, Oak Creek. (a) Present topography subtracted from the GOLEM simulated topography for Independence Creek, in map view (see text). Simulated topography is noticeably higher in the upper parts of the basin. (b) Present sub-ridgeline relief subtracted from GOLEM simulated sub-ridgeline relief for Independence Creek, in map view. Redistribution of relief comprises higher relief in the glacial system at high elevations and also in the lower U-shaped sections, but lower relief where the different tributaries come together. (c) Independence Creek. Longitudinal profiles drawn from the present topography (black) and simulated topography (pale grey) with the difference between the two in dark grey. Also shown are the interpolated ridgeline surfaces along the profiles (present topography—black, dashed; simulated topography—pale grey, dashed). Comparing the observed and simulated topography, both the valley floor and the ridgeline agree well at lower elevations and then diverge considerably higher up, with the simulated ridgeline and longitudinal profile considerably higher. (d) South Fork, Oak Creek. Key as for Independence Creek. The simulated profile undercuts the present topography in the middle reaches, suggesting headwall erosion in the glacial system (see text).

relation currently observed in nonglaciated basins, rather than to necessarily suggest the landscape now or in our simulations is in steady state. After seeing that the mean concavity and steepness produced the most realistic fluvial profiles in the one-dimensional case, we concentrated on these values here. Once the simulated topography had been generated, we calculated sub-ridgeline relief as before for comparison with relief in modern basins (Fig. 7) and to allow us to contrast ridgeline behaviour alongside any changes in the channels.

4.3.2. Results and interpretation

The GOLEM simulations accurately reproduced the modern topography in the nonglaciated basins, matching the topography of the basin and reproducing the total geophysical relief and its spatial distribution (Fig. 7). The simulations of glaciated basins revealed in more detail and in two dimensions the same patterns that were seen in our simple one-dimensional simulations (Fig. 10). In most cases, the simulated and present elevations are strikingly similar in the lower parts of the basin, but diverge noticeably in the upper part of the basin. Fig. 10a and c highlight that, in such instances, both ridgelines and valley floors are lower in the present topography. In other cases, the simulated topography undercuts the observed topography in the same way as in our one-dimensional cases (Fig. 10d). As before, the presence or absence of "undercutting" in the glaciated basins is independent of the degree of glaciation, and we attribute the undercutting to headwall erosion in the glacial system. Our calculation of sub-ridgeline relief shows that glaciation caused significant reorganisation of the relief structure, with greater relief at high elevations in the cirques, and reduced relief where tributaries come together lower in the basins in comparison with a simulated fluvial counterpart (Fig. 10b). The redistribution of relief is more pronounced the greater the degree of glaciation. However, our calculated geophysical relief is similar for the simulated fluvial topography and the current topography (Fig. 7). The only clear distinction between the two occurs in the fully glaciated basins, where geophysical relief is on average ~ 25 m greater using the observed topography (Fig. 7).

We attribute the differences in topography in the upper part of the basin in Fig. 10a to greater efficiency in downcutting at high elevations and/or headwall erosion (see below) by glaciers. Ridgelines could be lowered (Fig. 10c,d) either by periglacial ridgetop processes or through the mass wasting of hillslopes reacting to enhanced rates of downcutting by the valley glaciers. The redistribution of relief that is observed between simulated and observed topography indicates that glacial erosion mechanisms that both enhance and reduce relief have been active (Whipple et al., 1999), operating within the overall scheme of downward cutting at high elevations. The near-identical geophysical relief values in simulated and observed basins suggest that the major portion of the differences in relief between the current basins can be attributed to their sizes: nonglaciated and glaciated basins of the same size and shape have very similar relief. If our proposed headwall cutting incises an elevated plateau, the mean relief will be increased. However, if the topography is already dissected, the headwall cutting will act only to lower divides. In either case, this will be accompanied by lowering of valley floor, peak, and ridgeline elevations in the upper part of the basin.

5. Headwall erosion

As described above, both our one- and two-dimensional simulations led us to hypothesise that headwall erosion rates in the glacial system might exceed those in the fluvial system. Headwall erosion rates are not well understood in either the fluvial or glacial systems. We view this as a major unsolved problem in landscape evolution. A couple of mechanisms have been proposed to enhance headwall erosion rates in the glacial system. In the upper

Fig. 11. (a) Contour map of Tinemaha and Birch Creeks and the south fork of Big Pine Creek. Profiles plotted in (b)–(d) as illustrated. Notice the westward step in the divide at the head of Tinemaha Creek. (b) Tinemaha Creek, profile 1 (present topography—black; full-length simulation—medium grey; shortened simulation—pale grey; simulated longitudinal profiles varying concavity and steepness by $\pm 1\sigma$—dashed). Estimated headwall erosion: 500 m. (c) Tinemaha Creek, profile 2 (key as before). Estimated headwall erosion: 2150 m. (e) Tinemaha Creek, profile 3 (key as before). Estimated headwall erosion: 1400 m.

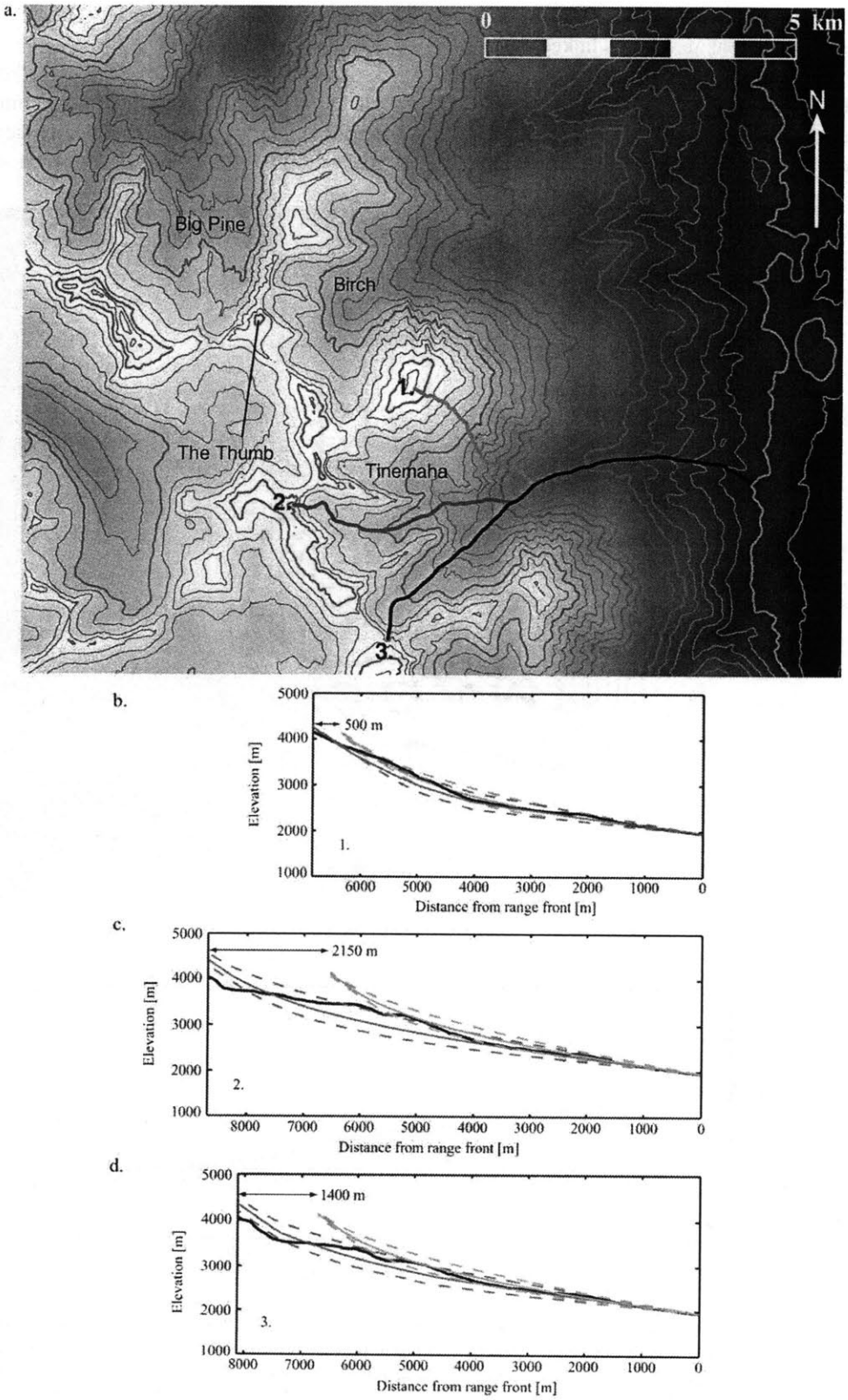
a.
0
5 km
N
Big Pine
Birch
The Thumb
Tinemaha
1
2
3
b.
500 m
Elevation [m]
1.
Distance from range front [m]
c.
2150 m
Elevation [m]
2.
Distance from range front [m]
d.
1400 m
Elevation [m]
3.
Distance from range front [m]

headwall, freeze–thaw processes govern erosion rates. Matsuoka and Sakai (1999) linked observed rockfalls in the Japanese Alps to seasonal thawing. In the lower headwall, the bergschrund allows water to reach the glacier bed, causing large amplitude subglacial water-pressure fluctuations that may facilitate rapid erosion by quarrying (Hooke, 1991; Hallet, 1996; Alley et al., 1999).

As shown in Fig. 9c, where we represent faster glacial headwall erosion with a simulated fluvial profile constructed for a shorter, reduced area basin, we can obtain a good fit between observed and

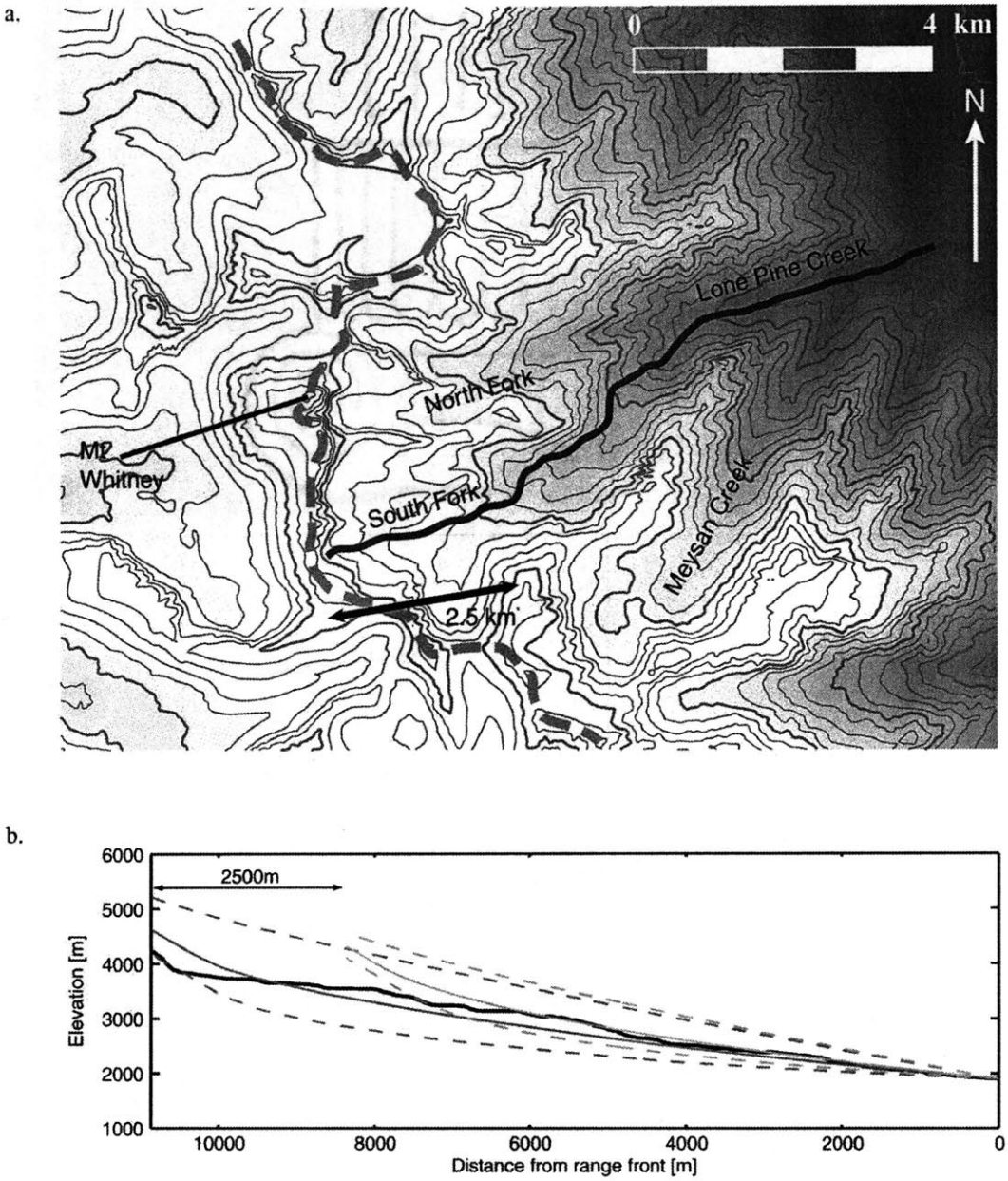

Fig. 12. Simulating headwall erosion in the south fork of Lone Pine Creek. (a) Contour map of the Lone Pine Creek basin. Notice the significant westward step in the divide at the head of Lone Pine Creek, passing just to the east of the summit of Mt Whitney. (b) Observed and simulated longitudinal profiles for Lone Pine Creek (present topography—black; full-length simulation—dark grey; shortened simulation—pale grey; simulated longitudinal profiles varying concavity and steepness by $\pm 1\sigma$—dashed). Estimated headwall erosion: 2500 m.

simulated profiles in the lower part of the basin. The headwall erosion represented in this way is the extra erosion beyond that which would have taken place in the fluvial system (i.e., we underestimate the total headwall erosion). We used Hack's Law parameters (Hack, 1957) to construct smaller basins of the same shape. For our purposes, Hack's Law can be written

$$A = k_h x^h \quad (4)$$

where A is drainage area, x is downstream distance along the longitudinal profile, and k_h and h are what we define as the Hack's Law constant and exponent, respectively. The constant and exponent were determined for each basin by regression analysis. We shortened the simulated drainage basins from the headwall end until the resulting longitudinal profile no longer undercut the present topography. In practice, this resulted in a fluvial profile that consistently matched the current topography up to ~3200 m, a little below the mean Quaternary ELA. The shorter profiles also reduce the amount of downcutting that is required in the upper part of the basin to move from the simulated nonglacial profile to the current profile, although the headwall erosion would still represent significant mass removal. Given the many unknowns in bedrock channel evolution and the uncertainty in our simulations of "expected" modern fluvial landforms, this argument for headwall erosion alone is perhaps unconvincing. However, the inferred amounts of headwall erosion are consistent with independent, if qualitative, field evidence for likely amounts of drainage divide retreat. For example, we suggest that the glacier in Birch Creek (Fig. 9b) has only cut headward ~100 m more than would have occurred under fluvial erosion, and we propose that this is because of competition with the south fork of Big Pine Creek, which lies at its head (Fig. 11a). Instead of divide

Table 2
Summary of divide migration results

Basin	Degree of glaciation	Headward migration (m)	Rate (mm/year)
Alabama	None	0	0
Black	None	0	0
Inyo	None	0	0
Pinyon	None	0	0
South Fork, Lubken	None	0	0
Symmes	None	0	0
Diaz	Minor	2500	1.25
Division	Minor	1500	0.75
Thibaut	Minor	400	0.20
Bairs	Moderate	550	0.28
Goodale	Moderate	2000	1.00
Hogback	Moderate	1400	0.70
North Fork, Bairs	Moderate	700	0.35
North Fork, Lubken	Moderate	1450	0.73
Red Mountain	Moderate	750	0.38
Armstrong	Significant	1000	0.50
George	Significant	850	0.43
North Fork, Oak	Significant	1200	0.60
Sardine	Significant	1400	0.70
Sawmill	Significant	3000	1.50
Shepherd	Significant	700	0.35
Taboose	Significant	900	0.45
Tuttle	Significant	1200	0.60
Birch	Full	100	0.05
Independence	Full	100	0.05
Lone Pine	Full	2500	1.25
South Fork, Oak	Full	2650	1.33
Tinemaha	Full	2150	1.08

migration, the combined action of these two glaciers has been to carve the horn known as The Thumb. The adjacent basin to the south, Tinemaha Creek (Figs. 9c and 11a), has cut a large "bite" out of the divide, which deviates noticeably to the west at its head. Here we require ~2150 m of "extra" headwall erosion to obtain a good fit between the simulated and observed profiles below ~3200 m (Fig. 11c). This headward cutting corresponds to an arguably reasonable rate of ~1.1 mm/year faster than the fluvial rate over the Quaternary (~2 Ma). The south fork of Lone Pine Creek, below Mt. Whitney, demonstrates a similar story (Fig. 12). Here, our best fit between the simulated profile and the observed glacial profile below ~3200 m requires shortening the simulated profile by ~2500 m (Fig. 12a). This again is consistent with the deviation of the divide around the head of the basin (Fig. 12b).

We also obtained a consistent story looking at the tributaries in selected basins. Fig. 11 illustrates our inferred variation in amounts of relative headwall erosion for three tributaries of Tinemaha Creek. Our method suggests that Tinemaha Creek is being enlarged in all directions, but is growing most rapidly at the range crest (profiles 2; Fig. 11c), lengthening the basin, rather than at the tops of its smaller tributaries (e.g., profile 3: Fig. 11d). This is consistent with what one might suggest from the basin morphology, as the head of the basin has a quite angular form with the "fastest growing" tributary at its apex, as opposed to a more typical morphology with a rounded head to the basin. Profile 1 (Fig. 11b) is essentially a nonglacial chute, so the fact that we attribute ~500 m of glacial headwall erosion to this profile illustrates the imperfect nature of the technique.

Table 2 summarises best-fit amounts of headwall erosion for each of our basins. The calculated headwall erosion rates are lower bounds on absolute headwall erosion rates because of the unknown headwall erosion rate that would have been taking place under the nonglacial regime, but they fall within the range of previously reported rockwall erosion rates in Alpine settings (Table 3). There is no correlation between degree of glaciation and rate of headwall erosion. Instead, local setting appears to be the major control on headwall erosion rate. We suggest that the slow headwall erosion in Shepherd and Independence Creeks is due not to competition, as in Birch Creek, but to the occurrence of transfluent ice at the head of the basin. We anticipate that an ice cap straddling the divide will act to protect the headwall, with relatively stagnant ice causing minor abrasion and insulating against freeze–thaw processes, and the lack of a bergschrund preventing water from reaching the glacier bed. Further studies of the mechanics of, and controls on, headward erosion by alpine glaciers are warranted.

6. Discussion

We have observed increasing relief with greater degree of glaciation in the basins of the eastern Sierra Nevada, but attribute this principally to the larger size of these basins. The amount of relief production that

Table 3
Published rockwall retreat rates for Alpine settings

Location	Lithology	Rockwall retreat rate (mm/year)			Source
		min	mean	max	
Alpine environments, present day					
Tatra Mountains	Dolomite	0.1		3.0	Kotarba, 1972
Front Range	Various		0.76		Caine, 1974
French Alps	Various	0.05		3.0	Francou, 1988
Japanese Alps	Sandstone and shale	0.03	0.1	0.3	Matsuoaka and Sakai, 1999
Alpine environments, Holocene					
Swiss Alps	Various	1.0		2.5	Barsch, 1977
Austrian Alps	Gneiss, schist	0.7		1.0	Poser, 1954

can be ascribed to the onset of glacial erosion is not tightly constrained, but is probably small. Given a prior, well-dissected fluvial landscape, relief will only be produced by glacial erosion through its ability to erode headward into a low-relief surface at a more rapid rate than the fluvial system, enlarging drainage basins. This will be important in the special case of erosion into a plateau surface. As a simple illustration, consider the limiting case of headward erosion into a very low-relief plateau surface. Suppose that the basin of interest has h=1.6 and k_h=5 (Eq. (4)) and begins the Quaternary with a length of 9 km, yielding a drainage area of $\sim 10^7$ m^2. This would result in a mean geophysical relief (from Fig. 7) of $\sim$200 m. Suppose an equivalent area with very low relief lies "upstream" of this, giving a mean geophysical relief of $\sim$100 m across the region as a whole. Now suppose that the basin is enlarged during the Quaternary by glacial headward erosion to cover the whole of the 2×10^7 m^2 area, corresponding to lengthening by $\sim$4.5 km or headward erosion at a rapid rate a little above 2 mm/year. From Fig. 7 again, this basin will now have a mean geophysical relief of $\sim$250 m, so that overall the region will have seen an increase in geophysical relief of only $\sim$150 m. This corresponds to a maximum isostatic response of $\sim$123 m. In general, while we suspect that glaciers could well erode headward at a faster rate than rivers, thus still being an agent of relief production, the difference is probably insufficient to have a major effect on mean relief and hence isostatic response. Instead, we find that in comparing simulated modern fluvial topography with observed glaciated topography, the major impact of glacial erosion during the Quaternary has been a substantial lowering of peaks, ridgelines, and valley floors high in the range (above $\sim$3200 m) and thus a major reduction of trunk stream relief. This substantial lowering suggests that at the elevations at which they have been present for the greatest portion of the Quaternary (Porter, 1989), glaciers are capable of eroding at faster rates than rivers, lowering the peaks at a faster rate than the isostatic uplift that they might induce.

We have demonstrated that enhanced glacial erosion was concentrated in a narrow band along the crest of the range (elevations >3200 m). Some glaciers have apparently cut predominantly downward and brought ridgelines down with them, while other glaciers have cut mostly in a horizontal, headward direction with less impact on ridgeline elevations. At present, the Sierra Nevada crest is at a quite uniform elevation throughout the study area. We speculate that, prior to glaciation, the range could well have had a more undulatory crest. As shown by Small and Anderson (1995), the combined effects of erosion at the range crest and deposition in the Great Valley to the west can lead to significant flexural–isostatic tilting of the Sierra Nevada block. If the Sierra Nevada block is modelled as a broken (along the eastern scarp) elastic plate, such erosional redistribution of mass may be sufficient to explain a significant fraction of the observed tilt of Miocene lava beds (e.g., Huber, 1981). If this effect has been significant during the Quaternary, the induced acceleration in relative baselevel fall on streams draining the eastern Sierra Nevada could potentially have steepened the river valleys and would be incorporated into our simulations of modern nonglacial topography. Full consideration of the possible implications would require analysis of the topography of the much larger western drainages and flexural–isostatic modelling of the Sierra Nevada block as a whole—an analysis beyond the scope of the present study. Our analysis instead focussed on the more general problem of relief evolution in adjacent glaciated and unglaciated drainage basins that have experienced the same tectonic history.

Our general conclusions are probably valid for other temperate mountain ranges in low-moderate uplift rate settings. In colder regions, glacial ice could be frozen to the bed, drastically reducing erosion rates (Braun et al., 1999; Cuffey et al., 2000) and permitting higher peak elevations (Whipple et al., 1999). It is not clear whether the glacial erosion system will behave differently in a rapidly uplifting mountain range, where glacial erosion might not keep pace with uplift, or the glaciers might at least have to steepen (analogous to the reaction of the fluvial system) to do so. We envision a number of competing factors. Glacier beds at high elevations are more likely to be at subfreezing temperatures, reducing erosion rates (Cuffey et al., 2000). However, these high elevations could also interrupt airflow, causing increased orographic precipitation, which at higher altitudes would also fall as snow year round, thus contributing to increased glaciation (as suggested by

Molnar and England, 1990). We note that the region around Nanga Parbat exhibits spectacular hillslopes sometimes covering a 3-km range in elevation. There are no hillslopes approaching this scale in the Sierra Nevada, and we hesitate to speculate on their likely impact on the relief structure or even on why such enormous steep slopes are able to develop. These slopes could cause greater snow avalanching, hindering development of glaciers on the slopes themselves, but at the same time this avalanching would contribute significant volumes of snow and ice to the glaciers at the base of the slopes, enhancing mass balance and erosion. If glacial erosion is not coupled effectively with hillslope erosion there would be a high potential for relief production. Avalanching would also bring rock debris onto the glacier surface, shielding it from ablation and further enhancing erosion. Recent authors have emphasised the potential importance of subglacial water in erosion processes (e.g., Alley et al., 1999), but we cannot speculate about the consequences of variations in the subglacial hydrology between the Sierra Nevada and other settings. At present, neither the importance of subglacial hydrology to erosion nor the response of the hydrological system to steepening are well constrained. Thus, we feel it would be unwise to extrapolate our results too far; further study in other settings is needed.

How might the topographic distinctions that we have found in the Sierra Nevada be attributable to factors other than the glaciation history? One of the most beneficial features of the eastern Sierra Nevada as the field site for this study was the relatively simple and uniform tectonic history. The major lithologic variation lies in the nature of jointing within the Cretaceous granites. Our reconnaissance field studies indicate that just a few valleys exhibit greater than average joint density and that the consequence of this is principally a greater volume of colluvium in the valley (e.g., Armstrong Canyon) to offset the steeper valley walls. Thus, no net effect on the estimation of relief from the DEM is noted. The nonglaciated basins are all shorter than their glaciated counterparts, so that their heads lie farther into the rain shadow generated by this mountain range. Possibly, fluvial basins sourced higher in the range with a greater discharge and higher erosivity would have reduced concavity and steepness in comparison with the current, shorter nonglaciated basins (Whipple et al., 1999) and hence be more similar in form to the current glaciated profiles. We believe that this would be a minor effect. The nonglaciated basins that we have studied have a considerable range in drainage area, but very consistent concavities and steepnesses (e.g., Alabama vs. Symmes Creeks). Such a pattern of shallower, larger fluvial basins would also be inconsistent with our observation that the lower parts of our glaciated profiles match very closely the simulated fluvial profiles using the steepness (k_s) and concavity (θ) of the modern nonglaciated basins.

7. Conclusions

We have demonstrated that glacial erosion is responsible for redistribution of relief, producing relief high in the drainage basin in the cirques, but resulting in lower relief where different tributaries converge. In the absence of a change in basin size, the net effect is to retain the same overall geophysical relief, so while glacial erosion mechanisms that both enhance and reduce relief have been active in the eastern Sierra Nevada, neither has been dominant. Glaciers have been responsible for bringing down both valley floors and ridgelines, suggesting that glaciers are capable of eroding at faster rates than rivers in this environment and that the glacial and hillslope systems are closely coupled. Whereas the glaciated basins in the eastern Sierra are associated with higher relief in comparison with their fluvial neighbours, this is principally due to basin size: the fluvial simulations based on the drainage networks of the glacial basins have geophysical relief similar to the current topography. Our preliminary attempts to evaluate the relative amounts of headward erosion in the fluvial and glacial systems suggest that, while local effects are very important, these headward erosion rates are generally higher in the glacial system. This leads to the possibility of enhanced relief production if this erosion cuts into a low relief surface, but the effect is likely to be small.

Our analyses indicate that the case for ridgeline uplift through isostatic response to enhanced valley erosion put forward by Molnar and England (1990) is exaggerated, at least for the Sierra Nevada. We note, however, that enhanced rates of erosion in the glacial

system will produce rugged topography and large volumes of sediment, both of which could be interpreted as reflecting relief production and misconstrued as evidence of accelerated late Cenozoic tectonism, as argued by Molnar and England (1990). At the same time, our results suggest that there will be a major negative feedback in the system proposed by Raymo and Ruddiman (1992) in that, whereas erosion rates may rise as a result of uplift and subsequent global cooling, the development of the glacial system will ultimately limit ridgeline elevations and relief. To return to the questions posed in the introduction, we find that, in the Sierra Nevada, glacial erosion is capable of reducing ridgeline elevations, but does not significantly enhance relief unless it enlarges a drainage basin into low-relief topography. However, the focussed glacial erosion above the ELA could contribute to far-field flexural–isostatic effects. We have identified the following areas for future research: (i) mechanisms, rates, and controls on headwall erosion in both the fluvial and glacial systems; (ii) the role of glacial erosion in areas of extreme tectonic activity; and (iii) limits to cirque headwall relief.

Acknowledgements

We would like to take this opportunity to thank Greg Tucker, Eric Leonard, Noah Snyder, and Eric Kirby for the many valuable discussions, Ryan Ewing for the long-suffering field assistance, and Noah Snyder, Julia Baldwin and Marin Clark for the helpful comments on early versions of this manuscript. The comments of an anonymous reviewer greatly improved the clarity and thoroughness of the manuscript. This work was supported by NSF grants EAR-9980465 and EAR-9725723 (to KXW), a NASA Graduate Fellowship (to SHB), a NASA GSFC Graduate Student Research Grant, and a GSA Fahnestock Award (to SHB).

References

Ahnert, F., 1984. Local relief and the height limits of mountain ranges. Am. J. Sci. 284 (9), 1035–1055.

Alley, R.B., Strasser, J.C., Lawson, D.E., Evenson, E.B., Larson, G.J., 1999. Glaciological and geological implications of basal-ice accretion in overdeepenings. In: Mickelson, D.M., Attig, J.W. (Eds.), Glacial Processes Past and Present. Geological Society of America Special Paper, vol. 337, pp. 1–9, Boulder, CO.

Barsch, D., 1977. Eine Abschälung von Schuttproduktion und Schutttransport im Bereich aktiver Blockgletscher der Schweizer Alpen. Z. Geomorphol., Suppl. 28, 148–160.

Bateman, P.C., 1965. Geology and tungsten mineralization of the Bishop District, California. U.S. Geol. Surv. Prof. Pap. 470, 208 pp.

Beaumont, C., Fullsack, P., Hamilton, J., 1992. Erosional control of active compressional orogens. In: McClay, K.R. (Ed.), Thrust Tectonics. Chapman & Hall, London, pp. 1–18.

Boulton, G.S., 1974. Processes and patterns of glacial erosion. In: Coates, D.R. (Ed.), Glacial Geomorphology. George Allen & Unwin, London, pp. 41–87.

Braun, J., Zwartz, D., Tomkin, J., 1999. A new surface-processes model combining glacial and fluvial erosion. Ann. Glaciol. 28, 282–290.

Brocklehurst, S.H., Whipple, K.X., 1999. Relief production on the eastern side of the Sierra Nevada, California. Am. Geophys. Union, Trans. 80 (46), F442.

Brocklehurst, S.H., Whipple, K.X., 2000. Hypsometry of glaciated landscapes in the western U.S. and New Zealand. Am. Geophys. Union, Trans. 81 (48), F504.

Brozović, N., Burbank, D.W., Meigs, A.J., 1997. Climatic limits on landscape development in the northwestern Himalaya. Science 276, 571–574.

Burbank, D.W., 1991. Late Quaternary snowline reconstructions for the southern and central Sierra Nevada, California and a reassessment of the "Recess Peak Glaciation". Quat. Res. 36 (3), 294–306.

Caine, N., 1974. The geomorphic processes of the alpine environment. In: Ives, J.D., Barry, R.G. (Eds.), Arctic and Alpine Environments. Methuen, London, pp. 721–748.

Chamberlin, T.C., 1899. An attempt to frame a working hypothesis of the cause of glacial periods on an atmospheric basis. J. Geol. 7: 545–584, 667–685, 751–787.

Clark, D.H., Gillespie, A.R., 1997. Timing and significance of late-glacial and Holocene cirque glaciation in the Sierra Nevada, California. Quat. Int. 38–39, 21–38.

Clark, D.H., Clark, M.M., Gillespie, A.R., 1994. Debris-covered glaciers in the Sierra Nevada, California, and their implications for snowline reconstructions. Quat. Res. 41 (2), 139–153.

Cuffey, K.M., Conway, H., Gades, A.M., Hallet, B., Lorrain, R., Severinghaus, J.P., Steig, E.J., Vaughn, B., White, J.W.C., 2000. Entrainment at cold glacier beds. Geology 28 (4), 351–354.

Flint, J.J., 1974. Stream gradient as a function of order, magnitude, and discharge. Water Resour. Res. 10 (5), 969–973.

Francou, B., 1988. Talus formation in high mountain environments: Alps and tropical Andes. Doctoral Thesis, Université de Paris XVII, France.

Gilchrist, A.R., Summerfield, M.A., Cockburn, H.A.P., 1994. Landscape dissection, isostatic uplift, and the morphologic development of orogens. Geology 22 (11), 963–966.

Gillespie, A.R., 1982. Quaternary glaciation and tectonism in the southeastern Sierra Nevada, Inyo County, California. PhD Thesis, California Institute of Technology, Pasadena, 695 pp.

Hack, J.T., 1957. Studies of longitudinal stream profiles in Virginia and Maryland. U.S. Geol. Surv. Prof. Pap. 294-B, 97 pp.

Hallet, B., 1996. Glacial quarrying: a simple theoretical model. Ann. Glaciol. 22, 1–8.

Hallet, B., Hunter, L., Bogen, J., 1996. Rates of erosion and sediment evacuation by glaciers: a review of field data and their implications. Global Planet. Change 12 (1–4), 213–235.

Hallet, B., Merrand, Y., Koppes, M.N., Anders, A., 2000. Recent advances in the study of glacial erosion through field research and theory. GSA Abstr. Prog. 32 (7), A328.

Hicks, D.M., McSaveney, M.J., Chinn, T.J.H., 1990. Sedimentation in proglacial Ivory Lake, Southern Alps, New Zealand. Arct. Alp. Res. 22 (1), 26–42.

Hooke, R.L., 1991. Positive feedbacks associated with erosion of glacial cirques and overdeepenings. Geol. Soc. Am. Bull. 103 (8), 1104–1108.

Huber, N.K., 1981. Amount and timing of Late Cenozoic uplift and tilt of the Central Sierra Nevada, California—evidence from the Upper San Joaquin River. U.S. Geol. Surv. Prof. Pap. 1197, 28 pp.

Koons, P.O., 1989. The topographic evolution of collisional mountain belts: a numerical look at the Southern Alps, New Zealand. Am. J. Sci. 289 (9), 1041–1069.

Kotarba, A., 1972. Comparison of physical weathering and chemical denudation in the Polish Tatra Mountains. In: Macar, P., Pissart, A. (Eds.), Processus Périglaciaires Études sûr le Terrain. Université Liège, Liège, Belgium, pp. 205–216.

Leopold, L.B., Wolman, M.G., Miller, J.P., 1964. Fluvial Processes in Geomorphology. Freeman, San Francisco, CA, 522 pp.

MacGregor, K.C., Anderson, R.S., Anderson, S.P., Waddington, E.D., 2000. Numerical simulations of glacial valley longitudinal profile evolution. Geology 28 (11), 1031–1034.

Matsuoka, N., Sakai, H., 1999. Rockfall activity from an alpine cliff during thawing periods. Geomorphology 28 (3–4), 309–328.

Merrand, Y., Hallet, B., 2000. A physically based numerical model of orogen-scale glacial erosion: importance of subglacial hydrology and basal stress regime. GSA Abstr. Prog. 32 (7), A329.

Molnar, P., England, P., 1990. Late Cenozoic uplift of mountain ranges and global climate change: chicken or egg? Nature 346, 29–34.

Montgomery, D.R., 1994. Valley incision and the uplift of mountain peaks. J. Geophys. Res. 99 (B7), 13913–13921.

Montgomery, D.R., Foufoula-Georgiou, E., 1993. Channel network source representation using digital elevation models. Water Resour. Res. 29 (12), 3925–3934.

Moore, J.G., 1963. Geology of the Mount Pinchot Quadrangle, Southern Sierra Nevada, California. U.S. Geol. Surv. Bull. 1130, 152 pp.

Moore, J.G., 1981. Geologic map of the Mount Whitney Quadrangle, Inyo and Tulare Counties, California, GQ-1545. US Geological Survey Map.

Porter, S.C., 1989. Some geological implications of average Quaternary glacial conditions. Quat. Res. 32 (3), 245–261.

Poser, H., 1954. Die Periglazial-Ersheinungen in der Umgebung der Gletscher des Zemmgrundes (Zillentaler Alpen). Göttinger Geogr. Abh. 15, 125–180.

Raymo, M.E., Ruddiman, W.F., 1992. Tectonic forcing of late Cenozoic climate. Nature 359, 117–122.

Sklar, L., Dietrich, W.E., 1998. River longitudinal profiles and bedrock incision models: stream power and the influence of sediment supply. In: Tinkler, K.J., Wohl, E.E. (Eds.), Rivers Over Rock. Geophysical Monograph, American Geophysical Union, Washington, DC, pp. 237–260.

Small, E.E., Anderson, R.S., 1995. Geomorphically driven Late Cenozoic rock uplift in the Sierra Nevada, California. Science 270, 277–280.

Small, E.E., Anderson, R.S., 1998. Pleistocene relief production in Laramide mountain ranges, western United States. Geology 26 (2), 123–126.

Snyder, N.P., Whipple, K.X., Tucker, G.E., Merritts, D.J., 2000. Landscape response to tectonic forcing: DEM analysis of stream profiles in the Mendocino triple junction region, northern California. Geol. Soc. Am. Bull. 112 (8), 1250–1263.

Sugden, D.E., John, B.S., 1976. Glaciers and Landscape Arnold, London, 376 pp.

Tarboton, D.G., Bras, R.L., Rodriguez-Iturbe, I., 1991. On the extraction of channel networks from digital elevation data. Hydrol. Processes 5 (1), 81–100.

Tomkin, J.H., Braun, J., 2000. The effect of glaciation on relief in an active orogen: a numerical modelling study. Earth Planet. Sci. Lett. Am. Geophys. Union, Trans. 81 (48), F504.

Tucker, G.E., Bras, R.L., 1998. Hillslope processes, drainage density, and landscape morphology. Water Resour. Res. 34 (10), 2751–2764.

Tucker, G.E., Slingerland, R.L., 1994. Erosional dynamics, flexural isostasy, and long-lived escarpments: a numerical modeling study. J. Geophys. Res. 99 (B6), 12229–12243.

Tucker, G.E., Slingerland, R.L., 1997. Drainage basin responses to climate change. Water Resour. Res. 33 (8), 2031–2047.

Wager, L.R., 1933. The rise of the Himalayas. Nature 132, 28.

Weissel, J.K., Pratson, L.P., Malinverno, A., 1994. The length-scaling properties of topography. J. Geophys. Res. 99 (B7), 13997–14012.

Whipple, K.X., Tucker, G.E., 1999. Dynamics of the stream-power river incision model; implications for height limits of mountain ranges, landscape response timescales, and research needs. J. Geophys. Res. 104 (B8), 17661–17674.

Whipple, K.X., Kirby, E., Brocklehurst, S.H., 1999. Geomorphic limits to climate-induced increases in topographic relief. Nature 401, 39–43.

Willgoose, G., 1994. A statistic for testing the elevation characteristics of landscape simulation models. J. Geophys. Res. 99 (B7), 13987–13996.

Chapter 3

Effects of Glacier Thickness on the Relief of Glaciated Landscapes

Simon H. Brocklehurst* and Kelin X. Whipple

Department of Earth, Atmospheric and Planetary Sciences, Massachusetts Institute of Technology, Cambridge MA 02139, USA

Prepared for submission to *Geological Society of America Bulletin*

* to whom correspondence should be addressed: email: shb@mit.edu, fax: 1-617-252-1800

Abstract

The development of relief in glaciated landscapes plays a crucial role in testing hypotheses relating climate change to tectonic processes. In particular, glaciers can only be responsible for peak uplift if they are capable of generating significant relief in formerly nonglaciated landscapes. Previous work has suggested that relief production in glaciated landscapes should scale with the thickness of the ice. Here we summarise a field-based test of this hypothesis in two mountain ranges in the western United States, the Sierra Nevada, California, and the western Sangre de Cristo Range, Colorado. We mapped last glacial maximum (LGM) trimlines to estimate the ice thickness at the equilibrium line altitude during the LGM. Comparing various measures of relief (hillslope, hanging valley and geophysical) with our ice thickness estimates indicates that relief production in glaciated mountain belts does indeed scale with ice thickness. Given that ice thickness is inversely related to ice surface slope for temperate glaciers, this suggests a crucial role for valley slope in relief production, and in turn a potentially major influence due to drainage basin size.

1. Introduction

Surface processes are recognised as playing a crucial role in the development of mountain ranges (e.g., Koons, 1995; Molnar and England, 1990; Small and Anderson, 1998; Whipple et al., 1999; Willett, 1999). Rapid incision can potentially focus crustal strain (e.g., Koons, 1995; Zeitler et al., 2001) or alter near-surface geothermal gradients (e.g., Mancktelow and Grasemann, 1997; Stüwe et al., 1994), while changes in the relief structure of the landscape will affect the isostatic response to erosion (e.g., Molnar and England, 1990; Small and Anderson, 1998; Whipple et al., 1999). The evolution of relief in response to climate change (and the onset of glaciation) is especially crucial in the debate over potential linkages between apparently synchronous mountain uplift in the Himalayas, the western United States, and elsewhere, and the onset of Quaternary glaciation (e.g., Molnar and England, 1990; Raymo and Ruddiman, 1992).

Molnar and England (1990) argued that evidence cited for accelerated rates of late Cenozoic tectonism might instead reflect enhanced erosion rates caused by a cooler and/or stormier climate. They argued that this enhanced erosion resulted in the generation of relief, and subsequent isostatic uplift of various mountain ranges across the globe. Whipple et al. (1999) argued that a stormier climate was unlikely to result in greater relief in the fluvial system, and furthermore stated, principally on the basis of theoretical arguments, that relief production by glaciers was likely to be more modest than that appealed to by Molnar and England (1990). Small and Anderson (1998) and Brocklehurst and Whipple (2002) presented evidence for only minor relief production by glaciers in the Wind River Range and the eastern Sierra Nevada (both in the western US), respectively.

This paper reports the results of a field test of the hypothesis outlined by Whipple et al. (1999) that relief production by glaciers should scale with ice thickness (and thus in turn also reflects downvalley gradient). We mapped Last Glacial Maximum (LGM) trimlines in both the Sierra Nevada and the Sangre de Cristos, reconstructed realistic glacier forms, and compared centreline ice thicknesses at the LGM equilibrium line altitude (ELA) with measures of relief in these landscapes. In summary, the hypothesis proposed by Whipple et al. (1999) is supported. In addition, we observed that lithology seems to play a more important role in shaping the glacial landforms of the Sangre de Cristos, where structural grain and bedding plane orientations are

more influential, compared with the generally homogeneous granites (and landforms) of the Sierra Nevada.

2. Background

"Relief" in any landscape varies with the scale over which it is measured. Accordingly, there are many different definitions for "relief" (Brocklehurst and Whipple (2002) give a partial summary). For the purposes of evaluating the potential geodynamic response to erosion, the relevant measure is the "geophysical relief" (Small and Anderson, 1998). The geophysical relief is defined as the volume of material "missing" below the peaks and ridges in a landscape, divided by the surface area. Small and Anderson (1998) demonstrated that, if remnants of a pre-erosion surface are preserved, one can estimate both geophysical relief and the total amount and distribution of erosion. Brocklehurst and Whipple (2002) described a similar approach to measuring the modern geophysical relief structure. Their "sub-ridgeline relief" indicates the relief between the valley floor and a ridgeline-related reference surface at every point in the basin. Thus it is an objective, quantitative measure of the spatial distribution of relief, although it does not indicate the amount of material eroded from the landscape. In addition to evaluating sub-ridgeline relief, we also focus on "hanging valley relief" and "hillslope relief". Hanging valley relief here is the difference in elevation between the base of a hanging valley and the centreline of the main valley directly below it. Hanging valleys are a component of relief characteristic of glaciated landscapes, and hold the potential to add a considerable amount of relief to the landscape. Hillslope relief here is the difference in elevation between the trimline above the cirque and the ridgeline above.

Whipple et al. (1999) proposed the following mechanisms whereby glacial erosion might increase the relief in a previously fluvially-sculpted landscape (see Fig. 5 in Whipple et al., 1999): valley widening, ice buttressing of rock slopes, and formation of hanging valleys and overdeepenings. Furthermore, Whipple et al. (1999) suggested that the potential relief increase due to ice buttressing, the width of parabolic glacial valley cross-sections and the relief production due to hanging valleys should all depend on ice thickness. Implicit in the argument for relief production associated with hanging valleys to scale with ice thickness is the assumption that there are not major icefalls at tributary junctions during a glacial maximum. Relief grows because ponding of ice from the tributaries against the thicker ice of the main glacier limits

erosion on the tributaries. This contrasts with the process envisioned by MacGregor et al. (2000), who argue that differences in ice flux set hanging valley height. Hanging valley height grows with time, limited only by the duration of ice occupation. Brocklehurst and Whipple (2002) further identified headwall erosion by glaciers at the expense of low relief topography as a relief enhancement mechanism, although this does not necessarily scale with ice thickness.

Acting in direct opposition to these relief-production mechanisms, Whipple et al. (1999) envisioned three relief reduction mechanisms: concentration of erosion at higher elevations, reduction of fluvial erosion downstream of glaciers, and acceleration of summit-lowering rates in the periglacial regime. Brocklehurst and Whipple (2002) determined that the glaciers of the eastern Sierra Nevada have been responsible for relief production only in their ability to enlarge basins. However, in all cases glaciers were responsible for redistribution of relief compared with their fluvial-sculpted counterparts, and thus at least some of both the relief production and relief reduction mechanisms must be active.

3. Field Sites

We carried out fieldwork and determined relief estimates in two ranges in the western US, the Sierra Nevada in California, and the western side of Sangre de Cristo Range in southern Colorado. The section of the Sierra Nevada of interest (Fig. 1a) focussed on the eastern side of the range, but also took in the headwaters of some of the basins draining to the west. This region comprises homogeneous Cretaceous granodiorites and quartz monzonites (Bateman, 1965; Moore, 1963, 1981). Present-day tectonic activity is dominated by strike-slip motion on the Owens Valley Fault farther to the east. However, the eastern range-front normal fault may still be active, contributing to fairly uniform uplift rates on the order of ~0.2 mm/yr (Gillespie, 1982). The glacial history of the range has been the focus of numerous studies (e.g., Benson et al., 1998; Burbank, 1991; Clark et al., 1994; Clark and Gillespie, 1997; Gillespie, 1982; Mathes, 1930; Wahrhaftig and Birman, 1965). The eastern side of the Sierra Nevada (Brocklehurst and Whipple, 2002) is more directly comparable with the western side of the Sangre de Cristos, while considering the western side of the Sierra Nevada allowed us to extend the ice thickness range in our comparison of ice thickness and relief development.

The section of the western Sangre de Cristo Range of interest is illustrated in Fig. 1b. The rocks here comprise Palaeozoic sedimentary units and Precambrian metamorphic rocks (Johnson

et al., 1987). The tectonic regime in the Sangre de Cristos is also consistent throughout the region of interest. The normal component of slip rates at the range front has averaged around 0.1-0.2 mm/yr during the late Pleistocene (McCalpin, 1986, 1987), comparable to rates measured in the Sierra Nevada. Inactive folds and thrust faults dominate the internal structure of the range, with a trend subparallel to the strike of the range (Fig. 1b) (Johnson et al., 1987). The glacial history is summarised by McCalpin (1981), while more recent research has tended to focus on cirque evolution (e.g., Olyphant, 1981) and rock glaciers (e.g., Burger et al., 1999).

We divided the drainage basins into 5 categories on the basis of the degree of glaciation experienced at the Last Glacial Maximum (LGM), using LGM ice extents from aerial photograph interpretation and field observations to supplement previous mapping (e.g., Gillespie, 1982; Johnson et al., 1987). This represents a proxy for relative ice extent throughout the Quaternary, but not the average conditions during the Quaternary (Porter, 1989), which are most obviously reflected in the modern landscape (Brocklehurst and Whipple, 2002). "Full glaciation" symbolizes LGM glaciers extending to the range front, while minor, moderate, and significant glaciers extended ~1/4, ~1/2, and ~3/4 of the length of the drainage basin, respectively.

4. Methods

4.1. DEM analyses

Our methods of topographic analysis follow those outlined by Brocklehurst and Whipple (2002). The source data are USGS 30-m digital elevation models (DEMs). We used a flow routing routine in ArcInfo to extract drainage network structures and individual drainage basins, in each case taking the downstream extent of the basin to lie at the range front. To analyse the distribution of relief, we followed the sub-ridgeline relief distribution method of Brocklehurst and Whipple (2002). In summary, a cubic spline surface is interpolated between the ridgelines surrounding a drainage basin (equivalent to stretching a rubber sheet across the top of the basin). This surface yields a ridgeline-related elevation at every point within the drainage basin. Any peaks within the basin that penetrate this surface are combined with the ridgelines surrounding the basin before interpolating an updated ridgeline-related surface. Subtracting the DEM from this surface yields a measure of the distance below the ridgelines for each point in the basin. Summing this 'sub-ridgeline relief' is then a measure of the 'missing mass' within the drainage

basin (although not necessarily the eroded mass), and dividing this number by the drainage area yields a length-scale relief measurement comparable to 'geophysical relief' (Small and Anderson, 1998). Again following a procedure described by Brocklehurst and Whipple (2002), we used a locally-calibrated 2-D fluvial landscape evolution model (GOLEM, Tucker and Slingerland, 1994) to compare the relief of the existing glaciated landscape with the relief of a fluvial landscape with the same drainage network. This simulated fluvial landscape represents how the drainage basin would look now had the glaciers never developed.

Hanging valley relief is one of the major components of relief in glacial landscapes, and is usually not a feature of fluvial landscapes. We identified the major hanging valleys from topographic maps and aerial photographs, and determined their height from steps observed in longitudinal profiles, extracted from the DEM, that run across the hanging valley step. We also calculated the hillslope relief at the heads of the major tributaries, measuring the difference in elevation between the trimline above the cirque and the ridgeline above.

4.2. Field methods

The trimline joins points on the valley side that mark the boundary between rock that was beneath ice during a glaciation below, and rock that was exposed subaerially, above. Thus the trimline is an indicator of ice thickness. Typically, the trimline separates smooth, glacially-polished rock below from more jagged outcrops above. We focussed on the most prominent trimline, the one from the last glacial maximum (LGM), to determine a proxy for ice thickness to compare with our relief estimates. In some cases, trimlines from minor, more recent glaciations were also present, at lower elevations on the hillside, while trimline remnants from earlier glaciations lying above the LGM trimlines were rare. However, in some cases we may have inadvertently mapped trimlines from prior glaciations. Our trimline mapping was conducted initially on the basis of aerial photograph and topographic map interpretation, and then verified with field observations. In practice, there were two principle means of identifying the trimline. Firstly, the trimline often represented a break in slope between steeper valley sides below and shallower slopes above, although this was not always the case; sometimes the LGM trimline lay within a steep cliff. Secondly, the trimline was often close to the top of, or inferred to be partially buried by, talus cones forming against the valley wall. Figure 2 shows examples of trimlines from the eastern Sierra Nevada and the western Sangre de Cristos. Below the LGM ELA, we

determined the margins of the glacier from lateral and terminal moraines, using field observations to supplement previously published mapping (e.g., Gillespie, 1982; Johnson et al., 1987), again attempting to focus on features related to the LGM glaciation.

4.3. Glacier reconstruction

Trimlines and moraine boundaries were digitised from topographic maps, interpolating across sections where the trimline could not be positively identified from either aerial photographs, topographic maps, or field observations. These glacier outlines were then used to fit a cubic spline surface as a smooth initial estimate for the glacier surface. This initial surface was then modified by adjusting valley centreline elevations to ensure that the calculated basal shear stress along the valley thalweg lay within the commonly observed range of 0.8 to 1.2 bars. Here, the basal shear stress, τ_b, is given by:

$$\tau_b = \rho g H S \tag{1}$$

where ρ is the ice density, g is the acceleration due to gravity, H is the ice thickness, and S is the surface slope of the ice. The modified elevations were then used in addition to the trimline data to recalculate the cubic spline surface, a second check was carried out, and then the centreline ice thicknesses were taken for comparison with our relief calculations.

5. Results

5.1. DEM analyses

Figure 3 shows the relationship between geophysical relief and drainage area for the drainage basins in the Sierra Nevada and the Sangre de Cristos. The solid symbols are the basins as extracted from the DEM, while the open symbols are the simulated fluvial basins. The Sierra Nevada and the Sangre de Cristos have responded in a very comparable fashion to the onset of glaciation. Glaciated basins have more mean relief, but this is due principally to their being larger; fluvial basins of the same size would have very similar missing mass. Thus glaciers in both ranges have only produced relief in their ability to enlarge drainage basins at the expense of low relief topography (Brocklehurst and Whipple, 2001, 2002). The only distinction between the

two ranges occurs at the largest drainage areas, where the glaciated basins in the Sangre de Cristos exhibit greater mean relief than their fluvial counterparts.

5.2. Field observations

Our field observations and topographic map interpretations suggest that lithology and structural grain play a much more important role in the drainage planform in the Sangre de Cristos. Whereas drainage basins in the eastern Sierra Nevada run essentially perpendicular to the range crest/front, many of the larger drainage basins in the western Sangre de Cristos hook around to run parallel with the range crest in their upper reaches (Fig. 1b) which is also parallel to the main structural grain. Furthermore, the valley cross-section in the upper part of the basin in these cases is often noticeably asymmetric (Fig. 4), with a shallower hillslope gradient on one side of the valley following bedding planes within the Palaeozoic sedimentary sequence. The opposite hillslope, cut across the beds, is much steeper.

5.3. Relief and ice thickness comparison

Figure 5 and Table 1 summarise the results of our ice thickness calculations and various relief estimates for basins on both sides of the Sierra Nevada and the western side of the Sangre de Cristos. For any given drainage basin there is a range in hanging valley and hillslope relief, so in Figures 5a and b we illustrate the range of both in each basin, and our best estimate for the LGM ELA ice thickness. With such a range in the data it is difficult to analyse the statistical significance of any trend. In Figure 5c we show the median hillslope relief for each basin along with a linear regression through these data. It is striking that there is essentially a 1:1 relationship between LGM ELA ice thickness and hillslope relief. Furthermore, the intercept of this best-fit line corresponds closely to the median hillslope relief values calculated in the same way for nonglaciated basins in the eastern Sierra Nevada. Figure 5d shows that the relationship between LGM ELA ice thickness and median hanging valley relief is also remarkably close to a 1:1 relationship. In addition to the 1:1 relationships for these datasets as a whole, both median hillslope relief and median hanging valley relief in both the eastern Sierra Nevada and Sangre de Cristos subsets have a near 1:1 relationship. However, the comparison between LGM ELA ice thickness and geophysical relief does not yield a strong correlation. In addition, variations in geophysical relief are much less than variations in hanging valley and hillslope relief. The major

trend in geophysical relief is for it to increase with drainage area, for both fluvial and glacial landscapes (Figure 3). Thus any correlation between ice thickness and geophysical relief likely reflects the fact that larger, shallower basins accumulate thicker ice than smaller, steeper basins. The weak correlation between ice thickness and geophysical relief despite the strong correlation between ice thickness and both hanging valley and hillslope relief indicates that both relief production and relief reduction mechanisms are active in these landscapes (Brocklehurst and Whipple, 2002; Whipple et al., 1999).

5.4 Extension to larger drainage basins

Our results from the Sierra Nevada and the Sangre de Cristos support the correlation between ice thickness and relief production suggested by Whipple et al. (1999). As a preliminary extension of this test to alternative settings, we examined the relief structure of glaciated drainage basins in the Bitterroots Range, Montana, and Glacier National Park (Brocklehurst and Whipple, in prep.-b). These represent larger basins and basins with a shallower down-valley gradient, respectively, and thus both had greater ice thicknesses during the LGM. Figure 3 illustrates how geophysical relief in these ranges compares with the results from moderately, significantly and fully glaciated drainage basins in the Sierra Nevada and the Sangre de Cristos. There is some degree of scatter in the data; they suggest that the thicker ice in Glacier National Park does cause greater geophysical relief, while mean relief increases with drainage area in the larger basins in the Bitterroots, but not in a linear fashion. Figure 3 also shows relief structure for a fluvial drainage basins of different sizes, achieved by using the drainage network and outline of Symmes Creek in the eastern Sierra Nevada in the landscape evolution model, GOLEM (Tucker and Slingerland, 1994), but using different cell sizes (Brocklehurst and Whipple, 2002). The relief of the simulated drainage basins also apparently rises less rapidly with drainage area in the larger basins.

6. Discussion

Our analyses indicate that the glaciated landscapes of the eastern Sierra Nevada and western Sangre de Cristos look very much alike. The two principle distinctions between the two are the reduced drainage basin relief (Whipple et al., 1999) in the Sangre de Cristos, and the greater degree of lithologic and structural control in the Sangre de Cristos. Geophysical relief is a

function of drainage area. Although drainage basin relief in the eastern Sierra Nevada is greater than in the Sangre de Cristos, geophysical relief in the two ranges is quite comparable. In both ranges simulated fluvial drainage basins have similar relief to observed glaciated basins of the same size, so that glaciers are principally responsible for net relief production in their ability to enlarge formerly fluvial basins at the expense of low relief topography (Brocklehurst and Whipple, 2002, in prep.-a). The only exception to this occurs in the largest drainage basins in the Sangre de Cristos, where glaciated basins have more mean relief than their fluvial simulations. This may reflect shallower down-valley gradients in the largest drainage basins in the range permitting thicker ice, and the development of greater relief in the upper part of the basin. Furthermore, the difference in relief is not sufficient to cause significant peak uplift. Given that this deviation between fluvial and glacial mean relief is seen only in the largest basins in the Sangre de Cristos, and is not observed in the Sierra Nevada where the greater total relief results in steeper down-valley gradients, suggests that there may be some threshold down-valley gradient below which glaciers will generate greater relief than rivers. Above this gradient there is still a difference in the distribution of relief between fluvial and glacial drainage basins.

Lithology and structure can be major controls on the development of glaciated landscapes (e.g., Augustinus, 1992, 1995). In the Sierra Nevada, lithology comprises regionally homogeneous granitoids. These granites exfoliate readily, allowing easy plucking of blocks from the valley floor, and perhaps permitting more rapid glacial erosion rates (Brocklehurst et al., in prep.). Qualitative regional variations in the degree of jointing in the bedrock appear to correlate with the amount of debris that collects in the glaciated basins. For example, Armstrong Creek in the eastern Sierra Nevada is characterised by highly jointed bedrock and very large volume moraines (e.g., Gillespie, 1982). In the Sangre de Cristo Range, the upper reaches of the larger basins are range-parallel, following the structural grain. It is difficult to evaluate when the drainage network took on this planform, which could well have occurred prior to the onset of glaciation in the range. However, the lithology clearly plays a key role in the evolution of the glaciated landscape. The cross-sections of these valley heads are asymmetric, as the valley walls on one side lie at a shallower angle parallel to bedding planes, while the valley walls opposite are noticeably steeper with angular steps cutting across each of the bedding planes.

We have demonstrated a correlation between centreline ice thickness and relief production in glaciated landscapes. In fact, the relationship between ice thickness and both

hanging valley and hillslope relief is remarkably close to 1:1. While we do not seek to overemphasise this as a 'rule' for the development of glaciated landscapes, it is certainly an interesting result that warrants further investigation. The close association between ice thickness and hanging valley relief suggests that the former limits the development of the latter, perhaps because the tributary ice ponds against the trunk stream (Whipple et al., 1999). This contrasts with the suggestion that tributary relief can grow without limits (MacGregor et al., 2000). Again this deserves further study. Variations in geophysical relief are less dramatic. Here the major correlation is between drainage area and geophysical relief, a relationship that also holds true for fluvial landscapes (and thus indicates that glaciers are also responsible for relief reduction). This suggests that if glaciers were to be responsible for significant relief production to cause flexural-isostatic peak uplift, it would be in glaciated drainage basins that are either larger or have lower relief, such that the lower down-valley slopes would allow the ice to be thicker. Our preliminary attempts to extend our study to ranges with larger glaciated basins (Bitterroots Range) confirm that mean relief does increase with drainage area, although not in a linear fashion. Also, our lower relief basins with thicker ice (Glacier National Park) exhibit modest additional relief production in terms of geophysical relief, principally due to the spectacular hanging valleys (e.g., Avalanche Creek, Brocklehurst and Whipple, in prep.-b). The importance of basin size for the development of glacial landscapes is discussed more fully elsewhere (Brocklehurst and Whipple, in prep.-a, c). It would be extremely valuable to extend this study with a more comprehensive evaluation of the glaciated landscapes of the Bitterroot Range and Glacier National Park, and larger ranges such at the Alps, where valley glacier ice thicknesses approach 1 km. The results presented here suggest that landscapes in the Alps should have even greater relief than the glaciated ranges studied in the western US, but it will be interesting to evaluate how this is partitioned between hillslope and hanging valley relief. Thicker ice should allow greater hanging valley relief, but unless drainage density is significantly reduced in the Alps, rock strength should limit hillslope relief.

7. Conclusion

Sub-ridgeline relief distributions from the eastern Sierra Nevada and the western Sangre de Cristos are similar, even though drainage basin relief in the Sierra Nevada is much greater. Geologic structure in the Sangre de Cristos exerts a strong influence on drainage basin

planforms, while inclined sedimentary bedding affects valley cross-sectional profiles. Hillslope and hanging valley relief tend to increase with LGM ELA ice thickness. The close relationship between trunk valley ice thickness and hanging valley relief suggests that hanging valley relief development is limited by ponding of ice against the trunk stream, rather than growing without limits. Variations in geophysical relief are less dramatic, suggesting that relief production on hanging valleys and hillslopes is countered by relief reduction elsewhere. The apparent correlation between ice thickness and geophysical relief is principally a reflection of changing basin size. Preliminary analyses comparing the Bitterroot Range with the Sangre de Cristos and Sierra Nevada confirm that geophysical relief production scales with basin size.

Acknowledgements

This work was supported by NSF grant EAR-9980465 (to KXW), a NASA GSFC Graduate Student Research Grant, a NASA Graduate Fellowship (to SHB), and a GSA Fahnestock Award (to SHB). We would like to thank Ryan Ewing and Noah Snyder for assistance in the field, and Ben Crosby and Darryl Granger for thorough reviews of early drafts of this manuscript.

Figure captions

Fig. 1. (a) Shaded relief map of the study site in the Sierra Nevada, California, highlighted on the inset map. On the eastern side of the range, three categories of basin, based on the degree of glaciation at the Last Glacial Maximum, are illustrated as follows: nonglaciated (bold), moderate glaciation (italic) and full glaciation (regular). Select basins on the western side of the range, as listed in Table 2, are also highlighted. (b) Shaded relief map of the study site on the western side of the Sangre de Cristo Range, Colorado, highlighted on the inset map. Key as in Figure 1a. Simplified structure after Johnson et al. (1987). Map shows the major folds and faults in the region of interest; subsidiary faults and folds have the same general orientation. CLA – Cotton Lake Anticline; GPS – Gibson Peak Syncline; MMT – Marble Mountain Thrust.

Fig. 2. Photographs of typical trimlines in the field. (a) Birch Creek, eastern Sierra Nevada. Prominent trimline occurs at the break in slope at the top of the vertical cliff-face at the base of the cliff, while a second remnant trimline occurs shortly above this. (b) Black Canyon, Sangre de Cristos. Trimline is typically more difficult to identify in the Sangre de Cristos. In this case it lies just above the top of the tallest talus cones.

Fig. 3. Geophysical relief versus drainage area for moderately, significantly and fully glaciated basins in the eastern Sierra Nevada and Sangre de Cristos, along with glaciated basins in Glacier National Park and the Bitterroot Range. Also shown is geophysical relief for a fluvial simulation of Symmes Creek, eastern Sierra Nevada, with different drainage areas achieved by changing the pixel size in the GOLEM simulation. Glacier ice tends to be thicker in Glacier National Park, where mean relief is also generally greater, while the larger glaciated basins in the Bitterroots also have greater relief. Mean relief tends to scale with drainage area in a similar fashion in glacial and fluvial basins, with the exception of Glacier National Park.

Fig. 4. Photograph illustrating lithologic control on glacial landforms in the Sangre de Cristos. Photograph is taken looking to the south towards San Isabel Lake and the cirque at the top of the San Isabel valley. To the east (left) of the lake, the shallow hillside is parallel to the dip-slope on

the sedimentary units, while to the west (right) of the lake, the hillside that cuts across the bedding in the sedimentary units is noticeably steeper.

Fig. 5. Comparison of various measures of relief with LGM ELA ice thicknesses in the Sierra Nevada and the Sangre de Cristos (see Table 2). In (a) and (b), symbols represent maximum and minimum values within each drainage basin, connected by a line of the same colour. (a) Hillslope relief. (b) Hanging valley relief. (c) Median hillslope relief for each of the (glaciated) basins in (a) and (b) indicated by closed symbols, along with a linear best-fit to these data. Median hillslope relief for nonglaciated basins in the eastern Sierra Nevada indicated by open symbols. The glaciated basin data are fit by a near 1:1 fit whose intercept coincides with the median hillslope relief for the nonglaciated basins. (d) Median hanging valley relief for each of the (glaciated) basins in (a) and (b). Again a linear best-fit line through all of these data indicates a relationship close to 1:1.

Table 1. Summary of ice thickness data.

Basin	LGM ELA ice thickness (m)	Relief (m)			Geophysical Relief (m)
		Hillslope	Hanging valley	Total	
Eastern Sierra					
Birch	~100	200-400	150-200	350-600	174
Independence	~160	300-550	150-250	450-800	206
Lone Pine	~120	250-500	200-300	450-800	240
North Fork, Oak	~130	250-350	150-200	400-550	214
Red Mountain	~80	200-500	100-150	300-650	232
Shepherd	~120	200-400	100-350	300-750	105
South Fork, Oak	~110	300-400	150-300	450-700	189
Tinemaha	~100	200-350	100-150	300-500	255
Sangre de Cristos					
Black	~80	120-350	75-100	195-450	178
Cotton	~140	150-400	150-250	300-650	312
Cottonwood	~180	200-450	100-200	300-650	233
Rito Alto	~150	150-400	120-250	270-650	282
Spanish	~100	150-300	75-100	225-400	174
Wild Cherry	~130	150-350	100-180	250-530	177
Willow	~115	250-450	100-200	350-650	255
Western Sierra					
Bubbs	~300	400-500	250-400	650-900	
Evolution	~240	400-600	200-400	600-1000	
Palisade	~200	400-600	250-400	650-1000	
Woods	~250	300-600	250-300	550-900	

References

Augustinus, P. C., 1992, The Influence of Rock Mass Strength on Glacial Valley Cross-Profile Morphometry: A Case Study from the Southern Alps, New Zealand: Earth Surface Processes and Landforms, v. 17, p. 39-51.

-, 1995, Glacial valley cross-profile development: the influence of in-situ rock stress and rock mass strength, with examples from the Southern Alps, New Zealand: Geomorphology, v. 14, p. 87-97.

Bateman, P. C., 1965, Geology and Tungsten Mineralization of the Bishop District, California, U.S. Geological Survey Professional Paper, 208 p.

Benson, L. V., May, H. M., Antweiler, R. C., Brinton, T. I., Kashgarian, M., Smoot, J. P., and Lund, S. P., 1998, Continuous Lake-Sediment Records of Glaciation in the Sierra Nevada between 52,600 and 12,500 ^{14}C yr B.P.: Quaternary Research, v. 50, p. 113-127.

Brocklehurst, S. H., and Whipple, K. X., 2001, Assessing the relative efficiency of fluvial and glacial erosion: Examples from the Sierra Nevada, California, and Sangre de Cristo Range, Colorado: GSA/GSL Earth Systems Processes Programmes with Abstracts, p. 81.

-, 2002, Glacial Erosion and Relief Production in the Eastern Sierra Nevada, California: Geomorphology, v. 42, no. 1-2, p. 1-24.

-, in prep.-a, Assessing the relative efficiency of fluvial and glacial erosion through fluvial landscape simulation.

-, in prep.-b, Hypsometry of glaciated landscapes.

-, in prep.-c, The response of glaciated landscapes to varying rock uplift rates.

Brocklehurst, S. H., Whipple, K. X., and Granger, D. E., in prep., Cosmogenic isotope inheritance in alpine glaciated basins.

Burbank, D. W., 1991, Late Quaternary Snowline Reconstructions for the Southern and Central Sierra Nevada, California and a Reassessment of the "Recess Peak Glaciation": Quaternary Research, v. 36, p. 294-306.

Burger, K. C., Degenhardt, J. J., Jr., and Giardino, J. R., 1999, Engineering geomorphology of rock glaciers: Geomorphology, v. 31, no. 1-4, p. 93-132.

Clark, D. H., Clark, M. M., and Gillespie, A. R., 1994, Debris-Covered Glaciers in the Sierra Nevada, California, and their Implications for Snowline Reconstructions: Quaternary Research, v. 41, p. 139-153.

Clark, D. H., and Gillespie, A. R., 1997, Timing and significance of late-glacial and Holocene cirque glaciation in the Sierra Nevada, California: Quaternary International, v. 38-39, p. 21-38.

Gillespie, A. R., 1982, Quaternary Glaciation and Tectonism in the Southeastern Sierra Nevada, Inyo County, California [PhD thesis]: California Institute of Technology, 695 p.

Johnson, B. R., Lindsey, D. A., Bruce, R. M., and Soulliere, S. J., 1987, Reconnaissance geologic map of the Sangre de Cristo Wilderness Study Area, south-central Colorado: USGS Miscellaneous Field Studies Map, v. MF-1635-B.

Koons, P. O., 1995, Modeling the Topographic Evolution of Collisional Belts: Annual Review of Earth and Planetary Sciences, v. 23, p. 375-408.

MacGregor, K. R., Anderson, R. S., Anderson, S. P., and Waddington, E. D., 2000, Numerical Simulations of Glacial Valley Longitudinal Profile Evolution: Geology, v. 28, no. 11, p. 1031-1034.

Mancktelow, N. S., and Grasemann, B., 1997, Time-dependent effects of heat advection and topography on cooling histories during erosion: Tectonophysics, v. 270, p. 167-195.

Mathes, F. E., 1930, Geologic History of the Yosemite Valley, USGS Professional Paper.

McCalpin, J. P., 1981, Quaternary geology and neotectonics of the west flank of the northern Sangre de Cristo Mountains, south-central Colorado [Doctoral thesis]: Colorado School of Mines, 287 p.

-, 1986, Quaternary Tectonics of the Sangre de Cristo and Villa Grove Fault Zones: Colorado Geological Survey Special Publication, v. 28, p. 59-64.

-, 1987, Recurrent Quaternary normal faulting at Major Creek, Colorado: An example of youthful tectonism on the eastern boundary of the Rio Grande Rift Zone, *in* Beus, S. S., ed., Geological Society of America Centennial Field Guide - Rocky Mountain Section, Geological Society of America, p. 353-356.

Molnar, P., and England, P., 1990, Late Cenozoic uplift of mountain ranges and global climate change: chicken or egg?: Nature, v. 346, p. 29-34.

Moore, J. G., 1963, Geology of the Mount Pinchot Quadrangle, Southern Sierra Nevada, California, US Geological Survey Bulletin, 152 p.

-, 1981, Geologic map of the Mount Whitney Quadrangle, Inyo and Tulare Counties, California, US Geological Survey Map.

Olyphant, G. A., 1981, Allometry and cirque evolution: Geological Society of America Bulletin, v. 92, p. 679-685.

Porter, S. C., 1989, Some Geological Implications of Average Quaternary Glacial Conditions: Quaternary Research, v. 32, p. 245-261.

Raymo, M. E., and Ruddiman, W. F., 1992, Tectonic forcing of late Cenozoic climate: Nature, v. 359, p. 117-122.

Small, E. E., and Anderson, R. S., 1998, Pleistocene relief production in Laramide mountain ranges, western United States: Geology, v. 26, p. 123-126.

Stüwe, K., White, L., and Brown, R., 1994, The influence of eroding topography on steady-state isotherms: Application to fission track analysis: Earth and Planetary Science Letters, v. 124, p. 63-74.

Tucker, G. E., and Slingerland, R. L., 1994, Erosional dynamics, flexural isostasy, and long-lived escarpments: A numerical modeling study: Journal of Geophysical Research, v. 99, no. B6, p. 12229-12243.

Wahrhaftig, C., and Birman, J. H., 1965, The Quaternary of the Pacific Mountain System in California, *in* Wright, H. E. J., and Frey, D. G., eds., The Quaternary of the United States: Princeton, N.J., Princeton University Press, p. 299-340.

Whipple, K. X., Kirby, E., and Brocklehurst, S. H., 1999, Geomorphic limits to climate-induced increases in topographic relief: Nature, v. 401, p. 39-43.

Willett, S. D., 1999, Orogeny and orography: The effects of erosion on the structure of mountain belts: Journal of Geophysical Research, v. 104, no. B12, p. 28957-28981.

Zeitler, P. K., Meltzer, A. S., Koons, P. O., Craw, D., Hallet, B., Chamberlain, C. P., Kidd, W. S. F., Park, S. K., Seeber, L., Bishop, M. P., and Shroder, J. F., 2001, Erosion, Himalayan Geodynamics, and the Geomorphology of Metamorphism: GSA Today, v. 11, no. 1, p. 4-9.

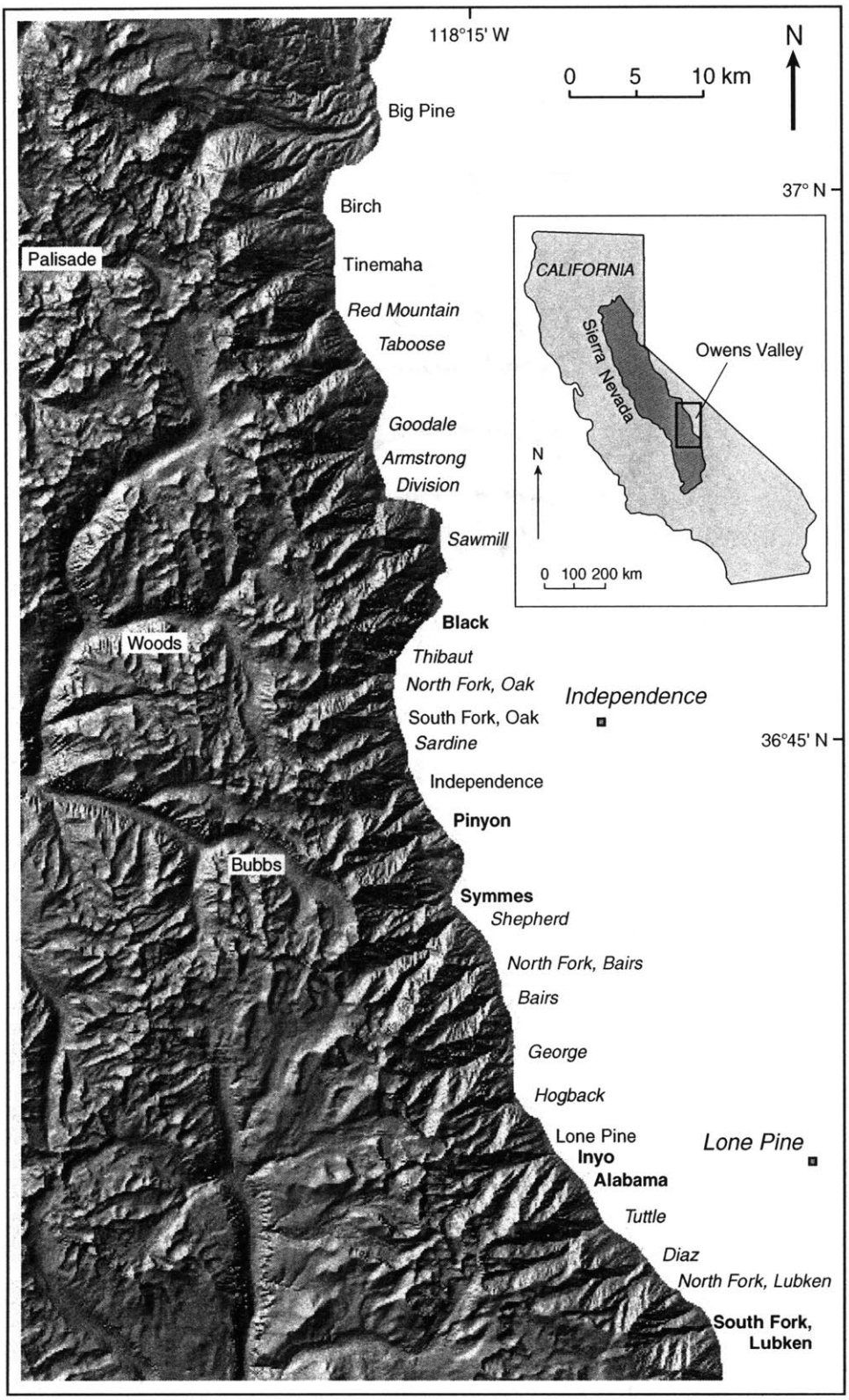
118°15' W
N
0 5 10 km
Big Pine
37° N
Birch
Palisade
Tinemaha
Red Mountain
Taboose
Goodale
Armstrong
Division
Sawmill
Black
Woods
Thibaut
North Fork, Oak
South Fork, Oak
Sardine
Independence
36°45' N
Independence
Pinyon
Bubbs
Symmes
Shepherd
North Fork, Bairs
Bairs
George
Hogback
Lone Pine
Inyo
Alabama
Lone Pine
Tuttle
Diaz
North Fork, Lubken
South Fork, Lubken
CALIFORNIA
Sierra Nevada
Owens Valley
N
0 100 200 km

Fig. 1a

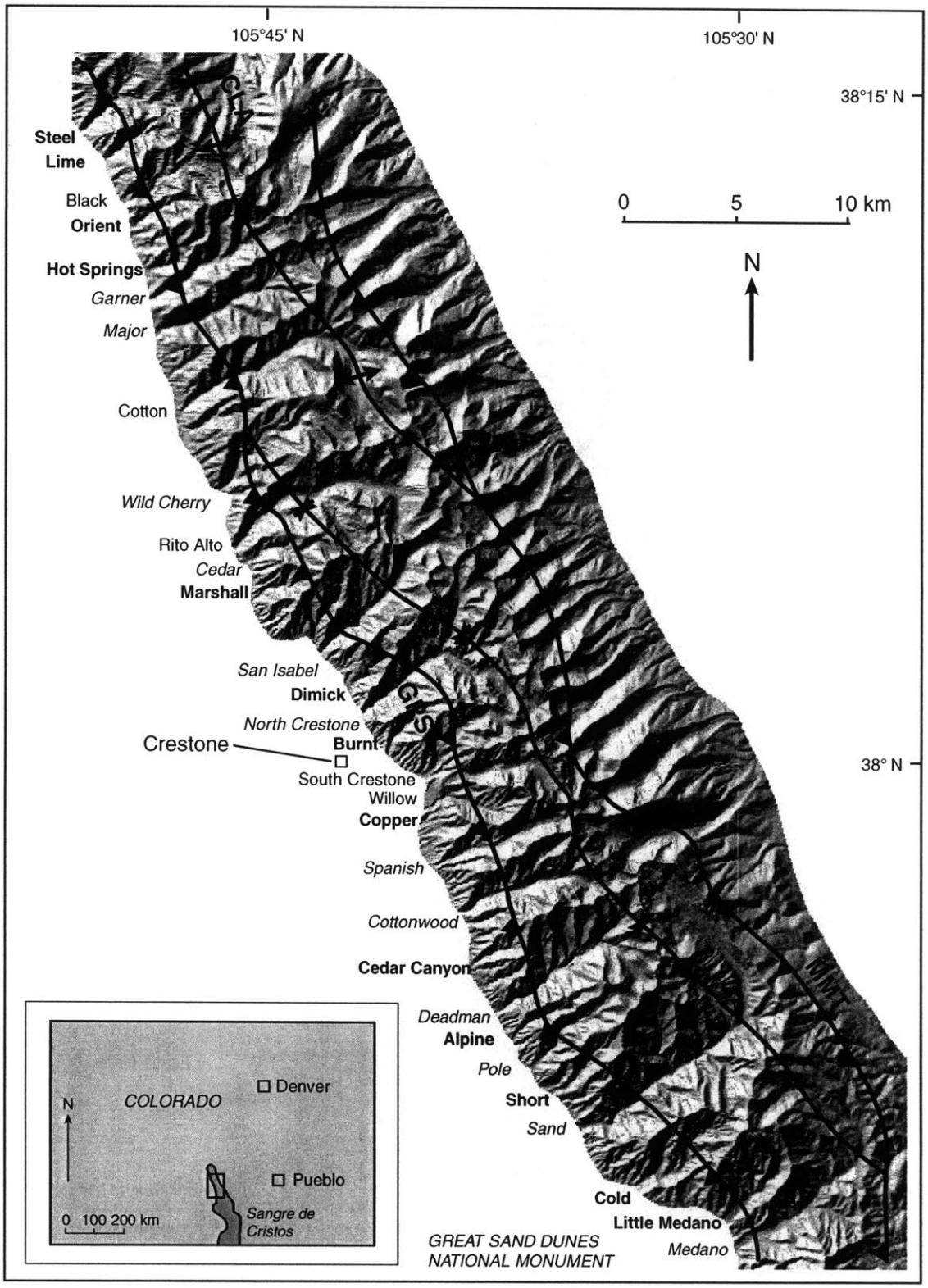
105°45' N
105°30' N
38°15' N
38° N
0 5 10 km
N
Steel
Lime
Black
Orient
Hot Springs
Garner
Major
Cotton
Wild Cherry
Rito Alto
Cedar
Marshall
San Isabel
Dimick
North Crestone
Crestone
Burnt
South Crestone
Willow
Copper
Spanish
Cottonwood
Cedar Canyon
Deadman
Alpine
Pole
Short
Sand
Cold
Little Medano
Medano
GREAT SAND DUNES
NATIONAL MONUMENT
CSF
CGS
MWT
COLORADO
Denver
Pueblo
Sangre de
Cristos
0 100 200 km

Fig. 1b

a.

b.

Fig. 2

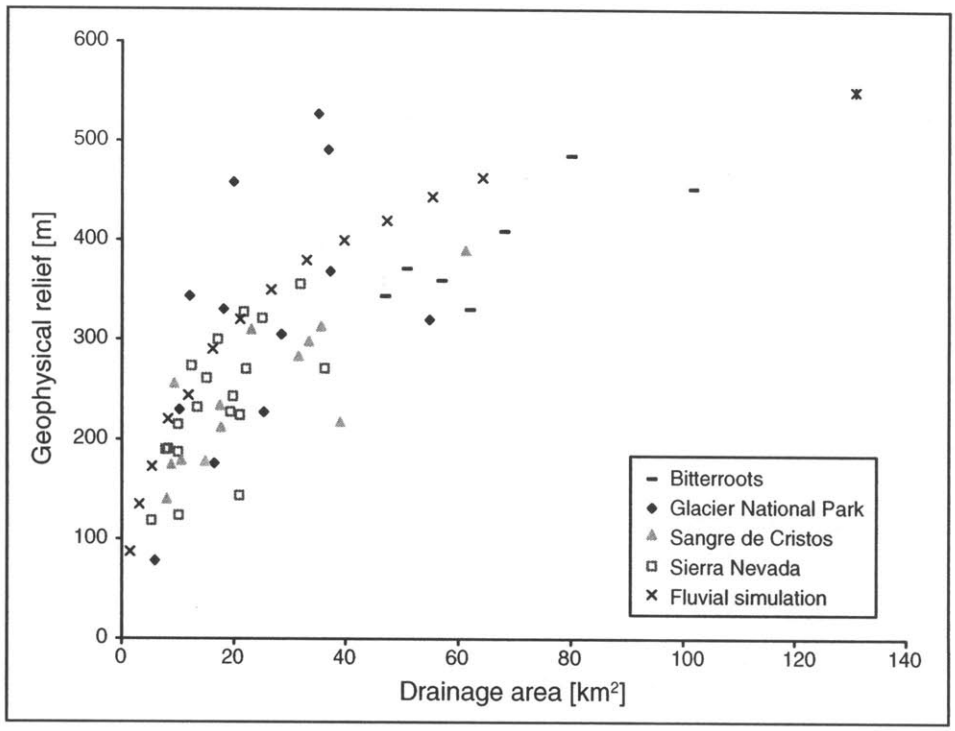
Geophysical relief [m]
Drainage area [km²]
0
100
200
300
400
500
600
0
20
40
60
80
100
120
140
Bitterroots
Glacier National Park
Sangre de Cristos
Sierra Nevada
Fluvial simulation

Fig. 3

Fig. 4

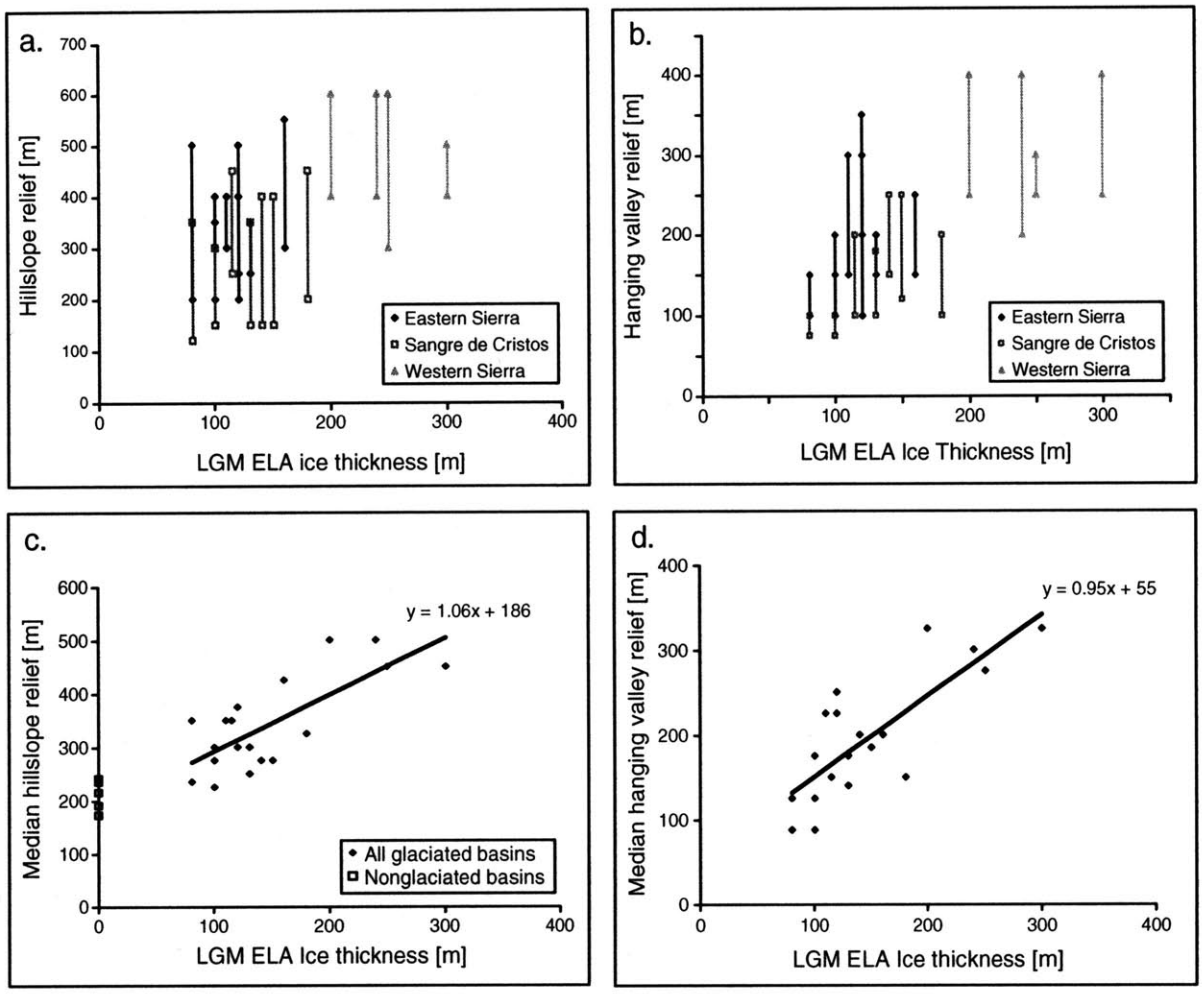
a.
Hillslope relief [m]
LGM ELA ice thickness [m]
Eastern Sierra
Sangre de Cristos
Western Sierra
b.
Hanging valley relief [m]
LGM ELA Ice Thickness [m]
Eastern Sierra
Sangre de Cristos
Western Sierra
c.
Median hillslope relief [m]
y = 1.06x + 186
All glaciated basins
Nonglaciated basins
LGM ELA Ice thickness [m]
d.
Median hanging valley relief [m]
y = 0.95x + 55
LGM ELA Ice thickness [m]

Fig. 5

Chapter 4

Assessing the relative efficiency of fluvial and glacial erosion through fluvial landscape simulation

Simon H. Brocklehurst* and Kelin X. Whipple

Department of Earth, Atmospheric and Planetary Sciences, Massachusetts Institute of Technology, Cambridge MA 02139, USA

Prepared for submission to *Geomorphology*

* to whom correspondence should be addressed: email: shb@mit.edu, fax: 1-617-252-1800

Abstract

Determining the relative rates of erosion by rivers and glaciers, and the topographic consequences of these two different styles of erosion, remains an outstanding problem in geomorphology. Here we demonstrate the insight into glacial erosion that can be gained through employing a locally calibrated fluvial erosion model to simulate how the landscape might look now had glaciation not occurred. We compare examples from the Sierra Nevada, California and the Sangre de Cristo Range, Colorado. In smaller drainage basins, glacial modification is focussed above the mean Quaternary equilibrium line altitude (ELA), where both ridgelines and valley floors are lowered as a consequence of glaciation. At lower elevations, small glaciers apparently widen valleys without incising the valley floor differently from what would have happened under non-glacial conditions. This may reflect the short residence time of the glaciers at their full extent, or differences in the subglacial drainage network between the glacier margins and the thalweg. In larger drainage basins, the pattern of glacial erosion is dramatically different. In this case, the glaciers have modified longitudinal profiles, as well as valley cross-sections, far below the mean Quaternary ELA. Possible causes for this difference in the larger basins include the larger accumulation area, greater shading, longer residence times for ice at its full extent, and the influence of the lower valley slope prior to glaciation on the subglacial hydrology. Current glacial landscape evolution models behave more like the large basin case.

1. Introduction

Glaciers are responsible for carving some of the most spectacular landscapes on Earth. Furthermore, they play a crucial role in hypotheses relating late Cenozoic climate change, erosion, and geodynamics (Hallet et al., 1996; Molnar and England, 1990; Raymo and Ruddiman, 1992; Raymo et al., 1988; Whipple et al., 1999). Such hypotheses cannot be addressed without considering the effects of changing from fluvial to glacial erosion as a result of climatic cooling. In this context, it is surprising that little is known about the rates of erosion achieved by glaciers, and even less about the distribution of this erosion in either space or time.

Most studies designed to evaluate relative rates of fluvial and glacial erosion have focussed on measuring long-term erosion rates from sediment yields. Hicks et al. (1990) used sediment yields in the Southern Alps of New Zealand to challenge the long-held view that glaciers are the more effective erosion agents. Hallet et al. (1996) used a global dataset to argue that glaciers are capable of eroding at significantly faster rates than rivers. In the most recent such study, Koppes and Hallet (2002) caution that the glacial erosion rates inferred from total sediment budgets in recently deglaciated fjords are representative only of tidewater glaciers during post-Little Ice Age retreat. They estimate a recent mean erosion rate of ~37 mm/yr for the Muir Glacier, but suggest a long-term rate of ~7 mm/yr, comparable to what can be achieved by rivers in some settings (Hallet et al., 1996).

As an alternative to estimating glacial erosion rates using sediment yields or interpretation of landforms, we suggest that it is informative to exploit our better understanding of the characteristic form of fluvial landscapes, and to compare observed glacial landscapes with predicted fluvial landscapes. In this study we compare observed landscapes with simulations of how the landscape might look now had glaciers never developed. As our understanding of the response of fluvial erosion to climate change improves, and a field site with a well-constrained base-level history is found, this approach could be extended to estimate how the landscape would have looked prior to the onset of glaciation. Nevertheless, the approach described here allows us to evaluate how mountain ranges may have developed over time due to climate cooling.

Prior work using a locally-calibrated fluvial erosion model in the Sierra Nevada indicated that the primary impact of glaciers in small catchments has been above the mean Quaternary equilibrium line altitude (ELA) (Brocklehurst and Whipple, 2002). As described by Porter (1989), the mean Quaternary ELA represents an ELA for 'average' Quaternary conditions,

typically midway between the current and last glacial maximum (LGM) ELAs. Glaciated landscapes often reflect erosion under these 'mean' conditions. Above this mean Quaternary ELA, glaciers have brought down both valley floors and ridgelines (Brocklehurst and Whipple, 2002). Below the mean Quaternary ELA, glaciers have widened valleys and carved characteristic U-shaped cross-sections, but without significantly incising the valley floor. Brocklehurst and Whipple (2002) also demonstrated how this approach could be used to evaluate relative rates of headwall erosion by glaciers in the Sierra Nevada.

Here we describe a more comprehensive evaluation of the tool of comparing current glacial landscapes with simulations of how the (fluvial) landscape might look now had glaciers never developed. We compare our results from the smaller basins on the eastern side of the Sierra Nevada with basins of a similar size and at a similar latitude on the western side of the Sangre de Cristo Range of southern Colorado. We also extend our analyses to some larger drainage basins, on both sides of the Sierra Nevada, and on the western side of the Sangre de Cristos. Glaciers in the larger basins have been responsible for modifying the longitudinal profile to much lower elevations, far below the mean Quaternary ELA. This suggests that processes in the ablation zone are noticeably different in these larger basins. We suspect that this reflects a combination of the larger accumulation area in the larger basins, thicker ice generating greater relief, longer residence time for ice in the lower part of the basin, and the lower slope on the fluvial longitudinal valley prior to glaciation, which may importantly influence subglacial hydrology, and thus the efficiency of glacial erosion (e.g., Alley et al., 1999; Hallet, 1996; Hooke, 1991).

2. Field Sites

This paper reports further details of our studies on the eastern side of the Sierra Nevada, adjacent to the Owens Valley (Fig. 1a), in addition to considering the western side of the Sangre de Cristo Range in southern Colorado (Fig. 1b), and the Kings River basin on the western side of the Sierra Nevada (Fig. 1c).

On the eastern side of the Sierra Nevada, we examined 2 large basins, Big Pine Creek and Bishop Creek, in addition to the 28 smaller basins previously described (Brocklehurst and Whipple, 2002). We selected this field site because of the relatively uniform climate, tectonic activity and lithology. The eastern scarp of the Sierra Nevada was produced by normal faulting,

beginning at ~5 Ma (Wakabayashi and Sawyer, 2001). The range front fault system may still be active, contributing to modest uplift rates (~0.2 mm/yr, Gillespie, 1982). This section of the Sierra Nevada comprises regionally homogeneous Cretaceous granodiorites and quartz monzonites (Bateman, 1965; Moore, 1963, 1981; Stone et al., 2001). Furthermore, the side-by-side occurrence of catchments ranging from displaying essentially no glacial modification to those with major glacial landforms holds the key to allowing local calibration of our fluvial erosion model and application to the neighbouring glaciated basins.

The western side of the Sangre de Cristo Range (Fig. 1b) comprises Paleozoic sedimentary units and Precambrian metamorphic rocks (Johnson et al., 1987). The tectonic regime is consistent throughout the region of interest. The normal component of slip rates on the range front fault system have averaged around 0.1-0.2 m/yr during the late Pleistocene (McCalpin, 1981, 1986, 1987), comparable to rates measured in the eastern Sierra Nevada. As in the eastern Sierra Nevada, the occurrence of neighbouring glacial and nonglacial basins allows local calibration of the fluvial erosion model.

Moving to the western side of the Sierra Nevada, the tectonic regime is generally thought to be that of a tilting crustal block (e.g., Huber, 1981). Uplift of the Sierra Nevada, westward tilting, and stream incision began at ~5 Ma, and Tertiary stream gradients were lower than modern ones (Wakabayashi and Sawyer, 2001). Granites are again the dominant lithology (e.g., Wakabayashi and Sawyer, 2001). Drainage networks here are much larger. We focussed on the Kings River drainage, which lies opposite the portion of the eastern side of the range studied. Due to the extensive glacial modification of the upper portion of the basin, it was necessary to calibrate the erosion model using smaller tributaries to the Kings River further downstream (Fig. 1c), and streams in the adjacent Kaweah River basin.

3. Methods

3.1 DEM analyses

A flow routing routine in Arc/Info was used to extract drainage networks from USGS 30m digital elevation models (DEMs). The downstream extent of each drainage basin was taken to coincide with the range front, to exclude the alluvial fan regime, and to allow consistent comparison between basins. Subsequent analyses and modelling were carried out using Matlab scripts.

Figure 2 compares representative longitudinal profiles from the Sangre de Cristos with those in the Sierra Nevada (Brocklehurst and Whipple, 2002). In both ranges, the longitudinal profiles of the nonglaciated basins look much like those seen in entirely unglaciated ranges (e.g., the Appalachians of Virginia and Maryland (Hack, 1957; Leopold et al., 1964)), the King Range, northern California (Snyder et al., 2000)). Increasing glacial influence is manifest as the development of a flatter section in the upper reaches of the profile, while the lower parts retain the shape of a bedrock stream. Full glaciation produces profiles with long, shallow sections separated by steeper steps, although the lower parts still resemble fluvial stream profiles. Figures 2a and 2b are at the same scale, and with no vertical exaggeration. The key difference between the longitudinal profiles of the Sangre de Cristos and the eastern Sierra Nevada is the reduced elevation range between the divide and the range front in the Sangre de Cristos, which in turn means that the average gradient of the Sangre de Cristos profiles is less.

3.2 Model calibration

The application of a fluvial landscape model here, to represent how the landscape might look now had glaciers never developed, was achieved by calibrating the model in the basins that have remained essentially unmodified by glaciers. The model simulates realistic fluvial topography by integrating the frequently observed power-law relationship between local slope, S, and drainage area, A, for fluvial topography (Fig. 3, Flint, 1974):

$$S = k_s A^{-\theta} \tag{1}$$

This power-law relationship is commonly observed in fluvial systems (Flint, 1974; Montgomery and Foufoula-Georgiou, 1993; Snyder et al., 2000; Tarboton et al., 1991; Willgoose, 1994), and under the special conditions of steady state (erosion rate equal to uplift rate at all points) the concavity, θ, and steepness, k_s, can be related to the parameters of bedrock channel erosion models (e.g., Whipple and Tucker, 1999). Since we merely sought to reproduce topography similar to the current state of the nonglaciated basins, we did not require that either the current fluvial topography or the simulated topography represent steady state conditions. The only assumption necessary is that the slope-area relationship for the nonglaciated basins (e.g., Fig. 3a, drainage area ~ 10 km^2) can be extrapolated to the greater drainage area of the glaciated basins

(< 110 km^2). Previous studies have demonstrated such a power-law relationship over larger ranges of drainage area (e.g., Baldwin et al., in press; Tarboton et al., 1991; Whipple and Tucker, 1999), as shown in Fig. 3b. We used only data from the trunk stream in our calculation. We calculated the steepness and concavity by linear regression in log-log space for each of the nonglacial basins, following techniques described by Snyder et al. (2000) and Brocklehurst and Whipple (2002). In summary, we excluded hillslopes and debris-flow dominated colluvial channels from the regression, and calculated slopes on interpolated 10m contour intervals. By selecting the downstream extent of the nonglaciated basins at the range front, we avoided regions of significant alluviation. Since θ and k_s are related, to determine a representative k_s we employed a mean value for θ from all of the nonglacial basins and repeated the regression for each basin to determine a 'fixed-θ' k_s (Snyder et al., 2000). The error-weighted mean values for θ and k_s that were used in the simulations are given in Table 1.

3.3. 1-D simulations

In order to obtain a smooth simulated profile we carried out a similar regression to determine a Hack law constant, k_h, and exponent, h (Hack, 1957), in the following relationship between drainage area and downstream distance, x, for each of the glacially-modified basins:

$$A = k_h x^h \tag{2}$$

Then for each of the glacially-modified basins we integrated the slope-area relationship:

$$S = -dz/dx = k k_h^{-\theta} x^{-h\theta} \tag{3}$$

This implicitly assumes that basin shape has not been significantly modified by glacial erosion. As discussed by Brocklehurst and Whipple (2002), in some cases elongation of the basins may be caused by headwall erosion (see below). In such cases, we assume basin shape has not been substantially altered. We set a maximum permitted hillslope and colluvial channel slope at the channel head of 40°, determined from slope histograms. We fixed the simulated outlet elevation to match the observed outlet elevation, reasoning that the glacial system has had very little opportunity to modify this elevation by either erosion (very short ice residence time in this

region even for the fully glaciated cases) or by deposition (most of the sediment continues to the alluvial fans below, and beyond). This is consistent with the observation that, especially in the smaller basins, the lower portions of glaciated basin longitudinal profiles have smooth concave forms rather than stepped profiles, and the close match between the lower parts of the observed and simulates profiles in the smaller basins.

It is striking that in some cases the simulated profile lies at a lower elevation than the observed profile (Figs. 9, 10). The simplest interpretation of this is that the river would have incised further had glaciers not developed upstream. Alternatively, some local complication, such as harder lithology, might cause deviation from the expected profile. However, our preferred interpretation is that the glaciers have been responsible for headwall retreat, which means that our simulated fluvial profile is too long to represent how a never-glaciated profile would look now, so has an overall slope that is too shallow (Brocklehurst and Whipple, 2002). We estimate the magnitude of headwall erosion by shortening (and steepening) the simulated profile until a good match is achieved in the lower reaches of the two profiles. This method has less precision in larger glaciated basins, where the glacier modifies the longitudinal profile to lower elevations.

A second complication in larger glaciated basins concerns the amount of sediment in the lower reaches of these basins, i.e., the current stream is heavily alluviated. In these cases it is not appropriate to employ the slope-area relationship calibrated in bedrock-channel dominated basins, since the alluviated channel will tend to have a shallower slope. In practice this is seen as the simulated profile lying above the observed profile at every location in the basin except at the outlet, where the two are forced to match. This issue is addressed by shortening the simulated profile from the downstream end, such that the observed and simulated profiles are tied at the base of the bedrock channel reach rather than at the outlet. This results in a reach over which the observed and simulated profiles match well, before diverging further upstream. On the eastern side of the Sierra Nevada and in the Sangre de Cristos we have field evidence for the location of the bedrock-alluvial transition, while on the western side of the Sierra Nevada this introduces considerable uncertainty into our analysis.

3.4. 2-D simulation

In order to extend our comparison between simulated fluvial and observed glacial landscapes to parts of the basin beyond merely the longitudinal profile, we needed to employ a 2-D landscape evolution model. This allowed us to use our sub-ridgeline relief method (Brocklehurst and Whipple, 2002) to project the ridgelines onto the longitudinal profile, to evaluate how they have responded to the onset of glaciation. We selected the Geologic-Orogenic Landscape Evolution Model (GOLEM, Tucker and Slingerland, 1994, 1997) to simulate most-likely present-day fluvial landforms. GOLEM incorporates tectonic uplift, weathering, hillslope transport, landsliding, and bedrock channel erosion and sediment transport. This list includes the most important landscape-forming processes in environments where chemical weathering is not significant. Bedrock channel erosion follows a shear-stress derived power-law relationship (e.g., Howard et al., 1994; Whipple and Tucker, 1999). We proscribe the basin outline and initial drainage pattern to allow direct comparison between simulated and observed topography. By fixing the basin outline we do not allow for the possibility that glaciers have been responsible for changing the shape of the basin, i.e., headwall erosion (Brocklehurst and Whipple, 2002). By running the landscape evolution model to a steady-state condition, we reproduce a slope-area relationship of the form shown in (1); we are not necessarily suggesting that the nonglaciated basins in this part of the Sierra Nevada are in steady state. Instead of using mean values for nonglaciated concavity and steepness calculated from the longitudinal profile data only, we calculated values using local slope and drainage area data at every point in each of the nonglaciated drainage basins.

4. Results

4.1 Smaller basins

The fluvial landscape simulation work presented by Brocklehurst and Whipple (2002) illustrated how some of the smaller, glaciated basins of the eastern Sierra Nevada might look now had glaciers never developed. Here we compare these results with those obtained from the western Sangre de Cristos.

The first step in using the approach described here is to verify that we can reproduce realistic nonglacial topography for an individual basin using our fluvial simulation, which uses mean values of θ and k_s from a series of basins (Table 1). As shown in Figures 4a and 5a, this is

achieved in both the Sierra Nevada and the Sangre de Cristos. Focussing on the cases where we do not see evidence of significant headwall erosion, the principle difference between how the glaciated basins might have looked and their current appearance is at higher elevations (Figs. 4b, c, 5b, c). Here glaciers have carved large cirque basins, lowering the valley floors. Furthermore, the 2-D simulations show that in both ranges the glaciers have apparently also brought the ridgelines down by a commensurate amount (Fig. 6). Thus there has not been significant generation of relief in terms of missing mass (Brocklehurst and Whipple, 2002).

At lower elevations, below the mean Quaternary ELA, the difference between the simulated and observed longitudinal profiles is minor, indicating little glacial incision of the valley floor (Figs. 4, 5), despite the clear U-shaped cross-section to the valleys (Figs. 7, 8). This suggests that glaciers carried out minimal downward cutting below the mean ELA during the LGM (when some of the glaciers extended to the range front), even though they were active in valley widening. The major difference between the results from the eastern Sierra Nevada and the western Sangre de Cristos is that there is less drainage basin relief in the Sangre de Cristos, so overall gradients are less. This is also shown in the nonglacial calibration data (Table 1); the mean concavities in the two ranges are essentially identical, but mean steepness is less in the Sangre de Cristos. Otherwise the results from the two ranges are quite comparable, despite the major contrast in lithology, and lesser differences in climate and tectonic setting.

Figures 9 and 10 illustrate cases from the Sierra Nevada and the Sangre de Cristo Range, respectively, where our interpretation of the simulated fluvial profile suggests significant headwall erosion. The amount of headwall erosion in addition to that which would have been achieved under purely fluvial conditions is estimated by shortening the simulated profile until it achieves a close match with the observed profile over the reach where the observed profile has a concave, step-free shape. The amount of "shortening" required is consistent with independent estimates obtained from our interpretation of divide migration due to headwall retreat. As shown in Figure 9, the divide at the head of Lone Pine Creek lies around 2.5 km further west than a line projected from points on the divide immediately north and south of the basin. Figure 10 illustrates interpreted headwall erosion at the head of Cottonwood Creek in the Sangre de Cristos. Here the head of the valley interrupts a ridgeline trending southwest from Crestone Needle, and also causes an eastward deviation in the range crest behind this. A more usual shape for the Cottonwood Creek basin would be for the main fork to follow the axis of the lower part

of the valley, which is instead followed by a modest tributary. Measuring back from the interrupted ridgeline, the valley extends a further ~2 km, comparable to the estimate gained independently from the simulation. In constrast, the cases where we do not see evidence for headwall erosion from our simulated profiles generally do not show divide migration at their head. For example, Birch Creek culminates in a horn, called The Thumb (see Figure 11 in Brocklehurst and Whipple, 2000).

4.2 Large basins

Figure 11 illustrates what happens when we extend our analyses to larger basins, using Big Pine Creek in the Sierra Nevada as an example. Attempting to fit the entire length of the basin produces a 1-D simulated profile (Fig. 11a) that lies significantly above the observed profile at every point upstream of the outlet. The simplest interpretation of this is that the glacier here has incised more rapidly than a river would have done at every point along the longitudinal profile. However, we suggest that this is not quite accurate; the lower reaches of Big Pine Creek are quite alluviated, and so trying to simulate an alternative profile with a bedrock erosion slope-area relationship is inappropriate. When we look at only that portion of the profile with some amount of bedrock in the channel, as indicated by field observations, we obtain a reasonable fit to a short section of the profile. This also involves modest glacial headwall erosion (shortening the simulated profile from the upstream end). Deviation between the simulated profile and the observed profile occurs far below the mean Quaternary ELA, even below the LGM ELA. Thus it seems clear that in this case (and also in Bishop Creek), the large glaciers have been responsible for actively incising the valley floor down to much lower elevations than in the smaller basins, even though the glaciers did not extend especially much further beyond the range front (Fig. 1). As in the smaller glaciated basins, the 2-D simulation (Fig. 11b) shows that the ridgelines have closely followed the response of the longitudinal profile, and thus there has not been major relief production. Figure 11c illustrates in 3-D the glacial modification of the longitudinal profile far below the ELA. Although the smaller basins in the Sierra Nevada show U-shaped cross-sections in the lower part of the basin (Fig. 7), it is only in the larger basins that this is accompanied by the incision of dramatic glacial steps.

Figure 12 illustrates preliminary 1-D simulations from the Bubbs and Palisade Creek tributaries to the Kings River. As in Big Pine Creek, our best fit involves shortening our

simulated profile from both the head (reflecting glacial headwall erosion) and the foot (reflecting an alluviated reach). Again there is significant deviation between the observed and simulated profiles at much lower elevations than in the smaller basins, and the glacial steps are more pronounced. However, calibrating the model on the western side of the range proved to be more tricky than on the eastern side, since in general there is greater glacial modification of the landscape, making nonglaciated basins more elusive, and also the greater range of basin sizes meant extrapolating parameters from small nonglaciated basins to very much larger glaciated basins. In addition, we currently lack field control on the extent of any alluviated channel reach; attempting to identify this from the longitudinal profile gives non-unique results, since the best fit also involves adjusting the headwall erosion component. This headwall erosion component is also difficult to constrain because it represents a much smaller portion of the overall basin length. Profiles on the western side of the range are also much more stepped than on the eastern side of the range; this may reflect lithologic variation, tectonics, or geomorphic process. In any case, this represents a further challenge to using a smooth concave fluvial profile to surmise how the range might look now had glaciation never occurred. In summary, our preliminary analyses of the large, low gradient basins on western side of the range suggest deep glacial scour all the way to the LGM terminus, consistent with the well-known observations of overdeepenings near glacial termini in Yosemite Valley and the Hetch Hetchy in the Sierra Nevada (e.g., MacGregor et al., 2000), and glaciated basins in the Wind River Range, Wyoming, and Glacier National Park, Montana. However, the scale of the basins on the western side of the Sierra Nevada means that we are pushing the limits of what we can hope to learn from this simulation technique.

5. Discussion

We have found very similar results applying our fluvial landscape simulation technique to both the eastern Sierra Nevada and the western Sangre de Cristos. The principle difference between the two is simply that there is more total relief in the Sierra Nevada, and so both observed and simulated profiles tend to be steeper. In detail, the two landscapes exhibit subtle differences, such as lithology exerting an influence on valley cross-sectional form in the Sangre de Cristos (Brocklehurst and Whipple, in prep.-a). However, the consistent results demonstrate that the approach outlined here provides valuable insight into the role of glaciers in sculpting mountain ranges.

It is important to note that the technique of fluvial landscape simulation is not readily applicable to the eastern side of the Sangre de Cristos. Here the moraines have a much greater volume than on the western side of the range, despite comparable drainage areas for the glaciated basins on the two sides of the range. This may reflect the prevailing wind preferentially blowing snow from the crest of the range into the basins on the eastern side, contributing to enhanced ice discharge during glacial times. The consequence, as far as our simulation method is concerned, is that the modern streams are still incising through these considerable piles of debris, rather than running close to bedrock, so a bedrock fluvial scaling relation is not appropriate.

This simulation technique has proven particularly adept at helping identify those cases where glaciers have caused significantly more headwall erosion and drainage basin enlargement than would have occurred under nonglacial conditions. This suggests the possibility of drainage capture by glaciers in a similar way to rivers in other settings. Drainage capture and relief inversion due to glacial erosion in the Sierra Nevada are considered more fully elsewhere (Brocklehurst et al., in prep.).

Our simulation studies have clearly demonstrated that larger glaciers have quite different behaviour from those in smaller basins. Large glaciers can erode more rapidly, particularly in the ablation zone, than their smaller brethren. Such a situation was also discussed by Hallet et al. (1996), who noticed that glacial erosion yields tend to increase with basin size. This they presumed to reflect an increase in effective erosion rates from small cirque glaciers to large, fast-moving glaciers. That we see major variations within a small range of the Sierra Nevada suggests that something more subtle is happening. The principal distinctions of the larger basins are that they have a larger accumulation area and that they would have had a lower overall slope prior to the onset of glaciation. In the smaller, steeper basins, the glaciers may be doing little more than 'avalanching' down the valley, with subglacial water percolating out readily. This is crucial, since subglacial water pressure fluctuations are thought to play a key role in erosion by quarrying(Alley et al., 1999; Hallet, 1996; Hooke, 1991). If water is readily flushed out, such fluctuations will not develop, and erosion rates may be retarded. On a shallower slope, the glaciers may well allow the development of more complicated subglacial water systems, thus permitting more rapid erosion. The larger accumulation area will result in a much larger ice discharge, and since most formulations for glacial erosion, whether through abrasion or quarrying, emphasise the importance of ice velocity, this may allow more rapid erosion rates.

The larger accumulation area may also allow the glacier to extend further down the valley for more extended periods of time, permitting greater degrees of glacial erosion. The shallow slope of the larger basins will also allow thicker ice to develop. Given the correlation between ice thickness and relief production (Brocklehurst and Whipple, in prep.-a; Whipple et al., 1999), it is possible that larger glaciers will be associated with taller hillsides, thus shading the glacier below and allowing it to extend to lower elevations. Brocklehurst and Whipple (in prep.-b) also find a scale-based distinction in the response of glaciated landscapes to rapid tectonic uplift. Large glaciers maintain their downvalley slope even in the face of the most rapid tectonic uplift, while small glaciers must apparently steepen to erode as rapidly, although not as much as rivers. The causes of the obvious distinctions between small basins normally occupied by modest cirque glaciers and large drainages featuring larger valley glaciers represent an important focus for future research.

A final question of glacial erosion dynamics to consider here is why it is that the smaller glaciers widen the valley floor without incising it. As demonstrated by Harbor (1992), starting from an initial V-shaped cross section, erosion driven by ice velocity will be focussed initially towards the development of a U-shaped cross section. It is possible that, due to the short residence times of these glaciers at their full LGM extents (Porter, 1989), the glaciers haven't been able to pass out of this stage as yet. We suggest that subglacial water may again play a crucial role. The subglacial water along the thalweg is likely to form a well-connected network for much of the annual cycle, reducing the possibility of large water-pressure fluctuations (Hallet, 1996; Hooke, 1991). Along the glacier margins, the subglacial drainage network may not be as well developed, while crevasses will allow meltwater to percolate to the base, potentially allowing greater water pressure fluctuations, and thus more rapid erosion. We thus highlight the role of subglacial water in erosion processes as a key focus for future research.

Our studies suggest that there is a range of possible behaviours for glacial erosion systems. Initial efforts on constructing glacial landscape evolution models have focussed on the larger-scale end of the spectrum (Braun et al., 1999; MacGregor et al., 2000; Merrand and Hallet, 2000; Oerlemans, 1984). Predictions of these models include large overdeepenings below the long-term ELA, in addition to overdeepenings associated with tributary junctions. We draw attention to the fact that we will only fully understand glacial erosion once we are able to use these models to explain the differences between smaller basins, where glacial modification is

concentrated above the ELA, and larger basins, which are capable of carving overdeepenings far below the ELA.

The principle limitation on applying fluvial landscape simulation to deduce the effects of glacial erosion on a mountain belt is the requirement that the model be locally calibrated. This stems from our current inability to precisely predict parameters in fluvial erosion formulations based purely on a set of climatic, tectonic and lithologic observations. However, it is mainly only at higher latitudes that glaciers will have sculpted every basin within a mountain range. The work presented here has demonstrated the applicability of this approach in two ranges with different lithologies and somewhat different climates. It will be interesting to move to other ranges, e.g., Southern Alps of New Zealand, to consider what this approach can tell us about the response of glaciers to rapid tectonic uplift rates. Preliminary results from the Manaslu region of the Himalayas (Whipple and Brocklehurst, 2000) emphasise the ability of glaciers to maintain a shallow gradient in spite of rapid uplift, unlike their fluvial counterparts (Brocklehurst and Whipple, in prep.-b; Brozovic et al., 1997). A second limitation lies in other factors that may cause fluvial profiles to deviate from a smooth concave profile, such as a local change in lithology. Using this simulation approach, such deviations would tend to be attributed to glacial processes, which may not always be accurate.

The analysis described here exploits the fact that we understand the characteristics of fluvial landscapes better than glaciated landscapes. It is important to emphasise that as yet we are unable to use this approach to establish convincingly how the range might have looked prior to glaciation, because of (i) uncertainty over how θ and k_s respond to climate change (Roe et al., 2002; Whipple et al., 1999); and (ii) lack of detailed understanding of the base-level history over the Quaternary as the Owens Valley fell with respect to the Sierra Nevada (Gillespie, 1982), while the range was being tilted down towards the west (e.g., Huber, 1981), in part through the flexural-isostatic response to erosional unloading and deposition (Small and Anderson, 1995), and how the San Luis Valley fell with respect to the Sangre de Cristo Range (e.g., McCalpin, 1981). Thus further improvements in terms of the response of rivers to specific forcing factors, such as climate change and lithologic variation, will further broaden the scope of this method. Understanding the response of rivers to climate change during the Quaternary will allow us to predict how mountain ranges would have looked prior to the onset of glaciation, while the ability to constrain erosion model parameters purely on the basis of climatic, tectonic and lithologic

parameters will allow application of this approach where local calibration of the fluvial erosion model is not possible.

The application of a simple formulation for bedrock channel profiles leads to problems when the valley floor becomes highly alluviated, and thus exhibits a shallower slope than predicted by the bedrock channel model. This can be solved in larger basins, where alluviation is a natural consequence of steadily increasing drainage area, by restricting the analysis to only the bedrock portions of the profile. However, where a small stream is choked by debris from the last glaciation, as in the eastern Sangre de Cristos, there is not a sufficiently long stretch of the longitudinal profile between the morainal debris and the glacially-modified upper section to realistically fit the model to.

Conclusion

We have used a fluvial erosion model to simulate how the glaciated basins of the Sierra Nevada and the western Sangre de Cristos might look now had the glaciers never developed. This has proven to be an effective tool in indicating how glaciated landscapes have developed, predicting rates of erosion relative to rivers, and the spatial distribution of glacial erosion. Results from the two ranges are very similar. For the smaller glaciated basins, we find that the glaciers have modified the landscape extensively above the mean Quaternary ELA, but have done little more than widen valleys below this level. A likely cause of this is the short residence time of glaciers at their maximum extent. In the larger glaciated basins, we find that the glaciers have incised the valley floor into characteristic steps much lower into the basin. We suggest that this is due to either the larger accumulation area or the lower initial slope prior to glaciation. The larger accumulation area will allow longer ice occupation of lower elevations and more rapid ice velocities. The lower slope will allow thicker ice and a more complicated subglacial drainage network. The causes of the important distinction between small basins occupied predominantly by cirque glaciers, and the larger basins with valley glaciers, represent an important focus for future research. In both large and small drainage basins, subglacial water may be playing a key role in the development of the glaciated landscape.

Acknowledgements

This work was supported by NSF grant EAR-9980465 (to KXW), a NASA Graduate Fellowship (to SHB), and a GSA Fahnestock Award (to SHB).

Figure captions

Fig. 1. (a). Study site in the Sierra Nevada, California, highlighted on the inset map. On the eastern side of the range, three categories of basin, based on the degree of glaciated at the Last Glacial Maximum, are illustrated as follows: nonglaciated (bold), moderate glaciation (italic) and full glaciation (regular). Big Pine Creek is a 'large' fully glaciated basin, whereas the remainder of the fully glaciated basins are 'small' (see text). (b). Study site on the western side of the Sangre de Cristo Range, Colorado, highlighted on the inset map. Three categories of basin, based on the degree of glaciated at the Last Glacial Maximum, are illustrated as follows: nonglaciated (bold), moderate glaciation (italic) and full glaciation (regular). (c). Kings River basin, on the western side of the Sierra Nevada, highlighting tributaries discussed in the text.

Fig. 2. Comparison of longitudinal profiles in the Sangre de Cristo Range and the eastern Sierra Nevada. (a) Sierra Nevada: Longitudinal profiles from Alabama Creek (nonglaciated, black), Division Creek (minor glaciation, medium grey, dashed), Red Mountain Creek (moderate glaciation, medium grey, solid), Tuttle Creek (significant glaciation, medium grey, dotted) and Lone Pine Creek (full glaciation, light grey). (b) Sangre de Cristos: Longitudinal profiles from Lime Creek (nonglaciated, black), Pole Creek (minor glaciation, medium grey, dashed), Wild Cherry Creek (moderate glaciation, medium grey, solid), Cottonwood Creek (significant glaciation, medium grey, dotted) and Rito Alto Creek (full glaciation, light grey).

Fig. 3. Slope-area plots. (a) Symmes Creek, a representative example from the nonglaciated basins in the study area used to constrain the fluvial simulation model. (b) Middle River, Virginia, illustrating the slope-area relationship over a significantly broader range of drainage area than the extrapolation employed here.

Fig. 4. Representative one-dimensional simulated profiles for small basins in the Sierra Nevada study area. (a) Symmes Creek, a non-glaciated basin. The darker line is the longitudinal profile extracted from the DEM, and the paler line is the simulated longitudinal profile. Horizontal lines are the modern (top), mean Quaternary (dashed) and LGM (bottom) ELAs at the range crest (Burbank, 1991). Notice the close agreement between the simulated and observed profiles for this representative example. (b) Red Mountain Creek, a partially glaciated basin. Key as for Symmes Creek. (c) Independence Creek, a small, fully glaciated basin. Key as for Symmes Creek. Notice the very close agreement between the observed and simulated profiles below the mean Quaternary ELA, and especially below the LGM ELA.

Fig. 5. Representative one-dimensional simulated profiles from the Sangre de Cristos. (a) Burnt Creek, a non-glaciated basin. The darker line is the longitudinal profile extracted from the DEM, and the paler line is the simulated longitudinal profile. Horizontal lines are the modern (top), mean Quaternary (dashed) and LGM (bottom) ELAs at the range crest (Richmond, 1965). Notice the close agreement between the simulated and observed profiles for this representative example. (b) North Crestone Creek, a partially glaciated basin. Key as for Burnt Creek. (c) Rito Alto Creek, a small, fully glaciated basin. Key as for Burnt Creek. As in the Sierra Nevada (Fig. 3), notice the very close agreement between the observed and simulated profiles below the mean Quaternary ELA, and especially below the LGM ELA.

Fig. 6. Two-dimensional simulations of (a) Independence Creek, Sierra Nevada, and (b) Rito Alto Creek, Sangre de Cristos. Longitudinal profiles drawn from the present topography (black) and simulated topography (pale grey) with the difference between the two in dark grey. Also shown are the interpolated ridgeline surfaces along the profiles (present topography—black, dashed; simulated topography—pale grey, dashed). ELAs indicated as in Figures 3 and 4. Comparing the observed and simulated topography, both the valley floor and the ridgeline agree well at lower elevations and then diverge considerably higher up, with the simulated ridgeline and longitudinal profile considerably higher. We suggest that both the valley floor and the ridgelines have been lowered by glacial erosion.

Fig. 7. 3-D perspective views of Independence Creek, showing the same extent as the longitudinal profile shown in Fig. 3c. (a) Shaded relief map draped on the topography. (b) Slope map draped on the topography. Notice how the valley floor is wide and flat, and the valley cross-section is U-shaped almost to the basin outlet.

Fig. 8. 3-D perspective views of Rito Alto Creek. (a) Shaded relief map draped on the topography. (b) Slope map draped on the topography.

Fig. 9. Simulating headwall erosion in the south fork of Lone Pine Creek, Sierra Nevada. (a) Contour map of the Lone Pine Creek basin. Notice the significant westward step in the divide at the head of Lone Pine Creek, passing just to the east of the summit of Mt Whitney. (b) Observed and simulated longitudinal profiles for Lone Pine Creek (present topography—black; full-length simulation—dark grey; shortened simulation—pale grey). Estimated headwall erosion: 2500 m.

Fig. 10. Simulating headwall erosion in Cottonwood Creek, Sangre de Cristos. (a) Contour map of the Cottonwood Creek basin. Notice the significant eastward step in the divide at the head of Cottonwood Creek, to the south of the Crestone Needle. (b) Observed and simulated longitudinal profiles for Lone Pine Creek (present topography—black; full-length simulation—dark grey; shortened simulation—pale grey). Estimated headwall erosion: 2000 m.

Fig. 11. (a) One-dimensional simulated profiles for Big Pine Creek, a large, fully glaciated basin. The black line is the longitudinal profile extracted from the DEM, the dark grey line is a simulated longitudinal profile for the full length of the basin, and the pale grey line is a simulated profile shortened from the foot of the valley to account for alluviation, and from the top of the valley to account for headwall erosion. Horizontal lines are the modern (top), mean Quaternary (dashed) and LGM (bottom) ELAs at the range crest (Burbank, 1991). (b) Longitudinal profiles extracted from 2-D GOLEM simulation for the non-alluviated portion of Big Pine Creek. Present topography (black) and simulated topography (pale grey) with the relief, measured as the distance between interpolated ridgeline (dashed) and valley floor (solid) in dark grey (solid for observed topography, dashed for simulated. ELAs as in (a). Comparing the observed and simulated topography, both the valley floor and the ridgeline agree well at lower elevations and

then diverge considerably higher up, with the simulated ridgeline and longitudinal profile considerably higher. However, distribution of relief is similar in the two cases. We suggest that both the valley floor and the ridgelines have been lowered by glacial erosion. (c) 3-D perspective view of shaded relief draped on topography for Big Pine Creek. Notice how glacial steps in the valley floor continue close to the mouth of the valley, along with extensive glacial modification in the upper parts of the basin.

Fig. 12. (a) One-dimensional simulated profiles for Bubbs Creek, glaciated tributary to the Kings River. Observed profile is in black, full length simulated profile in dark grey, and simulated profile shortened to account for headwall erosion (5 km) and to remove the alluvial section at the downstream end in pale grey. Horizontal lines are the modern (top), mean Quaternary (dashed) and LGM (bottom) ELAs at the range crest (Burbank, 1991). (b) One-dimensional simulated profiles for Palisade Creek, glaciated tributary to the Kings River. Key as for Bubbs Creek; headwall erosion is 2 km in this case. Notice how all simulated profiles have much higher divides than the observed profile, and glaciated steps in the observed profile are observed far below the ELA.

Table 1. Calibration parameters, with ± 1σ errors. k_s calculated using the calculated mean value of θ for each range.

Basin	θ	$\ln k_s$
Eastern Sierra Nevada		
Alabama	0.32±0.07	3.38±1.60
Black	0.20±0.07	3.49±1.67
Inyo	0.37±0.06	3.41±1.59
Pinyon	0.19±0.06	3.41±1.72
South Fork, Lubken	0.45±0.08	3.34±1.57
Symmes	0.37±0.05	3.32±1.68
Mean	*0.32±0.11*	*3.39±1.63*
Sangre de Cristos		
Alpine	0.20±0.08	2.95±1.39
Burnt	0.37±0.06	3.00±1.38
Cedar Canyon	0.44±0.06	3.05±1.39
Cold	0.36±0.05	3.01±1.44
Copper	0.33±0.06	3.16±1.41
Dimick	0.21±0.06	2.94±1.40
Hot Spring	0.26±0.07	2.99±1.38
Lime	0.19±0.13	3.02±1.42
Little Medano	0.27±0.05	2.94±1.43
Marshall	0.45±0.06	3.16±1.36
Orient	0.31±0.08	2.79±1.38
Short	0.38±0.06	3.14±1.40
Steel	0.24±0.08	2.92±1.45
Mean	*0.32±0.10*	*3.01±0.49*
Western Sierra Nevada		
Boulder	0.46±0.18	4.40±1.66
Deer	0.37±0.05	5.00±1.72
Kennedy	0.28±0.03	4.71±1.62
Middle	0.33±0.02	5.10±1.67
Monarch	0.44±0.02	4.48±1.61
Rough1	0.44±0.02	5.11±1.67
Rough2	0.52±0.02	4.99±1.75
Rough3	0.48±0.03	4.99±1.75
Rough4	0.65±0.04	5.02±1.72
Mean	*0.42±0.11*	*49.2±0.80*

References

Alley, R. B., Strasser, J. C., Lawson, D. E., Evenson, E. B., and Larson, G. J., 1999, Glaciological and geological implications of basal-ice accretion in overdeepenings, *in* Mickelson, D. M., and Attig, J. W., eds., Glacial Processes Past and Present: Geological Society of America Special Paper: Boulder, Colorado, Geological Society of America, p. 1-9.

Baldwin, J. A., Whipple, K. X., and Tucker, G. E., in press, Implications of the shear-stress river incision model for the timescale of post-orogenic decay of topography: Journal of Geophysical Research.

Bateman, P. C., 1965, Geology and Tungsten Mineralization of the Bishop District, California, U.S. Geological Survey Professional Paper, 208 p.

Braun, J., Zwartz, D., and Tomkin, J. H., 1999, A new surface-processes model combining glacial and fluvial erosion: Annals of Glaciology, v. 28, p. 282-290.

Brocklehurst, S. H., Granger, D. E., and Whipple, K. X., in prep., Implications of Old Glaciated Surfaces at High Elevations in the Sierra Nevada, California.

Brocklehurst, S. H., and Whipple, K. X., 2002, Glacial Erosion and Relief Production in the Eastern Sierra Nevada, California: Geomorphology, v. 42, no. 1-2, p. 1-24.

-, in prep.-a, Effects of Glacier Size and Thickness on the Relief of Glaciated Landscapes.

-, in prep.-b, The response of glaciated landscapes to varying rock uplift rates.

Brozovic, N., Burbank, D. W., and Meigs, A. J., 1997, Climatic Limits on Landscape Development in the Northwestern Himalaya: Science, v. 276, p. 571-574.

Burbank, D. W., 1991, Late Quaternary Snowline Reconstructions for the Southern and Central Sierra Nevada, California and a Reassessment of the "Recess Peak Glaciation": Quaternary Research, v. 36, p. 294-306.

Flint, J. J., 1974, Stream gradient as a function of order, magnitude, and discharge: Water Resources Research, v. 10, p. 969-973.

Gillespie, A. R., 1982, Quaternary Glaciation and Tectonism in the Southeastern Sierra Nevada, Inyo County, California [PhD thesis]: California Institute of Technology, 695 p.

Hack, J. T., 1957, Studies of longitudinal stream profiles in Virginia and Maryland: U.S. Geological Survey Professional Paper, v. 294-B, p. 97.

Hallet, B., 1996, Glacial quarrying: a simple theoretical model: Annals of Glaciology, v. 22, p. 1-8.

Hallet, B., Hunter, L., and Bogen, J., 1996, Rates of erosion and sediment evacuation by glaciers: A review of field data and their implications: Global and Planetary Change, v. 12, p. 213-235.

Harbor, J. M., 1992, Numerical modeling of the development of U-shaped valleys by glacial erosion: Geological Society of America Bulletin, v. 104, p. 1364-1375.

Hicks, D. M., McSaveney, M. J., and Chinn, T. J. H., 1990, Sedimentation in proglacial Ivory Lake, Southern Alps, New Zealand: Arctic Alpine Research, v. 22, p. 26-42.

Hooke, R. L., 1991, Positive feedbacks associated with erosion of glacial cirques and overdeepenings: Geological Society of America Bulletin, v. 103, p. 1104-1108.

Howard, A. D., Dietrich, W. E., and Seidl, M. A., 1994, Modeling fluvial erosion on regional to continental scales: Journal of Geophysical Research, v. 99, p. 13971-13986.

Huber, N. K., 1981, Amount and Timing of Late Cenozoic Uplift and Tilt of the Central Sierra Nevada, California - Evidence from the Upper San Joaquin River, U.S Geological Survey Professional Paper, 28 p.

Johnson, B. R., Lindsey, D. A., Bruce, R. M., and Soulliere, S. J., 1987, Reconnaissance geologic map of the Sangre de Cristo Wilderness Study Area, south-central Colorado: USGS Miscellaneous Field Studies Map, v. MF-1635-B.

Koppes, M. N., and Hallet, B., 2002, Influence of rapid glacial retreat on the rate of erosion by tidewater glaciers: Geology, v. 30, no. 1, p. 47-50.

Leopold, L. B., Wolman, M. G., and Miller, J. P., 1964, Fluvial Processes in Geomorphology: San Francisco, W.H. Freeman, 522 p.

MacGregor, K. C., Anderson, R. S., Anderson, S. P., and Waddington, E. D., 2000, Numerical Simulations of Glacial Valley Longitudinal Profile Evolution: Geology, v. 28, no. 11, p. 1031-1034.

McCalpin, J. P., 1981, Quaternary geology and neotectonics of the west flank of the northern Sangre de Cristo Mountains, south-central Colorado [Doctoral thesis]: Colorado School of Mines, 287 p.

-, 1986, Quaternary Tectonics of the Sangre de Cristo and Villa Grove Fault Zones: Colorado Geological Survey Special Publication, v. 28, p. 59-64.

-, 1987, Recurrent Quaternary normal faulting at Major Creek, Colorado: An example of youthful tectonism on the eastern boundary of the Rio Grande Rift Zone, *in* Beus, S. S., ed., Geological Society of America Centennial Field Guide - Rocky Mountain Section, Geological Society of America, p. 353-356.

Merrand, Y., and Hallet, B., 2000, A physically based numerical model of orogen-scale glacial erosion: Importance of subglacial hydrology and basal stress regime: GSA Abstracts with Programs, v. 32, no. 7, p. A329.

Molnar, P., and England, P., 1990, Late Cenozoic uplift of mountain ranges and global climate change: chicken or egg?: Nature, v. 346, p. 29-34.

Montgomery, D. R., and Foufoula-Georgiou, E., 1993, Channel Network Source Representation Using Digital Elevation Models: Water Resources Research, v. 29, no. 12, p. 3925-3934.

Moore, J. G., 1963, Geology of the Mount Pinchot Quadrangle, Southern Sierra Nevada, California, US Geological Survey Bulletin, 152 p.

-, 1981, Geologic map of the Mount Whitney Quadrangle, Inyo and Tulare Counties, California, US Geological Survey Map.

Oerlemans, J., 1984, Numerical Experiments on Large-scale Glacial Erosion: Zeitschrift fuer Gletscherkunde und Glazialgeologie, v. 20, p. 107-126.

Porter, S. C., 1989, Some Geological Implications of Average Quaternary Glacial Conditions: Quaternary Research, v. 32, p. 245-261.

Raymo, M. E., and Ruddiman, W. F., 1992, Tectonic forcing of late Cenozoic climate: Nature, v. 359, p. 117-122.

Raymo, M. E., Ruddiman, W. F., and Froelich, P. N., 1988, Influence of late Cenozoic mountain building on ocean geochemical cycles: Geology, v. 16, p. 649-653.

Richmond, G. M., 1965, Glaciation of the Rocky Mountains, *in* Wright, H. E., Jr, and Frey, G. D., eds., The Quaternary of the United States: Princeton, NJ, Princeton University Press, p. 217-230.

Roe, G. H., Montgomery, D. R., and Hallet, B., 2002, Effects of orographic precipitation variations on the concavity of steady-state river profiles: Geology, v. 30, no. 2, p. 143-146.

Small, E. E., and Anderson, R. S., 1995, Geomorphically Driven Late Cenozoic Rock Uplift in the Sierra Nevada, California: Science, v. 270, p. 277-280.

Snyder, N. P., Whipple, K. X., Tucker, G. E., and Merritts, D. J., 2000, Landscape response to tectonic forcing: DEM analysis of stream profiles in the Mendocino triple junction region, northern California: Geological Society of America Bulletin, v. 112, no. 8, p. 1250-1263.

Stone, P., Dunne, G. C., Moore, J. G., and Smith, G. I., 2001, Geologic Map of the Lone Pine 15' Quadrangle, Inyo County, California: U.S. Geological Survey Geologic Investigations Series, v. I-2617, p. Online version 1.0.

Tarboton, D. G., Bras, R. L., and Rodriguez-Iturbe, I., 1991, On the Extraction of Channel Networks from Digital Elevation Data: Hydrological Processes, v. 5, p. 81-100.

Tucker, G. E., and Slingerland, R. L., 1994, Erosional dynamics, flexural isostasy, and long-lived escarpments: A numerical modeling study: Journal of Geophysical Research, v. 99, no. B6, p. 12229-12243.

-, 1997, Drainage basin responses to climate change: Water Resources Research, v. 33, p. 2031-2047.

Wakabayashi, J., and Sawyer, T. L., 2001, Stream Incision, Tectonics, Uplift, and Evolution of Topography of the Sierra Nevada, California: Journal of Geology, v. 109, p. 539-562.

Whipple, K. X., and Brocklehurst, S. H., 2000, Estimating Glacial Relief Production in the Nepal Himalaya: GSA Abstracts with Programs, v. 32, p. A320.

Whipple, K. X., Kirby, E., and Brocklehurst, S. H., 1999, Geomorphic limits to climate-induced increases in topographic relief: Nature, v. 401, p. 39-43.

Whipple, K. X., and Tucker, G. E., 1999, Dynamics of the stream-power river incision model: Implications for height limits of mountain ranges, landscape response timescales, and research needs: Journal of Geophysical Research, v. 104, p. 17661-17674.

Willgoose, G., 1994, A statistic for testing the elevation characteristics of landscape simulation models: Journal of Geophysical Research, v. 99, no. B7, p. 13,987-13,996.

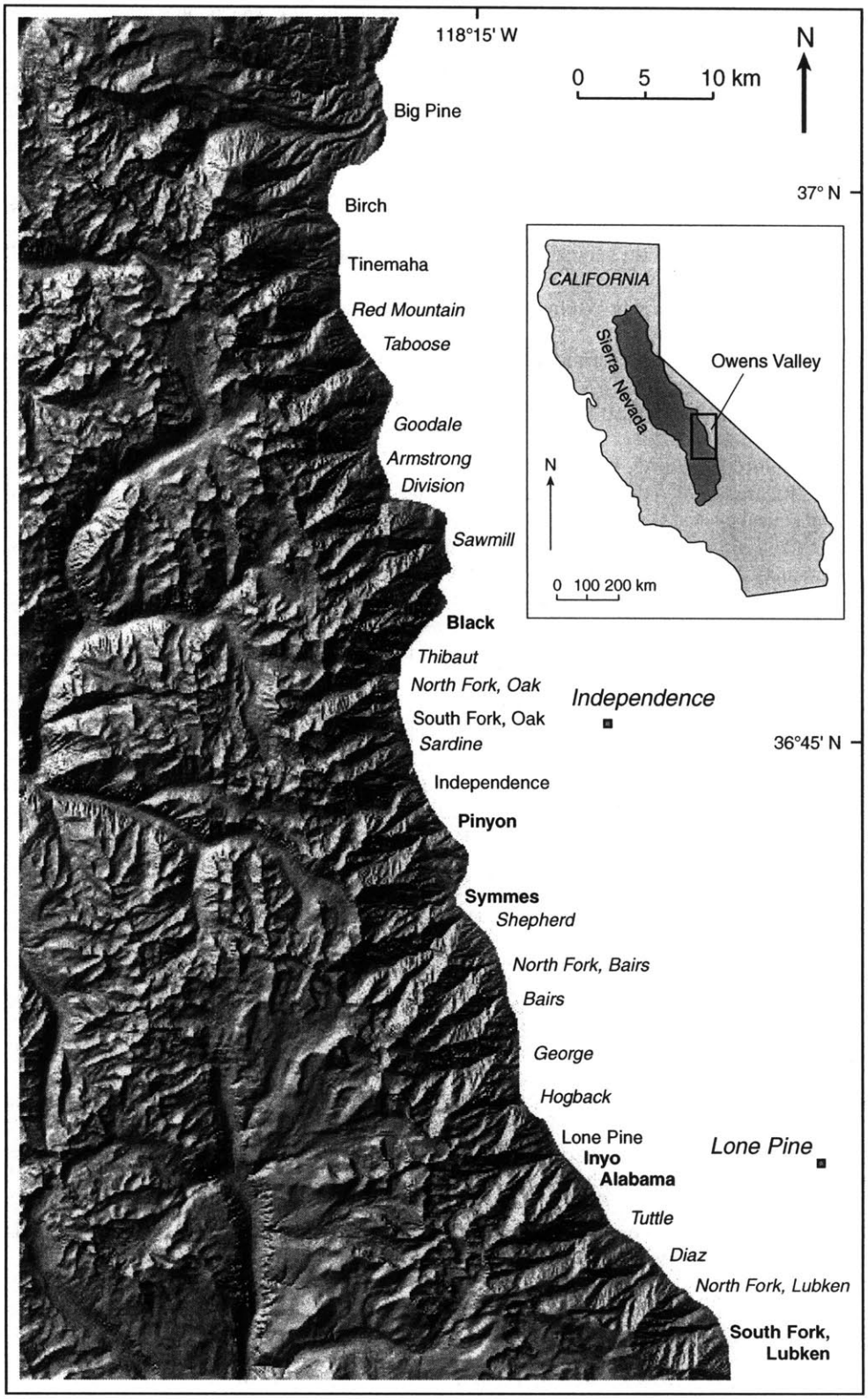
118°15' W
N
0 5 10 km
Big Pine
37° N
Birch
Tinemaha
Red Mountain
Taboose
CALIFORNIA
Sierra Nevada
Owens Valley
Goodale
Armstrong
Division
N
Sawmill
0 100 200 km
Black
Thibaut
North Fork, Oak
Independence
South Fork, Oak
Sardine
36°45' N
Independence
Pinyon
Symmes
Shepherd
North Fork, Bairs
Bairs
George
Hogback
Lone Pine
Inyo
Alabama
Lone Pine
Tuttle
Diaz
North Fork, Lubken
South Fork,
Lubken

Fig. 1a

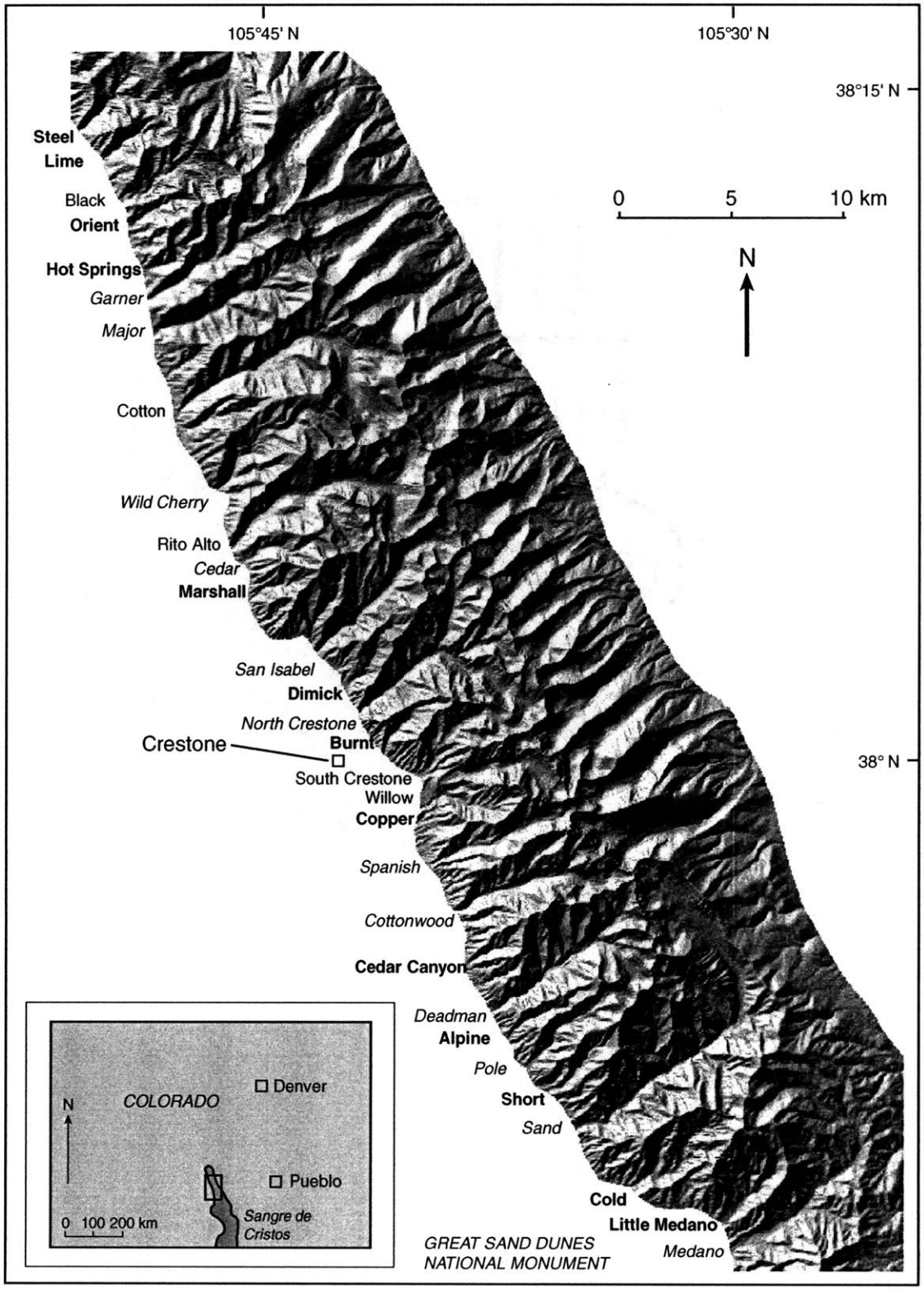
105°45' N
105°30' N
38°15' N
38° N
0 5 10 km
N
Steel
Lime
Black
Orient
Hot Springs
Garner
Major
Cotton
Wild Cherry
Rito Alto
Cedar
Marshall
San Isabel
Dimick
North Crestone
Crestone
Burnt
South Crestone
Willow
Copper
Spanish
Cottonwood
Cedar Canyon
Deadman
Alpine
Pole
Short
Sand
Cold
Little Medano
Medano
GREAT SAND DUNES
NATIONAL MONUMENT
N
COLORADO
Denver
Pueblo
0 100 200 km
Sangre de
Cristos

Fig. 1b

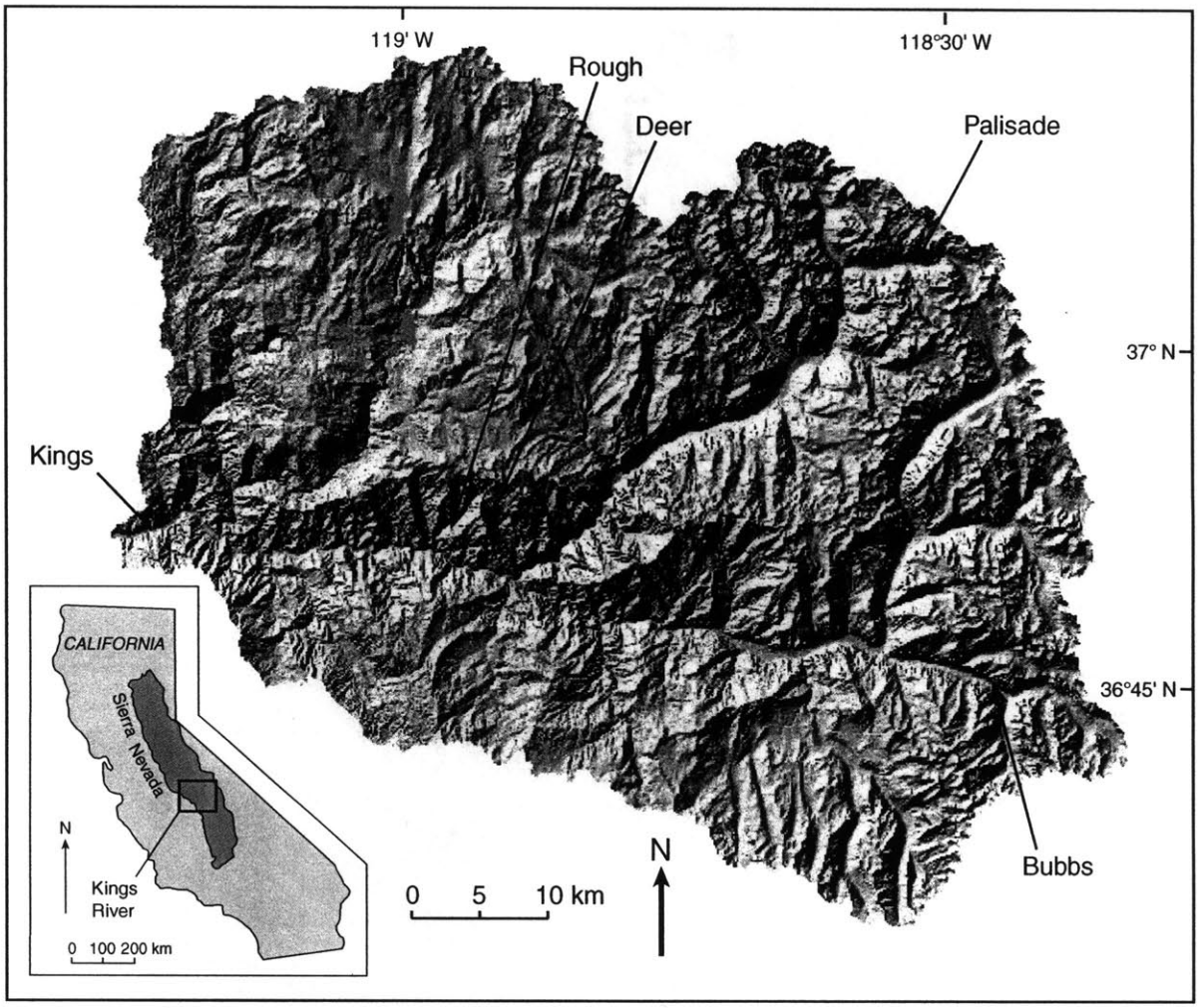
119' W
118°30' W
Rough
Deer
Palisade
37° N
Kings
36°45' N
Bubbs
CALIFORNIA
Sierra Nevada
N
Kings
River
0 100 200 km
0 5 10 km
N

Fig. 1c

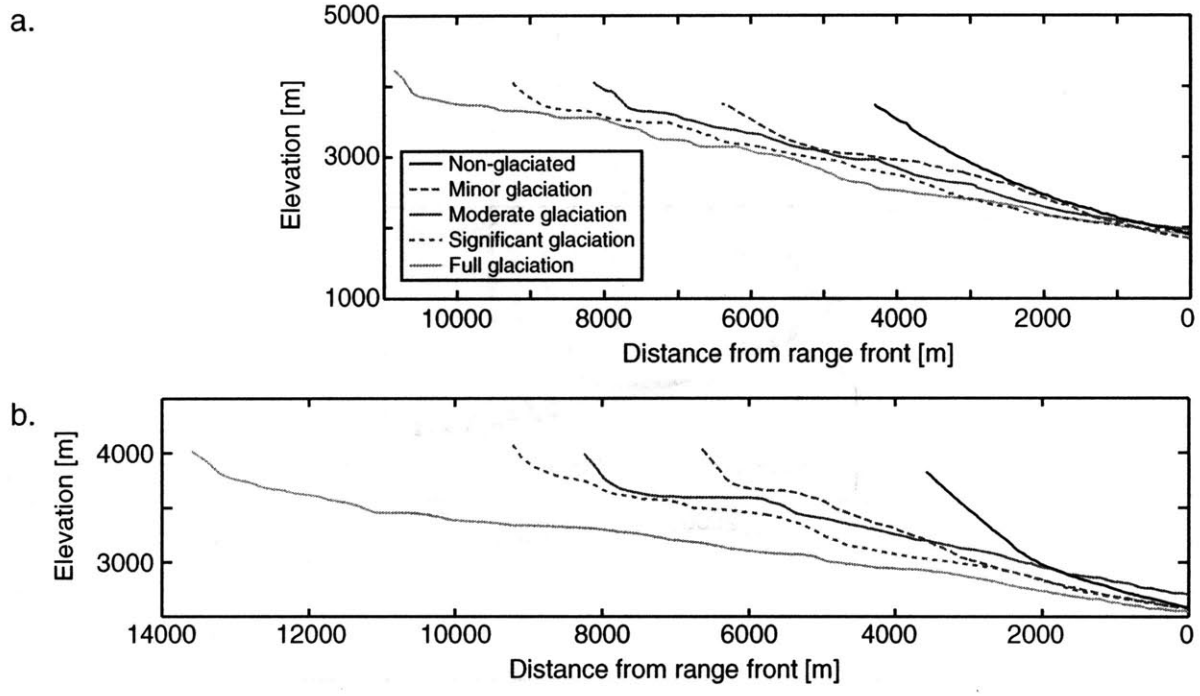
a.
Elevation [m]
5000
3000
1000
Non-glaciated
Minor glaciation
Moderate glaciation
Significant glaciation
Full glaciation
10000
8000
6000
4000
2000
0
Distance from range front [m]
b.
Elevation [m]
4000
3000
14000
12000
10000
8000
6000
4000
2000
0
Distance from range front [m]

Fig. 2

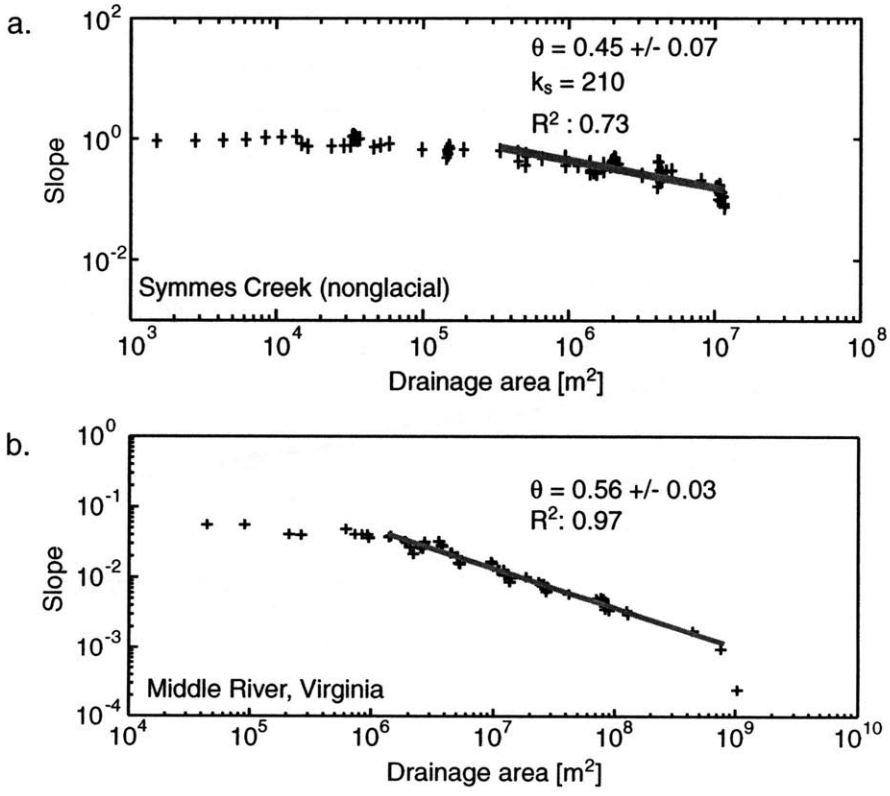
a.
Slope
θ = 0.45 +/- 0.07
k_s = 210
R^2 : 0.73
Symmes Creek (nonglacial)
Drainage area [m²]
b.
Slope
θ = 0.56 +/- 0.03
R^2: 0.97
Middle River, Virginia
Drainage area [m²]

Fig. 3

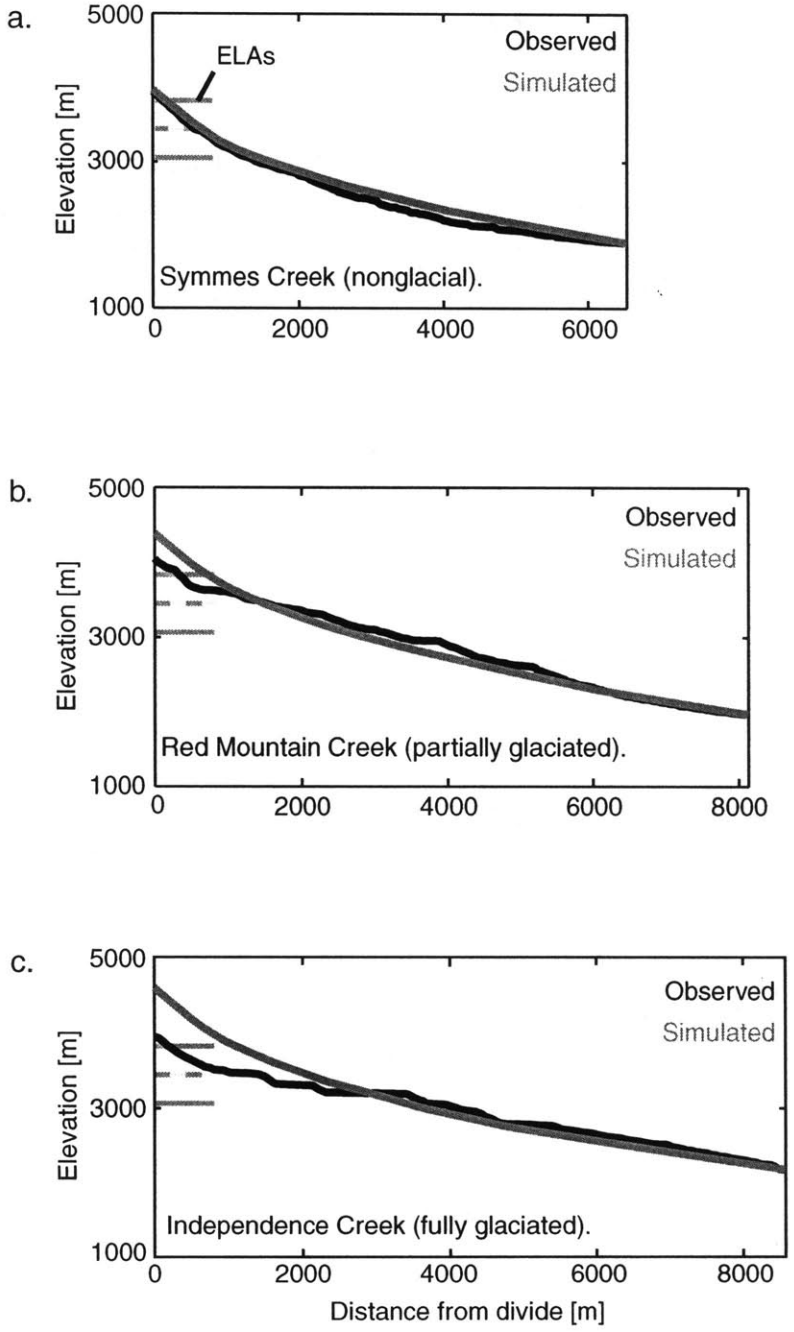
a.
5000
3000
1000
Elevation [m]
ELAs
Observed
Simulated
Symmes Creek (nonglacial).
0
2000
4000
6000
b.
5000
3000
1000
Elevation [m]
Observed
Simulated
Red Mountain Creek (partially glaciated).
0
2000
4000
6000
8000
c.
5000
3000
1000
Elevation [m]
Observed
Simulated
Independence Creek (fully glaciated).
0
2000
4000
6000
8000
Distance from divide [m]

Fig. 4

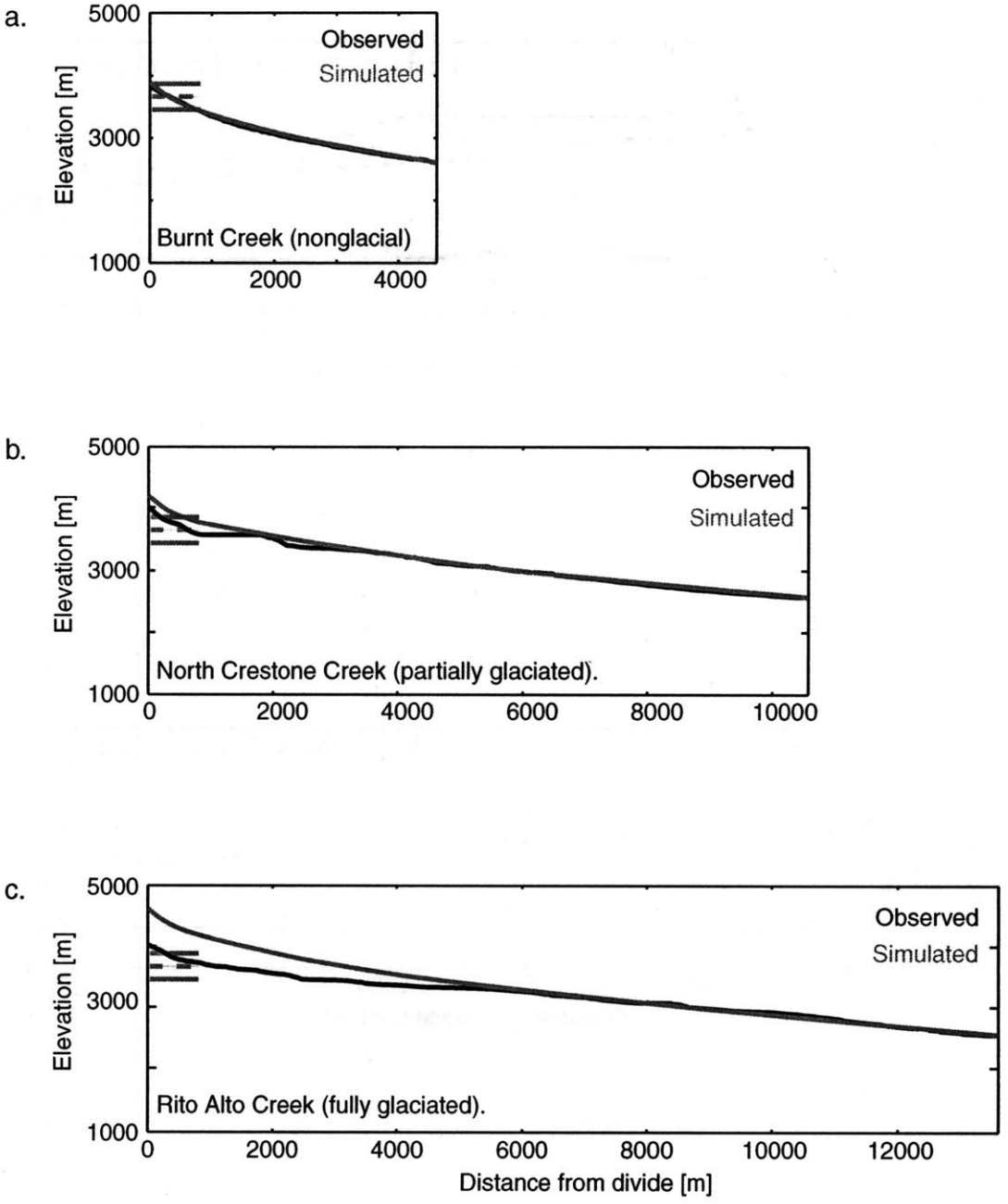
a.
Observed
Simulated
Elevation [m]
5000
3000
1000
Burnt Creek (nonglacial)
0
2000
4000
b.
Observed
Simulated
Elevation [m]
5000
3000
1000
North Crestone Creek (partially glaciated).
0
2000
4000
6000
8000
10000
c.
Observed
Simulated
Elevation [m]
5000
3000
1000
Rito Alto Creek (fully glaciated).
0
2000
4000
6000
8000
10000
12000
Distance from divide [m]

Fig. 5

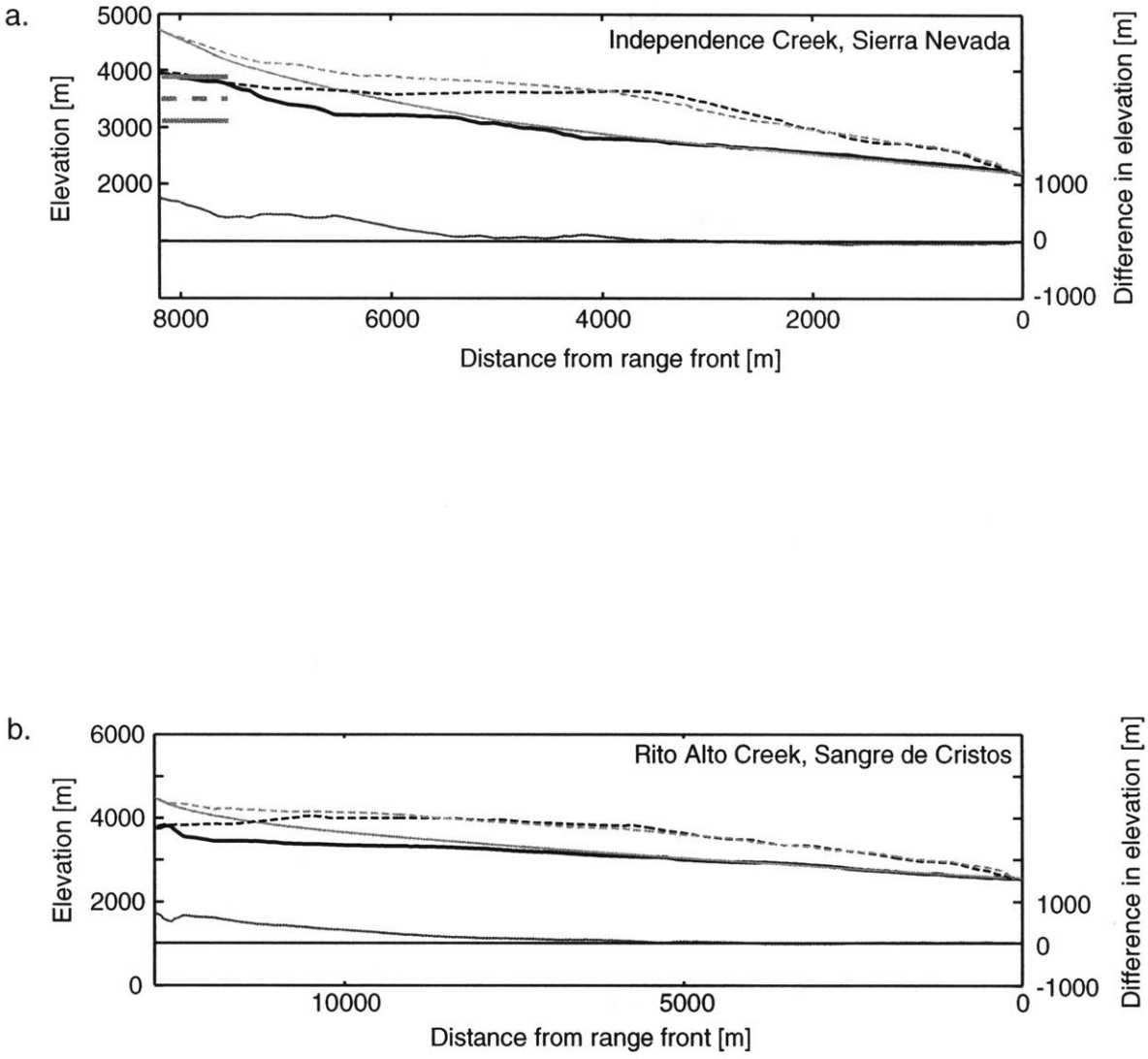
a.
Independence Creek, Sierra Nevada
Elevation [m]
5000
4000
3000
2000
8000
6000
4000
2000
0
Distance from range front [m]
1000
0
-1000
Difference in elevation [m]
b.
Rito Alto Creek, Sangre de Cristos
Elevation [m]
6000
4000
2000
0
10000
5000
0
Distance from range front [m]
1000
0
-1000
Difference in elevation [m]

Fig. 6

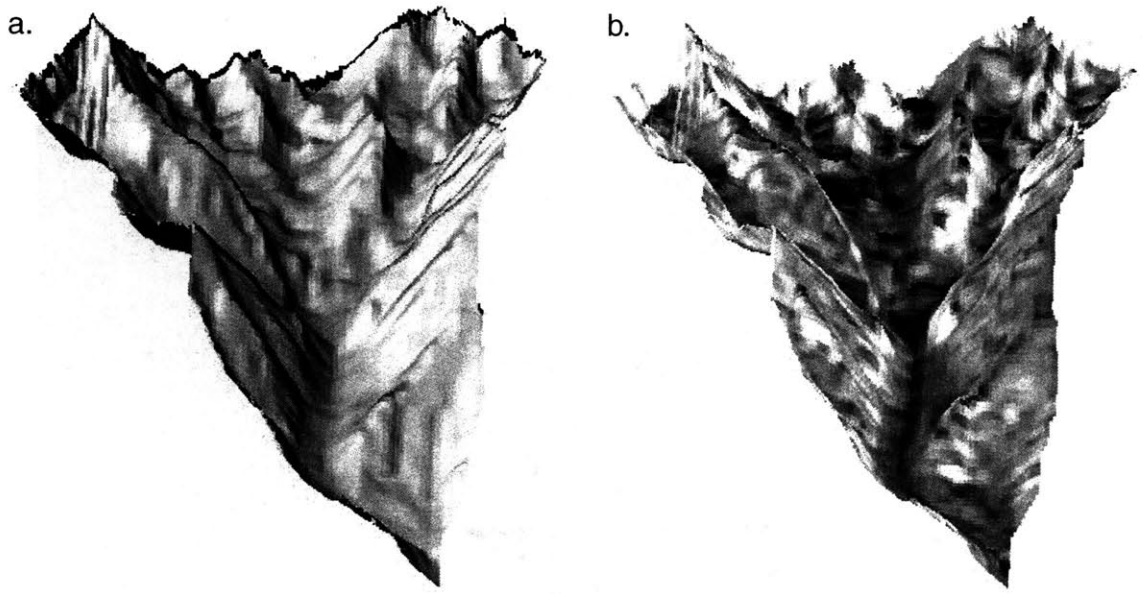

Fig. 7

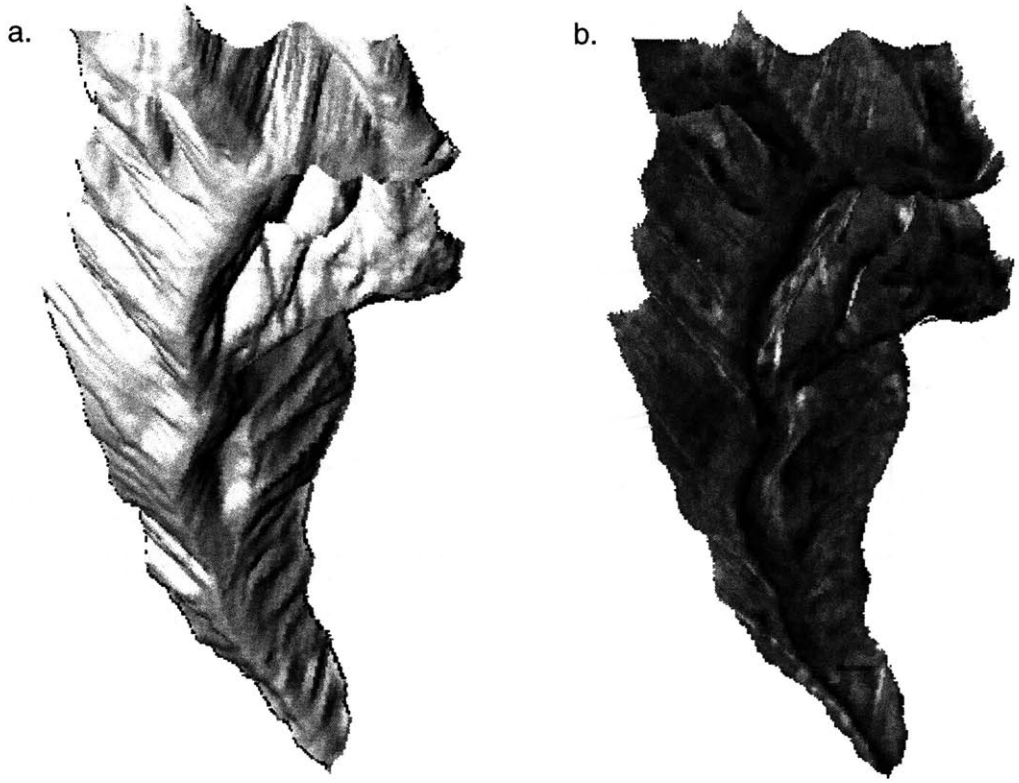

Fig. 8

a.

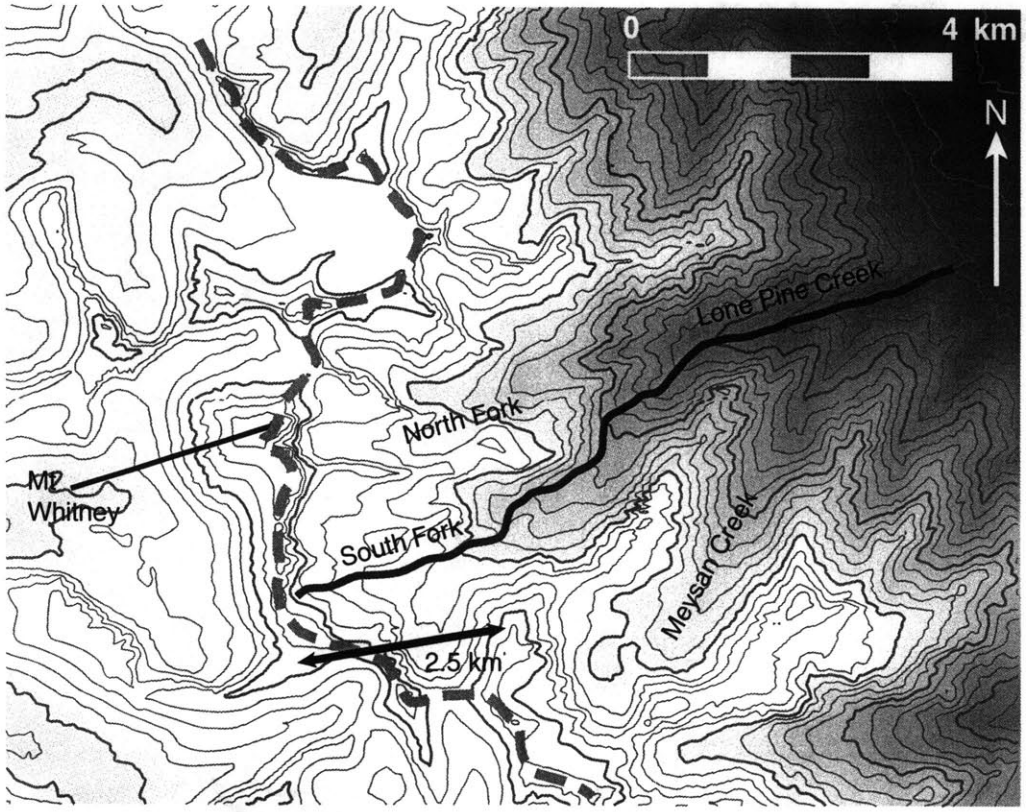
0
4 km
N
Lone Pine Creek
North Fork
Mt
Whitney
South Fork
Meysan Creek
2.5 km

b.

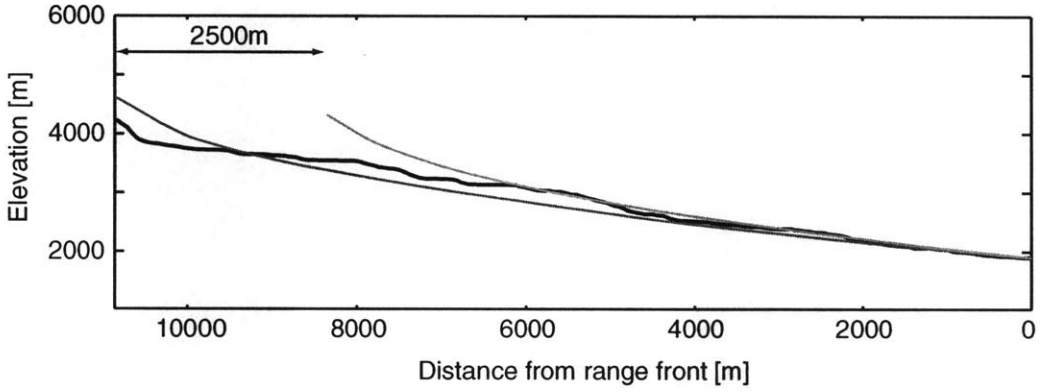
6000
4000
2000
2500m
Elevation [m]
10000
8000
6000
4000
2000
0
Distance from range front [m]

Fig. 9

a.

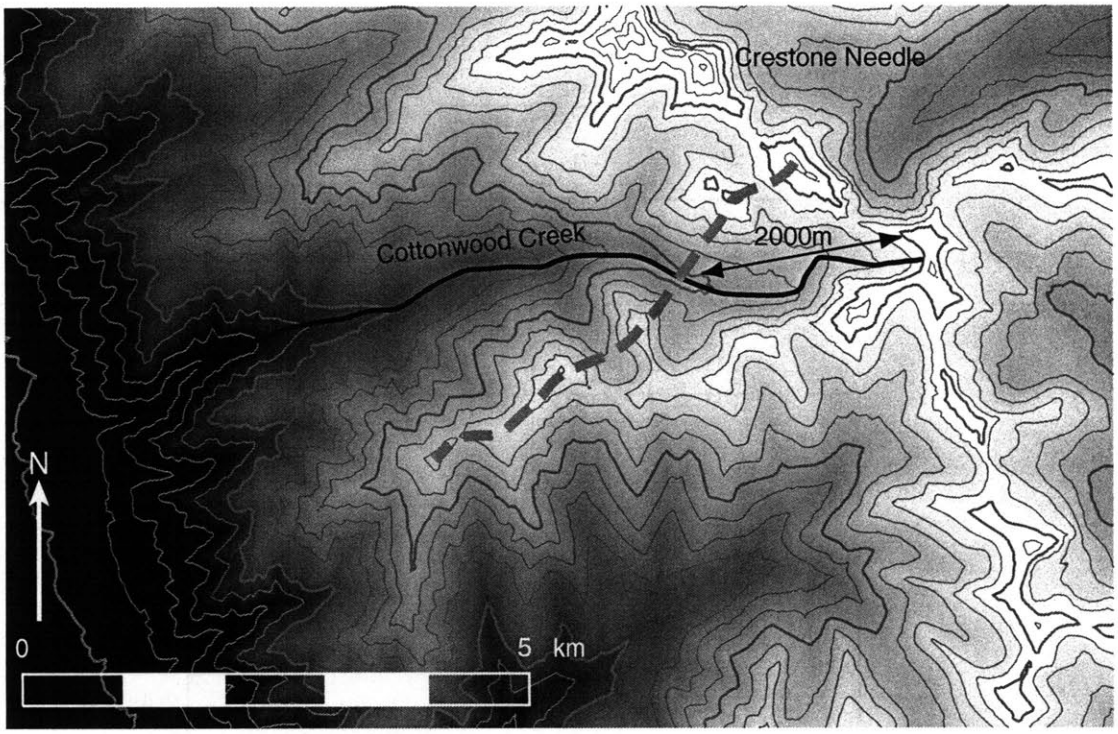
Crestone Needle
Cottonwood Creek
2000m
N
0
5 km

b.

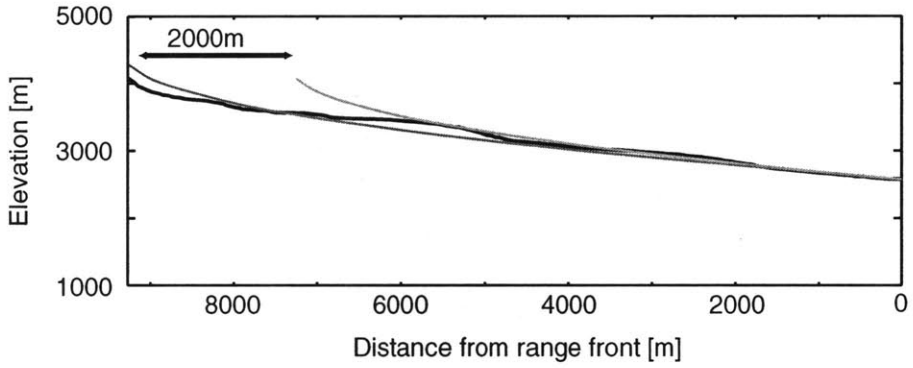
5000
3000
1000
2000m
Elevation [m]
8000
6000
4000
2000
0
Distance from range front [m]

Fig. 10

a.

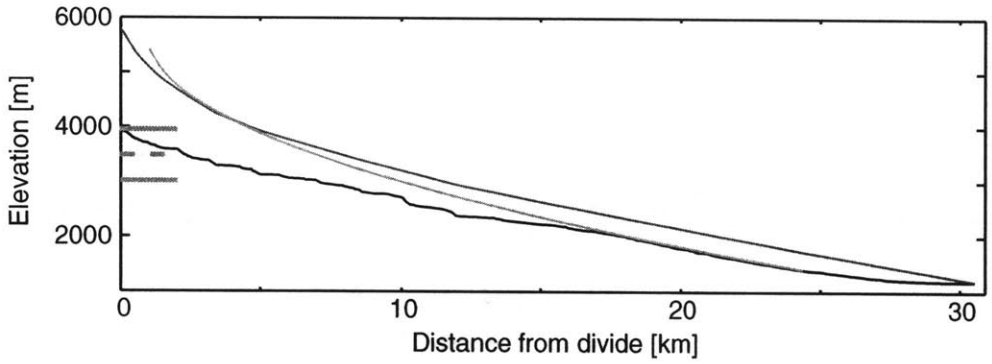
6000
4000
2000
Elevation [m]
0
10
20
30
Distance from divide [km]

b.

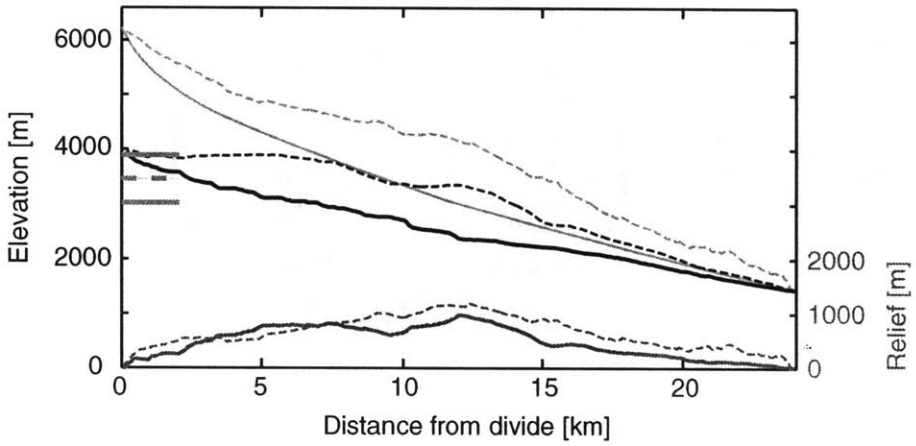
6000
4000
2000
0
Elevation [m]
0
5
10
15
20
Distance from divide [km]
2000
1000
0
Relief [m]

c.

Fig. 11

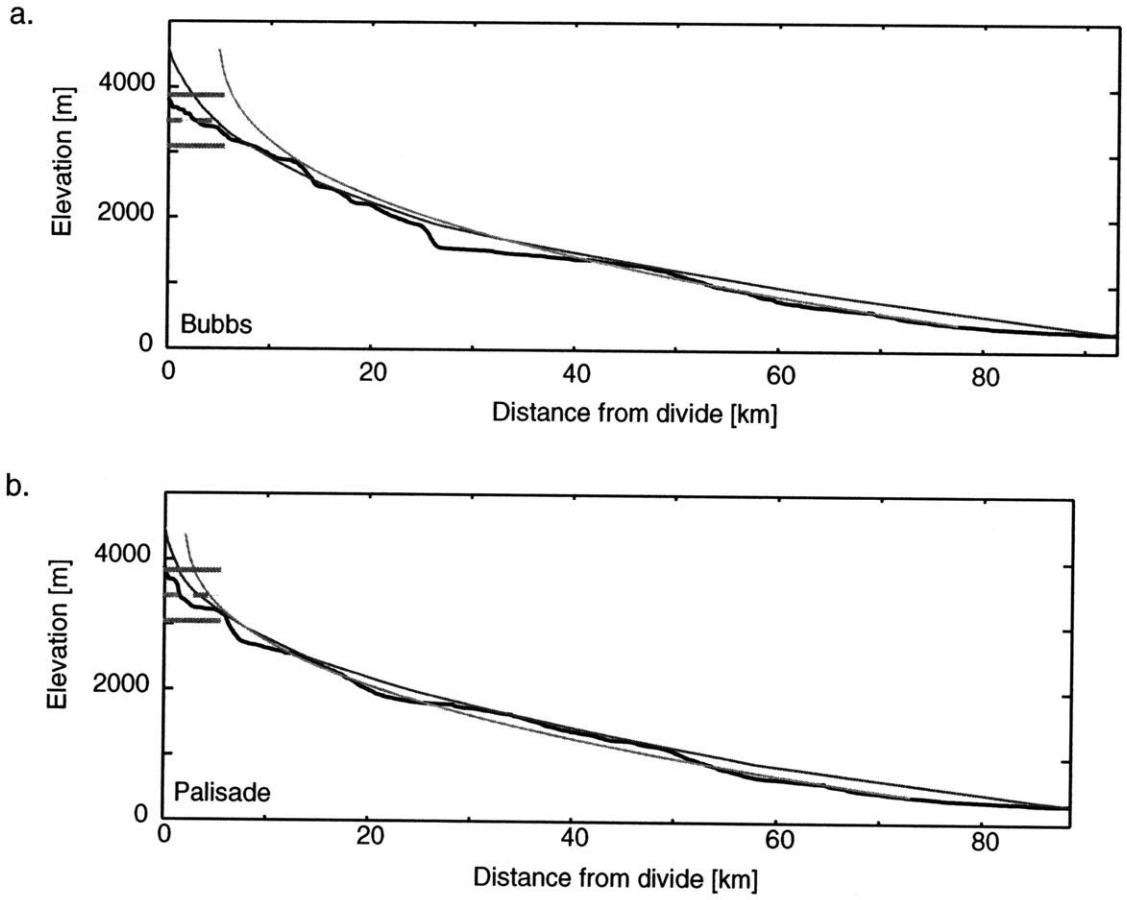
a.
Elevation [m]
4000
2000
0
Bubbs
0
20
40
60
80
Distance from divide [km]
b.
Elevation [m]
4000
2000
0
Palisade
0
20
40
60
80
Distance from divide [km]

Fig. 12

Chapter 5

Cosmogenic isotope inheritance in alpine glaciated basins in the eastern Sierra Nevada, California

Simon H. Brocklehurst* and Kelin X. Whipple

Department of Earth, Atmospheric and Planetary Sciences, Massachusetts Institute of Technology, Cambridge MA 02139, USA

Darryl E. Granger

Department of Earth and Atmospheric Sciences, Purdue University, West Lafayette IN 47907, USA

Prepared for submission to *Geology*

* to whom correspondence should be addressed: email: shb@mit.edu, fax: 1-617-252-1800

Abstract

Previous studies of the cosmogenic nuclide content of bedrock surfaces exposed during the most recent deglaciation have suggested that, under certain circumstances, isotopes produced during the prior interglacial may not have been completely removed during the last glaciation. These inherited isotopes would cause anomalously old calculated exposure ages. Previous work on the problem of inheritance in glacial settings has focussed on erosion by ice sheets. We test the importance of inheritance in a temperate alpine glacial setting. Guided by our previous studies of glaciated landscapes in the eastern Sierra Nevada, California, we identified a series of sites most likely to record inheritance, i.e., to have experienced minimal erosion during the last glaciation. We sampled glacially-polished bedrock along the floors of three small drainages and, below the mean Quaternary equilibrium line altitude, found exposure ages shortly postdating the last glacial retreat, indicating that glaciers did incise the valley floor at least ~2 m during the last glacial maximum. This implies minimum glacial erosion rates on the order of ~0.2-1 mm/yr. We suggest that inheritance will only be found in glaciated regions in the absence of quarrying, which in turn suggests inheritance is unlikely in the valley floor in temperate alpine glacial settings. More important problems are the presence of snow and postglacial debris, which both cause calculated deglaciation ages to underestimate the time since deglaciation.

Keywords: *cosmogenic isotopes, inheritance, glacial erosion*

1. Introduction

Glacial erosion plays a crucial role in the development of many mountain ranges. An improved understanding of temporal and spatial variations in glacial erosion rates is crucial in order to understand how glaciated landscapes are evolving now, and how they might have developed from prior fluvial landscapes due to late Cenozoic cooling. This in turn is essential in testing hypotheses relating climate change and tectonic processes (e.g., Molnar and England, 1990; Raymo and Ruddiman, 1992; Whipple et al., 1999).

Cosmogenic nuclides are seeing increasing use as a means of determining ages and rates in geomorphic settings (e.g., Bierman, 1994; Gosse and Phillips, 2001). However, before either rates or ages can be determined, an accurate production rate is needed. The eastern Sierra Nevada has been the setting for a number of studies using the apparently well-constrained glacial history to determine production rates (e.g., Nishiizumi et al., 1989). In addition to some controversy over the details of the glacial history (e.g., Clark and Gillespie, 1997), previous workers have also suggested that, in at least some settings, inheritance of remnant cosmogenic isotopes produced during a prior interglacial may affect apparent ages for the most recent deglaciation (e.g., Briner and Swanson, 1998; Fabel and Harbor, 1999). Here we describe a field test of the importance of inheritance in a temperate alpine glacial setting. Based on our previous work (e.g., Brocklehurst and Whipple, 2002), we selected sites in the eastern Sierra Nevada most likely to record inheritance, and determined ^{10}Be ages for polished bedrock samples.

Previous studies on the possible role of inheritance in glacial settings have tended to focus on erosion by continental-scale ice sheets. Briner and Swanson (1998) used cosmogenic isotopes to examine the magnitude, rate and spatial distribution of glacial erosion over Mount Erie, a large stoss-and-lee landform in the Puget Sound region, Washington, which was submerged beneath 1200-1500 m of ice during the last glaciation. They showed that quarrying was an efficient process, but that in the absence of glacial quarrying, the Cordilleran ice sheet may have abraded as little as 1-2 m of bedrock, insufficient to reset the cosmogenic clock. Harbor et al. (1999) found anomalously old apparent ^{10}Be exposure ages on Mt Tjuolmma, Sweden. This they interpreted as an inheritance signal, indicating that erosion by the most recent Fennoscandian ice sheet (probably cold-based at this point) did not completely remove inherited cosmogenic radionuclides. At the scale of alpine glaciers, Horn et al. (1996) used cosmogenic radionuclides to demonstrate patterns of erosion in a glacial valley cross-section, namely an

extensive area of significant erosion in the central portion of the valley, and decreasing erosion rates towards the ice margin. Fabel and Harbor (1999) were able to use inherited cosmogenic radionuclides and an independent estimate for the time interval between the penultimate and last deglaciation in the Wind River Range, Wyoming, to calculate erosion rates for this period.

Here we describe the results of a cosmogenic isotope study designed to test the hypothesis that inheritance may be a problem in bedrock samples from a temperate alpine glacial setting. We identified 3 drainage basins in the eastern Sierra Nevada exhibiting widespread bedrock outcrop and apparent minor glacial incision along the part of the valley below the mean Quaternary ELA (Brocklehurst and Whipple, 2002). We sought inheritance in polished bedrock samples deglaciated since the Last Glacial Maximum (LGM), during the Tioga glaciation (Blackwelder, 1931), which would indicate that a thickness less than ~2 m was eroded during the LGM. This represents the depth over which cosmogenic isotope production falls to the level resolvable by accelerator mass spectrometry (~5% of the surface production rate). Such inheritance would be reflected in surface exposure ages exceeding the last major deglaciation age (the end of the Tioga glaciation) of ~14 ka (Benson et al., 1998; Bierman et al., 1996; Clark et al., 1995; Clark and Gillespie, 1997). Secondarily, this would also provide a test of the resolution of our fluvial landscape simulation technique that suggests minor incision in the ablation zone of small glaciers (Brocklehurst and Whipple, 2002, in prep.).

2. Field Site

The eastern Sierra Nevada was selected for our prior studies because of the range of degrees of glacial modification exhibited in adjacent drainage basins within a zone of relatively uniform tectonic activity, lithology, and climate. On the regional scale, the lithologies consist of homogeneous Cretaceous granodiorites and quartz monzonites (Bateman, 1965; Moore, 1963, 1981; Stone et al., 2001). Uplift rates associated with the range-front normal fault system are fairly uniform, on the order of ~0.2 mm/yr (Gillespie, 1982). The eastern Sierra Nevada represent an ideal location to examine the importance of inheritance in alpine glacial settings because of the preservation of glacially-polished, striated surfaces to sample, and the carefully studied glacial history (e.g., Benson et al, 1998; Clark and Gillespie, 1997; Gillespie, 1982). Brocklehurst and Whipple (2002; in prep.) compared observed topography with simulated fluvial topography that was designed to illustrate how the range might look now had the glaciers never

developed. They proposed that, over the length of the Quaternary, glaciers have done little to incise the landscape at elevations below the mean Quaternary ELA (Porter, 1989). However, while the longitudinal profile has a smooth, concave shape in these reaches, looking much like a fluvial profile, the valley cross-sections are clearly U-shaped, reflecting some amount of glacial landscape modification. Given that the glaciers have not carved characteristic steps low in the basin, this would seem to represent a likely candidate if inheritance were to be a problem in temperate alpine glaciated landscapes.

The Sierra Nevada has been the site of many previous cosmogenic isotope studies, although most of these have sought to establish a chronology for glacial deposits. Phillips et al. (1990) determined the chronology of glacial deposits at Bloody Canyon, just north of the area studied here, using cosmogenic ^{36}Cl. Phillips et al. (1996) then obtained a more detailed record of Tioga glacial advances, at 31±1, 25±1, 19±1, and 16±1 ^{36}Cl ka. The region has also been the setting for a vigorous debate regarding the calibration of the ^{10}Be production rate (Gosse and Phillips, 2001). Nishiizumi et al. (1989) determined the ^{10}Be production rate assuming deglaciation of the Sierra Nevada occurred 11,000 years ago. However, Clark et al. (1995), Bierman et al. (1996), Clark and Gillespie (1997) and Benson et al. (1998) have argued, on the basis of more recent radiocarbon dating from lake-sediment cores, that deglaciation concluded by ~14,000 years ago, if not earlier. Thus the production rate of Nishiizumi et al. (1989) is around 20% too high. Here we use the updated production rates of Stone (2000).

3. Cosmogenic dating

3.1 Sampling strategy

We collected glacially-polished bedrock samples at various elevations along the valley axes of Meysan (a tributary to Lone Pine), Red Mountain and South Fork, Oak Creeks (see Table 1 and Figs. 1 and 2). We sampled along the valley floor to determine if there was a relationship between elevation (and thus ice occupation time, ice dynamics, etc.) and degree of inheritance. These drainage basins were chosen because of the large areal extent of bedrock exposed in each of these valleys. While the streams in each of these valleys run mostly on bedrock, each valley still contains a large volume of morainal deposits. Thus in each case we took samples from the fronts of bedrock noses close to the main stream. In addition, the bedrock surfaces sampled in the South Fork, Oak Creek have a significant downvalley slope. Such sites are likely to have had any

sole moraine removed rapidly following deglaciation. To increase the likelihood of finding inheritance, we selected sites with glacially polished bedrock, indicating minimal postglacial erosion, and sampled at highs in the local microtopography, avoiding areas with evidence of plucking of an overlying layer of joint blocks or an exfoliation sheet. In Meysan Creek, we sampled the Whitney granodiorite (Stone et al., 2001), in South Fork, Oak Creek we sampled a metarhyolite (Moore, 1963), and from Red Mountain Creek, a quartz monzonite (Bateman, 1965). Sample sites are illustrated in Figure 3. Given a typical density of 2.7 g/cm^3 and a penetration length of 170 g/cm^2, the depth of erosion required to reset the cosmogenic clock (i.e., to erode down to where the prior production would have been at the detection limit of ~5% of its surface value), is ~1.89m (Briner and Swanson, 1998). In each case we sampled the upper surface of the bedrock to a depth of 2-4 cm (see Table 2). In addition, in Meysan Creek we identified boulders of the same granodiorite seated upon the glacially-polished surface and unlikely to have been moved during the postglacial history, as indicated by weathering predominantly on the uppermost surface of the boulder, and the presence of soil and small cobbles between the boulder and the underlying bedrock. We sampled both the glacially polished underside of the boulder and the underlying bedrock with which it was in contact, along with a nearby, exposed polished surface. The same age recorded on the underside of the boulder and the underlying bedrock (which we argue it has been overlying since the LGM) would indicate that there was no inheritance in the bedrock surface.

3.2 Methods

We isolated quartz by selectively dissolving other minerals in aqua regia, pyrophosphoric acid, and dilute HF/HNO_3 in an ultrasonic bath (e.g., Granger et al., 2001). Samples were dissolved in HF and HNO_3 and spiked with ~0.7 mg Be. Fluorides were eliminated by repeated fuming in H_2SO_4, and Be was purified by ion chromatography and selective hydroxide precipitation. BeO was prepared for accelerator mass spectrometry (AMS) and mixed with Ag. Measurements were made at PRIME Lab.

We assumed that spallogenic production scales with star production in emulsions, as described by Lal (1991), using the ^{10}Be/star production ratio of Stone (2000). We also considered muon production (Heisinger et al., 2002a; Heisinger et al., 2002b), although this proved to be a

minor component. We measured shielding of our samples at 30° azimuth intervals, and calculated shielding factors according to Dunne et al. (1999).

3.3 Results

Our calculated ^{10}Be ages are shown in Table 1 and Figure 4. We generally obtained ages younger than the last deglaciation, at or before ~15,000 ka (Benson et al., 1998; Clark and Gillespie, 1997). One sample, SHB-00-07, perhaps marginally predates deglaciation, but the resolution of the lake core records and the precision of the cosmogenic dating do not permit conclusive evidence of inheritance. Thus we do not see any clear evidence of inherited ^{10}Be. In general, more than ~2 m of material was eroded by the glaciers during the last glaciation. Calculated ages that postdate deglaciation probably reflect (early) removal of glacial sediment that initially buried the samples. The presence of glacial polish on the sampled bedrock means that the surfaces have not eroded significantly during the current interglacial. There is not a straightforward pattern to the distribution of calculated ^{10}Be exposure ages along the lengths of the valleys studied. Samples SHB-00-01A, -01B, and -01C represent the polished underside of a small boulder (~50cm diameter), the polished bedrock immediately beneath the boulder in situ, and a nearby, exposed polished bedrock surface, respectively. Samples SHB-00-01A and –01B returned the same ^{10}Be exposure age, within error, indicating that there is no pre-LGM inheritance in the bedrock surface. That sample SHB-00-01C also returned the same age suggests that it had a debris cover of similar thickness to the –01B boulder removed comparatively recently.

4. Discussion

We have not found any evidence for inheritance in the glaciated drainage basins of the eastern Sierra Nevada. This suggests that the alpine glaciers in this part of the Sierra Nevada have been sufficiently active to reset the cosmogenic clock, even in the ablation zone. This contrasts with the results of recent studies of erosion by ice sheets (Briner and Swanson, 1998; Harbor et al., 1999), and one study of alpine glaciation (Fabel and Harbor, 1999).

Our exposure ages slightly postdate the deglaciation of this part of the Sierra Nevada (Clark et al., 1995; Clark and Gillespie, 1997). The distribution of ages has a greater spread than

we would expect from measurement uncertainty alone. The spread must be due to the "geological" uncertainties of till, snow, etc., which will always make ages appear younger. The most likely causes for this are (a) the presence of snow cover since deglaciation, and (b) despite our efforts to avoid the problem, we were unable to avoid samples that were buried beneath a sole moraine for at least part of the postglacial history. While it is difficult to separate these two effects, we suggest that both have played an important role in the postglacial history of the eastern Sierra Nevada.

Many of our exposure ages cluster around 12.5 ka. If we assume that glaciation occurred at 15 ka, we have underestimated the age by ~17%. If we were to attribute this to snow cover, using a penetration length of 170 g/cm^2, this represents a mean annual average of ~31 cm (water equivalent) of snow, or ~93 cm if we assume that the snow is only present for 4 months of the year. For a typical Sierra Nevada snow density of ~0.35 g/cm^3, this equates to ~266 cm of snow. The California Department of Water Resources maintains a snow survey site at ~3100 m in Sawmill Creek, within the study area described here. Since 1926, mean April snow thickness has been 133±60 cm (48±24 cm water equivalent). Obviously snow thickness varies considerably on a regional basis and also on an annual basis, let alone over the Holocene. This simple calculation suggests that while significant, snow cover perhaps cannot completely account for our age underestimates, and that debris cover is also important. The one site where we come closest to the deglaciation age, in Red Mountain Creek, is also the most exposed site, and least likely to accumulate snow (or debris).

In considering the role of debris cover, our samples from Red Mountain and South Fork, Oak Creeks come closer to the time of deglaciation than those from Meysan Creek. This is consistent with the fact that the Red Mountain and South Fork, Oak Creeks samples were collected from bedrock rises somewhat above the modern stream, and would have been cleared of overlying sediment more rapidly than the Meysan Creek samples, which came from closer to the stream elevation. There is not a straightforward pattern to the distribution of calculated ^{10}Be exposure ages along the lengths of the valleys studied, suggesting that exposure-age dating does not have the resolution to isolate glacier retreat after the LGM, or a systematic pattern to the amounts of erosion beneath LGM glaciers. Instead local circumstances are more important.

In Meysan Creek, our field observations indicate that, although abrasion is certainly responsible for the glacial polish observed, the dominant mode of glacial erosion is

plucking/quarrying of exfoliating granite blocks, typically 30-50 cm thick. Given that our results suggest at least ~2 m of incision during the last glacial occupation, this suggests that at least 4-7 plucking events occurred during this time. Taking an estimate for the duration of the glaciation of ~11 ka (Benson et al., 1998), implies a maximum recurrence interval for plucking events of ~ 1.5-3 ka, and a minimum mean erosion rate of ~0.2 mm/yr. Alternatively, if we assume that all the erosion occurred during the most recent of the Tioga advances, with a duration of only ~2 ka (Phillips et al., 1990), we estimate a maximum recurrence interval of ~0.3-0.5 ka, and a minimum rate of ~1 mm/yr. The bedrock sampled in Red Mountain and South Fork, Oak Creeks, is fractured on a finer scale, so the plucking of joint blocks is less obvious. However, our minimum estimates for glacial incision rate remain the same. The calculated incision rate of ~0.2-1 mm/yr is comparable with estimates for the rate of offset on the range-bounding normal fault system (~0.2 mm/yr, Gillespie, 1982). This suggests that at least during the glaciation the mountains were either at topographic steady state, or perhaps in net decline, given that (i) this is a minimum estimate, and (ii) we hypothesise (Brocklehurst and Whipple, 2002) that there has been significantly greater glacial erosion at higher elevations.

Briner and Swanson (1998) also found quarrying to be sufficiently fast to reset the cosmogenic clock during the last glaciation; only in those areas eroding solely by abrasion did they find inheritance. This suggests that in areas where plucking is active, incision rates will generally exceed ~0.2 mm/yr. Furthermore, given that we sought those sites most likely to exhibit inheritance in this setting, we suggest that special circumstances are required for exceptionally slow erosion rates beneath temperate valley glaciers. Restriction to solely abrasion, particularly in the absence of concentrated abrasive material, seems to be one possibility (Briner and Swanson, 1998). This may be possible in situations where there is minimal subglacial water and therefore not the potential for the water pressure fluctuations that are thought necessary for efficient plucking (Hallet, 1996), or alternatively if the bedrock is resistant to fracture. Alternatively, freezing of ice to the basal bedrock (e.g., Harbor et al., 1999) may limit glacial erosion rates. Both of these circumstances are more likely to be found in either high latitude mountain belts or beneath continental-scale ice sheets than in temperate alpine glaciers.

Previous work, in which a locally-calibrated fluvial erosion model was used to simulate what the landscape might look like now had glaciers never developed, suggested that, in small, glaciated basins in the Sierra Nevada, glaciers have incised little below the mean Quaternary

ELA (Brocklehurst and Whipple, 2002). However, the cosmogenic isotope test presented here did not have sufficient resolution to isolate this region of reduced incision from the remainder of the valley profile. In other words, if we had found inheritance, this would have strongly supported the findings of the simulation study. The lack of inheritance, however, does not reject the hypothesised reduction in incision rate, because we cannot resolve the thickness required to reset the cosmogenic clock (< 2 m) on the scale of our simulated longitudinal profiles (relief > 2000 m). There is no question that small glaciers have modified the landscape far more significantly above the mean Quaternary ELA.

Conclusion

We have sought inheritance in bedrock exposure age dating in the temperate alpine glacial setting by selecting sites in the valley floor of eastern Sierra Nevada drainages that were the most likely candidates for inheritance. However, all of our measured surface exposure ages postdate the most recent deglaciation, and so we see no evidence of inheritance. We suggest that inheritance will only be a problem in cases where ice is frozen to the bed, or in settings where plucking is not active, for example if the lithology is extremely resistant to fracture, or there is insufficient variation in basal water pressure to drive fracturing. We caution that postglacial snow and debris cover may be far more important factors in interpreting cosmogenic exposure ages as deglaciation ages in alpine glacial settings.

Acknowledgements

This work was supported by NSF grant EAR-9980465 (to KXW/DEG), a NASA Graduate Fellowship (to SHB), and a GSA Fahnestock Award (to SHB). We would like to thank Jason Gulley for assistance with sample preparation, and the staff at PRIME Lab.

Figure captions

Fig. 1. Shaded relief map of the eastern Sierra Nevada, showing the locations of our sample sites.

Fig. 2. Longitudinal profiles of the sampled basins, illustrating sample locations each of the valleys. (a) Meysan Creek, tributary to Lone Pine Creek. (b) Red Mountain Creek. (c) South Fork, Oak Creek.

Fig. 3. Field photos of sample sites. (a) Sample SHB-00-01, Meysan Creek. Main picture shows the sampled boulder (see text) in situ prior to sampling. Inset: (top) the underside of the boulder, and (bottom) the bedrock surface beneath the boulder. (b) SHB-00-08, Red Mountain Creek. (c) SHB-00-12, South Fork, Oak Creek.

Fig. 4. Calculated ^{10}Be age versus elevation for each of the sampled catchments. Errors shown are purely analytical. There is not a systematic pattern to the ages versus elevation, indicating that this technique cannot resolve glacier retreat. Samples in Red Mountain and South Fork, Oak Creeks have generally been exposed for longer than samples in Meysan Creek.

Table 1. Summary of cosmogenic isotope data. Production rates, shielding factors, etc., calculated as noted in text. Errors indicated are purely analytical.

Sample	Basin	Elevation (km)	^{10}Be age (ka)
SHB-00-01A	Meysan	3.04	10.9±0.4
SHB-00-01B	Meysan	3.04	10.0±0.4
SHB-00-01C	Meysan	3.04	10.6±0.4
SHB-00-02A	Meysan	3.30	9.5±0.3
SHB-00-02C	Meysan	3.30	12.4±0.3
SHB-00-04	Meysan	3.09	12.6±0.4
SHB-00-05	Meysan	2.94	9.4±0.6
SHB-00-06	Meysan	2.77	11.2±0.5
SHB-00-07	Red Mountain	2.89	11.2±0.5
SHB-00-08	Red Mountain	3.11	14.5±0.4
SHB-00-09	Red Mountain	2.82	13.6±0.5
SHB-00-11	South Fork, Oak	2.76	12.2±0.8
SHB-00-12	South Fork, Oak	2.89	11.7±0.6

References

Bateman, P. C., 1965, Geology and Tungsten Mineralization of the Bishop District, California, U.S. Geological Survey Professional Paper, 208 p.

Benson, L. V., May, H. M., Antweiler, R. C., Brinton, T. I., Kashgarian, M., Smoot, J. P., and Lund, S. P., 1998, Continuous Lake-Sediment Records of Glaciation in the Sierra Nevada between 52,600 and 12,500 ^{14}C yr B.P.: Quaternary Research, v. 50, p. 113-127.

Bierman, P. R., 1994, Using in situ produced cosmogenic isotopes to estimate rates of landscape evolution: A review from the geomorphic perspective: Journal of Geophysical Research, v. 99, p. 13885-13896.

Bierman, P. R., Larsen, P., Clapp, E., and Clark, D. H., 1996, Refining estimates of 10Be and 26Al production rates: Radiocarbon, v. 38, no. 1, p. 149.

Blackwelder, E., 1931, Pleistocene glaciation in the Sierra Nevada and Basin ranges: Geological Society of America Bulletin, v. 42, p. 865-922.

Briner, J. P., and Swanson, T. W., 1998, Using inherited cosmogenic 36Cl to constrain glacial erosion rates of the Cordilleran ice sheet: Geology, v. 26, p. 3-6.

Brocklehurst, S. H., and Whipple, K. X., 2002, Glacial Erosion and Relief Production in the Eastern Sierra Nevada, California: Geomorphology, v. 42, no. 1-2, p. 1-24.

-, in prep., Rates of glacial erosion in the ablation zone: evidence from fluvial landscape simulation.

Clark, D. H., Bierman, P. R., and Larsen, P., 1995, Improving in Situ Cosmogenic Chronometers: Quaternary Research, v. 44, p. 367-377.

Clark, D. H., and Gillespie, A. R., 1997, Timing and significance of late-glacial and Holocene cirque glaciation in the Sierra Nevada, California: Quaternary International, v. 38-39, p. 21-38.

Dunne, J., Elmore, D., and Muzikar, P. F., 1999, Scaling factors for the rates of production of cosmogenic nuclides for geometric shielding and attenuation at depth on sloped surfaces: Geomorphology, v. 27, p. 3-11.

Fabel, D., and Harbor, J., 1999, The use of in-situ produced cosmogenic radionuclides in glaciology and glacial geomorphology: Annals of Glaciology, v. 28, p. 103-110.

Gillespie, A. R., 1982, Quaternary Glaciation and Tectonism in the Southeastern Sierra Nevada, Inyo County, California [PhD thesis]: California Institute of Technology, 695 p.

Gosse, J. C., and Phillips, F. M., 2001, Terrestrial in situ cosmogenic nuclides: theory and application: Quaternary Science Reviews, v. 20, no. 14, p. 1475-1560.

Granger, D. E., Riebe, C. S., Kirchner, J. W., and Finkel, R. C., 2001, Modulation of erosion on steep granitic slopes by boulder armoring, as revealed by cosmogenic ^{26}Al and ^{10}Be: Earth and Planetary Science Letters, v. 186, p. 269-281.

Hallet, B., 1996, Glacial quarrying: a simple theoretical model: Annals of Glaciology, v. 22, p. 1-8.

Harbor, J., Fabel, D., Stroeven, A., and Elmore, D., 1999, Constraining erosion rates under the Fennoscandian ice sheet; new evidence from cosmogenic isotopes: Abstracts with Programs - Geological Society of America, v. 31, no. 7, p. 48.

Heisinger, B., Lal, D., Jull, A. J. T., Kubik, P. W., Ivy-Ochs, S., Knie, K., and Nolte, E., 2002a, Production of selected cosmogenic radionuclides by muons: 2. Capture of negative muons: Earth and Planetary Science Letters, v. 200, p. 357-369.

Heisinger, B., Lal, D., Jull, A. J. T., Kubik, P. W., Ivy-Ochs, S., Neumaier, S., Knie, K., Lazarev, V., and Nolte, E., 2002b, Production of selected cosmogenic radionuclides by muons: 1. Fast muons: Earth and Planetary Science Letters, v. 200, p. 345-355.

Horn, L. L., Dahms, D., James, A., Harbor, J., and Elmore, D., 1996, Reconstructing spatial patterns of glacial erosion; a new approach using cosmogenic radionuclides: Abstracts with Programs - Geological Society of America, v. 28, no. 7, p. 56.

Lal, D., 1991, Cosmic ray labeling of erosion surfaces: in situ nuclide production rates and erosion models: Earth and Planetary Science Letters, v. 104, p. 424-439.

Molnar, P., and England, P., 1990, Late Cenozoic uplift of mountain ranges and global climate change: chicken or egg?: Nature, v. 346, p. 29-34.

Moore, J. G., 1963, Geology of the Mount Pinchot Quadrangle, Southern Sierra Nevada, California, US Geological Survey Bulletin, 152 p.

-, 1981, Geologic map of the Mount Whitney Quadrangle, Inyo and Tulare Counties, California, US Geological Survey Map.

Nishiizumi, K., Winterer, E., Kohl, C., Klein, J., Middleton, R., Lal, D., and Arnold, J., 1989, Cosmic ray production rates of 10^Be and 26^Al in quartz from glacially polished rocks: Journal of Geophysical Research, v. 94, no. B12, p. 17,907-17,915.

Phillips, F. M., Zreda, M. G., Benson, L. V., Plummer, M. A., Elmore, D., and Sharma, P., 1996, Chronology for Fluctuations in Late Pleistocene Sierra Nevada Glaciers and Lakes: Science, v. 274, p. 749-751.

Phillips, F. M., Zreda, M. G., Smith, S. S., Elmore, D., Kubik, P. W., and Sharma, P., 1990, Cosmogenic Chlorine-36 Chronology for Glacial Deposits at Bloody Canyon, Eastern Sierra Nevada: Science, v. 248, p. 1529-1532.

Porter, S. C., 1989, Some Geological Implications of Average Quaternary Glacial Conditions: Quaternary Research, v. 32, p. 245-261.

Raymo, M. E., and Ruddiman, W. F., 1992, Tectonic forcing of late Cenozoic climate: Nature, v. 359, p. 117-122.

Stone, J. O., 2000, Air pressure and cosmogenic isotope production: Journal of Geophysical Research, v. 105, no. B10, p. 23753-23759.

Stone, P., Dunne, G. C., Moore, J. G., and Smith, G. I., 2001, Geologic Map of the Lone Pine 15' Quadrangle, Inyo County, California: U.S. Geological Survey Geologic Investigations Series, v. I-2617, p. Online version 1.0.

Whipple, K. X., Kirby, E., and Brocklehurst, S. H., 1999, Geomorphic limits to climate-induced increases in topographic relief: Nature, v. 401, p. 39-43.

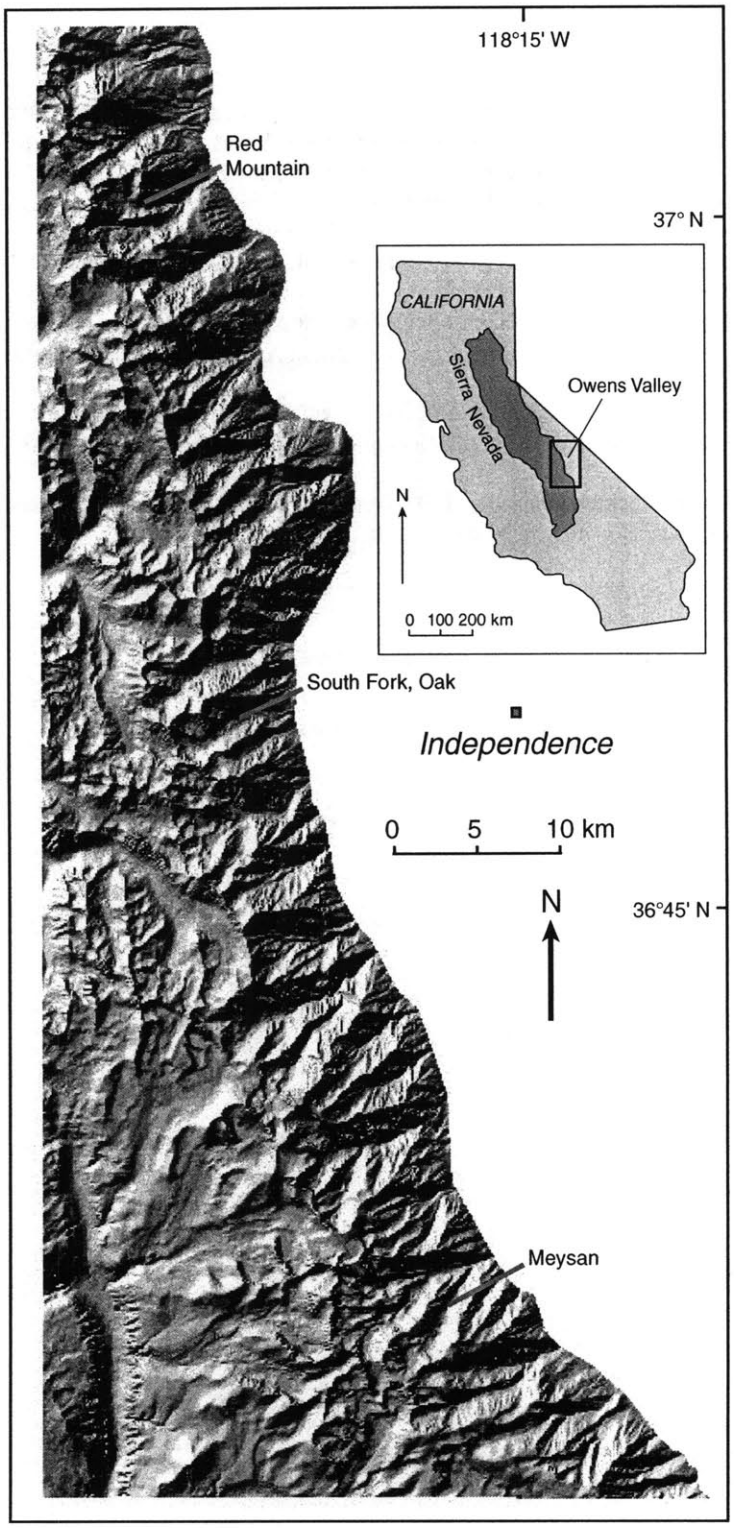
118°15' W
Red
Mountain
37° N
CALIFORNIA
Sierra Nevada
Owens Valley
N
0 100 200 km
South Fork, Oak
Independence
0 5 10 km
N
36°45' N
Meysan

Fig. 1

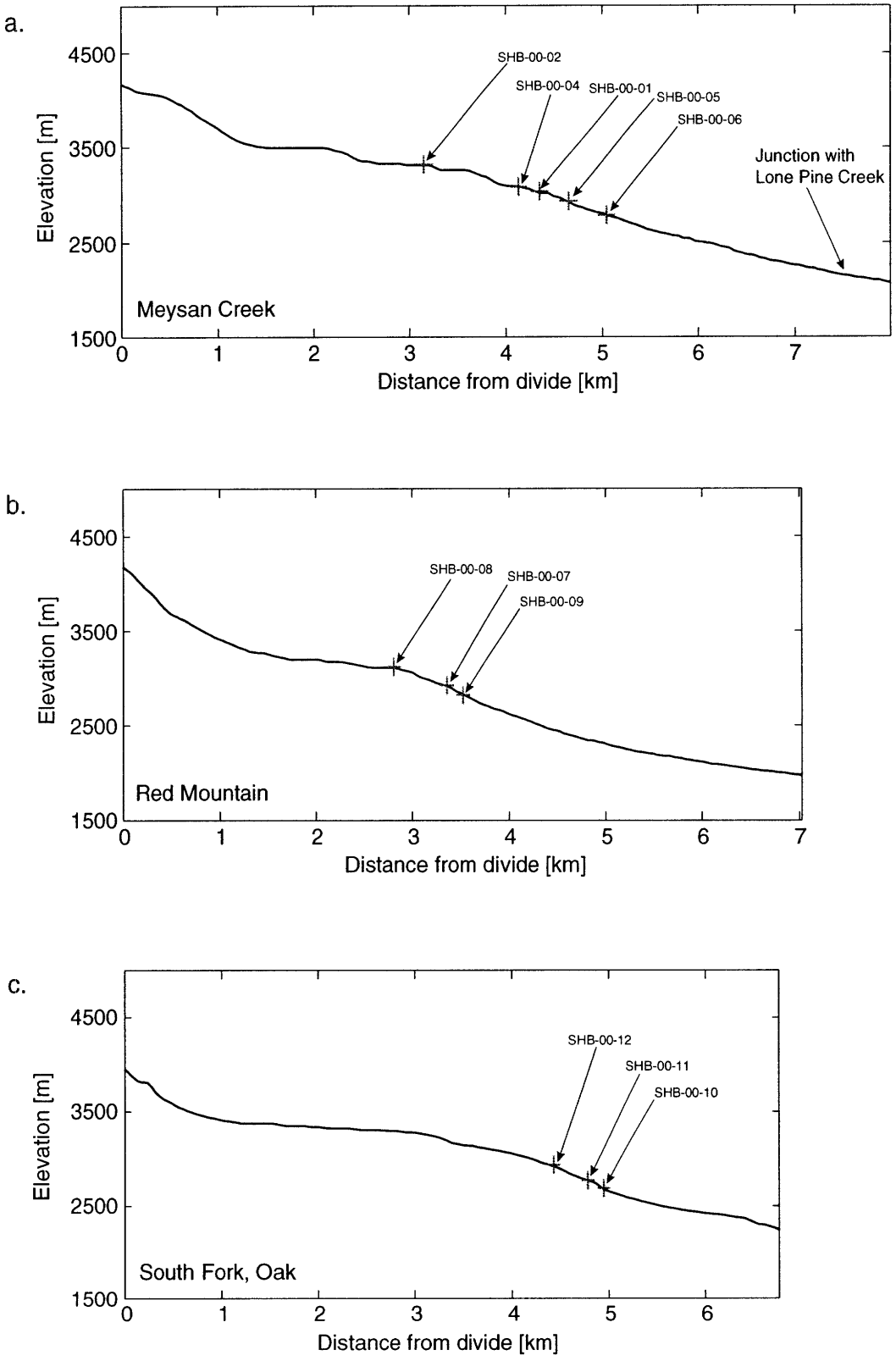
a.
SHB-00-02
SHB-00-04
SHB-00-01
SHB-00-05
SHB-00-06
Junction with
Lone Pine Creek
Meysan Creek
Elevation [m]
Distance from divide [km]
b.
SHB-00-08
SHB-00-07
SHB-00-09
Red Mountain
Elevation [m]
Distance from divide [km]
c.
SHB-00-12
SHB-00-11
SHB-00-10
South Fork, Oak
Elevation [m]
Distance from divide [km]

Fig. 2

Fig. 3a

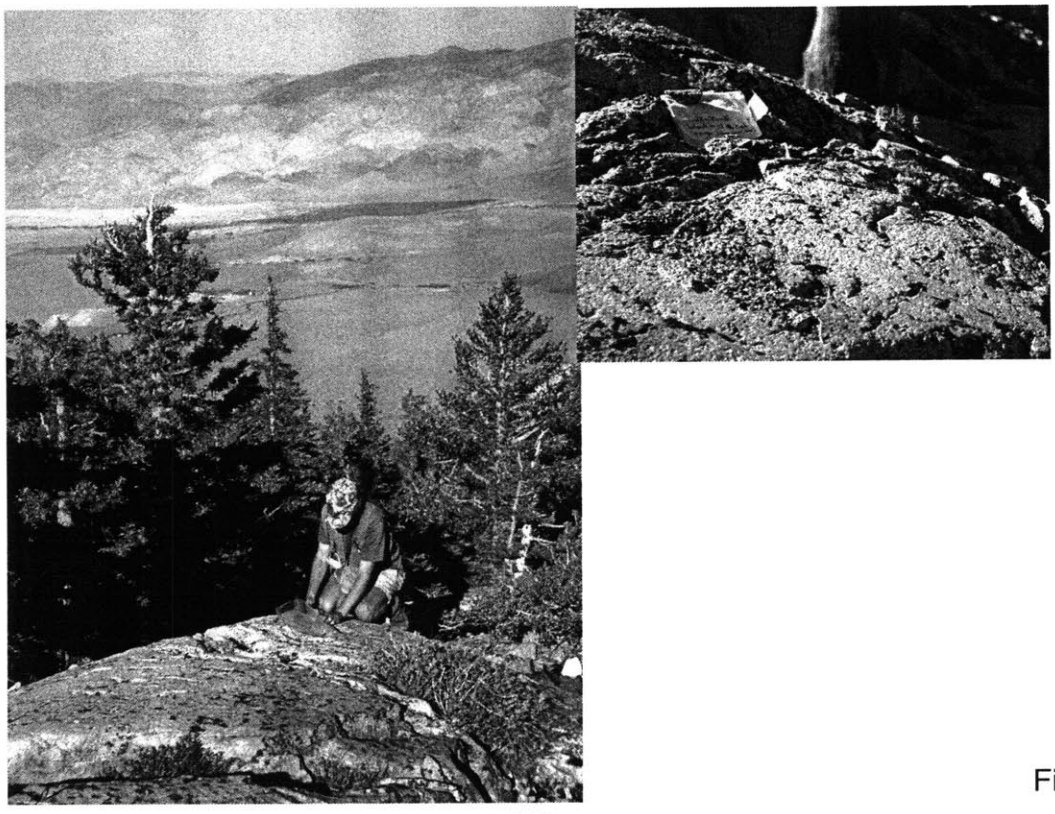

Fig. 3b

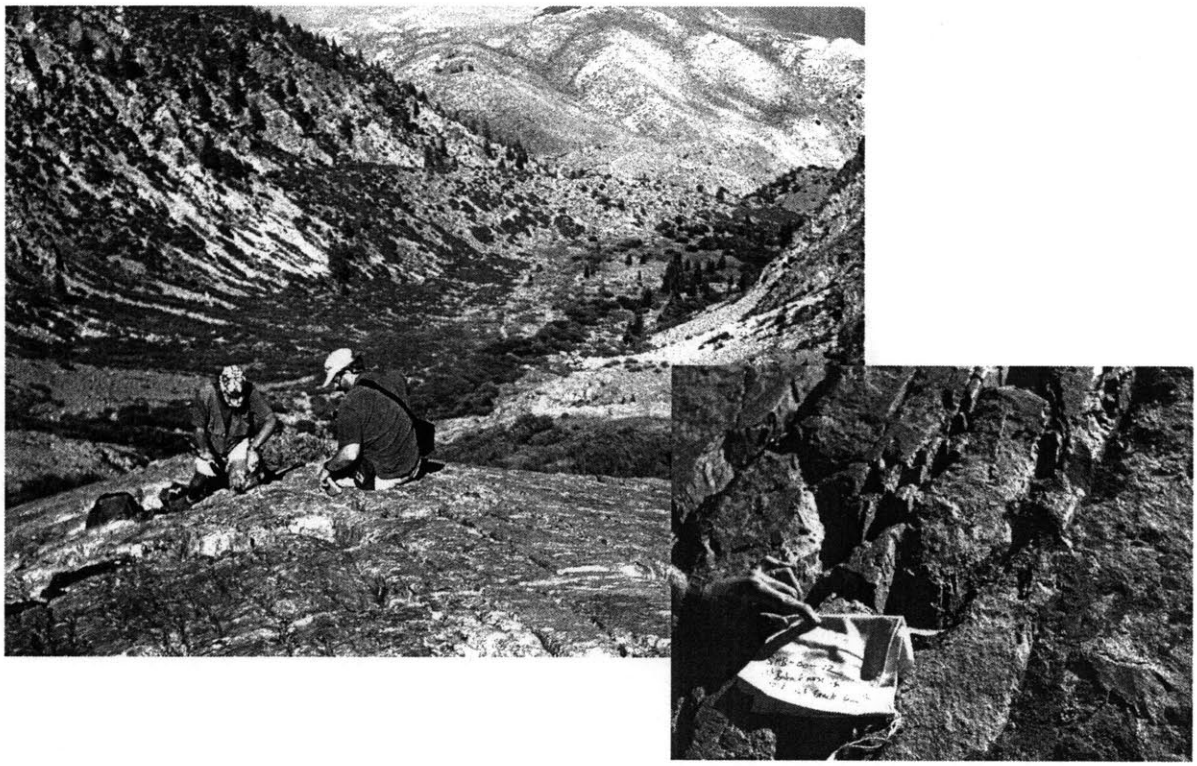

Fig. 3c

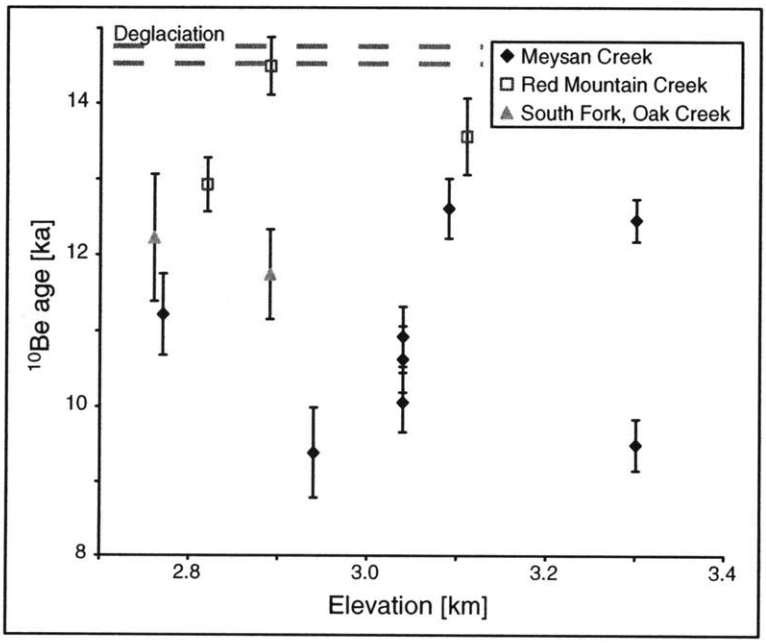
Deglaciation
Meysan Creek
Red Mountain Creek
South Fork, Oak Creek
^{10}Be age [ka]
14
12
10
8
2.8
3.0
3.2
3.4
Elevation [km]

Fig. 4

Chapter 6

Implications of Old Glaciated Surfaces at High Elevations in the Sierra Nevada, California

Simon H. Brocklehurst*

Department of Earth, Atmospheric and Planetary Sciences, Massachusetts Institute of Technology, Cambridge MA 02139, USA

Darryl E. Granger

Department of Earth and Atmospheric Sciences, Purdue University, West Lafayette IN 47907, USA

Kelin X. Whipple

Department of Earth, Atmospheric and Planetary Sciences, Massachusetts Institute of Technology, Cambridge MA 02139, USA

Prepared for submission to *Geology*

* to whom correspondence should be addressed: email: shb@mit.edu, fax: 1-617-252-1800

ABSTRACT

We propose that widespread, enigmatic, old surfaces near the crest of the Sierra Nevada represent former glacial valley floors. Field observations indicate that some of the boulders present amongst the diamict on these surfaces must have been carried into their current position by glaciers. Cosmogenic isotope dating supports qualitative field evidence that the deposits on these low relief surfaces are of varying ages. Both modelling studies and field evidence have shown that glacial headwall erosion is an important process. Thus we infer that the glacial drainages of the eastern Sierra Nevada are subject to a cycle of drainage capture and relief inversion events, similar to the evolution of fluvial drainage networks. These processes produce diamict-covered surfaces at various stages of evolution from clearly U-shaped forms to stranded, flatter surfaces at the range crest. We suggest that this continued process of reorganisation of the drainage network might limit major relief production by glaciers.

Keywords: relief inversion, glacial erosion, summit flats

INTRODUCTION

A detailed understanding of the evolution of relief in glaciated mountain ranges is an essential step in testing hypotheses relating global cooling and mountain uplift (e.g., Molnar and England, 1990; Raymo et al., 1988; Small and Anderson, 1995, 1998; Whipple et al., 1999). Molnar and England (1990) suggested that relief production by glaciers is potentially a major contributor to late Cenozoic uplift of mountain peaks, although Small and Anderson (1998) demonstrated only modest relief production by glaciers in the Wind River Range. Both of these studies focussed on changes in relief due to vertical incision. Here we emphasise that the reorganisation of drainage networks in glaciated landscapes could also play a key role in the development of relief in glaciated landscapes. Furthermore, both the transition from fluvial to glacial erosion, and the subsequent continued development of the glacial system, are crucial. Brocklehurst and Whipple (2002) focussed on the former, demonstrating that both relief production and relief reduction processes due to glacial erosion (Whipple et al., 1999) have been active in the Sierra Nevada; here we focus on the latter.

A surprisingly common feature of glaciated mountain ranges is the presence of isolated patches of low relief topography near the crest of the range, amongst the more common arêtes and horns (e.g., Anderson, 2002). These low relief surfaces are commonly known as summit flats, and have been identified throughout glaciated mountain ranges in the western U.S. (e.g., Anderson, 2002; Small et al., 1997) and in the Himalayas (e.g., Bishop and Shroder, 2000; Shroder et al., 1993). Of those studied by Small et al. (1997), only those in the Sierra Nevada exhibit evidence of prior glaciation, in the form of glacial striations and erratic boulders (Gillespie, 1982), as opposed to the larger surfaces, featuring numerous tors and dominated by in situ weathering, described by Small et al. (1997) in the Wind River, Beartooth and Front Ranges. Summit flats in the Sierra Nevada (Fig. 1) are generally one of two types; larger surfaces with widespread exposure of striated bedrock that clearly reflect transfluent ice flow during glaciations (e.g. Taboose Pass, Gillespie, 1982), and smaller surfaces covered in debris, occasionally showing the contact with the underlying bedrock, and often high above modern glacial valley floors. We focus on the smaller summit flats, and suggest that they provide important evidence of the evolution of the drainage network in glaciated environments.

Given the preservation of diamict on these low relief surfaces, including striated boulders (Gillespie, 1982), and the common, but subtle, U-shaped cross-section on many of them, we

suggest that these surfaces were at one time located in the valley floor. The process whereby a former valley bottom becomes a ridge, bounded by newly formed valleys on each side, is referred to as either relief inversion (e.g., Pain and Ollier, 1995) or topographic inversion (e.g., Hasbargen and Paola, 2000). Prior work has tended to focus on fluvial landscapes. Pain and Ollier (1995) suggest that inversion of relief occurs only when materials on valley floors are, or become, more resistant to erosion than the adjacent valley slopes. In their experimental drainage basins cut into homogeneous material, Hasbargen and Paola's (2000) topographic inversion occurs when streams migrate to occupy former ridge locations.

Drainage capture refers to the process whereby headward erosion by one stream allows it to extend into the watershed of a neighbour, and thus "capture" drainage area from it (e.g., Bishop, 1995; Clark et al., submitted; Schumm, 1977). It is plausible that a single event, related to the opening of the Owens Valley, caused a one-time rearrangement of the drainage network of the eastern Sierra Nevada, from the network related to the summit flats, to the current drainage network (Eric Small, pers. comm.). However, we favour the hypothesis that the eastern Sierra Nevada drainage network represents an ongoing cycle of drainage captures, relief inversions, and degrading summit flats, driven by glacial erosion. This is supported by (i) modelling and topographic analyses suggesting that headwall erosion by glaciers is an important process in the Sierra Nevada (Brocklehurst and Whipple, 2002); (ii) field evidence for numerous diamict-covered, low-relief surfaces of various apparent ages at the crest of the Sierra Nevada; and (iii) cosmogenic isotope analyses that demonstrate the different ages of two such developing surfaces.

EVIDENCE FOR HEADWALL EROSION

Brocklehurst and Whipple (2002) used a locally-calibrated fluvial landscape evolution model to simulate how the drainage basins of the eastern Sierra Nevada might look now had glaciers never developed. Glaciers have been responsible for both downward erosion in the higher reaches of glaciated drainage basins, and considerable amounts of headward erosion and drainage basin extension, at rates up to ~1 mm/yr faster than would have been achieved by rivers.

Figure 2 illustrates the same technique of fluvial landscape simulation applied to two drainage basins of interest here. The method for estimating glacial headwall erosion, described in

more detail by Brocklehurst and Whipple (2002), exploits the fact that glaciers apparently do not significantly modify the lower reaches of the basin from a typical concave fluvial profile. We adjust the length of the simulated fluvial profile, keeping the outlet position fixed, until we achieve a close match between the simulated and observed profiles in the lower half of the basin. The amount of shortening of the fluvial profile required equates to the extra headward erosion attributable to glacial erosion, which is supported by independent evidence (Brocklehurst and Whipple, 2002). We argue below that Sardine Canyon (Fig. 2a) has been beheaded by the Golden Trout Lakes tributary to Independence Creek (Fig. 2b). The observed longitudinal profile for Sardine Canyon emphasises the lack of a headwall at the crest of the basin. The simulated profile for the whole length of the basin dramatically undercuts the observed topography. Our preferred interpretation is that if the basin were sculpted only by fluvial erosion, it would be shorter, i.e., there was considerable headward erosion by the glacier that occupied the full extent of Sardine Canyon before it was beheaded. However, in this case the situation is complicated by the change in drainage area caused by beheading, and the lack of a headwall. The new cirque developing beneath the flat, uppermost part of Sardine Canyon (e.g., Gillespie, 1982) is also seen clearly in the longitudinal profile. Our method indicates that the tributary to Independence Valley lying directly beneath the current head of Sardine Canyon has cut headward ~1.5 km further than it would have done under fluvial conditions (Fig. 2b).

FIELD OBSERVATIONS

The summit flats shown in Figure 1 were predominantly identified from stereo pairs of aerial photographs. We concentrate on those surfaces that do not exhibit clear evidence of transfluent ice flow during glaciation. Features common to these summit flats include a covering of diamict, a shallow surface slope, and in many instances, a subtle U-shaped cross section. However, these surfaces encompass a spectrum from tiny, isolated patches surrounded on almost all sides by steep cliffs (e.g., University Peak), to broad, sediment-laden valley floors with higher topography on some sides (e.g., Sardine Canyon).

Figure 3 illustrates the surface on the northeast ridge of University Peak. Gillespie (1982) described the contact shown, diamicton overlying the Bullfrog quartz monzonite, as a very sharp boundary, with silt, sand and boulders directly overlying a smooth rock surface. This contrasts with the gradational contact zone expected for nivated surfaces or felsenmere (i.e., in situ

weathering, Anderson, 2002; Matthes, 1900; Small et al., 1997), and suggests a depositional origin for the diamicton. Gillespie (1982) reported signs of polish and fluting, with an orientation of 064° (between the current trends of Onion Valley and its Robinson Lake tributary, which bound the northeast ridge of University Peak), that represents a water-worn or glaciated surface subsequently modified by wind erosion. Finally, the smooth arête rising towards University Peak, characterised by deeply eroded joints in striking contrast to the more freshly plucked cliffs on either side, may represent a remnant of an ancient glacially sculpted valley wall, related perhaps to the interpreted valley floor below.

Our field mapping has focussed on surfaces that perhaps more clearly represent former valley floors. We carried out careful mapping of the float and collected samples for cosmogenic isotope dating from two surfaces, at the head of Sardine Canyon, and at Baxter Pass, as shown in Figure 1. In addition, Small et al. (1997) collected cosmogenic isotope samples from the summit flat adjacent to Lone Pine Peak.

The head of Sardine Canyon has long been regarded as something of an enigma (Gillespie, 1982). As shown in Figure 4, the valley head exhibits a U-shaped cross-sectional form typical of many glaciated valleys. However, the floor is covered in a thick layer of gruss and occasional large boulders, and there is no headwall at the head of the valley. Instead, a near-vertical cliff plunges down to the Golden Trout Lake basin to the west, a drop of some 300m, suggesting that Sardine Canyon has been beheaded. The contact between the diamicton and the underlying granodiorite bedrock is sharp, similar to that on University Peak. The bedrock surface ramps up at the head of the valley, reflecting either the eroded head of the canyon having been only a little further to the west, or a step in the prior glacial valley floor. Given the thickness of the diamict layer (up to 20 m) and the degree of grussification (very few larger boulders remain), it seems clear that the upper part of this basin was not occupied with flowing ice during the last glaciation. As noted by Gillespie (1982), the absence of any trace of a stream channel and the abundance of clay and mud suggest this part of Sardine Canyon represents a nivated valley (Matthes, 1900), i.e., it was modified only by snow rather than ice during recent glaciation.

It could be argued that the majority of the sediment lining the valley floor has a colluvial origin, as the fractured bedrock of the valley walls is clearly descending into the valley. Indeed, a distinct line down the centre of the valley separates the colluvium derived from either side of the valley. However, at the highest point on the diamict-covered valley floor, at the top of the cliffs

rising from the Golden Trout Lake basin, we found several conspicuous boulders of a striking white biotite leucogranite (Fig. 5a), that careful mapping of the valley walls demonstrated was not derived from the current confines of Sardine Canyon. Instead the same leucogranite was found in a small outcrop partway down the cliff descending into the Golden Trout Lakes basin, and in the float on both sides of this basin (Fig. 4). The outcrop below Sardine Canyon was in the form of a small, subvertical, dyke surrounded by more widespread country rock, both pink granite and grey granodiorite (Fig. 6). The leucogranite boulders at the top of Sardine Canyon also displayed smooth, occasionally striated, undersides, suggesting glacial transport, and many protruded upright from the gruss. Uneven, 'crenulation' weathering further suggested that the boulders were weathered at the surface, rather than being weathered at depth and more recently exhumed. Thus we deduced that this sample was an erratic carried to its present position at some time prior to beheading of the valley. However, we did not find the erratic lithology in outcrop at an elevation above the crest of Sardine Canyon, and thus we cannot pinpoint precisely where the boulders might have come from. We collected samples of several of the erratic boulders at the head of the valley for ^{10}Be exposure-age dating, to determine a minimum age for the timing of the event that beheaded Sardine Canyon. In addition, we collected a sample from a heavily weathered, wide, flat, stable boulder in the centre of the valley floor just downhill of the valley head (Fig. 5b). This boulder lay in the widest, flattest part of the valley floor, apparently out of reach of the typical colluvial deposits that cover the remainder of the valley.

Just to the north of Baxter Pass, a similar low relief surface is present, again covered with a thick layer of diamicton, and apparently undermined by a small, unnamed cirque glacier that developed on the south side of the Baxter Lakes (Fig. 7). A very limited exposure of jointed bedrock on the northern side of the surface makes a subvertical contact with the diamicton that caps the remainder of the ridge. Ice on this surface here may still connect with the ice below during times of glaciation. The Baxter Pass surface is characterised by a much coarser deposit, comprising a blanket of only slightly weathered boulders up to 2 m in diameter, with no gruss. Furthermore, the undermining valley is much smaller, narrower and less well established than the Golden Trout Lakes basin. We surmise that this surface is still in the process of being abandoned as an active glacial valley floor, making it considerably younger than the head of Sardine Canyon, and perhaps in a different stage of its evolution. Again we collected samples of erratic boulders for exposure-age dating, to test the hypothesis that this surface is considerably

younger than that at the head of Sardine Canyon. The sampled boulders are believed to be erratic because the lithologies were not identified in the bedrock of the hillsides rising above the surface.

COSMOGENIC DATING

Samples SHB-01-20, SHB-01-21 and SHB-01-22 were taken from the erratic boulders at the head of Sardine Canyon, and sample SHB-01-28 from the large, flat boulder just downvalley of this. Samples SHB-01-29, SHB-01-30 and SHB-01-31 come from erratic boulders on the surface just north of Baxter Pass. The samples were taken from flat areas not subject to either erosion or transport. We suggest that both surfaces are on the way to becoming summit flats, and thus are earlier in their evolution than the University Peak surface (Fig. 3). In each case we selected boulders that had neither spalled nor rotated recently, and collected samples from the top surface, to a depth of 2-4 cm (see Table 1). We isolated quartz by selectively dissolving other minerals in aqua regia, pyrophosphoric acid, and dilute HF/HNO_3 in an ultrasonic bath (e.g., Granger et al., 2001). Samples were dissolved in HF and HNO_3 and spiked with ~0.7 mg Be. Fluorides were eliminated by repeated fuming in H_2SO_4, and Be was purified by ion chromatography and selective hydroxide precipitation. BeO was prepared for accelerator mass spectrometry (AMS) and mixed with Ag. Measurements were made at PRIME Lab.

We assumed that spallogenic production scales with star production in emulsions, as described by Lal (1991), using the ^{10}Be/star production ratio of Stone (2000). We also considered muon production (Heisinger et al., 2002a; Heisinger et al., 2002b), although this proved to be a minor component. Given that our samples are all within 2-4 cm of the surface, the mean production rate experienced by the sample as a whole is within a few percent of the surface production rate. We measured shielding of our samples at 30° azimuth intervals, and calculated shielding factors according to Dunne et al. (1999).

The results are shown in Table 1. We show effective ages, assuming zero erosion, and nominal erosion rates, assuming steady erosion. We report only the analytical error, not errors associated with uncertainties in the production rate, etc. The erratic boulders at the top of Sardine Canyon have ^{10}Be ages that correspond very closely to Tioga deglaciation at ~15 ka (Benson et al., 1998; Clark and Gillespie, 1997). This age is surprisingly young given that the boulders have clearly experienced glacial transport, and yet the uppermost reaches of Sardine Canyon are very

unlikely to have developed a cirque glacier during Tioga times. We suggest that the young ages relate to removal of material associated with cliff retreat in the neighbouring Golden Trout Lake basin. Cliff retreat is clearly active, as evidenced by the large volumes of talus, and the boulders lie very close to this cliff (Fig. 5). The boulders may well have been exhumed as the deposit that they lie in was undermined. Perhaps processes associated with nivation, i.e., the presence of permanent snow in the upper part of Sardine Canyon, enhanced the rate of periglacial creep in the diamict, thus exhuming the glacially-transported, but previously buried, boulders around the time of deglaciation. Alternatively, the periglacial processes acting on the cliff-face may have been more effective during the glaciation, undermining the overlying diamict and exhuming these boulders. This exhumation of glacially-transported boulders suggests that excavating a boulder for burial age determination would provide a better estimate for the abandonment of the cirque. The large, stable boulder in Sardine Canyon has an effective ^{10}Be age that is significantly older. We feel that this age is a truer reflection of the time since a cirque glacier occupied the upper part of the valley. The nominal erosion rate is also comparable to the rate at which phenocryst relief is produced on freshly deglaciated bedrock surfaces, ~2 cm since the Tioga deglaciation. The age of SHB-01-28 is also very much comparable with the effective ages of ~200 ka determined by Small et al. (1997) for boulders on a summit flat adjacent to Lone Pine Peak, just to the south of the samples described here (although the focus of the study by Small et al. (1997) was to estimate erosion rates rather than ages on these surfaces). It may be that this is the age at which saturation is achieved, i.e., equilibrium between isotope production and removal by either radioactive decay or weathering. The two effective ^{10}Be ages from Baxter Pass both predate Tioga deglaciation, but are also significantly younger than the large boulder in Sardine Canyon.

DISCUSSION

Combining our observations with those of prior workers (e.g., Gillespie, 1982), we argue that at least some of the old surfaces at the crest of the Sierra Nevada represent abandoned palaeo-glacial valley floors, and thus indicate that topographic inversion has occurred. Furthermore, both qualitative evidence and cosmogenic isotope dating indicate that the materials deposited on these surfaces have varying ages. In addition, we have previously demonstrated (Brocklehurst and Whipple, 2002) that headwall erosion by glaciers is an active process in the

Sierra Nevada. Thus we conclude that these old surfaces represent a continuing cycle of drainage capture, relief inversion, and degradation (as outlined below), rather than a single drainage reorganisation event. Glaciated landscapes thus exhibit dynamic drainage reorganisation processes similar to those observed in fluvial systems.

We suggest the following model for the evolution of these high, diamict-covered surfaces, from their proposed former state as a glacial valley floor, to their ultimate state as an isolated, low-relief surface at the range crest. In the first stage, a cirque is abandoned. An apparently common process is beheading of drainage basins by headward migration of younger, lower glacial valleys. This is in progress just north of Baxter Pass. Once beheaded, in the absence of a cirque glacier, the remnants of the cirque will gradually fill as periglacial weathering and rockfall erode the valley walls. As this fill continues to accumulate in the valley, relief and downvalley gradient will decrease, and it will become increasingly likely that any snow that accumulates will form a stagnant ice patch rather than a flowing glacier. This represents the current situation in Sardine Canyon. In the absence of glacial, fluvial or landsliding processes, erosion will be primarily due to periglacial creep. Thus there will not be an effective mechanism for transporting the debris from the valley. Meanwhile, continued valley widening in the neighbouring, active valleys will undermine the former valley floor, such that it will become an isolated high, completing the topographic inversion. However, given the extremely low relief on such surfaces, they are likely to be quite stable and long-lived, eroded only at the margins by diffusive processes or undermining due to cliff retreat, and upon the surface by weathering. This represents the current state of the surface just northeast of University Peak.

This demonstration of relief inversion in the Sierra Nevada, as opposed to the recent development of a 'new' drainage network incised at the expense of formerly low relief topography, suggests that it is unlikely that a large amount of relief has been developed by the onset of glacial erosion. This runs contrary to the expectations of Molnar and England (1990).

CONCLUSION

We have combined field observations, aerial photograph interpretation and cosmogenic dating to demonstrate the presence of former valley floors of different ages at the crest of the Sierra Nevada. We suggest that the occurrence of different-aged surfaces reflects continuing

processes of headwall erosion, drainage capture, and topographic inversion. Thus drainage capture and relief inversion are active processes in glacial landscapes, and processes other than tectonics can trigger drainage network rearrangement.

ACKNOWLEDGEMENTS

This work was supported by NSF grant EAR-9980465 (to KXW/DEG), a NASA Graduate Fellowship (to SHB), and a GSA Fahnestock Award (to SHB). We would like to thank Amy Draut, Karen Viskupic, Ryan Ewing, and Noah Snyder for assistance in the field, Jason Gulley for assistance with sample preparation, and the staff at PRIME Lab.

Figure captions

Fig. 1. Shaded relief map of a portion of the eastern Sierra Nevada, with high, low relief surfaces highlighted. Green indicates surfaces that had transfluent ice during the last glaciation, red indicates more isolated surfaces that did not. The sites described in the text lie just to the northeast of University Peak, at the head of Sardine Canyon, and immediately north of Baxter Pass. Note the widespread distribution of these old surfaces.

Fig. 2. Longitudinal profiles of (a) Sardine Canyon, and (b) the eastern fork of the Golden Trout Lakes basin. Observed longitudinal profile is shown in black, simulated fluvial longitudinal profile for the full length of the basin in light grey, and simulated profile shortened to match the lower part of the observed profile and thus evaluate headwall erosion in dark grey (see methodology in Brocklehurst and Whipple (2002)). Note the absence of a headwall in Sardine Canyon, and the development of a new cirque partway down the valley, at about 3250 m elevation. We predict considerable headward erosion in Sardine Canyon prior to its beheading. In the eastern fork of the Golden Trout Lakes basin, we predict around 1.5 km of headwall erosion in excess of what would have been achieved by fluvial erosion.

Fig. 3. Photograph of the ridgetop surface just to the northeast of University Peak, showing diamict directly overlying shallowly-dipping bedrock surface.

Fig. 4. 3-D oblique shaded relief view of the head of Sardine Canyon and Golden Trout Lakes basin, with location of the erratic boulders sampled in Sardine Canyon, the boulder sampled lower in Sardine Canyon, and locations of the erratic in outcrop and float in the Golden Trout Lakes basin.

Fig. 5. (a) Photograph of the erratic boulders at the crest of Sardine Canyon from which samples SHB-01-20, -01-21, and -01-22 were taken. (b) Photograph of the boulder lower in Sardine Canyon that sample SHB-01-28 was taken from. Main photograph shows the location of the boulder in the middle of a flat section of the valley floor, inset shows detail of the boulder.

Fig. 6. Photograph of the outcrop of the erratic lithology beneath the upper reaches of Sardine Canyon. Main picture shows the cliff beneath the head of Sardine Canyon. Sample site lies on the skyline, just off the left of the picture. Outcrop of the erratic lithology lies near the base of the cliff, as shown. Inset shows the detail of the erratic lithology in outcrop, showing relationship between intrusive white erratic lithology and surrounding granodiorite (grey) and granite (pink).

Fig. 7. (a) 3-D oblique shaded relief view of the Baxter Pass region. (b) Photograph looking southwest of the ridgetop surface immediately north of Baxter Pass, as indicated in (a).

Table 1. Summary of cosmogenic isotope data. Production rates, shielding factors, etc., calculated as noted in text. Errors indicated are purely analytical.

Sample	Location	Rock type	Elevation (m)	(^{10}Be)* (10^6 at g^{-1})	^{10}Be age (ka)	Nominal ^{10}Be erosion rate (m/My)
SHB-01-21	Sardine Canyon	Biotite leucogranite	3694	0.877	14.7±0.5	40.4±1.4
SHB-01-28	Sardine Canyon	Granite	3628	11.11	194.9±2.2	2.82±0.03
SHB-01-30	Baxter Pass	Granite	3704	1.253	20.7±0.5	28.5±0.7
SHB-01-31	Baxter Pass	Granite	3704	3.134	51.8±1.3	11.2±0.3
LP-1*	Lone Pine Peak		3750	11.4	182.4±4.8	2.98±0.08
LP-2*	Lone Pine Peak		3750	5.9	94.4±3.2	6.01±0.20
LP-3*	Lone Pine Peak		3750	13.2	211.2±4.8	2.53±0.06

* effective ages calculated from data given by Small et al. (1997), using updated production rates used elsewhere in this study.

References

Anderson, R. S., 2002, Modeling the tor-dotted crests, bedrock edges, and parabolic profiles of high alpine surfaces of the Wind River Range, Wyoming: Geomorphology, v. 46, no. 1, p. 35-58.

Benson, L. V., May, H. M., Antweiler, R. C., Brinton, T. I., Kashgarian, M., Smoot, J. P., and Lund, S. P., 1998, Continuous Lake-Sediment Records of Glaciation in the Sierra Nevada between 52,600 and 12,500 ^{14}C yr B.P.: Quaternary Research, v. 50, p. 113-127.

Bishop, M. P., and Shroder, J. F., Jr, 2000, Remote sensing and geomorphometric assessment of topographic complexity and erosion dynamics in the Nanga Parbat massif, *in* Khan, M. A., Treloar, P. J., Searle, M. P., and Jan, M. Q., eds., Tectonics of the Nanga Parbat Syntaxis and the Western Himalaya: Geological Society, London, Special Publications: London, The Geological Society of London, p. 181-200.

Bishop, P., 1995, Drainage rearrangement by river capture, beheading and diversion: Progress in Physical Geography, v. 19, no. 4, p. 449-473.

Brocklehurst, S. H., and Whipple, K. X., 2002, Glacial Erosion and Relief Production in the Eastern Sierra Nevada, California: Geomorphology, v. 42, no. 1-2, p. 1-24.

Clark, D. H., and Gillespie, A. R., 1997, Timing and significance of late-glacial and Holocene cirque glaciation in the Sierra Nevada, California: Quaternary International, v. 38-39, p. 21-38.

Clark, M. K., Royden, L. H., Whipple, K. X., Burchfiel, B. C., Schoenbohm, L. M., Zhang, X., Tang, W., Wang, E., and Chen, L., submitted, Surface Uplift, Tectonics, and Erosion of Eastern Tibet from Large-Scale Drainage Patterns: Tectonics.

Dunne, J., Elmore, D., and Muzikar, P. F., 1999, Scaling factors for the rates of production of cosmogenic nuclides for geometric shielding and attenuation at depth on sloped surfaces: Geomorphology, v. 27, p. 3-11.

Gillespie, A. R., 1982, Quaternary Glaciation and Tectonism in the Southeastern Sierra Nevada, Inyo County, California [PhD thesis]: California Institute of Technology, 695 p.

Granger, D. E., Riebe, C. S., Kirchner, J. W., and Finkel, R. C., 2001, Modulation of erosion on steep granitic slopes by boulder armoring, as revealed by cosmogenic ^{26}Al and ^{10}Be: Earth and Planetary Science Letters, v. 186, p. 269-281.

Hasbargen, L. E., and Paola, C., 2000, Landscape instability in an experimental drainage basin: Geology, v. 28, no. 12, p. 1067-1070.

Heisinger, B., Lal, D., Jull, A. J. T., Kubik, P. W., Ivy-Ochs, S., Knie, K., and Nolte, E., 2002a, Production of selected cosmogenic radionuclides by muons: 2. Capture of negative muons: Earth and Planetary Science Letters, v. 200, p. 357-369.

Heisinger, B., Lal, D., Jull, A. J. T., Kubik, P. W., Ivy-Ochs, S., Neumaier, S., Knie, K., Lazarev, V., and Nolte, E., 2002b, Production of selected cosmogenic radionuclides by muons: 1. Fast muons: Earth and Planetary Science Letters, v. 200, p. 345-355.

Lal, D., 1991, Cosmic ray labeling of erosion surfaces: in situ nuclide production rates and erosion models: Earth and Planetary Science Letters, v. 104, p. 424-439.

Matthes, F. E., 1900, Glacial sculpture of the Big Horn Mountains, Wyoming: U.S. Geological Survey Annual Report, v. 21, no. 2, p. 171-190.

Molnar, P., and England, P., 1990, Late Cenozoic uplift of mountain ranges and global climate change: chicken or egg?: Nature, v. 346, p. 29-34.

Pain, C. F., and Ollier, C. D., 1995, Inversion of relief - a component of landscape evolution: Geomorphology, v. 12, p. 151-165.

Raymo, M. E., Ruddiman, W. F., and Froelich, P. N., 1988, Influence of late Cenozoic mountain building on ocean geochemical cycles: Geology, v. 16, p. 649-653.

Schumm, S. A., 1977, The Fluvial System: New York and London, Wiley, 338 p.

Shroder, J. F., Jr, Owen, L., and Derbyshire, E., 1993, Quaternary glaciation of the Karakoram and Nanga Parbat Himalaya, *in* Shroder, J. F., Jr, ed., Himalaya to the Sea: Geology, Geomorphology and the Quaternary: London, Routledge, p. 132-158.

Small, E. E., and Anderson, R. S., 1995, Geomorphically Driven Late Cenozoic Rock Uplift in the Sierra Nevada, California: Science, v. 270, p. 277-280.

-, 1998, Pleistocene relief production in Laramide mountain ranges, western United States: Geology, v. 26, p. 123-126.

Small, E. E., Anderson, R. S., Repka, J. L., and Finkel, R., 1997, Erosion rates of alpine bedrock summit surfaces deduced from in situ 10Be and 26Al: Earth and Planetary Science Letters, v. 150, p. 413-425.

Stone, J. O., 2000, Air pressure and cosmogenic isotope production: Journal of Geophysical Research, v. 105, no. B10, p. 23753-23759.

Whipple, K. X., Kirby, E., and Brocklehurst, S. H., 1999, Geomorphic limits to climate-induced increases in topographic relief: Nature, v. 401, p. 39-43.

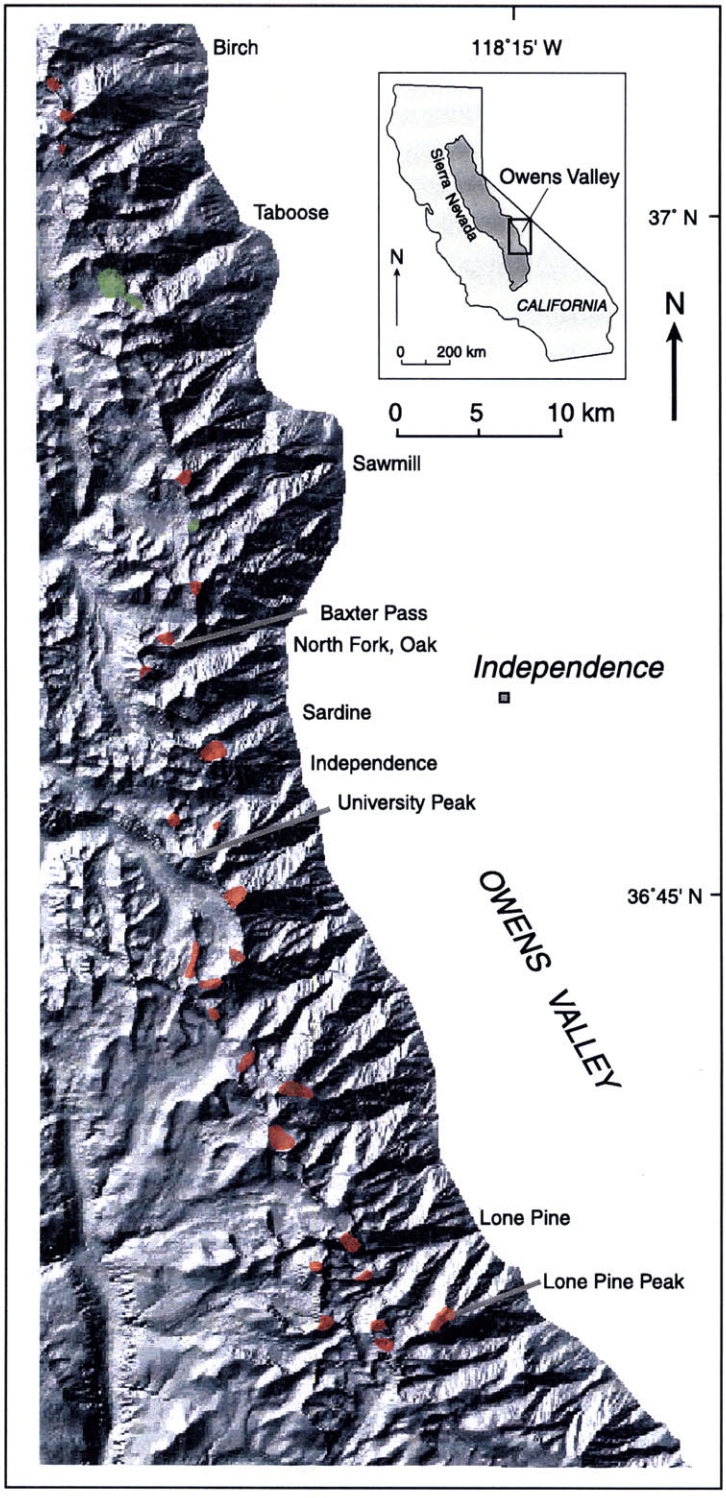
Birch
118°15' W
Taboose
Owens Valley
Sierra Nevada
37° N
N
CALIFORNIA
0 200 km
0 5 10 km
N
Sawmill
Baxter Pass
North Fork, Oak
Independence
Sardine
Independence
University Peak
36°45' N
OWENS VALLEY
Lone Pine
Lone Pine Peak

Fig. 1

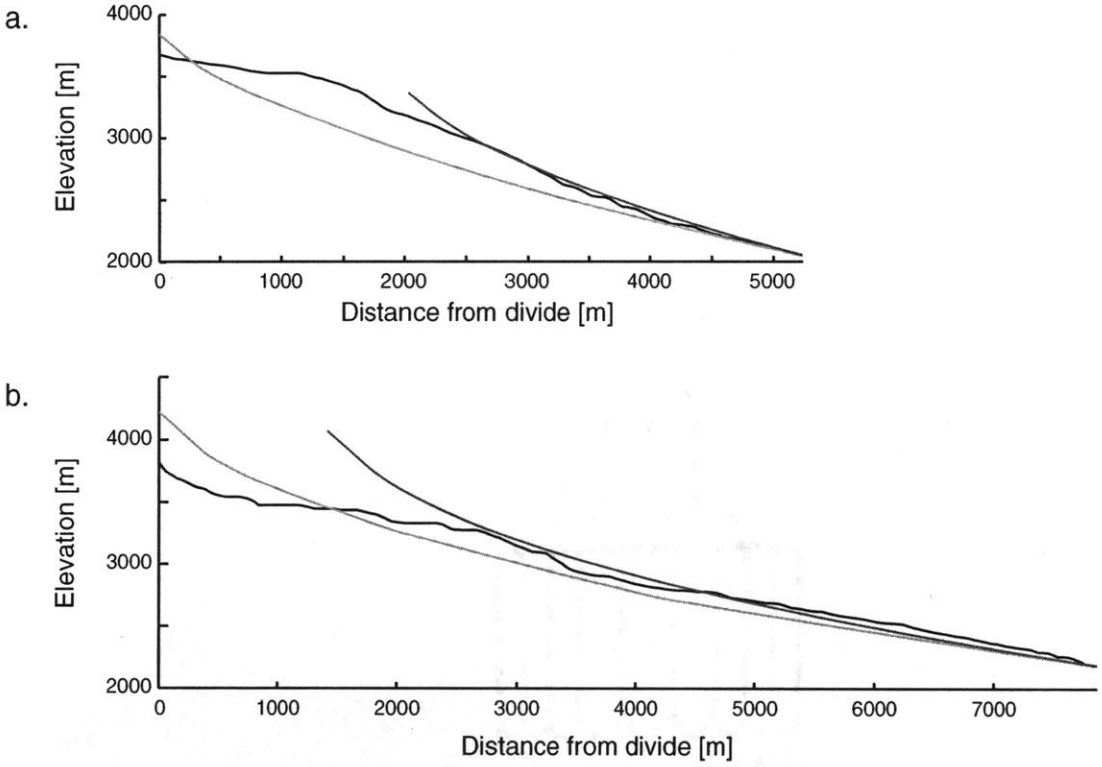
a.
Elevation [m]
4000
3000
2000
0
1000
2000
3000
4000
5000
Distance from divide [m]
b.
Elevation [m]
4000
3000
2000
0
1000
2000
3000
4000
5000
6000
7000
Distance from divide [m]

Fig. 2

Fig. 3

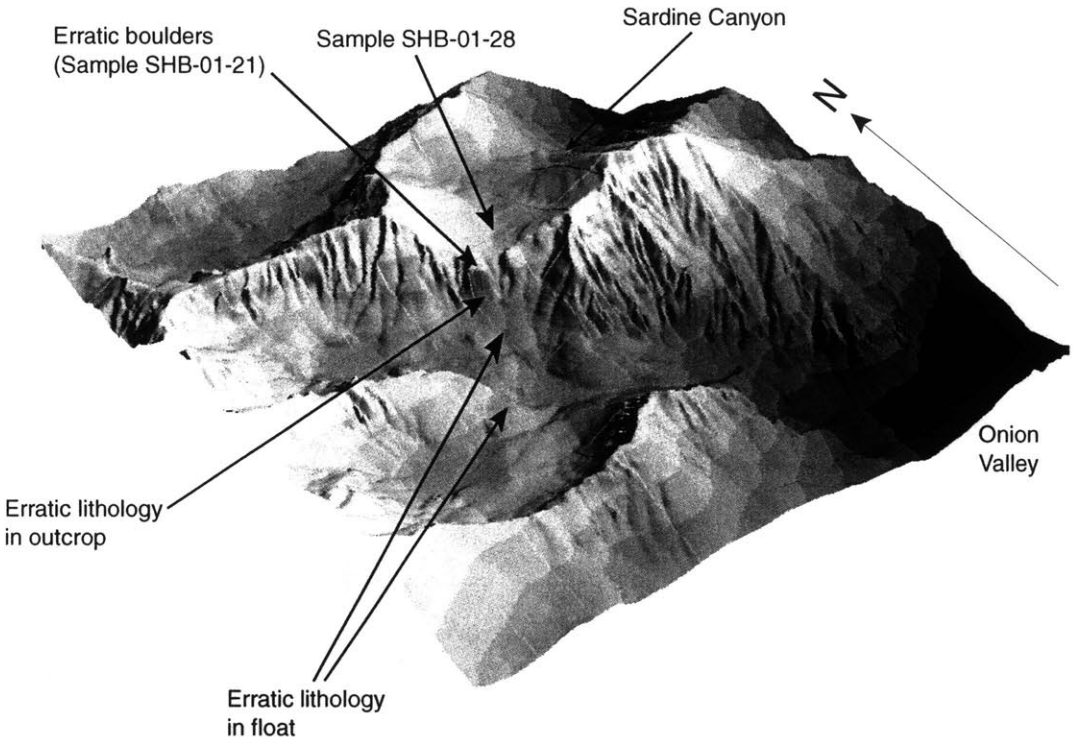
Erratic boulders
(Sample SHB-01-21)
Sample SHB-01-28
Sardine Canyon
N
Onion
Valley
Erratic lithology
in outcrop
Erratic lithology
in float

Fig. 4

a.

b.

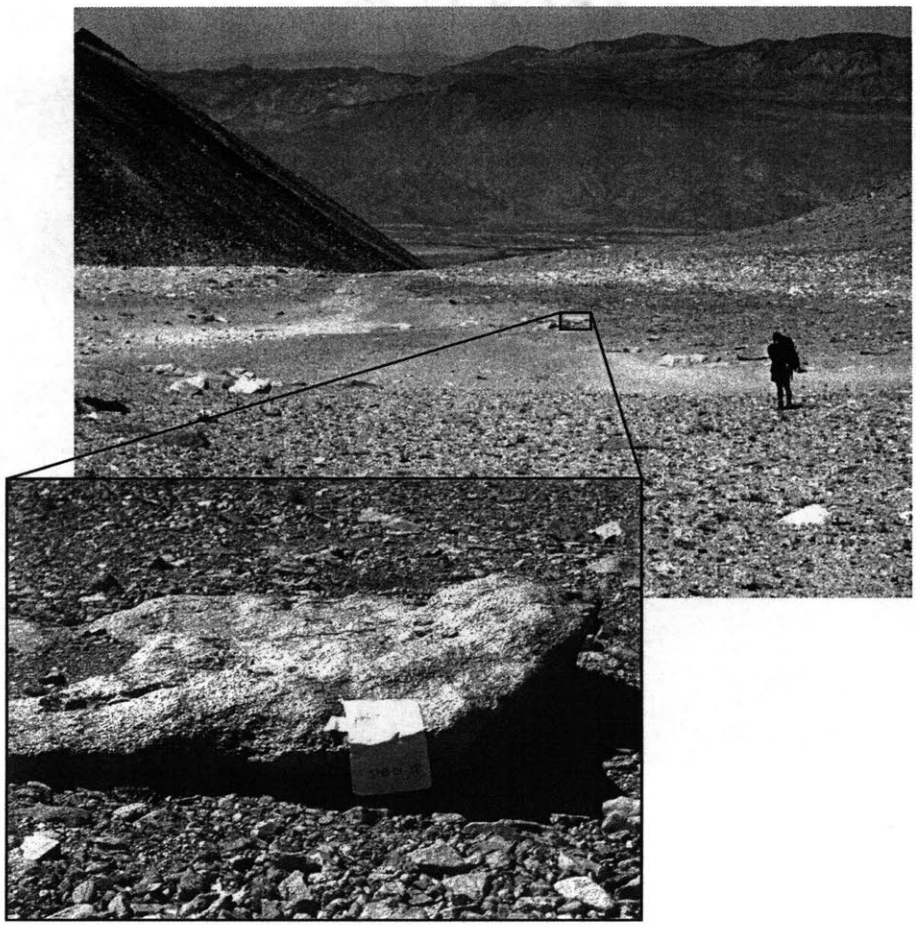

Fig. 5

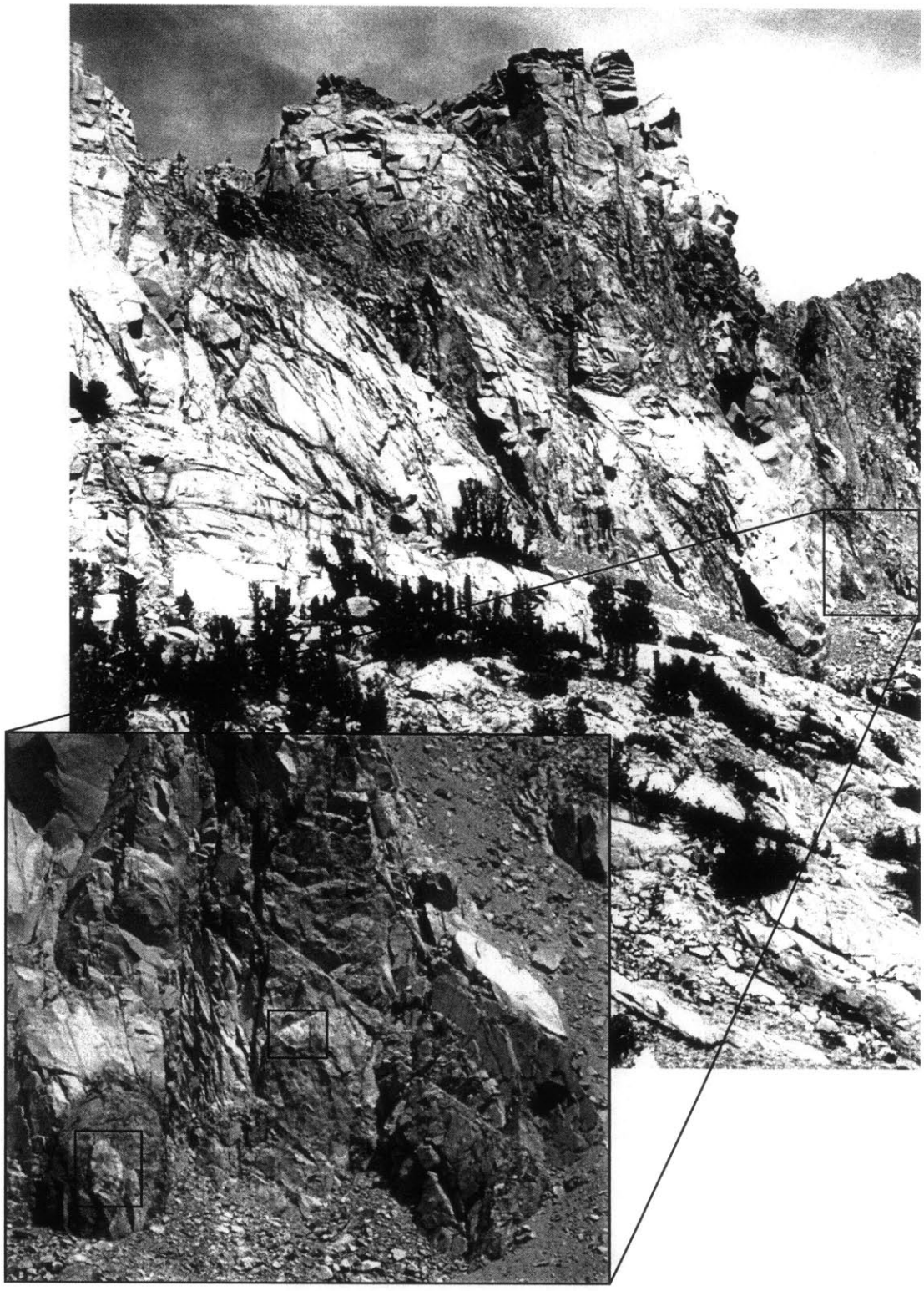

Fig. 6

a.

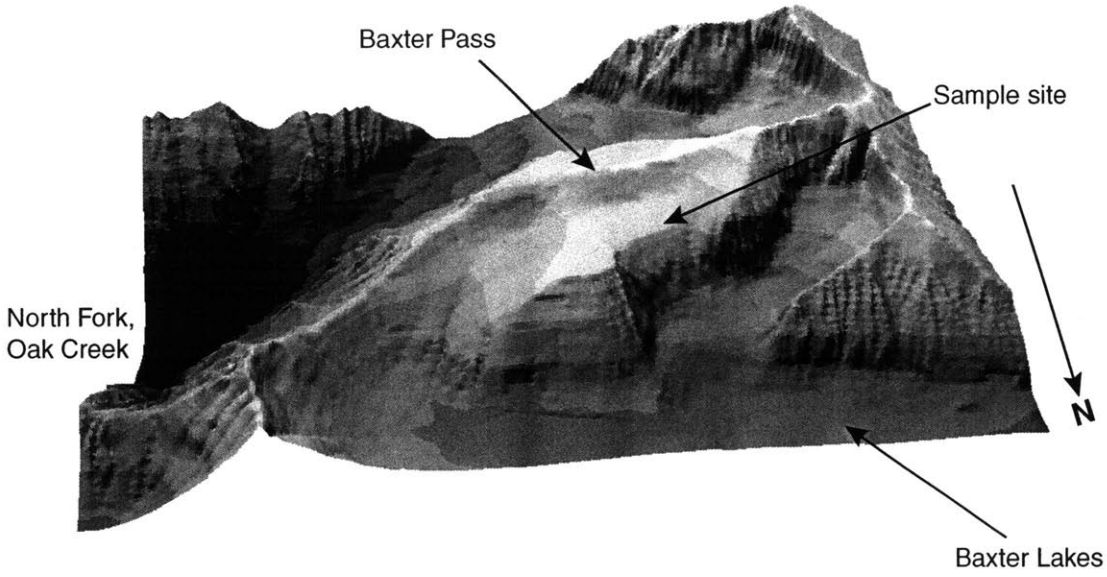

b.

Fig. 7

Chapter 7

Hypsometry of Glaciated Landscapes

Simon H. Brocklehurst* and Kelin X. Whipple

Department of Earth, Atmospheric and Planetary Sciences, Massachusetts Institute of Technology, Cambridge MA 02139, USA

Prepared for submission to: *Earth Surface Processes and Landforms*

*to whom correspondence should be addressed: Email: shb@mit.edu, fax: 1-617-252-1800

Abstract

Hypsometry (frequency distribution of elevations) is often used to characterise landscape morphology, traditionally in the context of the degree of fluvial dissection. Recently, the hypsometry of glaciated regions has been used to make inferences about how rates of glacial erosion compare with tectonic uplift rates. However, many factors other than tectonics can also exert a major influence on the hypsometry of a glaciated landscape, resulting in a wide variety of hypsometries. We have taken a closer look at the hypsometry of glaciated landscapes in the western U.S. and New Zealand. Using examples from the eastern Sierra Nevada, California, the western Sangre de Cristo Range, Colorado, and the Ben Ohau Range, New Zealand, we demonstrate that, all else being equal, the hypsometries of neighbouring basins can indicate the relative degree of glacial modification in each. A selection of drainage basins from the Rocky Mountains show that the position of the equilibrium line altitude (ELA) within the drainage basin relief is a dominant variable in determining the hypsometry of a glaciated basin. This appears to be a nonlinear effect; once the ELA falls to some critical level within the basin, the glaciers scour deeply below the ELA, causing a noticeably different hypsometry. The hypsometry of an arbitrary region encompassing many drainage basins can disguise the variation present in the hypsometries, and thus landforms, of the individual basins. Unique local circumstances, such as the presence of an icecap (Waiho Basin, Southern Alps), substantial hanging valleys (Avalanche Creek, Glacier National Park), a narrow outlet canyon (Sawmill Creek, Sierra Nevada), and isolated geologic structures (Baker Creek, Sierra Nevada), can have a major impact on the hypsometry of an individual basin compared with its neighbours.

Keywords: *hypsometry, glacial erosion, glaciated landscapes*

1. Introduction

Potential interactions between climate change and tectonic processes have sparked much interest in recent years, as authors have debated whether tectonic processes can influence global climate or indeed climate change can drive tectonic processes (e.g., Brozovic et al., 1997; Molnar and England, 1990; Raymo and Ruddiman, 1992; Small and Anderson, 1998; Whipple et al., 1999). In order to evaluate the role of climatic cooling during the late Cenozoic, it is particularly important to understand the role of glaciers in shaping the evolving landscape, because most active mountain ranges in temperate latitudes have been at least partially glaciated (e.g., Braun et al., 1999; Brocklehurst and Whipple, 2002; Brozovic et al., 1997; MacGregor et al., 2000; Merrand and Hallet, 2000; Tomkin and Braun, 2000). Hypsometry (frequency distribution of elevations) is an important tool in the study of glaciated landscapes using digital topographic data. For example, Brozovic et al. (1997) used the hypsometry of glaciated landscapes in the Nanga Parbat region to examine their response to varying tectonic uplift rates. In another recent example, Montgomery et al. (2001) used hypsometry to argue for the relative importance of fluvial, glacial, and tectonic processes along the Andes. However, our preliminary studies (Brocklehurst and Whipple, 2000) suggested that hypsometry can be non-unique, and other factors, such as the degree of glaciation and the presence of an icecap, can also cause considerable variation in the hypsometries of glaciated landscapes. This paper explores the variety in the hypsometry of glaciated landscapes in the absence of dramatic tectonic activity (i.e., considering only rock uplift rates <~1 mm/yr).

Hypsometry describes the distribution of elevation within an area of interest, and has several different guises. Typically, 'hypsometry' refers to a frequency distribution of elevations. The hypsometric curve then represents the fraction of basin area below a given height, often reported in nondimensional terms by normalising the elevations relative to the total elevation range in the area of interest. The hypsometric integral is the area under this normalised curve, which by definition must lie in the range 0 to 1, and typically varies between ~0.3 and ~0.6 in fluvial landscapes. The region of interest is arbitrary, ranging from a single drainage basin (e.g., Strahler, 1952) to entire continents (e.g., Harrison et al., 1983). Hypsometry has classically been used in fluvial landscapes to differentiate between erosional landforms at progressive stages in their evolution (Schumm, 1956; Strahler, 1952). Strahler (1952) asserted that the hypsometric

integral decreases as a landscape "matures", or during post-orogenic topographic decay. Willgoose and Hancock (1998) showed that hypsometry is strongly dependent on channel network and catchment geometry, and is a scale-dependent descriptor of landforms, as fluvial processes become more dominant with respect to hillslopes in larger basins. Hurtrez et al. (1999) also reported that hypsometry is dependent on drainage area. Lifton and Chase (1992) demonstrated that lithology influences the hypsometric integral at smaller scales.

The hypsometry of glaciated landscapes has not been explored in such detail. Hypsometry places an important control on glacier mass balance (e.g., Furbish and Andrews, 1984; Porter, 1970; Small, 1995). When the equilibrium line altitude (ELA) moves as a result of climate change, the rate at which the extent of glaciated terrain in the landscape changes depends on hypsometry. If a large portion of a region lies at an elevation similar to the ELA, small changes in ELA can significantly affect the proportion of surface area covered by glaciers. Further, the faster accumulation area is lost during climate amelioration and ELA rise, the faster the glacier terminus must retreat, and the faster the area subjected to glacial erosion decreases (Small, 1995). Kirkbride and Matthews (1997) found that, in the Ben Ohau Range of New Zealand, an increasing glacial influence is manifest as smoother, more concave long profiles and U-shaped cross-profiles associated with a higher proportion of the land area at lower elevation. In terms of hypsometry, this puts a greater proportion of the landscape at lower elevations within the basin.

Recent studies have focussed on interpreting the hypsometry of glaciated landscapes in terms of their response to tectonic activity. Brozovic et al. (1997) found that in the northwestern Himalaya, the hypsometry of glaciated landscapes is independent of tectonic uplift rates, but is correlated with the extent of glaciation, and thus they concluded that glacial erosion rates can compete with uplift rates in actively deforming regions without increasing valley slope. Montgomery et al. (2001) argued that hypsometry demonstrated the relative dominance of fluvial, glacial and tectonic processes in the Andes. They deduced that rivers dominate the northern Andean landscape, neither fluvial nor glacial erosion can compete with tectonics in the dry central portion of the Andes, and that glaciers dominate landscapes in the southern Andes, in spite of tectonic uplift. While we agree with the interpretations in this case, we caution that in general interpretations made from hypsometry can be non-unique. As we show here, other

factors, such as varying degrees of glaciation and ELA position, can produce similar variations in hypsometry.

We have carried out a comprehensive series of analyses to assess the influences of the degree of glaciation, the position of the equilibrium line altitude (ELA), and the selection of a drainage basin versus an arbitrary region on the hypsometry of glaciated landscapes, in the absence of rapid (here meaning >1 mm/yr) rock uplift. We selected field sites in the western U.S. and the South Island of New Zealand in order to isolate each of these factors and assess the influence of each on hypsometry and thus landscape form. The effect of more rapid tectonic uplift rates on the hypsometry of glaciated mountain ranges is considered elsewhere (Brocklehurst and Whipple, in prep.-b).

2. Motivation

Given that glaciated landforms are quite distinct from their fluvial counterparts (e.g., Benn and Evans, 1998; Sugden and John, 1976), it seems reasonable to infer that such differences will be reflected in the hypsometry of the two landscapes, with the degree of glacial modification of the landscape reflected in relative change in the hypsometry. Many authors argue that glacial erosion is focussed at and above the ELA (e.g., Andrews, 1972; MacGregor et al., 2000), and we have shown in the eastern Sierra Nevada that the mean Quaternary ELA (Porter, 1989) marks the lower limit of major landscape modification (Brocklehurst and Whipple, 2002). Thus it would follow that the position of the ELA within the drainage basin of interest would have a major influence on the landscape. Recent work has examined large (i.e., multiple drainage basin), arbitrary regions of landscapes to deduce the relative importance of glacial and tectonic processes (Brozovic et al., 1997; Montgomery et al., 2001). However, given that no two drainage basins are exactly alike, it would seem that selecting arbitrary regions, while appropriate for regional-scale studies, might obscure some of the local details that would otherwise be visible in the hypsometry of individual basins. Finally, the potential exists in glacial landscapes for significant local variations in landforms that are caused, for instance, by ice caps and hanging valleys.

Thus we sought to test the following four hypotheses, focussing on individual drainage basins, a natural unit for landscape analysis, with the exception of the comparison with arbitrary portions of the landscape:

i. Hypsometry is an effective indicator of long-term degree of glaciation.

ii. The position of the ELA within the drainage basin relief has a significant influence on the hypsometry of a glaciated basin.

iii. The hypsometry of large, arbitrary regions can mask the detail and variation shown by individual drainage basins.

iv. Unique local circumstances, such as the presence of icecaps and hanging valleys can have a profound effect on the hypsometry.

3. Methods

We employed two different methods of analysing hypsometry. The first method (e.g., Fig. 3a-c) is a simple *histogram* of the frequencies in different elevation bins, for instance as employed by Brozovic et al. (1997). The chosen bin size is a compromise between not gaining enough information with too large a bin size, and obscuring the signal with scatter in the data with too small a bin size. In practice, we found a 100m bin size to be most appropriate. Secondly, we generate a *hypsometric curve* (e.g., Fig 3d), normalised elevation plotted against normalised cumulative area (e.g., Strahler, 1952). The area under this curve, which by definition lies in the range 0 to 1, is the hypsometric integral. Our analyses within the US were carried out using 30m digital elevation models (DEMs) from the USGS, whereas for the New Zealand examples we used a 50m DEM from TerraLink.

To test hypothesis (i), we sought drainage basins within a short latitudinal range that exhibit varying degrees of glacial modification (determined independently from published geologic maps, our own field observations, and aerial photograph and topographic map interpretation). This criterion was satisfied by the eastern side of the Sierra Nevada, California (Figs. 1a, 2a), the western side of the Sangre de Cristo Range, southern Colorado (Figs. 1a, 2b), and the eastern side of the Ben Ohau Range, New Zealand (Figs. 1b, 2c, Kirkbride and Matthews, 1997).

On the regional scale, the section of the Sierra Nevada studied (Fig. 2a) consists of homogeneous Cretaceous granodiorites and quartz monzonites (Bateman, 1965; Moore, 1963, 1981). Present-day tectonic activity is dominated by strike-slip motion on the Owens Valley Fault farther to the east, although the range-front normal fault system may still be active, contributing to fairly uniform uplift rates on the order of ~0.2 mm/yr (Gillespie, 1982).

The section of the Sangre de Cristos of interest lies on the western side of the range (Fig. 2b). The principle lithologies in this region are Palaeozoic sedimentary units and Precambrian metamorphic rocks (Johnson et al., 1987). The tectonic regime in the Sangre de Cristos is also constant throughout the region analysed here. Normal faulting slip rates at the range front have averaged around 0.1-0.2 mm/yr during the late Pleistocene (McCalpin, 1986, 1987), comparable to rates measured in the Sierra Nevada.

In this study we consider the drainage basins on the eastern side of the Ben Ohau Range (Fig. 2c). The dominant lithologies include greywacke and argillaceous metasediments, with some minor schist and localised volcanic rocks (Spörli and Lillie, 1974). There is along strike variation in the time since initiation of uplift, which Kirkbride and Matthews (1997) used to evaluate the rate of development of glacial landforms. Rock uplift rates inferred from fission track data of ~0.8 mm/yr (Tippett and Kamp, 1995a, b) agree well with uplift rates of ~1 mm/yr obtained from monitoring of the range-bounding Ostler Fault Zone (Blick et al., 1989).

In the Sierra Nevada and the Sangre de Cristos we can examine the full spectrum from basins essentially lacking any glacial modification through to what we call "fully glaciated" drainages, i.e., basins that at the last glacial maximum (LGM) contained glaciers extending to the range front. The extent of glaciation at the LGM in the Ben Ohau Range varied from small cirque glaciers at the southern end of the range to glaciers extending beyond the basin outlet at the northern end of the range.

To test hypothesis (ii), we focussed on "fully-glaciated" catchments in the Rocky Mountains, from the Sangre de Cristo Range in southern Colorado, north through the Bitterroot Range in southern Idaho, to Glacier National Park in northern Montana (Fig. 1a). From south to north, the mean Quaternary ELA steadily declines, both in absolute terms and also within the drainage basin relief of the catchments studied. We also devised a second test of hypothesis (ii). Focussing on Independence Creek in the eastern Sierra Nevada, we isolated successive subsets of the catchment with outlets at different elevations. With the mean ELA fixed, raising the selected outlet elevation has the effect of artificially lowering the ELA within the sampled basin relief.

To test hypothesis (iii), we constructed a comparison of drainage basin hypsometry with the hypsometry of arbitrary regions of the landscape by extracting arbitrary subsets of the Sierra Nevada landscape, both smaller than and larger than the individual basins. We followed the same

hypsometric methods summarised above, and then compared the results with those from the individual drainage basins in the same region.

Finally, in order to evaluate hypothesis (iv), we examined the potentially extreme impacts of: (a) an ice-cap, by looking at the hypsometry of basins draining the west side of Mt Cook in the Southern Alps of New Zealand (Brocklehurst and Whipple, in prep.-b); (b) prominent hanging valleys, in Glacier National Park; (c) narrow outlet canyons, in the eastern Sierra Nevada; and (d) local geologic structures, also in the Sierra Nevada.

4. Results

4.1. Hypsometry as an indicator of the degree of glaciation

Figure 3 illustrates hypsometry and hypsometric curves for 28 drainage basins on the eastern side of the Sierra Nevada (Brocklehurst and Whipple, 2002). We highlight three representative examples with bold lines, with the remaining basins shown with faint lines on the hypsometric curve plot (Fig. 3d). In Figures 3a-c, the dashed grey lines illustrate the modern and LGM ELAs for each drainage basin taken from regional trends (Burbank, 1991). (Note that by definition local LGM ELA must vary between nonglaciated and glaciated basins). As shown, the regional ELA gradient is modest. Inyo Creek preserves no evidence of glacial occupation during the Quaternary. Hogback Creek developed a small glacier that never reached the range front. Lone Pine Creek supported a larger glacier that extended to the range front at the Last Glacial Maximum (LGM). There is a consistent pattern to the hypsometry as a function of the degree of glaciation across all of the drainages studied. In general, nonglaciated basins have a frequency distribution of elevations skewed towards lower elevations, and thus a low hypsometric integral. Increasing to moderate glaciation causes a more even frequency distribution and an intermediate hypsometric integral. Further glacial modification results in both the peak in the frequency distribution becoming skewed towards higher elevations and higher hypsometric integrals. Figure 4 shows the same plots for 31 basins draining the western side of the Sangre de Cristos, again highlighting three representative examples. As before, Figures 4a-c illustrate, with dashed grey lines, modern and LGM ELAs from regional trends (Richmond, 1965). Marshall Creek, like Inyo Creek in the Sierra Nevada, preserves no significant evidence of glacial modification. The glacier in Wild Cherry Creek never reached the range front, whilst the Rito Alto Creek glacier

did extend to the range front at the LGM. The pattern observed in the hypsometry is much the same as in the Sierra Nevada (Fig. 3), although the relief of the Sangre de Cristo range is about half that of the Sierra Nevada.

In comparison with the Sierra Nevada, the Ben Ohau Range has a much stronger gradient in ELA (both current and LGM), varying from close to the outlet elevation of the basins in the northern part of the range, to near the crest of the range in the south, as shown by the dashed grey lines in Figures 5a-c (Porter, 1975). The highlighted, representative examples from the Ben Ohau Range show a trend relating to glacial impact that is the opposite of that seen in the eastern Sierra Nevada and the western Sangre de Cristo Range. During the last major glaciation, McMillan River had a small cirque glacier at its head, Whale River developed a small valley glacier, and Black Birch River had a glacier that extended beyond the range front as a tributary to the Tasman Glacier. In this case, the least glacial modification results in a frequency distribution skewed towards high elevation (reflecting a very modest cirque glacier). Increasing degrees of glaciation then shift the mode of the frequency distribution to successively lower elevations, correspondingly decreasing the hypsometric integral. This is consistent with what Kirkbride and Matthews (1997) report, namely that "increasing glacial influence is manifest as smoother, more deeply concave long profiles and U-shaped cross-profiles associated with a higher proportion of the land at lower elevation".

This result suggests that there is some fundamental difference between the eastern Sierra Nevada and the western Sangre de Cristos compared with the Ben Ohau Range. We suggest that this is due to the position of the mean Quaternary ELA within the total relief of the mountain range. In general, glaciated landscapes predominantly reflect the glaciers that would have been present under a mean Quaternary ELA (Porter, 1989). Furthermore, our previous work has demonstrated that there is a close correlation between the mean Quaternary ELA and the position of the majority of landscape modification by glaciers in basins of this scale in the eastern Sierra Nevada (Brocklehurst and Whipple, 2002). If the ELA is proportionally lower within the basin, it seems logical to infer that a higher proportion of the basin will have been subjected to major glacial modification, development of wide valley floors and U-shaped cross-sections, etc., and that this will be reflected in the hypsometry. This hypothesis is tested in the next section.

4.2. Influence of ELA position on hypsometry

We have attempted to quantify the relative ELA position within the total elevation range of the basin using the following formula:

$$ELA_{norm} = \frac{ELA_{Qm} - z_0}{z_{\max} - z_0} \quad (1)$$

Here ELA_{norm} is the relative mean Quaternary ELA position, ELA_{Qm} is the mean Quaternary ELA, defined as midway between the modern and LGM ELAs (Porter, 1989), z_0 is the outlet elevation for the basin, and z_{max} is the maximum elevation in the basin. As defined, a value of 1 for ELA_{norm} indicates a mean Quaternary ELA at the highest point in the basin, and a value of 0 indicates a mean Quaternary ELA at the outlet. Here we are interested in variations in hypsometry as ELA_{norm} declines, i.e., as the ELA becomes proportionally lower in the basin. Mean values for ELA_{norm} are 0.67, 0.64 and 0.57 for the Sangre de Cristos, Bitterroots and Glacier National Park respectively. Figure 6 compares the hypsometries of fully glaciated basins in these three ranges, highlighting Rito Alto Creek in the Sangre de Cristo Range, Sawtooth Creek in the Bitterroots, and Walton Creek in Glacier National Park. Again these are representative examples of each of the study areas. In each case the LGM glaciers extended at least to the range front, but as indicated by the thick grey lines (and the differing ELA_{norm} values), the ELA position within the relief of the basin varies markedly. The result of lowering the ELA within the relief of the range is to shift the major peak in hypsometry to lower elevations, and, consequently, to reduce the hypsometric integral. It is interesting to note that the shift in the peak in the frequency distribution is far greater than the shift in ELA. In addition there seems to be nonlinearity in the response, in that the slight decline in ELA_{norm} from 0.64 to 0.57 produces a big difference in hypsometry, perhaps because the glacier is able to overdeepen below the ELA (Brocklehurst and Whipple, in prep.-a).

As a further test of this idea, we picked subsets of Independence Creek with outlets at ~2100m, ~2500m and ~2700m, in comparison with the basin outlet at the range front which lies at ~1900 m (Fig. 7). This yields ELA_{norm} values of 0.57, 0.39 and 0.30, respectively, compared with 0.66 for the full extent of the basin. As before, the proportional lowering of the ELA, here achieved by raising the basin outlet, lowers the hypsometric integral. The peak in hypsometry also shifts towards the basin outlet.

4.3. Comparing arbitrary regions and drainage basins

Figure 8 illustrates the effects of selecting a larger, arbitrary section of topography from the eastern Sierra Nevada, in comparison with representative drainage basins within this area. The selected portion runs from Independence Creek in the north to Lone Pine Creek in the south, and as such encompasses these two fully glaciated basins, five partially glaciated basins (Shepherd, North Fork Bairs, Bairs, George, and Hogback) and four nonglaciated basins (Pinyon, Symmes, Inyo, and Alabama – see Fig. 2a). The result of combining these basins into a larger unit is a hypsometry that looks much like a partially glaciated basin, both in the frequency distribution and the hypsometric curve (Fig. 8). The effect of choosing a region encompassing all of this variation in degree of glaciation has been to effectively average the variation. In other words, the overall frequency distribution is the sum of the frequency distributions of all of the basins within the range of interest, and the hypsometric curve is an 'average' of all of the hypsometric curves. A casual observer would look at Figure 8 and decide that the eastern Sierra Nevada as a whole can be described as 'partially glaciated', which is a valid interpretation, but misses the wide variety of landforms within this portion of the range. Arbitrary regions of the landscape at scales comparable to or smaller than a drainage basin can be quite unrepresentative. For example, a narrow swath of topography parallel to the long axis of a basin, running down the valley floor will look quite different from a swath running along the ridgeline separating two drainage basins.

4.4. Importance of local circumstances

Our search for examples of unique local circumstances having a major impact on the hypsometry of individual drainage basins showed that at least three different situations may be reflected in the hypsometry: ice caps, hanging valleys, and unusual basin shapes.

As an example of the influence of an ice-cap, we show the hypsometry of the Waiho River (Fig. 9a), which lies immediately to the south of Callery River (Fig. 9b) in the Mt Cook region of the Southern Alps (Brocklehurst and Whipple, in prep.-b). The two basins have experienced similar degrees of glaciation, but a significant proportion of the Waiho Basin lies beneath a permanent ice sheet at high elevation. This is seen quite clearly in the hypsometry as a

peak in the frequency distribution at the very top of the basin, which is also reflected in an increase in the hypsometric integral (Fig. 9c).

In Avalanche Creek in Glacier National Park, the two major tributaries both form hanging valleys above the main stream. This is also readily identified in the hypsometric curve of this basin in comparison with its neighbours, for example, Snyder Creek. The hanging valleys result in a greater proportion of the valley lying at higher elevation, and thus the hypsometric integral is significantly higher.

Sawmill Creek in the eastern Sierra Nevada looks much like its' neighbouring partially glaciated drainage basins, with the exception that it drains into the Owens Valley through a deep canyon rather than a typical V-shaped valley. As shown in Fig. 11, this difference is a feature that can be identified in the hypsometric curve, as a particularly small fraction of the drainage basin area lies at low elevations, compared with, for example, nearby Taboose Creek.

Baker Creek in the eastern Sierra Nevada (Fig. 2a) traverses the fault-bounded, low-relief Coyote warp (e.g., Bateman, 1965) between the cirque at its' head and the outlet into the Owens Valley (Fig. 12a). This broad flat region in the upper-middle portion of the basin is reflected in both the frequency distribution of elevations, as a dramatic peak, and in the hypsometric curve, as a large proportion of the area within a narrow elevation range (Fig. 12). Notice how Baker and nearby Red Mountain Creeks have quite comparable hypsometric integrals, but the shape of the hypsometric curve for Baker Creek is much flatter in the middle section. In this case it is important to note that without independent knowledge of the unique local setting of this basin, one might attribute hypsometry of this style to dramatic glacial modification, whereas glacial modification in this basin has in fact been comparatively minor.

5. Discussion

Given the obvious distinctions between fluvial and glacial landscapes, it follows that the two should have different hypsometries. The differences between the two that we describe in this study are consistent with expectations based on studies of glacial landforms and erosion (e.g., Benn and Evans, 1998; Sugden and John, 1976). We would anticipate that a fluvial landscape characterised by narrow, downstream-sloping valley floors and angle-of-repose hillslopes would have a smooth frequency distribution of elevations. Meanwhile, a glacial landscape of wide, flat valley floors and cirque basins would logically have a frequency distribution featuring a single,

dramatic peak, especially if the basin is dominated by a solitary cirque floor (Andrews, 1972; Brozovic et al., 1997). Furthermore, given the close association between the mean Quaternary ELA and the region of valley longitudinal profile flattening (i.e., cirque floor development, Brocklehurst and Whipple, 2002), it is reasonable that the location of the mode in the frequency distribution should be related to the mean Quaternary ELA.

We have demonstrated a spectrum of changes in hypsometry due to glaciation, as illustrated in Figure 13. As shown in the eastern Sierra Nevada and the western Sangre de Cristo Range, at the onset of glaciation, driven here by local changes in ELA, the peak in the frequency distribution of elevations shifts towards higher elevations in a relative sense; equivalently the hypsometric curve rises and the hypsometric integral increases. This reflects the development of cirque floors high in the range. The rise in the hypsometric curve is further accentuated by cirque glaciers bringing down ridgelines as well as flattening the valley floors above the mean Quaternary ELA (Brocklehurst and Whipple, 2002), thus decreasing the elevation range over which the hypsometric curve is normalised. In the Ben Ohau Range or Glacier National Park, further lowering of either local or regional ELA causes the mode to shift back towards lower elevations, and the hypsometric integral to decrease again, as the larger glaciers incise the whole of the valley floor. Comparing Figures 2d and 6d, this glacial erosion will drive the hypsometry towards, and then beyond, the typical fluvial case, accentuating skewness towards low elevations and thus small values for the hypsometric integral. For example, Walton Creek in Glacier National Park also has a lower hypsometric integral than the larger fluvial basins described by Hurtrez et al. (1999) in the Siwalik Hills of Nepal. It is important to note that, within a restricted area of a given mountain range (e.g., over ~50 km), only two of the three styles of hypsometric curve in Fig. 13a will be present. Either the red (nonglaciated) and green (mainly cirque glaciers, with a high ELA) curves, or the green and the blue (valley glaciers, with a lower ELA) curves will be present. Both the nonglaciated and cirque glacier curves can occur in a region with fairly uniform regional ELAs, while the transition from cirque to valley glaciers requires substantial lowering of regional ELA. The full spectrum, from nonglaciated to valley glaciers, will require either significant climatic cooling or an increase in precipitation (and ELA lowering), and thus the nonglaciated and valley glacier landforms would be seen at different times, or a considerable larger spatial range. The Ben Ohau Range comes close to having all three because of the pronounced rainshadow effect in this region, but does not exhibit any truly nonglaciated valleys.

Thus there will not be circumstances where a nonglaciated basin might be confused with a glaciated basin intermediate between the cirque (high ELA) and valley glacier (low ELA) cases, and hypsometry remains a valuable tool for examining the degree of glaciation.

As shown in Figure 13b, the progression from landscapes featuring only modest cirque glaciers to basins dominated by large valley glaciers is somewhat reminiscent of the classic sequence of fluvial landscape evolution described by Strahler (1952). He proposed that 'young', recently uplifted, fluvially-eroded landscapes have high hypsometric integrals, while increasing incision and 'maturity' result in lower hypsometric integrals as a greater proportion of the landscape is brought down to lower elevations, culminating in 'monadnock' landscapes with few peaks surrounded by extensive, low relief regions.

The effect of lowering ELA within the elevation range of a basin appears to be non-linear. In the Independence Creek example, a wide range of ELA_{norm} produced only modest variations in frequency distributions and hypsometric curves, because the basin only has modest-sized cirques, and the cirque glaciers only seldom spilled into the valley floor below. Meanwhile the examples across the western US showed much less ELA_{norm} variation but dramatic differences in frequency distributions and hypsometric curves. We suggest that this may reflect a fundamental difference between landscape forms produced by cirque glaciers, and larger valley glaciers with longer residence times in the valley. Furthermore, the relative drop in ELA between El Capitan and Walton Creeks is small, but the change in landscape form is dramatic; this suggests that once the ELA falls to some critical level within the basin, the glacier can scour deeply below the ELA, causing this noticeably different hypsometry.

The use of hypsometry is by definition a tool that attempts to describe a whole region or drainage basin with a single curve or statistic. In some cases this is desirable, and we have shown that hypsometry can be an efficient tool in assessing the impact of glaciers on a landscape. Hypsometry can be a valuable tool at the scale of comparing drainage basins or neighbouring regions. However, particular features of the region of interest may be lost amongst the much larger population of elevations. Within an individual basin, for example, the hypsometry will not tell you how many steps there are in the glacial longitudinal profile. Similarly, a study that combines several watersheds into larger landscape units will result in the loss of the details of specific basins, but this broad scale characterisation of the landscape might be all that is necessary. Hypsometry is a valuable tool for characterising the dominant processes active in a

given landscape, but we would hesitate to use it to try to elucidate the details of the erosion processes acting at a sub-basin scale. We have also demonstrated that unique local circumstances can influence hypsometry, sometimes in quite profound ways. Hanging valleys, ice caps, narrow outlet canyons and geologic structures are amongst the features of glaciated landscapes that may affect hypsometry. Thus we suggest that hypsometry should not be used in isolation when making quantitative assessments of glaciated landscapes.

In their study of the Andes, Montgomery et al. (2001) attributed moderate hypsometric integrals in the northern part of the range to fluvial processes dominating landscape evolution, high hypsometric integrals in the central portion of the range to tectonics dominating over either fluvial or glacial erosion, and low hypsometric integrals in the southern part to dominance by glacial erosion. While we agree with their conclusions in this special case, with the Altiplano clearly playing a role in the high hypsometric integrals in the central part of the range, in general this progression of hypsometric curves could also be achieved by having a steady progression of glacial influence from none in the north (moderate hypsometric integral), through minor modifications by small cirque glaciers in the central region (high hypsometric integral), to large glaciers with a low ELA in the southern part of the range (low hypsometric integral). Furthermore, as described above, studying large blocks of topography like this can potentially mask major interbasin variations in topography. This also applies to the study around Nanga Parbat carried out by Brozovic et al. (1997); this region is discussed in more detail by Brocklehurst and Whipple (Brocklehurst and Whipple, in prep.-b). Here we simply emphasise the large variations between individual drainage basins that might be overlooked by this regional approach.

Kirkbride and Matthews (1997) attribute the varying amounts of glacial modification in the Ben Ohau Range to variations in time since initiation of glaciation. According to their conceptual model, the northern end of the range began rising earlier, intersected the regional ELA sooner and thus has experienced a longer period of glaciation. Furthermore ELAs are proportionally lower in the northern part of the range, so glacial modification can extend to lower in the basin. We caution that the initial condition for this landscape may have been a rising low relief bench similar to the low relief landscapes further to the east (and thus looking like a miniature Altiplano in terms of hypsometry), rather than a more typical fluvially dissected landscape. Thus the landforms (as reflected in the hypsometric curve) in the southern part of the

range may represent minor reworking of this landscape rather than major modification by cirque glaciers. Furthermore, for the basins at the southern end to continue to evolve towards the landforms of the more northerly basins will require relative lowering of the ELA. Basins scoured down towards the elevation of the outlet would require substantial lowering of the ELA in absolute terms, or uplift of the whole basin, including the outlet, with respect to the ELA. Therefore we agree that it is the progressive northwest advection of the Ben Ohau Range into the wetter region near the Main Divide of the Southern Alps (and correspondingly lower ELAs) that is dominantly responsible for the trends in hypsometry along the range.

This study has purposely avoided regions with either significant gradients in tectonic uplift rate or extremely rapid uplift rates, as we sought to isolate other factors that might influence the hypsometry of glaciated landscapes. The use of hypsometry as a tool for assessing the response of glaciated landscapes to tectonic uplift, alongside other geomorphologic techniques, is considered elsewhere (Brocklehurst and Whipple, in prep.-b). We have also focussed on landscapes produced by small, alpine glaciers, at the expense of their larger counterparts, or ice caps and ice sheets. In these settings, as suggested by the example of the Waiho River basin, described above, we would anticipate even more exaggerated departures from the hypsometry of fluvial landscapes. However, great care would have to be taken to clarify whether the study concerned the ice surface or the valley floor beneath the ice, since these would differ quite significantly in terms of their hypsometries in regions of thick and/or widespread ice.

6. Conclusions

We have carried out a broad survey of the hypsometry of glaciated landscapes. Both the frequency distribution of elevations and the hypsometric curve can indicate the relative degree of glacial modification in neighbouring basins. We have identified a continuous spectrum of frequency distributions of elevations and hypsometric curves reflecting increasing modification of initially fluvial landscapes. The transition from nonglaciated to glaciated conditions tends to skew the frequency distribution to higher elevations, while further glacial modification, requiring lowering of the ELA, shifts the peak back towards lower elevations. Thus, amongst drainage basins that have been fully glaciated, the most important influence on the hypsometry is the relative position of the ELA within the relief, measured between the basin outlet and the top of the highest peak. The second part of the spectrum is reminiscent of the classic fluvial landscape

development described by Strahler (1952). Given the range of different hypsometries exhibited by drainage basins with different glaciation histories, using arbitrary regions of the landscape to determine hypsometry can mask some of the detail present in the individual drainage basins, although this approach will generally provide a good indication of the overall influence of glaciers on the landscape. Finally, unique local circumstances, such as the presence of ice-caps, major hanging valleys, narrow outlet canyons, and isolated geologic structures, can introduce major variations into the hypsometry of a glaciated landscape.

Acknowledgements

This work was supported by NSF grant EAR-9980465 (to KXW), NASA grant SENH99-0209-0172 (to KXW) and a NASA Earth System Science Graduate Fellowship (to SHB). We would like to thank Julia Baldwin and Nicole Gasparini for their careful reviews of an early version of this manuscript.

Figure Captions

Fig. 1. Location maps for the areas examined in this study. (a). Western US: Sierra Nevada, Sangre de Cristo Range, Bitterroot Range, Glacier National Park. (b). South Island, New Zealand: Ben Ohau Range, Waiho Basin (Southern Alps).

Fig. 2. (a) Shaded relief map of drainage basins studied in the eastern Sierra Nevada, California. Location of study site shown in inset map. (b) Shaded relief map of drainage basins studied in the Sangre de Cristo Range, southern Colorado. Location of study site shown in inset map. (c) Shaded relief map of drainage basins studied in the Ben Ohau Range, South Island, New Zealand. Location of study site shown in inset map.

Fig. 3. Hypsometry of the eastern Sierra Nevada. Modern (dashed) and Last Glacial Maximum (dotted) regional equilibrium line altitudes for the crest of the range from Burbank (1991). (a). Non-glaciated Inyo Creek. (b). Partially glaciated Hogback Creek. (c). Glaciated Lone Pine Creek. (d). Hypsometric curves and integrals (area under the hypsometric curve) for Inyo (red), Bairs (blue) and Lone Pine (green) Creeks (dark tones), and the remaining basins in the range following the same colour scheme (red – nonglaciated; blue – partially glaciated; green – fully glaciated) in pale tones. The highlighted examples are representative of the hypsometric curves and integrals of non-glaciated, partially glaciated and glaciated basins respectively. Notice how increasing degree of glaciation causes a shift in the mode of the frequency distribution to higher elevations, corresponding to an increase in the hypsometric integral. This reflects the development of wide, flat cirque floors and flattening of the glacial valley longitudinal profile at high elevation (Brocklehurst and Whipple, 2002; Brozovic et al., 1997).

Fig. 4. Hypsometry of the Sangre de Cristo Range. Modern (dashed) and LGM (dotted) regional ELAs for the crest of the range from Richmond (1965). (a). Non-glaciated Steel Creek. (b). Partially glaciated Wild Cherry Creek. (c). Glaciated Rito Alto Creek. (d). Hypsometric curves and integrals for Steel (red), Wild Cherry (blue) and Rito Alto (green) Creeks (dark tones), and the remaining basins in the range following the same colour scheme (red – nonglaciated; blue – partially glaciated; green – fully glaciated) in pale tones. The highlighted examples are

representative of the hypsometric curves and integrals of non-glaciated, partially glaciated and glaciated basins respectively. As in the Sierra Nevada, an increasing degree of glaciation causes a shift in the mode of the frequency distribution to higher elevations, along with a decrease in hypsometric integral, reflecting the development of the wide, flat-bottomed glacial trough.

Fig. 5. Hypsometry of the Ben Ohau Range. Modern (dashed, grey) and LGM (dotted, grey) regional ELAs for the crest of the range from Porter (1975). (a). Non-glaciated McMillan River. (b). Partially glaciated Whale River. (c). Glaciated Black Birch River. (d). Hypsometric curves and integrals for McMillan (red), Whale (blue) and Black Birch (blue) Rivers (dark tones), and the remaining basins in the range following the same colour scheme in pale tones. Here an increasing degree of glacial modification causes a shift in the mode of the frequency distribution to lower elevations, along with an increase in the hypsometric integral, reflecting glacial modification down to lower elevations. This is the opposite trend from that seen in the Sierra Nevada and the Sangre de Cristos.

Fig. 6. Comparative hypsometries from the western US. Note varying regional ELA positions; modern (dashed, grey), mean Quaternary (solid, grey) and LGM (dotted, grey) for the crests of each range (from Richmond, 1965). (a). Rito Alto Creek, Sangre de Cristos. (b). Sawtooth Creek, Bitterroots. (c). Walton Creek, Glacier National Park. (d). Hypsometric curves and integrals for Rito Alto (blue), Sawtooth (purple) and Walton (orange) Creeks in bold tones, and other fully glaciated basins in each range in pale tones, following the same colour scheme (data from Table 4). Notice how the position of the ELA declining within the relief of the basin (decreasing ELA_{norm}) causes the mode of the frequency distribution to shift lower in the basin, below the LGM ELA in the case of Walton Creek. This is also reflected in a dramatic reduction in the hypsometric integral. An ELA position lower within the drainage basin relief allows much greater glacial modification of the landscape, with wide, flat valley floors developing near the basin outlet, even though this may be below the LGM ELA, particularly for large, low gradient glaciers.

Fig. 7. (a). Sub-basins used to illustrate effect of changing ELA on hypsometry in Independence Creek. (b). Hypsometries for the Independence Creek basin subsets illustrated in Fig. 6a. (c).

Hypsometric curves and integrals for the same basin subsets, using the same colour scheme (blue – outlet at 2100m; purple – outlet at 2500m; orange – outlet at 2700m). As in Figure 6, decreasing ELA_{norm} results in the mode of the frequency distribution lying closer to the outlet, and thus a lower hypsometric integral, although the effect is less dramatic here.

Fig. 8. Hypsometry of a large portion of the study region in the eastern Sierra Nevada (compare with Fig. 2). (a). Selected region, bounded by the drainage divide to the west and the range front to the east. Compare with Figure 2a. (b). Frequency distribution of elevations for this arbitrary region (black, bold), together with shapes (not to same scale) of frequency distributions of Inyo (dark grey – nonglacial), Bairs (medium grey – partially glaciated), and Lone Pine (light grey – fully glaciated) Creeks, taken from Figs. 3a-c. (c). Hypsometric curve for this large portion of the landscape (black, bold) compared with the hypsometric curves for Inyo (dark grey), Bairs (medium grey) and Lone Pine (light grey) Creeks, from Fig. 3d. Notice how the hypsometry of this large portion of the landscape effectively combines the hypsometries of the basins with varying degrees of glaciation within its' boundaries, resulting in a hypsometry that looks like a 'partially glaciated' landscape.

Fig. 9. Hypsometry of neighbouring basins on the western side of the Southern Alps. Modern (dashed) and LGM (dotted) ELAs from Porter (1975). (a). Hypsometry of Waiho River basin. (b). Hypsometry of Callery River basin. (c). Hypsometric curve and integral for Waiho (black) and Callery (grey) River basins. The large ice cap near the range crest in the Waiho River basin introduces a large spike in the frequency distribution, also reflected in the significantly higher hypsometric integral.

Fig. 10a. Digital elevation model of Avalanche Creek, Glacier National Park. Notice how the two tributaries are hanging valleys above the main valley below. (b). Hypsometry of the Avalanche Creek basin. (c). Hypsometric curves for Avalanche Creek (black) and nearby Snyder Creek (grey). Notice how the presence of significant hanging valleys in Avalanche Creek causes a much greater proportion of the basin to lie at higher elevations.

Fig. 11. Hypsometric curves for Sawmill Creek (black) and Taboose Creek (grey) in the eastern Sierra Nevada (Fig. 2a). Sawmill Creek enters the Owens Valley through a narrow canyon, whereas Taboose Creek has a more typical fluvial V-shaped cross-section. This is reflected in Sawmill Creek having a much smaller proportion of the basin at low elevations.

Fig. 12a. Longitudinal profile of Baker Creek, eastern Sierra Nevada, emphasising the low relief of the Coyote warp. (b). Frequency distribution of elevations for Baker Creek. The large spike at ~3100 m reflects the large, low relief extent of the Coyote warp, while the smaller peak at ~3600 m reflects the cirque floors above this. (c). Hypsometric curves for Baker Creek (black) and nearby Red Mountain Creek (grey), which does not traverse the Coyote warp. Notice how the two are quite similar, except for the flatter section of the Baker Creek curve, which reflects the high proportion of the area within a narrow range of elevation on the Coyote warp.

Fig. 13. (a). Cartoon to illustrate effects of progressive glacial modification of an initial fluvial landscape (dark grey). Initial development of cirque glaciers associated with a high ELA will raise the hypsometric curve and integral (light grey). Lowering of the ELA and development of large valley glaciers will then lower the hypsometric curve back through its initial shape to a significantly lower position, with a correspondingly lower hypsometric integral (black). (b). Hypsometric curves for fluvial landscapes, after Strahler (1952), showing evolution from young stage (dark grey), through mature equilibrium stage (light grey), to monadnock stage (black).

Table 1. Summary of Sierra Nevada hypsometry data. Basins listed in alphabetical order. Mean values for hypsometric integral are: nonglaciated, 0.46; minor glaciation, 0.52; moderate glaciation, 0.52; significant glaciation, 0.57; full glaciation, 0.58.

Basin	Degree of glaciation	Hypsometric Integral
Alabama	None	0.452
Black	None	0.532
Inyo	None	0.427
Pinyon	None	0.485
South Fork, Lubken	None	0.396
Symmes	None	0.491
Diaz	Minor	0.531
Division	Minor	0.592
Thibaut	Minor	0.443
Bairs	Moderate	0.478
Goodale	Moderate	0.607
Hogback	Moderate	0.521
North Fork, Bairs	Moderate	0.448
North Fork, Lubken	Moderate	0.532
Red Mountain	Moderate	0.532
Armstrong	Significant	0.533
George	Significant	0.589
North Fork, Oak	Significant	0.590
Sardine	Significant	0.581
Sawmill	Significant	0.590
Shepherd	Significant	0.552
Taboose	Significant	0.569
Tuttle	Significant	0.542
Birch	Full	0.567
Independence	Full	0.563
Lone Pine	Full	0.575
South Fork, Oak	Full	0.589
Tinemaha	Full	0.624

Table 2. Summary of Sangre de Cristos hypsometry data. Basins listed in alphabetical order Mean values for hypsometric integral are: nonglaciated, 0.46; partially glaciated, 0.50; fully glaciated, 0.52

Basin	Degree of glaciation	Hypsometric integral
Alpine	None	0.449
Burnt	None	0.437
Cedar Canyon	None	0.502
Cold	None	0.401
Copper	None	0.395
Dimick	None	0.423
Hot Springs	None	0.463
Lime	None	0.500
Little Medano	None	0.471
Marshall	None	0.411
Mill	None	0.523
Orient	None	0.447
Short	None	0.439
Steel	None	0.510
Cedar	Partial	0.533
Cottonwood	Partial	0.516
Deadman	Partial	0.542
Garner	Partial	0.432
Major	Partial	0.432
Medano	Partial	0.388
North Crestone	Partial	0.532
Pole	Partial	0.479
Sand	Partial	0.511
San Isabel	Partial	0.558
Spanish	Partial	0.503
Wild Cherry	Partial	0.518
Black	Full	0.469
Cotton	Full	0.538
Rito Alto	Full	0.569
South Crestone	Full	0.483
Willow	Full	0.521

Table 3. Summary of Ben Ohau Range hypsometry data. Basins are listed from south to north. Mean values for hypsometric integral are: minor glaciation, 0.51; moderate glaciation, 0.49; full glaciation, 0.44.

Basin	Degree of glaciation	Hypsometric integral
Darts Bush	Minor	0.523
Fraser	Minor	0.519
Dry	Minor	0.524
Gladstone	Minor	0.504
McMillan	Minor	0.534
Top McMillan	Minor	0.516
Mackenzie	Minor	0.482
Duncan	Minor	0.493
Boundary	Minor	0.501
Jacks	Moderate	0.534
Whale	Moderate	0.483
Twin	Moderate	0.492
Dead Horse	Moderate	0.485
Bush	Moderate	0.459
Freds	Full	0.466
Birch Hill	Full	0.449
Hoophorn	Full	0.394
Sawyer	Full	0.465
Black Birch	Full	0.438

Table 4. Summary of hypsometry data for other fully glaciated basins in the western US, as illustrated in Fig 6 (in addition to the fully glaciated basins in the Sangre de Cristos, Table 2).

Basin	Range	Hypsometric integral
Lincoln	Glacier National Park	0.292
Harrison	Glacier National Park	0.408
Walton	Glacier National Park	0.329
Grinnell	Glacier National Park	0.334
Swift	Glacier National Park	0.344
Iceberg	Glacier National Park	0.364
Sprague	Glacier National Park	0.396
Snyder	Glacier National Park	0.411
Mineral	Glacier National Park	0.433
Mill	Bitterroots	0.520
Blodgett	Bitterroots	0.510
Fred Burr	Bitterroots	0.514
Sawtooth	Bitterroots	0.508
Roaring Lion	Bitterroots	0.527
Rock	Bitterroots	0.438
Tin Cup	Bitterroots	0.463

References

Andrews, J. T., 1972, Glacier power, mass balances, velocities and erosion potential: Zeitschrift fur Geomorphologie N.F. Suppl. Bd., v. 13, p. 1-17.

Bateman, P. C., 1965, Geology and Tungsten Mineralization of the Bishop District, California, U.S. Geological Survey Professional Paper, 208 p.

Benn, D. I., and Evans, D. J. A., 1998, Glaciers and Glaciation: London, Arnold, 734 p.

Blick, G. H., Read, S. A. L., and Hall, P. T., 1989, Deformation monitoring of the Ostler Fault Zone, South Island, New Zealand: Tectonophysics, v. 167, p. 329-339.

Braun, J., Zwartz, D., and Tomkin, J. H., 1999, A new surface-processes model combining glacial and fluvial erosion: Annals of Glaciology, v. 28, p. 282-290.

Brocklehurst, S. H., and Whipple, K. X., 2000, Hypsometry of Glaciated Landscapes in the western U.S. and New Zealand: EOS, v. 81, no. 48, p. F504.

-, 2002, Glacial Erosion and Relief Production in the Eastern Sierra Nevada, California: Geomorphology, v. 42, no. 1-2, p. 1-24.

-, in prep.-a, Rates of glacial erosion in the ablation zone: evidence from fluvial landscape simulation.

-, in prep.-b, The Response of Glaciated Landscapes to Varying Rock Uplift Rates.

Brozovic, N., Burbank, D. W., and Meigs, A. J., 1997, Climatic Limits on Landscape Development in the Northwestern Himalaya: Science, v. 276, p. 571-574.

Burbank, D. W., 1991, Late Quaternary snowline reconstructions for the southern and central Sierra Nevada, California, and a Reassessment of the "Recess Peak Glaciation": Quaternary Research, v. 36, p. 294-306.

Furbish, D. J., and Andrews, J. T., 1984, The use of hypsometry to indicate long-term stability and response of valley glaciers to changes in mass-transfer: Journal of Glaciology, v. 30, no. 105, p. 199-211.

Gillespie, A. R., 1982, Quaternary Glaciation and Tectonism in the Southeastern Sierra Nevada, Inyo County, California [PhD thesis]: California Institute of Technology, 695 p.

Harrison, C. G. A., Miskell, K. J., Brass, G. W., Saltzman, E. S., and Sloan, J. L., II, 1983, Continental hypsography: Tectonics, v. 2, p. 357-378.

Hurtrez, J.-E., Sol, C., and Lucazeau, F., 1999, Effect of Drainage Area on Hypsometry from an Analysis of Small-Scale Basins in the Siwalik Hills (Central Nepal): Earth Surface Processes and Landforms, v. 24, p. 799-808.

Johnson, B. R., Lindsey, D. A., Bruce, R. M., and Soulliere, S. J., 1987, Reconnaissance geologic map of the Sangre de Cristo Wilderness Study Area, south-central Colorado: USGS Miscellaneous Field Studies Map, v. MF-1635-B.

Kirkbride, M., and Matthews, D., 1997, The Role of Fluvial and Glacial Erosion in Landscape Evolution: The Ben Ohau Range, New Zealand: Earth Surface Processes and Landforms, v. 22, p. 317-327.

Lifton, N. A., and Chase, C. G., 1992, Tectonic, climatic and lithologic influences on landscape fractal dimension and hypsometry: implications for landscape evolution in the San Gabriel Mountains, California: Geomorphology, v. 5, p. 77-114.

MacGregor, K. C., Anderson, R. S., Anderson, S. P., and Waddington, E. D., 2000, Numerical Simulations of Glacial Valley Longitudinal Profile Evolution: Geology, v. 28, no. 11, p. 1031-1034.

McCalpin, J. P., 1986, Quaternary Tectonics of the Sangre de Cristo and Villa Grove Fault Zones: Colorado Geological Survey Special Publication, v. 28, p. 59-64.

-, 1987, Recurrent Quaternary normal faulting at Major Creek, Colorado: An example of youthful tectonism on the eastern boundary of the Rio Grande Rift Zone, *in* Beus, S. S., ed., Geological Society of America Centennial Field Guide - Rocky Mountain Section, Geological Society of America, p. 353-356.

Merrand, Y., and Hallet, B., 2000, A physically based numerical model of orogen-scale glacial erosion: Importance of subglacial hydrology and basal stress regime: GSA Abstracts with Programs, v. 32, no. 7, p. A329.

Molnar, P., and England, P., 1990, Late Cenozoic uplift of mountain ranges and global climate change: chicken or egg?: Nature, v. 346, p. 29-34.

Montgomery, D. R., Balco, G., and Willett, S. D., 2001, Climate, tectonics and the morphology of the Andes: Geology, v. 29, no. 7, p. 579-582.

Moore, J. G., 1963, Geology of the Mount Pinchot Quadrangle, Southern Sierra Nevada, California, US Geological Survey Bulletin, 152 p.

-, 1981, Geologic map of the Mount Whitney Quadrangle, Inyo and Tulare Counties, California, US Geological Survey Map.

Porter, S. C., 1970, Quaternary glacial record in Swat Kohistan, West Pakistan: Geological Society of America Bulletin, v. 81, no. 5, p. 1421-1446.

-, 1975, Equilibrium-line altitudes of late Quaternary glaciers in the Southern Alps, New Zealand: Quaternary Research, v. 5, p. 27-47.

-, 1989, Some Geological Implications of Average Quaternary Glacial Conditions: Quaternary Research, v. 32, p. 245-261.

Raymo, M. E., and Ruddiman, W. F., 1992, Tectonic forcing of late Cenozoic climate: Nature, v. 359, p. 117-122.

Richmond, G. M., 1965, Glaciation of the Rocky Mountains, *in* Wright, H. E., Jr, and Frey, G. D., eds., The Quaternary of the United States: Princeton, NJ, Princeton University Press, p. 217-230.

Schumm, S. A., 1956, Evolution of drainage systems and slopes in badlands at Perth Amboy, New Jersey: Geological Society of America Bulletin, v. 67, p. 597-646.

Small, E. E., 1995, Hypsometric forcing of stagnant ice margins: Pleistocene valley glaciers, San Juan Mountains, Colorado: Geomorphology, v. 14, p. 109-121.

Small, E. E., and Anderson, R. S., 1998, Pleistocene relief production in Laramide mountain ranges, western United States: Geology, v. 26, p. 123-126.

Spörli, K. B., and Lillie, A. R., 1974, Geology of the Torlesse Supergroup in the northern Ben Ohau Range, Canterbury, New Zealand: New Zealand Journal of Geology and Geophysics, v. 17, p. 115-141.

Strahler, A. N., 1952, Hypsometric (area-altitude) analysis of erosional topography: Geological Society of America Bulletin, v. 63, p. 1117-1141.

Sugden, D. E., and John, B. S., 1976, Glaciers and Landscape: London, Arnold, 376 p.

Tippett, J. M., and Kamp, P. J. J., 1995a, Geomorphic Evolution of the Southern Alps, New Zealand: Earth Surface Processes and Landforms, v. 20, p. 177-192.

-, 1995b, Quantitative relationships between uplift and relief parameters for the Southern Alps, New Zealand, as determined by fission track analysis: Earth Surface Processes and Landforms, v. 20, p. 153-175.

Tomkin, J. H., and Braun, J., 2000, The effect of glaciation on relief in an active orogen: a numerical modelling study: EOS, v. 81, no. 48, p. F504.

Whipple, K. X., Kirby, E., and Brocklehurst, S. H., 1999, Geomorphic limits to climate-induced increases in topographic relief: Nature, v. 401, p. 39-43.

Willgoose, G., and Hancock, G., 1998, Revisiting the Hypsometric Curve as an Indicator of Form and Process in Transport-Limited Catchments: Earth Surface Processes and Landforms, v. 23, p. 611-623.

a.

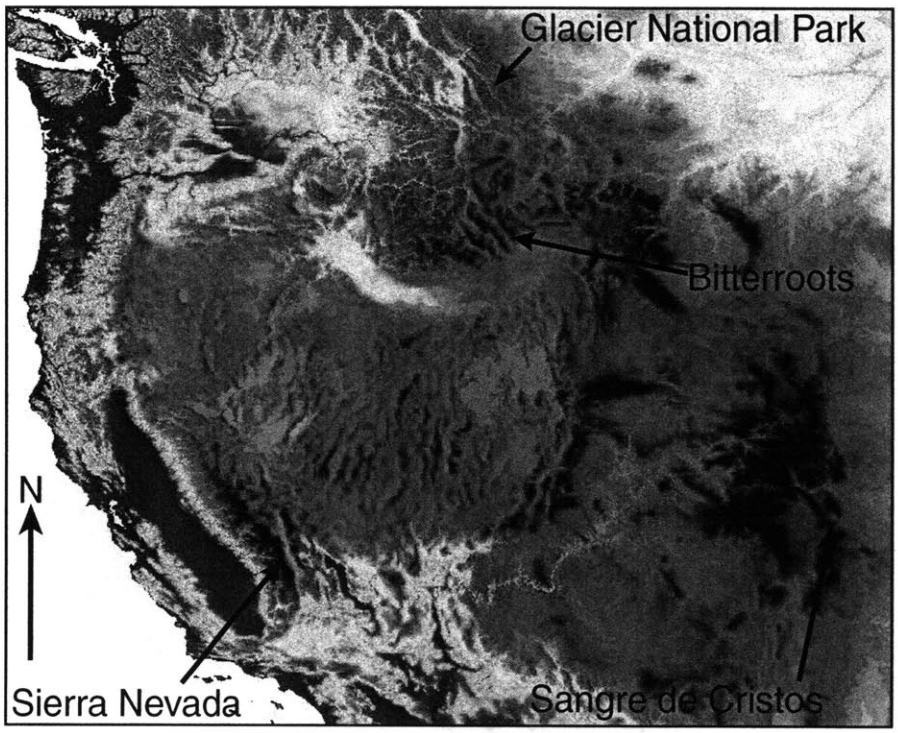
Glacier National Park
Bitterroots
N
Sierra Nevada
Sangre de Cristos

b.

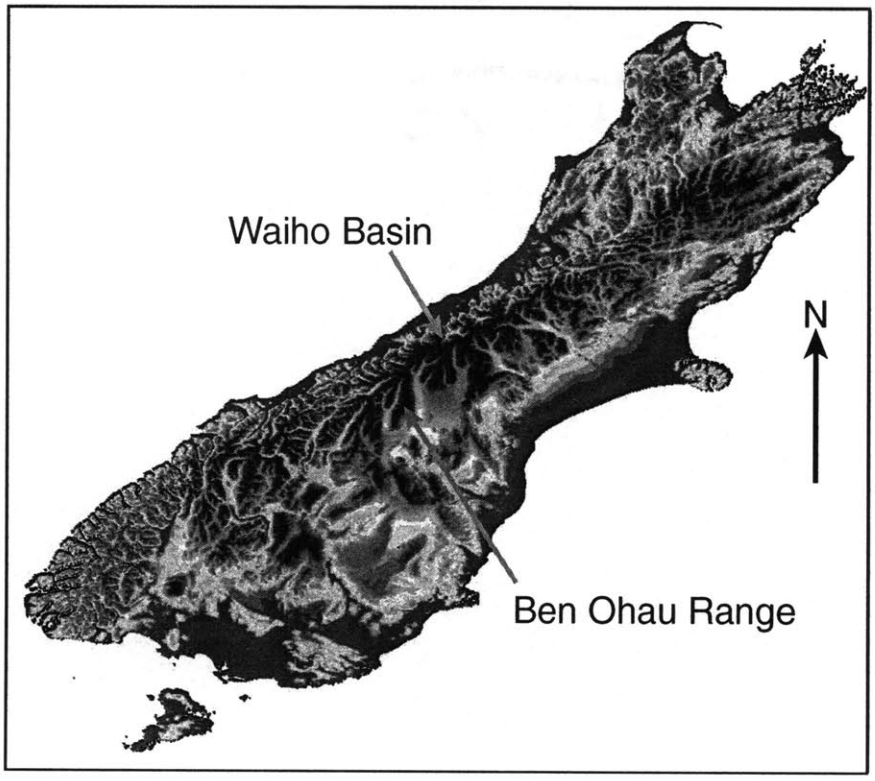
Waiho Basin
N
Ben Ohau Range

Fig. 1

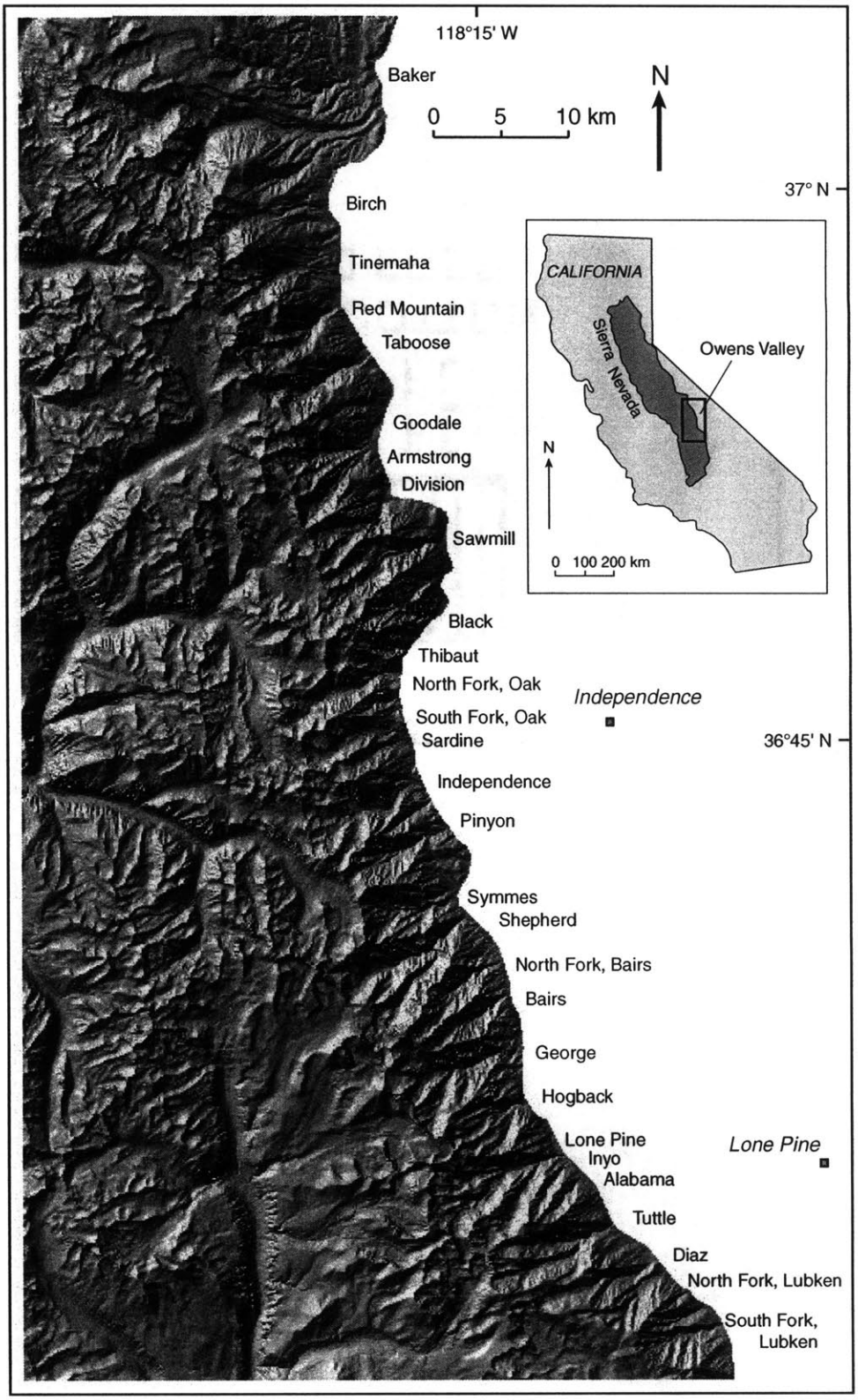
118°15' W
Baker
0 5 10 km
N
37° N
Birch
Tinemaha
Red Mountain
Taboose
Goodale
Armstrong
Division
Sawmill
Black
Thibaut
North Fork, Oak
South Fork, Oak
Sardine
Independence
Pinyon
Symmes
Shepherd
North Fork, Bairs
Bairs
George
Hogback
Lone Pine
Inyo
Alabama
Tuttle
Diaz
North Fork, Lubken
South Fork,
Lubken
Independence
36°45' N
Lone Pine
CALIFORNIA
Sierra Nevada
Owens Valley
N
0 100 200 km

Fig. 2a

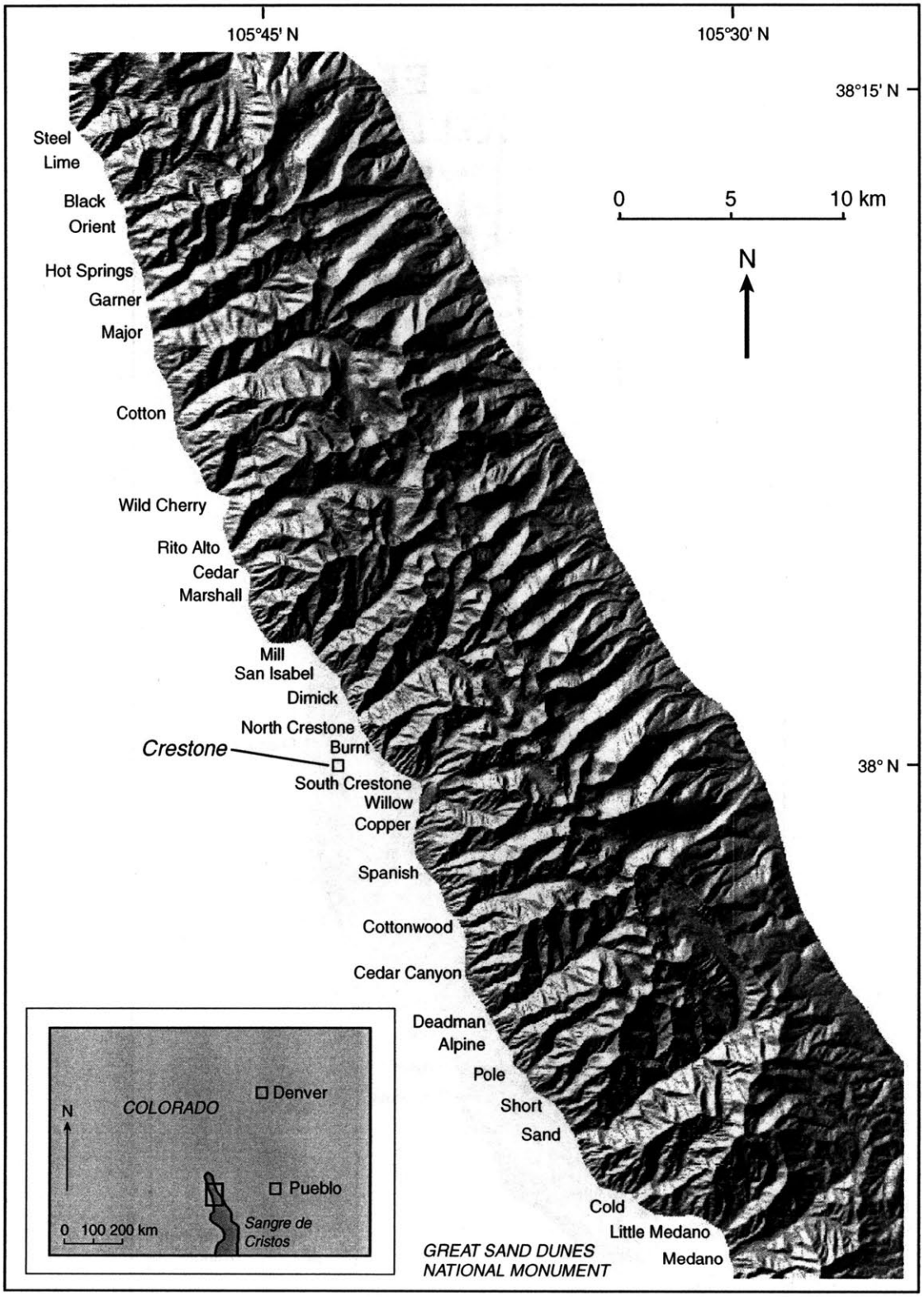
105°45' N
105°30' N
38°15' N
38° N
0 5 10 km
N
Steel
Lime
Black
Orient
Hot Springs
Garner
Major
Cotton
Wild Cherry
Rito Alto
Cedar
Marshall
Mill
San Isabel
Dimick
North Crestone
Crestone
Burnt
South Crestone
Willow
Copper
Spanish
Cottonwood
Cedar Canyon
Deadman
Alpine
Pole
Short
Sand
Cold
Little Medano
Medano
GREAT SAND DUNES
NATIONAL MONUMENT
COLORADO
Denver
Pueblo
Sangre de
Cristos
0 100 200 km

Fig. 2b

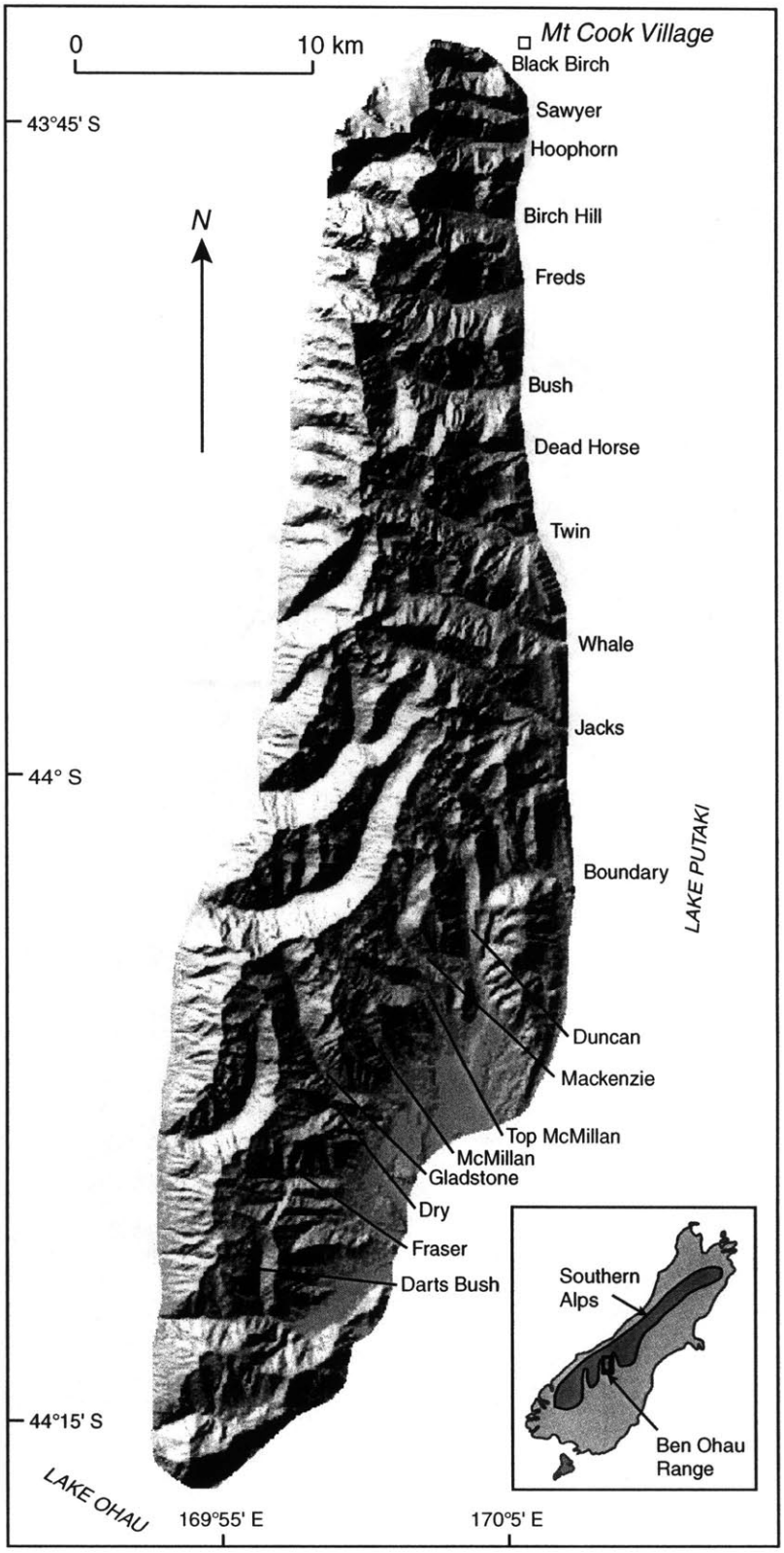
0
10 km
Mt Cook Village
Black Birch
Sawyer
Hoophorn
Birch Hill
Freds
Bush
Dead Horse
Twin
Whale
Jacks
Boundary
Duncan
Mackenzie
Top McMillan
McMillan
Gladstone
Dry
Fraser
Darts Bush
43°45' S
44° S
44°15' S
N
LAKE PUTAKI
LAKE OHAU
169°55' E
170°5' E
Southern Alps
Ben Ohau Range

Fig. 2c

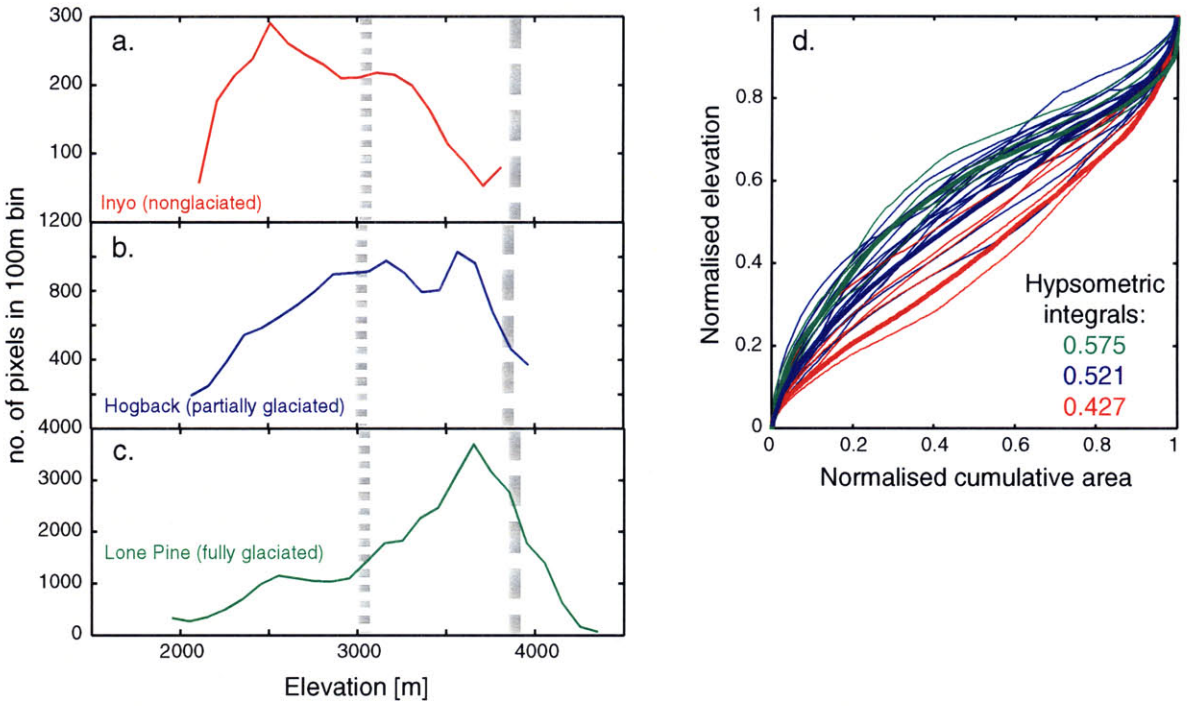
a.
Inyo (nonglaciated)
b.
Hogback (partially glaciated)
c.
Lone Pine (fully glaciated)
no. of pixels in 100m bin
Elevation [m]
d.
Normalised elevation
Normalised cumulative area
Hypsometric integrals:
0.575
0.521
0.427

Fig. 3

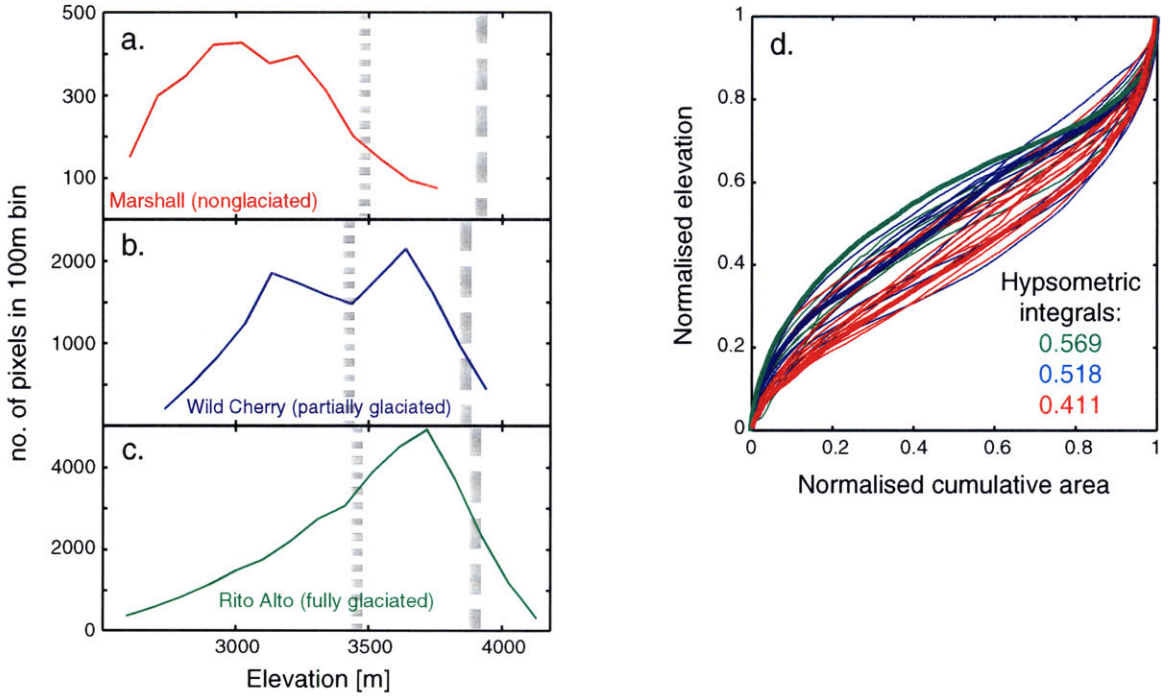
a.
Marshall (nonglaciated)
b.
Wild Cherry (partially glaciated)
c.
Rito Alto (fully glaciated)
no. of pixels in 100m bin
Elevation [m]
d.
Normalised elevation
Normalised cumulative area
Hypsometric integrals:
0.569
0.518
0.411

Fig. 4

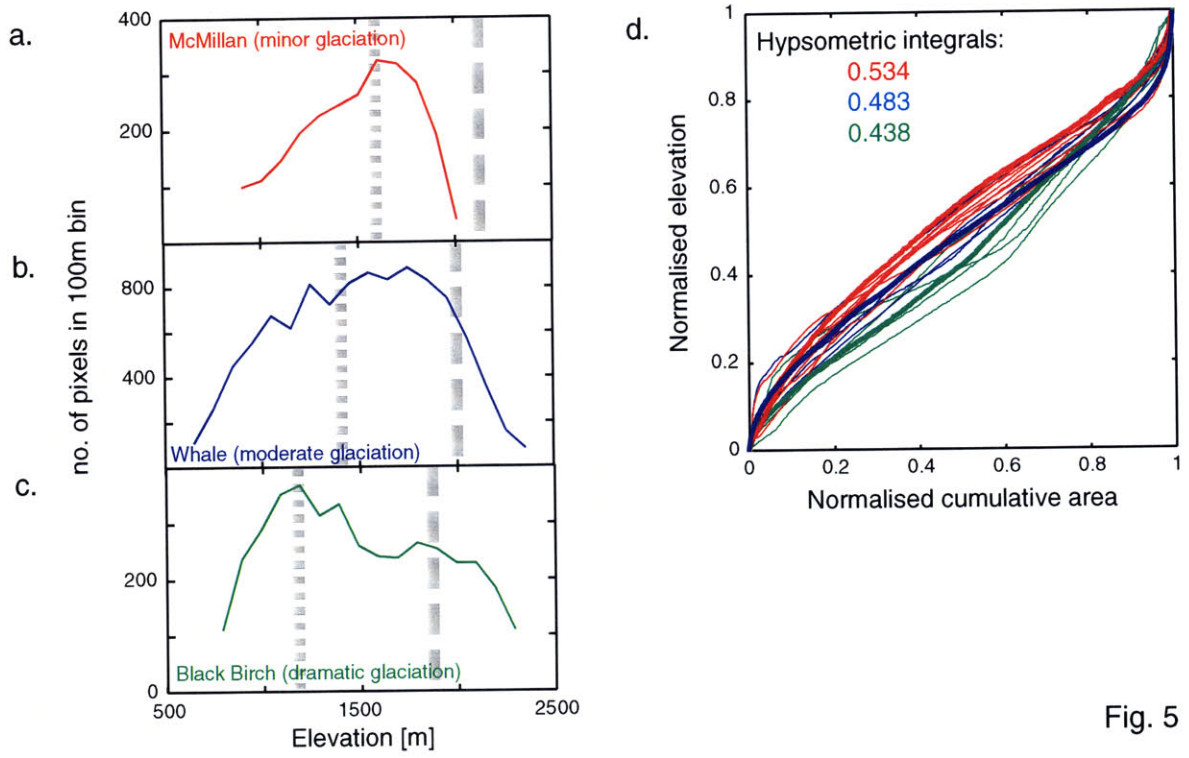
a.
b.
c.
d.
McMillan (minor glaciation)
Whale (moderate glaciation)
Black Birch (dramatic glaciation)
no. of pixels in 100m bin
Elevation [m]
Hypsometric integrals:
0.534
0.483
0.438
Normalised elevation
Normalised cumulative area

Fig. 5

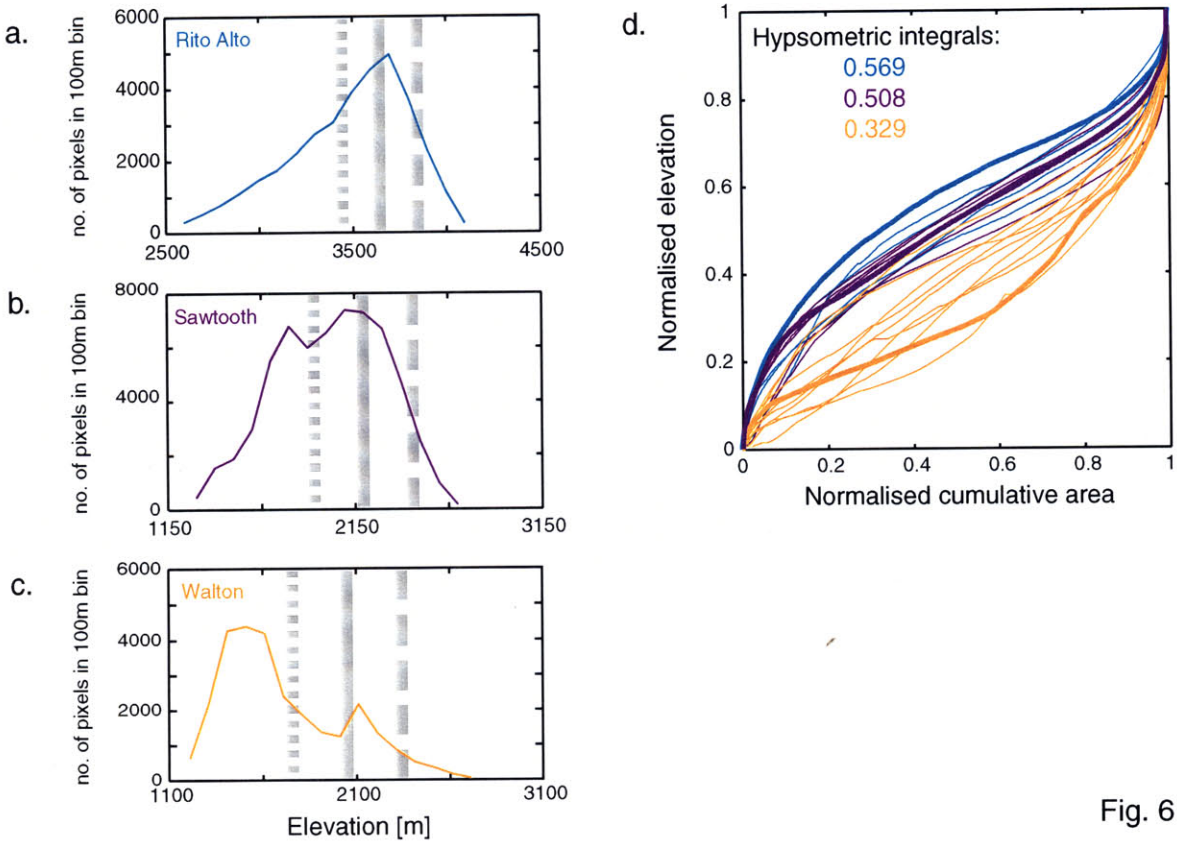
a.
b.
c.
d.
Rito Alto
Sawtooth
Walton
no. of pixels in 100m bin
Elevation [m]
Hypsometric integrals:
0.569
0.508
0.329
Normalised elevation
Normalised cumulative area

Fig. 6

a.

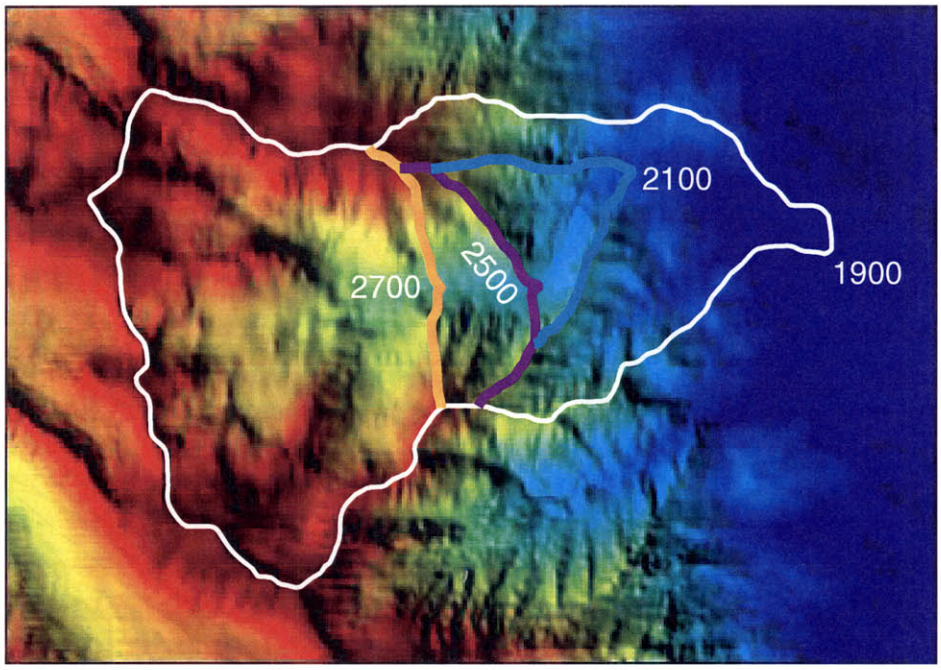
2100
2500
2700
1900

b.

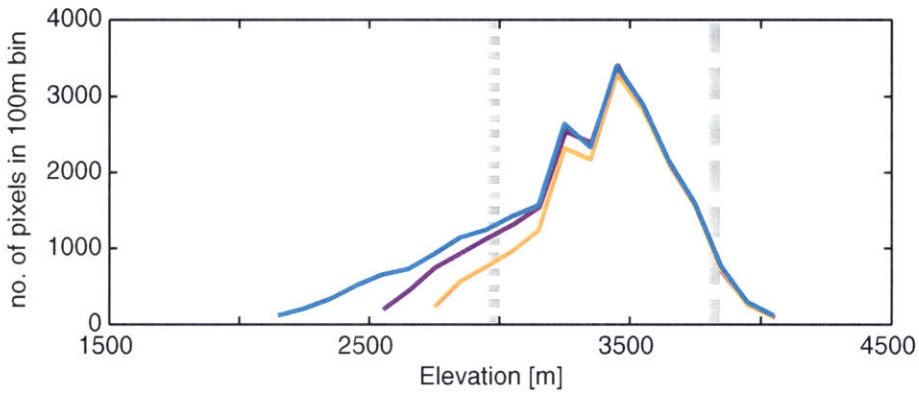
4000
3000
2000
1000
0
no. of pixels in 100m bin
1500
2500
3500
4500
Elevation [m]

c.

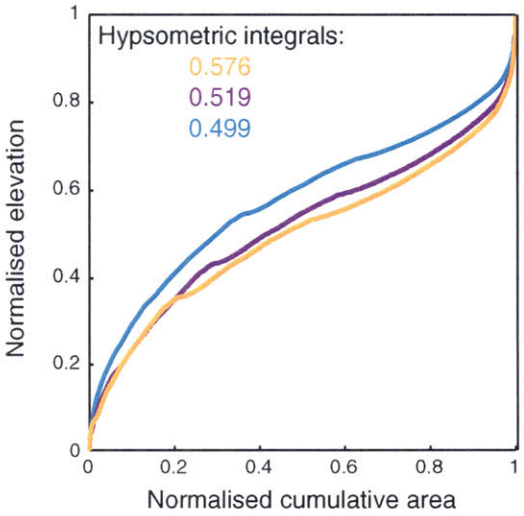
Hypsometric integrals:
0.576
0.519
0.499
1
0.8
0.6
0.4
0.2
0
Normalised elevation
0
0.2
0.4
0.6
0.8
1
Normalised cumulative area

Fig. 7

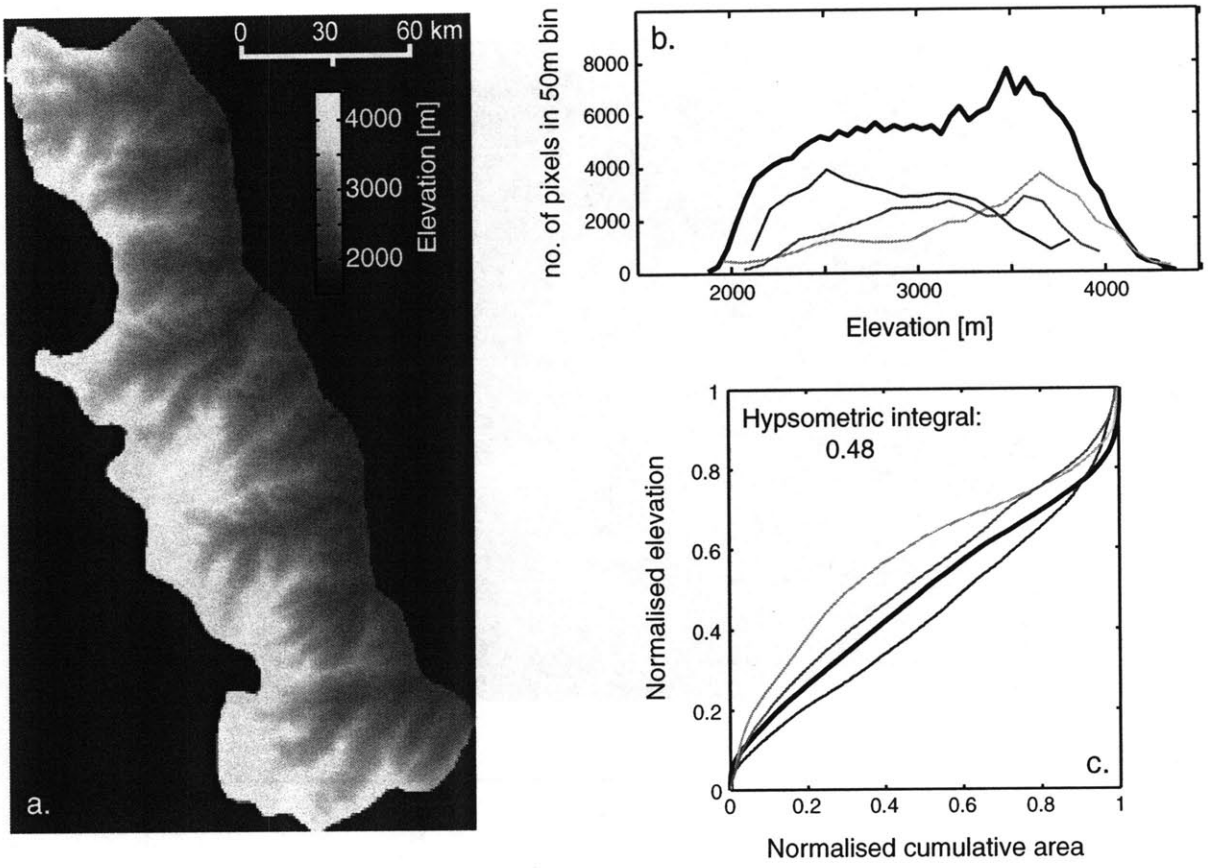
0
30
60 km
4000
3000
2000
Elevation [m]
a.
b.
no. of pixels in 50m bin
8000
6000
4000
2000
0
2000
3000
4000
Elevation [m]
Hypsometric integral:
0.48
Normalised elevation
1
0.8
0.6
0.4
0.2
0
0
0.2
0.4
0.6
0.8
1
c.
Normalised cumulative area

Fig. 8

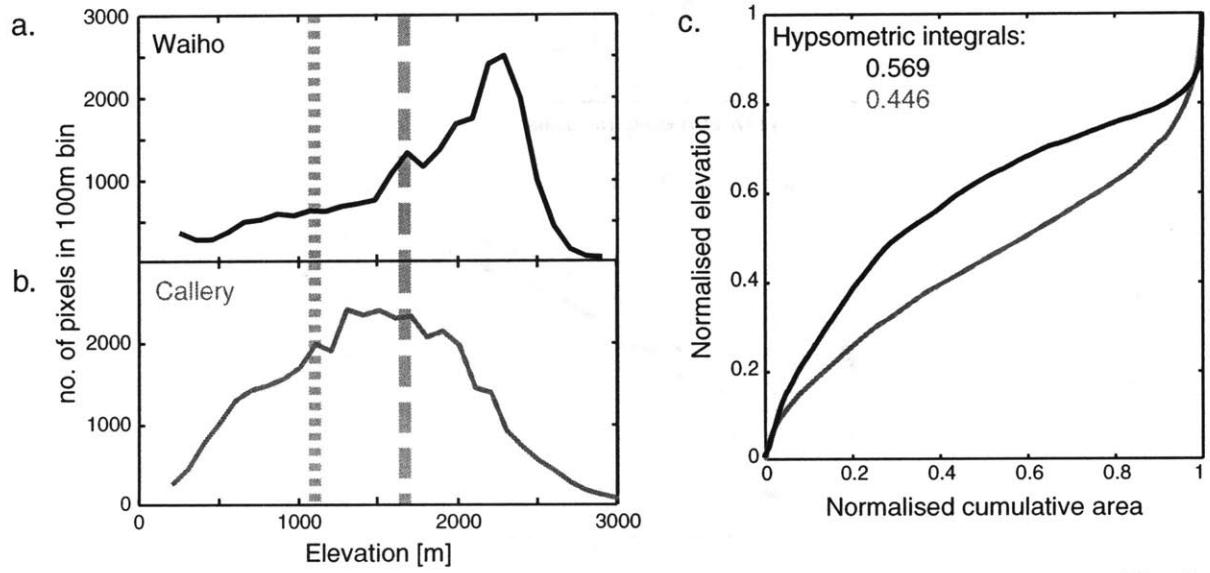
a.
Waiho
b.
Callery
no. of pixels in 100m bin
3000
2000
1000
0
1000
2000
3000
Elevation [m]
c.
Hypsometric integrals:
0.569
0.446
Normalised elevation
1
0.8
0.6
0.4
0.2
0
0
0.2
0.4
0.6
0.8
1
Normalised cumulative area

Fig. 9

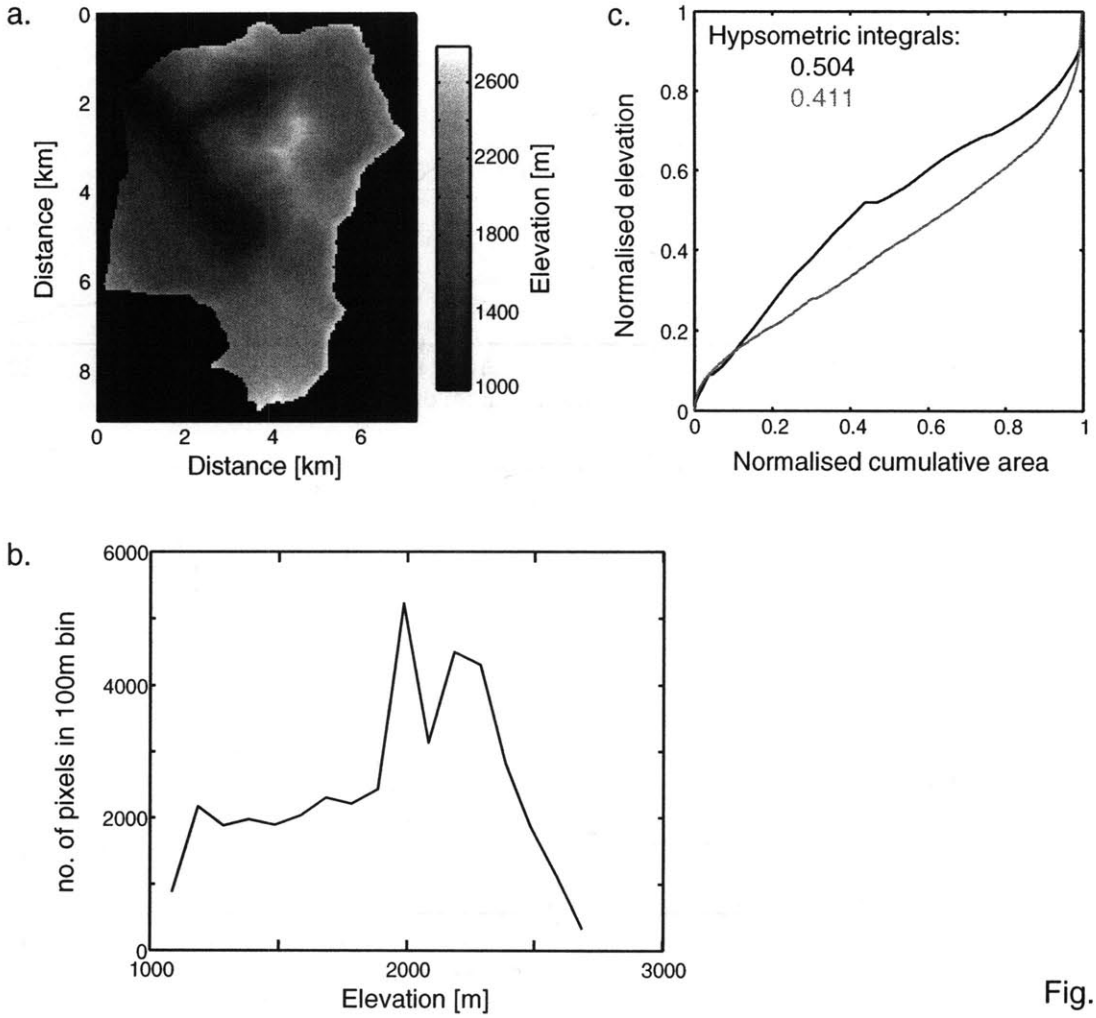
a.
Distance [km]
Distance [km]
Elevation [m]
2600
2200
1800
1400
1000
c.
Hypsometric integrals:
0.504
0.411
Normalised elevation
Normalised cumulative area
b.
no. of pixels in 100m bin
Elevation [m]

Fig. 10

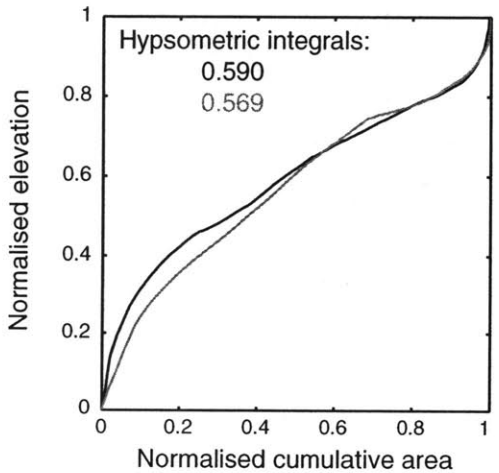
Hypsometric integrals:
0.590
0.569
Normalised elevation
Normalised cumulative area

Fig. 11

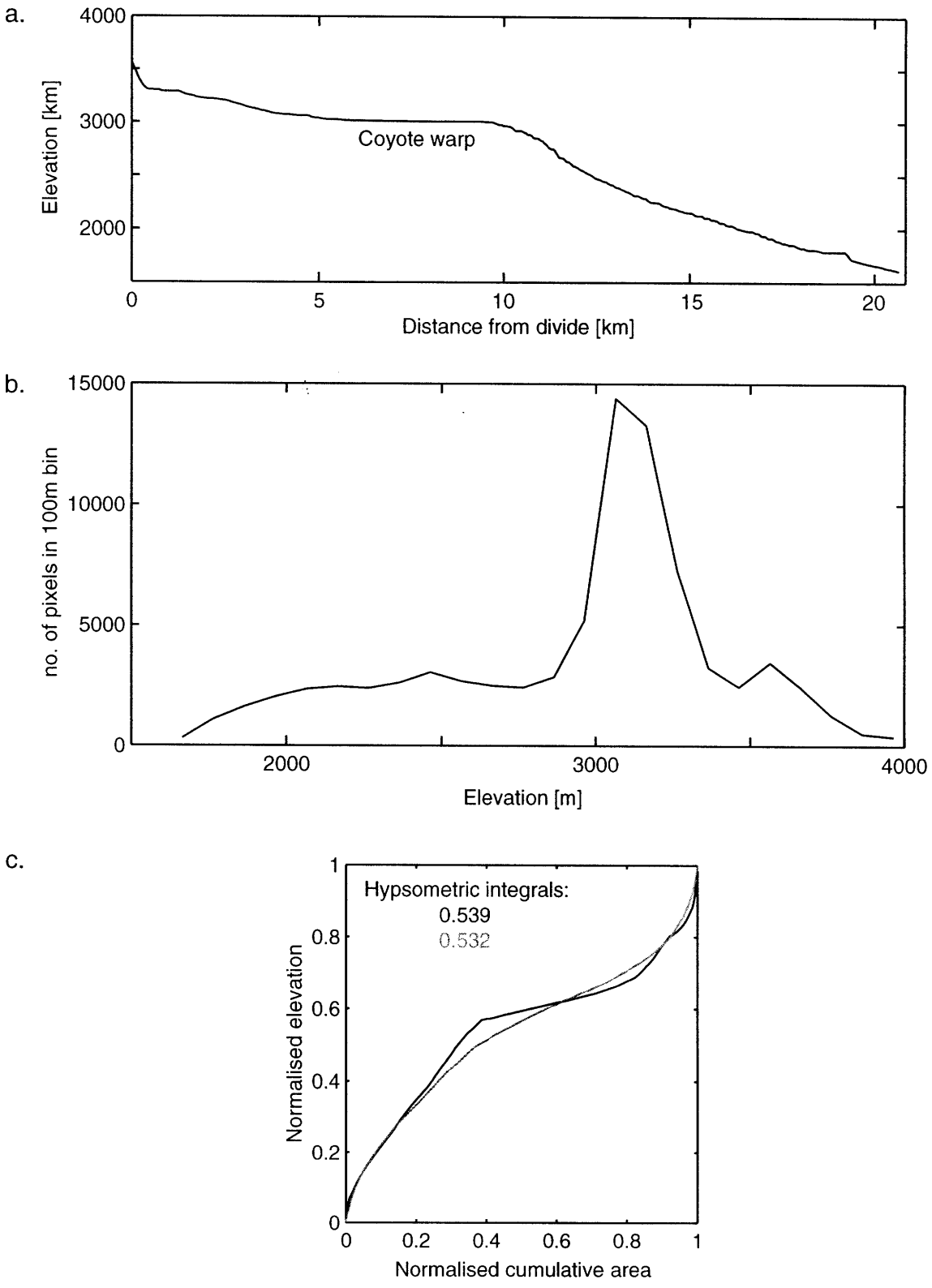
a.
4000
3000
2000
Elevation [km]
Coyote warp
0
5
10
15
20
Distance from divide [km]
b.
15000
10000
5000
0
no. of pixels in 100m bin
2000
3000
4000
Elevation [m]
c.
1
0.8
0.6
0.4
0.2
0
Normalised elevation
Hypsometric integrals:
0.539
0.532
0
0.2
0.4
0.6
0.8
1
Normalised cumulative area

Fig. 12

a.

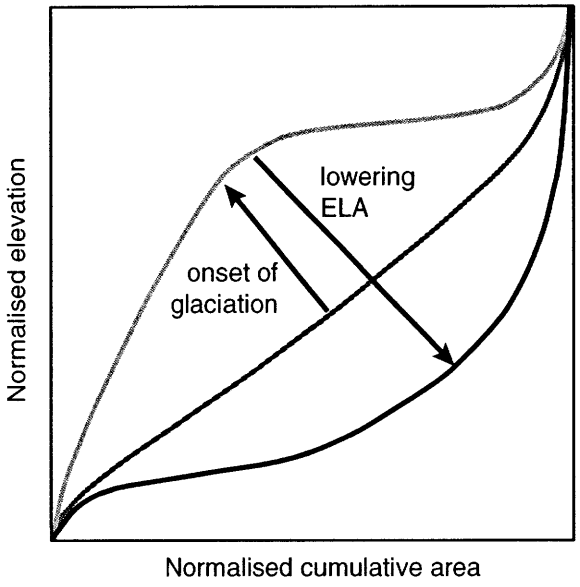
lowering
ELA
onset of
glaciation
Normalised elevation
Normalised cumulative area

b.

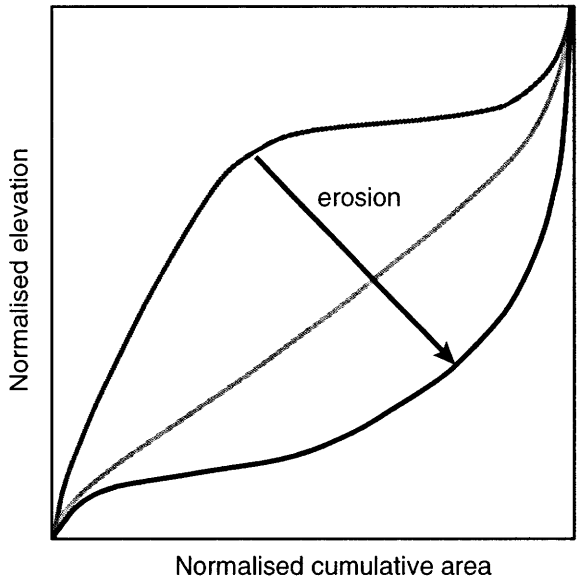
erosion
Normalised elevation
Normalised cumulative area

Fig. 13

Chapter 8

The Response of Glaciated Landscapes to Varying Rock Uplift Rates

Simon H. Brocklehurst* and Kelin X. Whipple

Department of Earth, Atmospheric and Planetary Sciences, Massachusetts Institute of Technology, Cambridge MA 02139, USA

Prepared for submission to: *Geological Society of America Bulletin*

* to whom correspondence should be addressed: email: shb@mit.edu, fax: 1-617-252-1800

Abstract

The response of glaciated landscapes to rapid tectonic uplift is an important aspect of proposed interactions between plate tectonic processes and climate change. Rivers typically respond to more rapid rock uplift in part by increasing their channel gradient. In contrast, the "glacial buzzsaw hypothesis" suggests that glaciers can erode as fast as the fastest tectonic uplift rates without any steepening of the landscape. However, it has not been established how this is achieved. Do glaciers have a specific response to rapid rock uplift? We examined longitudinal profiles and hypsometry for glaciated basins in areas of spatially variable rock uplift rate in the Southern Alps, New Zealand, and around Nanga Parbat, Pakistan. The response of these glaciated landscapes to rapid rock uplift comprises: (i) Development of tall, steep headwalls. Around Nanga Parbat, headwalls several kilometres high can constitute >50% of the basin relief. (ii) Weak steepening of longitudinal profiles. Larger glaciated basins maintain shallow slopes despite rapid rock uplift. (iii) Steepening of the basin as a whole (as shown in the hypsometry), dominated by hillslope lengthening.

At rapid rock uplift rates, although glaciers can incise the valley floor swiftly, they cannot bring down adjacent hillslopes sufficiently fast to prevent them from reaching exceptional heights. The hillslope gradient does not increase; rather drainage density decreases. This lengthening of hillslopes causes regional mean elevation to rise slightly with increasing rock uplift rate, but much less than expected in unglaciated ranges. This has important implications for the interplay between surface processes and tectonics.

Keywords: glacial erosion; tectonic uplift

1. Introduction

The potential for important interactions between climate change, tectonics and surface processes has received considerable attention in recent years (Beaumont et al., 1992; Beaumont et al., 2001; Koons, 1995; Molnar and England, 1990; Raymo and Ruddiman, 1992; Willett, 1999; Zeitler et al., 2001). Raymo and co-workers (e.g., Raymo and Ruddiman, 1992) suggested that increasing the elevation of mountain belts is a major influence on global climate, through enhanced weathering and drawdown of CO_2, greater albedo, and disturbance of atmospheric circulation patterns. Meanwhile, Molnar and England (1990) proposed that climate change caused the development of relief, isostatic uplift, and thus the appearance of synchronous tectonic uplift of many different mountain belts around the globe. While the Himalayas and the Southern Alps of New Zealand have proven to be attractive field sites for more detailed analyses of the coupling between surface and tectonic processes (Fig. 1), most of the surface processes models employed have focussed on fluvial and diffusive processes as the major erosive agents (e.g., Beaumont et al., 1992; Beaumont et al., 2001; Koons, 1995; Willett, 1999). For example, Willett (1999) models a cross-section through the Mt Cook region of the Southern Alps (Fig. 1b) with a surface processes model whose only component is a fluvial incision model. Landslides, avalanches and glacial erosion are clearly active in this landscape, and arguably are the dominant erosion processes (Fig. 1b). One purpose of this paper is to assess the significance of neglecting glacial erosion in modelling the dynamics of active mountain belts, i.e., posing the questions, how different are the evolution of fluvial and glacial landscapes in rapidly uplifting settings, and what are the implications of this for the dynamics of a developing orogen?

A second, complementary purpose of this paper is to test the "glacial buzzsaw hypothesis" proposed by Brozovic et al. (1997). They observed that different regions of the landscape around Nanga Parbat all had similar hypsometry (frequency distribution of elevations) with respect to the snowline, despite widely varying tectonic uplift rates. That the landscape does not show significant variation despite the extreme differences in rock uplift rates suggests that the glaciers that dominate the Nanga Parbat landscape are capable of keeping pace with some of the fastest rock uplift rates on the globe without a commensurate increase in either valley slope or glacier accumulation area (landscape area above the ELA). Thus, according to the glacial buzzsaw hypothesis, regional mean elevations are limited to a level closely related to the regional snowline. However, Brozovic et al. (1997) included the important caveat that localised

peaks, such as Nanga Parbat itself, may penetrate the 'snowline envelope', and reach much higher elevations. Our study was motivated by the observation in the Southern Alps that the glacial buzzsaw hypothesis is not strictly accurate. One prediction of the hypothesis is that mean elevation should follow variations in the snowline/ELA rather than variations in rock uplift rate. However, as shown in Figure 2, mean topography rises in association with interpreted rock uplift rates around Mt Cook, while the ELA is at a much more uniform level across the region (Porter, 1975).

Of particular importance to attempts to relate tectonics and climate change is the change from mostly fluvial landscapes prior to late Cenozoic cooling to the subsequent development of significant alpine glaciation. We have previously examined the key distinctions between fluvial and glacial landscapes in the slowly uplifting eastern Sierra Nevada, California (Brocklehurst and Whipple, 2002), the Sangre de Cristo Range, Colorado (Brocklehurst and Whipple, 2001), and the Ben Ohau Range, New Zealand (Brocklehurst and Whipple, 2000). In comparison with expectations for a fluvial landscape, Sierra Nevadan glaciers have brought down both the valley floor and neighbouring ridgelines in the part of the landscape above the approximate mean Quaternary equilibrium line altitude (ELA) (Porter, 1989), but have done little to incise below this elevation, despite obvious widening of the valley to form characteristic U-shaped cross-sections. Furthermore, the glaciers in the eastern Sierra Nevada have generated only minor relief, through their ability to enlarge basins by headwall erosion at the expense of low relief topography. Here we seek to examine the response of glaciers to more rapid rates of rock uplift, once more in the context of how this compares with our expectations for fluvial landscapes. This allows us to consider how alpine landscapes in areas of fast uplift have responded to the onset of late Cenozoic glaciation, which in turn influences how their relief has developed, and ultimately the nature and strength of feedbacks between climate and tectonics.

This paper begins with a summary of previous studies on the relationship between tectonic rock uplift and erosional processes in both fluvial and glacial settings. We then outline the three principle methods that we have used to analyse glacial landscapes experiencing varying rates of rock uplift (hypsometry, and longitudinal profile and hillslope analyses) and describe the two field sites selected for this study, the Southern Alps of New Zealand, and the north-western Himalaya of Pakistan. Our results show that both hypsometry and longitudinal profile slope can be affected by increasing rock uplift rates, but the principle response of glaciated landscapes to

rapid rock uplift is the development of tall, steep hillslopes, which the glaciers at their bases apparently have little control over. In turn, this suggests that peaks may continue to rise, even though the majority of the landscape is kept in check by the glacial buzzsaw. We conclude that the isolated peaks mentioned by Brozovic et al. (1997) are an important part of glaciated landscapes, with considerable importance for atmospheric dynamics, avalanche risk, glacial dynamics, and orographic precipitation. In terms of potential coupling between glacial erosion and tectonic processes, the potential for large glacial valley floors to maintain their elevation in the face of rapid rock uplift is quite distinct from the response of most rivers. Even the Indus River is forced to steepen to maintain its elevation as it traverses the rapidly uplifting Nanga Parbat-Haramosh axis (Burbank et al., 1996). Outside zones of very localised uplift, such as the Nanga Parbat massif, the presence of towering hillslopes does cause the mean topography of glaciated landscapes to rise in response to tectonic uplift, although in a style quite different from fluvially-incised landscapes.

2. Background

We follow England and Molnar (1990) in making a careful distinction between exhumation (the uplift of a given package of rocks with respect to the Earth's surface), rock uplift (the uplift of a given package of rocks with respect to a reference level such as the geoid) and surface uplift (the uplift of the Earth's surface with respect to a reference level such as the geoid). It is exhumation that is readily measured using thermochronologic techniques (barring complications due to particle trajectories and thermal evolution), and rock uplift that causes a response in surface processes. For a simple definition of topographic steady state (i.e., the mean elevation of some portion of the Earth's surface is invariant with time), considering vertical motions only, exhumation and rock uplift are equal. Otherwise an assumption is required to place a given region within the spectrum from erosion matching rock uplift (steady state) to negligible erosion (surface uplift equals rock uplift). As emphasised by Willett and Brandon (2002), for long-term topographic steady state in most mountain belts it is necessary to consider horizontal as well as vertical components to particle trajectories, while Stüwe and Barr (1998) emphasise the importance of the dynamics of the whole crustal column for steady-state mean topography. However, the discussion that follows is generally restricted to the vertical components of both uplift and erosion.

The response of rivers to changes in rock uplift rate is well understood, at least in qualitative terms. Relief evolution in fluvial environments is most strongly dependent on the response of the bedrock channel system (Whipple et al., 1999). The well-known "stream power erosion law" (e.g., Howard et al., 1994; Howard and Kerby, 1983; Whipple and Tucker, 1999) appears sufficiently robust to characterise the response of these bedrock channels to a change in the tectonic uplift regime in a semi-quantitative manner. According to the stream power erosion law, local erosion rate is a power-law function of upstream drainage area, A, and local channel gradient, S, such that a river profile evolution equation can be written (Howard et al., 1994):

$$\frac{dz}{dt} = U(x,t) - KA^m S^n \tag{1}$$

where dz/dt is the rate of change of bed elevation, U is rock uplift rate (defined relative to base-level), K is a dimensional coefficient of erosion, and m and n are positive constants that reflect erosion processes, basin hydrology and channel hydraulic geometry. At steady state ($dz/dt = 0$), channel gradient is proportional to rock uplift rate to the $1/n$ power:

$$S = \left(\frac{U}{K}\right)^{\frac{1}{n}} A^{-\frac{m}{n}} \tag{2}$$

Debate continues on the quantitative application of this model, particularly in terms of internal feedbacks that influence the effective values of model parameters (especially K and n). The uncertainties and internal feedbacks include the sensitivity to rock uplift rate (e.g., Kirby and Whipple, 2001), the role of sediment flux and grain size (e.g., Sklar and Dietrich, 1998; Sklar and Dietrich, 2001; Whipple and Tucker, 2002), the role of a critical threshold stress for initiation of erosion (e.g., Snyder et al., in review), the influence of orographic precipitation (e.g., Roe et al., 2002), the importance of storm distributions (Tucker and Bras, 2000), and the importance of river width adjustments (e.g., Snyder et al., 2000). However, the qualitative response of fluvial landscapes to uplift are relatively well understood. The response of the glacial system is much less certain, even at this qualitative level.

Burbank et al. (1996) found that hillslope angles in the Nanga Parbat region are largely independent of rock uplift rates, whether glacial or fluvial erosion controls the lower boundary condition for the hillslope. The uniformly high mean slopes among all areas suggest a common threshold controlling all of them, namely bedrock landsliding. It is generally accepted that landsliding is the dominant agent of hillslope erosion in a high-relief, tectonically active setting. This process is commonly modelled by assuming that there exists a threshold hillslope gradient, S_h, below which the mass movement rate is negligible, and above which the transport rate becomes effectively infinite (e.g., Burbank et al., 1996; Densmore et al., 1998; Howard et al., 1994; Tucker and Slingerland, 1994)

The expected relationship between drainage density and uplift rate for bedrock river channels can be explained as follows (Howard, 1997; Tucker and Bras, 1998; Tucker and Whipple, in press). Substituting the threshold hillslope angle for landsliding, S_h, in (2) and solving for the area of a zero-order catchment, A_0 (equivalently the drainage area for fluvial channel initiation), at which the required channel slope equals the maximum hillslope gradient:

$$A_0 = \left(\frac{U}{K}\right)^{\frac{1}{m}} S_h^{-\frac{n}{m}} \tag{3}$$

Since A_0 varies directly with uplift rate, a more rapidly uplifted catchment should have a lower drainage density in addition to a steeper channel gradient (and thus greater relief). This inverse relation between relief and drainage density is supported by data from the badlands of the western U.S. (Howard, 1997), and from the northern Japanese Alps and adjacent ranges (Oguchi, 1997).

At the scale of interest for a potential coupling between erosion and geodynamics, it is changes in the mean topography of the overlying landscape that are important, rather than the details of the hillsides and valley floors in the landscape. A number of authors have recently demonstrated the potential for important coupling between surface processes and the geodynamics of active orogens. However, these have focused almost exclusively on rivers as the principle agents of erosion. For example, Willett (1999) uses a fluvial erosion model to demonstrate how orographic precipitation acting to increase fluvial erosion on one side of a mountain range with respect to the other can noticeably affect tectonic deformation. Willett

(1999) cites the Southern Alps of New Zealand as an example of the asymmetry characteristic of wind in the direction opposite to the motion of the subducting plate, while in the Olympic Mountains the dominant wind is in the direction of subduction. Beaumont et al. (2001) explain the ductile extrusion of high-grade metamorphic rocks between coeval normal- and thrust-sense shear zones in the Greater Himalayan sequence as a consequence of channel flow in the middle to lower crust. However, their model requires significant focused surface denudation (using a generic, slope-dependent erosion rule) to cause the lower crustal material to penetrate to the surface. Zeitler et al. (2001) note the coincidence of active metamorphic massifs with deep river gorges in the syntaxes at each end of the Himalayan range, together with the records of extremely rapid erosion in these regions, and suggest that erosion plays an integral role in collisional dynamics. They suggest that erosion can mediate the development and distribution of both deformation and metamorphic facies, accommodate crustal convergence, and locally instigate high-grade metamorphism and melting. Given that glaciers have been argued to erode at least as rapidly as rivers (Hallet et al., 1996), it seems plausible that they could play a similarly significant role in the dynamics of active mountain belts

Merrand and Hallet (2000) made the first attempt to couple a glacial landscape evolution model with adjustable tectonic uplift. Their model includes seasonal evolution of glacier mass balance, basal hydrology and thermal regime, bedrock erosion, and sediment accumulation and subsequent remobilisation. When they apply this model to glaciers of the Chugach-St. Elias Range, Alaska, specific patterns of tectonic forcing are required to sustain the topography necessary to maintain large glaciers over long timescales. This suggests complex coupling between tectonic and surface processes in the glacial environment.

Brozovic et al. (1997) observed a coincidence between a peak in hypsometry (frequency distribution of elevations), a low in slope-elevation distributions, and the snowline, across regions of widely differing uplift rates in the Nanga Parbat region of Pakistan. This they interpreted as evidence that glaciers can erode as fast as the most rapid tectonic uplift rates, and that glacial landscapes are essentially unaffected by variations in tectonic uplift rate, with the exception of a few isolated peaks. Montgomery et al. (2001) reached a similar conclusion with their large-scale look at the topography of the Andes. They claimed to be able to distinguish three latitudinal zones in the range: in the northern region, the landscape is dominated by fluvial erosion; in the middle latitudes neither fluvial nor glacial erosion can compete with tectonic

uplift rates; and in the southern region, the landscape is dominated by glacial erosion. The implication is that glacial landscapes are not significantly affected by tectonic processes.

3. Field Areas

To test the effect of differing rock uplift rates on glaciated landscapes, we sought glaciated mountain ranges where local gradients in exhumation rate have been demonstrated, and convincingly argued as reflecting gradients in rock uplift rate. Furthermore, in the ideal case other geomorphic factors such as climate and lithology would be held roughly constant over the region in question, so that the effects of rock uplift could be isolated. Our field areas of choice were the Southern Alps of New Zealand (Fig. 3a), and the Nanga Parbat region of the northwestern Himalayas (Fig. 3b).

In the Southern Alps, Tippett and Kamp (1993) obtained a comprehensive suite of apatite and zircon fission-track samples for the 300 km long central section of the range. They estimated pre-uplift palaeotemperatures of apatites from each sample by comparing measured values of fission-track age and mean length with data relating these variables to temperature in deep hydrocarbon well sections in the Otway Basin, Australia. By assuming a normal pre-uplift geothermal gradient of 27.5±2.5 °C/km in the region that became the Southern Alps, and showing that the initial mean elevation here was close to sea level, the amount of rock uplift was estimated for each sample. A trend surface of rock uplift ages from a subset of the data was then used to calculate rock uplift rates. Of interest here is the along-strike variation in rock uplift rate, which is most rapid around Mount Cook, and declines to both the northeast and southwest (Fig. 2c). Subsequent criticism of Tippett and Kamp's (1993) work has focussed on the fact that they neglected the role of lateral motion in the thermal conditions experienced by a rock traversing the orogen (e.g., Batt and Braun, 1999), and has questioned the zircon partial annealing zone temperatures used (Walcott, 1998). Batt et al. (2000) also question the extrapolation of trends observed in low temperature fission track data (generally seen as constraining shallow crustal behaviour) to constrain older and deeper levels of crustal behaviour. While Batt et al. (2000) suggest a modified early evolution of the range on the basis of muscovite and biotite K/Ar and $^{40}Ar/^{39}Ar$ analyses, they leave Tippett and Kamp's (1993) story of the recent (post 5 Ma) history essentially unchanged, and it is this time period that is of interest here in considering the role of late Cenozoic glaciers in sculpting the modern landscape. Variation in rock uplift perpendicular

to the strike of the range is debated. Tippett and Kamp (1993) favour the most rapid rock uplift occurring at the Alpine Fault, Batt et al. (2000) prefer uniform rates across a 10-20 km wide zone adjacent to the fault before tailing off to the southeast, in particular in the southern part of the range, and Adams (1980) envisions maximum rock uplift rates some 7 km southeast of the fault. However, all authors agree on the pattern of along-strike variations in uplift rate, and in the context of this study, focussed on the northwest side of the Main Divide of the Southern Alps, it is the along-strike variations in rock uplift rate that are far more important than the subtleties of variations perpendicular to the strike. In Figure 2 and subsequent figures we plot rock uplift rates from Tippett and Kamp (1993) along a transect ~10 km from the Alpine Fault. The portion of the Southern Alps studied here is composed almost exclusively of the Alpine schist (e.g., Mason, 1962).

Zeitler (1985) was the first to report extremely young fission track and $^{40}Ar/^{39}Ar$ cooling ages from the Nanga Parbat region. Zeitler documented a zone of young ages associated with the Nanga Parbat-Haramosh Massif (NPHM) with older ages to either side. He obtained exhumation rates from paired apatite and zircon fission track ages and an assumed geothermal gradient, obtaining rates exceeding 0.5 mm/yr only within the NPHM. Burbank et al. (1996) also interpreted Zeitler's (1985) fission track ages in terms of exhumation rates, although they assumed reasonable bounds for the geothermal gradient and treated apatite and zircon data independently. Their calculated rates peak at 4-10 mm/yr for apatite, and 2-4 mm/yr for zircon, in the localised area of rapid exhumation along the NPHM (Fig. 3b). Exhumation is slower (< 2 mm/yr) to either side of this zone. Gardner and Jones (1993) examined sediment yields to calculate rates of glacial erosion of 4-6 mm/yr for the Raikot glacier on the northern side of the Nanga Parbat massif, while Burbank et al. (1996) used ^{10}Be and ^{26}Al exposure-age dating of strath terraces to calculate incision rates of 2-12 mm/yr for the Indus River where it cuts across the Nanga Parbat massif, north of the peak. This correspondence between short-term incision and long-term exhumation rates suggests that both are indeed recording something close to the rock uplift rate. Burbank et al. (1996) argue for slightly accelerating denudation rates during the Pleistocene, in which case these exhumation rates will slightly overestimate rock uplift rates. However, this is probably a minor effect, and in any case the pattern of rock uplift rate variation remains robust. The Nanga Parbat massif comprises mostly leucogranites, some with cooling

ages as young as 1-10 Ma, while the surrounding terranes include a variety of metasedimentary gneisses and orthogneisses (e.g., Schneider et al., 1999).

4. Methods

The key to our examination of the effects of uplift rate on glaciated valleys was to compare drainage basins experiencing differing exhumation rates (and presumably comparably differing uplift rates) while as many other potentially influencing factors (climate, lithology, etc.) as possible remained essentially uniform. We employed four principal measures of surface topography to analyse the two glaciated mountain ranges: hypsometry, valley floor steepness, and hillslope gradient and relief. We applied all of these measures to a range of drainage basins of different sizes and exhumation rates in each range. The digital elevation models (DEMs) that we use define the surfaces of any ice present, rather than the elevations of bedrock beneath this ice (a major undertaking typically requiring the use of ground-penetrating radar or shallow seismic profiling). This data limitation clearly introduces some amount of error, since we are seeking to study the (bedrock) landforms of these environments. However, in cases other than range-crest ice-caps (see below), the thickness of the ice is seldom more than a hundred metres, which serves mainly to provide a smooth representation of the underlying bedrock. The principle conclusions of this study are therefore not affected by the occasional presence of modern ice.

4.1 Hypsometry

We employed three different approaches to examine the hypsometry, opting to study individual drainage basins rather than arbitrary portions of the landscape (see Brocklehurst and Whipple, in prep.-a). The first method uses a simple *histogram* of the frequencies in different elevation bins (Figs. 4a, 5a). The second uses a normalised *cumulative frequency* of the area above a given elevation plotted against elevation (Figs. 4b, 5b). Both of these were employed by Brozovic et al. (1997). From the cumulative frequency plot we also calculate an interquartile range, the change in elevation between the 25^{th} and 75^{th} percentiles of the elevation distribution. Finally we generated a *hypsometric curve*, normalised elevation plotted against normalised cumulative area (e.g., Strahler, 1952). The area under this curve, which by definition lies in the range 0 to 1, is the *hypsometric integral* (Figs. 4c, d, 5c, d).

4.2 Valley floor steepness

In the case of fluvial erosion, the response to rock uplift is typically measured using the steepness, k_s, the constant in the power-law relationship between local stream gradient, S, and drainage area, A (e.g., Flint, 1974):

$$S = k_s A^{-\theta} \tag{4}$$

In the unique case of steady state ($dz/dt = 0$) and spatially uniform K, U, m and n, the uplift rate influence on k_s for fluvial erosion is seen by comparing (2) and (3), assuming that none of the components of K are affected by changes in rock uplift rate; $k_s = (U/K)^{1/n}$, and $\theta = m/n$. The steepness parameter is less relevant in glaciated environments, since the above power law cannot be cast in terms of a glacial erosion model, and the longitudinal profiles of glaciated valleys do not follow a power law form. Rather glacial longitudinal profiles are characterised by a series of steps and overdeepenings (e.g., Benn and Evans, 1998; Brocklehurst and Whipple, 2002; Hooke, 1991; MacGregor et al., 2000; Sugden and John, 1976). However, we found in the field areas studied here that the glacial longitudinal profiles were often characterised by three distinct sections (see Fig. 6), a constant-gradient hillslope, a low concavity middle section in the zone most frequently occupied by ice ($\theta \sim 0.4$), and a more concave section below this ($\theta \sim 0.7$), displaying far greater fluvial influence. Each of these sections tended to be generally smooth. Therefore we calculated steepness, k_s, for the middle, glaciated, low concavity section of the profile, for the purposes of comparison both inter-basin and with our understanding of the fluvial case. Furthermore, since k_s and θ are correlated, we calculated a reference slope, S_r, to allow us to compare slope in basins with differing concavities (Sklar and Dietrich, 1998). S_r is calculated using the steepness and concavity of a given basin profile, with a single reference drainage area, A_r, that is the same for all basins studied, and chosen to lie in the middle of the range of data on a log slope-log area plot (see Fig. 6).

$$S_r = k_s A_r^{-\theta} \tag{5}$$

Since S_r varies directly with uplift rate, a more rapidly uplifted catchment should have a steeper reference slope.

4.3 Hillslope angle and relief

We took a detailed look at the straight hillslope reach above the channel head, described above (section 1 in Fig. 6). Our expectation for a fluvial setting in an active mountain range is that hillslopes will be at the angle of repose regardless of rock uplift rate (e.g., Burbank et al., 1996), and that the critical drainage area for channel initiation will roughly scale with uplift rate. On the longitudinal profile, the hillslope is generally characterised as a linear slope. However, we delimit the hillslope in slope-area space, where it is readily identified by uniform rather than downstream decreasing gradient (Fig. 6). We used the slope-area data to calculate the mean slope and the vertical relief on the hillslope, for both the flow line with the greatest drainage area (the trunk) and the flow line descending from the highest point on the basin perimeter.

5. Results

We present the results in the order described above (see Tables 1 & 2). The results from the Southern Alps can be more systematically presented since our chosen drainage basins lie along a transect parallel to the range along which inferred rock uplift rates vary systematically, whereas our drainage basins in the Nanga Parbat region are more scattered in space. In summary, we see slight evidence that glacial valley floors steepen in response to more rapid uplift. However, the major response of glaciated landscapes to more rapid uplift rates is the generation of towering cirque headwalls, valley sides, and glacial horns. This is the major cause of an apparent steepening seen in the cumulative frequency plots of hypsometry, in slight decreases of the hypsometric integral, and in an increase of regional mean elevation. The change in all of these measures reflects the longer hillslopes that develop in the areas of highest rock uplift rate.

5.1. Hypsometry

Figure 4 shows a representative pair of examples to illustrate the impact of varying uplift rates on the hypsometry of glaciated landscapes in the Southern Alps. The Callery River, just north of Mt Cook, is being uplifted faster than the Kokatahi River, near the northern end of the study transect (see Figs. 2, 3). The hypsometric curve and integral for the two drainages (Figs. 4c, d) show only minor variation, which would suggest that this tool does not readily distinguish variations in uplift rate. However, if we backtrack and remove the normalisation from this plot

(Fig. 4b) it becomes apparent that the hypsometry can show distinct variations with uplift rate. A higher uplift rate causes a shallower slope in the cumulative frequency plot (a wider interquartile range, equivalent to a wider elevation range in the basic hypsometry plot, Fig. 4a), and suggests that glacial landscapes overall steepen in response to faster uplift rates, in a fashion broadly similar to their fluvial counterparts. Despite these differences, in general we reproduce the major result of Brozovic et al. (1997), a close correlation between the snowline and the dominant peak in the frequency distribution of elevations. However, given the much reduced elevation in the Southern Alps compared with the Nanga Parbat region, the peak in the frequency distribution of elevations is much less dramatic.

Figure 5 shows a similar pair of examples from the Nanga Parbat region. The Patro Gah and the Ameges Gah face one another across the Indus River, but the Patro lies within the high uplift zone of the Nanga Parbat massif, draining from the west side of the mountain, whereas the Ameges lies in the lower uplift zone further to the west. The pattern seen in the hypsometry and cumulative frequency plots (Figs. 5a, b) is much the same as that for the Southern Alps examples described above, except that the uppermost two per cent or so of the Patro Gah lies across a range of almost 1500m (Fig. 5b), far greater than the equivalent ~500m for the Callery. These towering hillslopes (described in more detail below) are sufficient to cause a significant difference in the hypsometric curve and integral, since the hypsometric integral is normalised by the whole elevation range.

5.2. Longitudinal profile steepness

As described above, these results highlight the slope of the commonly observed glacially-dominated section of the longitudinal profiles (Fig. 6). In the Southern Alps we employed a reference area, A_r, of 5 x 10^6 m^2, while for the Nanga Parbat region a reference area of 10^7 m^2 was used. Note that the precise value of A_r chosen does not significantly affect the pattern of the results. Figure 7 illustrates S_r values for each of the basins in our Southern Alps transect. We have distinguished the larger basins that developed significant glaciers and reached all the way back from the range front to the range crest from the variety of smaller basins that didn't extend as far from the range front. The smaller basins demonstrate a wide scatter in their steepness, possibly reflecting the variety of local circumstances among these basins, many of which experience only the most rapid uplift rates immediately adjacent to the Alpine Fault. The larger

basins show a minor degree of steepening (higher S_r values) around Mt Cook in the centre of the profile, as the second-order polynomial fit to the large basin data rises slightly (however, the second-order polynomial fit is only a slight improvement on a straight line fit). A third-order polynomial fit to the small basin data shows a similar pattern in the Mt Cook region, but also rises towards the southern end of the profile, where the dynamics of the orogen may be slightly different (Batt et al., 2000). Again the improvement from a straight line fit is modest.

Figure 8a shows in map view the S_r values for a selection of basins in the Nanga Parbat region, while Figure 8b is a histogram separated into higher and lower rock uplift rate regions. In this case the very largest basins show quite shallow reference slopes even in the high uplift zone, but amongst the smaller basins there is a definite trend to higher S_r values either within, or closely adjacent to, the high uplift zone of the Nanga Parbat-Haramosh axis.

In summary, our results suggest that smaller, glaciated basins, some of which show greater fluvial influence, do steepen in response to more rapid rock uplift. However, as the glaciers increase in size, towards the largest cases in the Nanga Parbat region, the tendency to steepen decreases; glaciated valleys can have remarkably gentle downvalley gradients even in zones of very rapid rock uplift.

5.3. Hillslope gradient/relief

We notice a striking correlation between hillslope height and tectonic uplift rate. Focussing on the hillslopes descending from the highest point in each basin (although the story is essentially the same for the maximum drainage area profiles), the correlation in the Southern Alps (Fig. 9) is obscured only by the presence of a major ice cap close to Mt Cook that prevents us from obtaining the true headwall height from the digital elevation model. Otherwise there is a slight rise in foot of hillslope elevation in the central portion of the study area (reflecting the minor steepening of glaciated sections described above), but a far more striking rise in hillslope heights.

In the Nanga Parbat region the results are even more spectacular (Fig. 10). Here we observe that hillslopes can exceed 3 km in height, which can represent around half of the basin relief and approaches half of the height of the peaks above sea level. All of the > 2 km hillslopes lie within the zone of high uplift, or close to it. We have observed similar tall hillslopes in other parts of the Himalaya, such as the Manaslu region of Nepal (Whipple and Brocklehurst, 2000),

and have seen indications of a similar correlation between hillslope height and uplift rate in southern Alaska (Meigs and Sauber, 2000; Merrand and Hallet, 2000).

Figure 11 is an alternative illustration of the importance of the hillslopes in the Southern Alps. The two 3-D perspective pictures show the intersection of a transparent surface roughly representing the modern ELA with a shaded, solid surface representing the topography. Figure 11a shows the region around Mt Cook, illustrating the near range crest ice caps, but otherwise only the steep hillslopes protrude above the ELA. Figure 11b shows a region further to the south, where there are none of the ice caps, rock uplift rates are reduced, and hillslopes are not as tall. Consequently the peaks here protrude less far above the ELA.

6. Discussion

6.1 Summary of observations

The results outlined above suggest that glaciers are capable of eroding valley floors at rates comparable to the most rapid tectonic uplift rates, and without major steepening of their longitudinal profile. In the larger basins of the Southern Alps that develop substantial glaciers, we observe only minor, if any, steepening of the longitudinal profile in association with increasing uplift rates. The smaller basins in the Southern Alps that show scattered steepening patterns might not have experienced sustained glacial erosion. In the Nanga Parbat region the very largest glaciers (which are somewhat larger than their New Zealand counterparts) are essentially undisturbed by the most rapid tectonic uplift rates, while smaller basins are steeper in the high uplift zone than in the neighbouring regions. Thus glacier size seems to represent a determining factor in the glacier's response to tectonic uplift. Merrand and Hallet (2000) suggest that rapid incision by large glaciers might be achieved by high basal water pressures (approaching 80% of the hydrostatic pressure). This allows the glacier to be close to floating, facilitating extremely efficient erosion by plucking/quarrying. In general, the lack of response of large glaciers and the minor response of smaller glaciers supports the glacial buzzsaw hypothesis (Brozovic et al., 1997). The major response to rapid tectonic uplift occurs in the hillslopes surrounding these alpine basins, a caveat in the glacial buzzsaw hypothesis that we draw particular attention to here. Evidently the glaciers are unable to bring down the hillslopes at the same rates as the valley floor incision and impressive, towering cirque headwalls develop as a result. These headwalls can in some cases comprise between a third and a half of the peak height.

Furthermore, as these hillslopes 'advance' downvalley at the expense of the valley floor, drainage density is noticeably reduced.

Figure 12 summarises in cartoon form, then, the main features of glacial valley longitudinal profiles that we have observed in slowly (Brocklehurst and Whipple, 2002, in prep.-b) and rapidly uplifting (this study) settings. In the smaller, glaciated basins of the Sierra Nevada (Fig. 12a), the major impact of glaciers is to lower valley floors and ridgelines above the mean Quaternary ELA. Below this the valleys are widened to a U-shaped cross-section, but the longitudinal profile does not deviate significantly from a typical fluvial profile. Larger, glaciated basins in slowly uplifting settings (Fig. 12b) show a glacial influence much further below the long-term mean ELA, carving steps down to much lower elevations. Moving to more rapidly uplifting settings, the smaller basins appear to steepen in response to rapid rock uplift (Fig. 12c), although less so than one would expect for a fluvial setting. Meanwhile, the larger glaciers (Fig. 12d) can apparently incise at rates comparable to the most rapid rock uplift without any steepening of the longitudinal profile. However, the glaciers are unable to erode the cirque headwall at the same rate, instead the glaciers appear to simply slide off the hillside, allowing the headwall to grow to staggering heights, with a noticeable commensurate decrease in drainage density.

The presence of these giant hillslopes then has the effect of steepening the landscape as a whole, as observed in the cumulative frequency hypsometry. In broad regions of rapid uplift, these hillslopes constitute a sufficiently high percentage of the landscape to cause a rise in regional mean elevation. Mean topography rises more significantly in the Southern Alps than it does in the Nanga Parbat region, perhaps because the zone of rapid uplift in the Nanga Parbat massif is so localised due to structural control; essentially only one horn develops because of these dramatic headwalls. Meanwhile in the Southern Alps the broader swell in uplift allows a wider zone of towering hillslopes, and thus a change in mean topography.

6.2 Importance of glacial erosion in landscape evolution models

There are three important considerations that motivate the introduction of glacial erosion processes into geodynamic models: (a) the different response of mean topography of fluvial and glacial landscapes to uplift. This is the key variable in coupling tectonic and surface processes; (b) the contrasting development of relief in fluvial and glacial landscapes, since this will

determine the flexural-isostatic response to incision and thus set peak heights; and (c) the different responses of the fluvial and glacial systems to climate change.

In the case of minor rock uplift rates, the onset of glacial erosion will generally cause lowering of mean topography with respect to expectations for fluvial systems (Brocklehurst and Whipple, 2002, in prep.-b). In the face of more rapid uplift, glaciated landscapes will steepen little, if at all, while their fluvial counterparts will steepen significantly. These represent very different upper boundary conditions to a geodynamic model. Although not directly comparable, Beaumont et al. (1996) illustrate significant differences in the internal dynamics of their model of the Southern Alps between model runs in which surface denudation is total (topography is instantly eroded to sea-level) and runs in which surface denudation is more modest. We do not suggest that glacial erosion acts like 'total denudation', but in denuding the landscape in a noticeably different fashion than fluvial erosion it may well have an important impact on orogen development.

In this context, Merrand and Hallet (2000), Braun et al. (1999) and Tomkin and Braun (2002) have presented promising initial efforts at incorporating glacial erosion into a landscape evolution model. Merrand and Hallet (2000) used a 1-D glacial erosion model to, among other things, constrain the pattern of tectonic uplift of the Chugach-St. Elias mountains required to maintain large glaciers over long time periods. However they have yet to apply the model to other settings, or to couple the surface processes model to an explicit model for the geodynamics of the orogen. Braun et al. (1999) and Tomkin and Braun (2002) developed a 2-D landscape evolution model incorporating glacial erosion. However, the application of the model was somewhat limited by the necessary employment of a shallow-ice approximation for ice dynamics, and they also haven't yet coupled their surface processes model to a geodynamic model. We are greatly encouraged by the progress demonstrated by these models, and on the basis of the evidence presented here strongly advocate further development of similar models. At a more general level, it would also be instructive to introduce a simplified "glacial buzzsaw", along the lines of Beaumont et al.'s (1996) 'total denudation' (although at an elevation some distance above sea-level) to a coupled tectonic-erosion model to examine the response of the orogen. In particular, it would be interesting to examine the effects of changing the elevation of the buzzsaw through time to simulate climate change. In order to fully account for our observations here, the buzzsaw elevation would also need to incorporate some uplift-rate

dependence, since we have shown that, in the extremes of rapid uplift (and only where this occurs over a broad region), the development of towering hillslopes will raise mean topography.

The towering hillslopes also clearly represent an increase in relief, such that while mean topography may decline as a result of the onset of glacial erosion, peak heights may indeed rise (Molnar and England, 1990). Although this will not have a direct effect on the internal dynamics of the orogen, this has implications for atmospheric dynamics, precipitation patterns, etc., which in turn will have some feedback to the erosion processes. The importance of towering hillslopes and peak heights in the geomorphology of alpine regions is discussed more fully in the next section.

Fluvial and glacial erosion will potentially have different sensitivity to climate change. Glaciers may well erode most efficiently as a consequence of a cycle of advance and retreat, allowing weathering of destabilised hillslopes during glacier retreat stages, and efficient removal of colluvial debris during glacier advance. Meanwhile rivers will be a more constant presence in the landscape, although their ability to erode will depend on storminess of the climate, sediment load, and other climate-related parameters (e.g., Whipple et al., 1999).

6.3 Geomorphic significance of towering hillslopes

We have demonstrated the exceptional scale of hillslopes in glaciated mountain ranges, especially in the Nanga Parbat region. Similar hillslopes are found throughout the Himalayas (e.g., Whipple and Brocklehurst, 2000), and in Alaska (e.g., Meigs and Sauber, 2000). The following is a brief list of the possible influences of steep, ice-free, bedrock hillslopes, especially when they reach several kilometres tall. (i) Giant hillslopes are major sources of snow accumulation and redistribution (e.g., Hewitt, 1993). Snow does not accumulate on the steepest slopes; it avalanches to the floor below. These avalanches are a major contributor to glacier mass balance, and an understanding of periglacial hillslope evolution is essential to questions of avalanche risk. Also, high peaks will influence wind patterns and thus the redistribution of snow by aeolian processes. (ii) Avalanches and rockslides on these hillslopes are major agents of debris transfer to the glaciers below (e.g., Hewitt, 1993, 1998). (iii) These hillslopes form a major component of peak elevation, which is responsible for disrupting atmospheric circulation patterns and determining the effects of orographic precipitation. In extreme cases the rainshadow may begin on the windward side of the range (e.g., Barry, 1992). (iv) Near-divide hillslope

processes determine drainage capture events, which we have shown occur in glacial as well as fluvial environments (Brocklehurst et al., in prep.).

These giant hillslopes clearly represent an important avenue for future research. Given the crucial role of peak heights in hypotheses relating climate change to tectonic processes (Molnar and England, 1990; Raymo and Ruddiman, 1992; Raymo et al., 1988), as well as the potential influence on mean topography, and thus crustal dynamics and orogen evolution (e.g., Beaumont et al., 1992; Beaumont et al., 2001; Willett, 1999), it is vital that we better understand the distribution of these hillslopes, the processes responsible for their development, and the circumstances which allow them to grow to such unusual and spectacular heights in the Himalayas. Furthermore, in the Himalayas these hillslopes play a vital role in the dynamics of the glaciers at their bases, in that the major component of positive mass balance for the glaciers is the snow that avalanches from the valley walls. In addition, Hewitt (1993) has argued that the overwhelming preponderance of debris brought to, and accumulating along, glacier margins in the Himalayas comes from the rockfalls and rockslides descending from these hillslopes, even more so than in other regions, where erosion directly by glaciers plays a more important role. It is hard to evaluate whether the current dominance by rockfalls is typical merely of interglacial times when glacier ice is thin and valley walls are potentially unstable (Whipple et al., 1999). Shading by the valley walls and insulation from the thick debris cover will allow glaciers to descend to much lower altitudes than would otherwise be the case. This then represents a further feedback on the evolution of mean elevation and topographic relief. Previous work on hillslopes in glaciated landscapes has tended to focus on the role of lateral hillsides in setting the U-shaped cross-section of glacial valleys (e.g., Augustinus, 1992, 1995). In these cases rock slope failure is most active following glacier retreat, when the removal of the glacier buttress promotes rock failure through the redistribution of internal rock stresses (e.g., Augustinus, 1995). Given that ice extents will fluctuate far less with climate change at the headwall than they do lower in the valley, it is likely that different processes play a crucial role at the headwall. Most landscape evolution models tend to assume that hillslopes are closely coupled to the rivers or glaciers at their bases. Here we have demonstrated a situation where this is not true, and it is important to understand how unique this case is, under what circumstances glaciers fail to bring down hillslopes at the same rates as valley floors, and whether this represents a transient condition, or something more long-lived. The Southern Alps have been glaciated for most of their existence,

and yet their tallest peaks are not especially high, which may indicate that there is some limit to how high/long headwalls and valley sides can grow in glaciated landscapes. Clearly the role of steep, ice-free hillslopes is crucial in the development of both glaciers and the landscape that they shape.

We also suggest that hillslopes of this magnitude represent a useful geomorphological tool for identifying zones of rapid tectonic uplift within a glaciated mountain range, given the clear correlation that we have demonstrated between hillslope height and uplift rate. Following this approach, we would suggest that the zone of high uplift shown on Fig. 3 perhaps should be extended a little to the west, around Rakaposhi, since it is in this region that the only giant hillslopes outside of the mapped high uplift zone occur. However, given that we have used independent thermochronologic data to argue for the correlation between tall hillslopes and rapid rock uplift, this idea needs further verification before we can confidently employ the presence of tall hillslopes as an indicator of rapid rock uplift.

7. Conclusion

We have carried out a series of topographic analyses designed to elucidate the response of glaciated landscapes to variations in uplift rate, and in particular to some of the most extreme uplift rates in the world. The principle response of the glaciated landscape to rapid uplift is the development of towering hillslopes, comprising between a third and a half of the elevation of some Himalayan peaks. This cirque headwall lengthening and (downvalley) advance is commensurate with a decrease in drainage density, and in some cases an increase in mean elevation. A secondary response is a minor steepening of the section of the valley floor dominated by glaciers, although the largest glaciated valleys are not affected in this way. Thus the size of a glacier seems to affect its response to rapid uplift. The impact of the giant hillslopes on the landscape as a whole can be seen with frequency distribution or cumulative frequency plots of hypsometry, but will only be observed clearly in hypsometric curves in the cases of the most dramatic, giant hillslopes. Apparently glaciers can incise their valley floor swiftly, but in areas of rapid uplift they are, at least at first, unable to bring down the neighbouring hillslopes at comparable rates. The lengthening of hillslopes causes mean elevation to rise slightly with increasing rock uplift rate, although much less than expected in nonglaciated ranges. This has important consequences for the interplay between surface and geodynamic processes, and we

strongly advocate the further development of landscape evolution models incorporating glacial erosion. Coupled tectonic-erosion models incorporating either a simple glacial buzzsaw or a more complex landscape evolution model are also encouraged.

We suggest that mapping of hillslope distributions may represent a geomorphological tool for estimating relative uplift rates in glaciated landscapes. Peak heights in glaciated mountain belts play a crucial role in many hypotheses relating climate change and tectonic processes, while periglacial hillslopes have important implications for glacier mass balance, debris transfer, and avalanche hazard. Thus the controls on the development of hillslopes in tectonically active, glaciated mountain belts represent an important area for future research.

Acknowledgements

This work was supported by NSF grant EAR-9980465 (to KXW), NASA grant SENH99-0209-0172 (to KXW) and a NASA Earth System Science Graduate Fellowship (to SHB). We would like to thank Bob Anderson, Bernard Hallet, Doug Burbank and Chris Beaumont for valuable discussions, and Ben Crosby and David Mohrig for careful reviews of earlier versions of this manuscript.

Figure captions

Fig. 1. Photographs of typical glaciated landscapes in active tectonic settings. (a) Khumbu Basin, Mt Everest region, Nepal. There is around 4 km of relief between the valley glacier and the highest peak. (Photograph taken by Karen Viskupic). (b) Mt Cook region, Southern Alps, New Zealand.

Fig. 2. Profile of mean topography along the crest of the Southern Alps. (a) Location of profile, on the South Island of New Zealand. (b) 1 km digital topographic data, averaged over a circle of radius 20 km to determine mean topography, showing the location of the profile in (c), parallel to the strike of the Southern Alps. Mt Cook lies close to the centre of the profile. (c) Mean topography along the line illustrated in (b) in black, modern (grey, solid) and last glacial maximum (grey, dashed) equilibrium line altitudes, and rock uplift rate pattern (grey, dotted). Equilibrium line altitude data from Porter (1975). Exhumation rate data inferred from Tippett

and Kamp (1993) (see discussion in text). Horizontal black line illustrates the extent of the profiles in Figures 7 and 9. The rise in mean elevation associated with more rapid exhumation (and inferred more rapid uplift) suggests that the "glacial buzzsaw hypothesis" is not appropriate in this setting.

Fig. 3. Shaded relief maps of the study areas, with the basins analysed in this study highlighted in red, and major peaks indicated. (a) Southern Alps. Rock uplift rates are highest in the Mount Cook area (Fig. 2c). The Callery and Kokatahi basins highlighted are examined in more detail in Figs. 4 and 6. (b) Nanga Parbat region. High uplift zone from Zeitler (1985) bounded by white dashed lines. The Ameges, Diamir and Patro basins highlighted are examined in more detail in Figs. 5 and 7.

Fig. 4. Hypsometry of the Kokatahi (pale grey – slower uplift) and Callery (dark grey – faster uplift) River basins, Southern Alps. (a) Frequency distribution of elevations. ELA estimates from Porter (1975). (b) Cumulative frequency plot, with interquartile range calculated as indicated. (c) Hypsometric curve for the Kokatahi River basin. (d) Hypsometric curve for the Callery River basin. The hypsometric curves alone suggest that there is little difference in landscape between these two drainage basins. However, the frequency distribution and cumulative frequency plot, which are not normalised by elevation, show that the Callery Basin is steeper as a whole than the Kokatahi.

Fig. 5. Hypsometry of the Ameges (pale grey – slower uplift) and Patro (dark grey – faster uplift) Gah basins, Nanga Parbat region. (a) Frequency distribution of elevations. (b) Cumulative frequency plot, with interquartile range calculated as indicated. (c) Hypsometric curve for the Ameges Gah basin. (d) Hypsometric curve for the Patro Gah basin. ELA estimates from Holmes (1993). The frequency distribution for the Patro Gah highlights the hillslopes at the top of the basin. These are not areally extensive, but add significantly to the relief of the basin. The cumulative plot suggests that, outside of the highest hillslopes, the Patro Gah is slightly steeper than the Ameges, and again highlights the extra relief due to the hillslopes. The hillslopes are also tall enough significantly modify the hypsometric curve, since this is normalised by the difference in elevation across the whole of the basin.

Fig. 6. Longitudinal profiles of (a) the Callery River, Southern Alps, and (b) the Diamir Basin, Nanga Parbat. Labels (1), (2) and (3) highlight the three zones of distinct concavity values, $\theta \sim 0$ (hillslope), $\theta \sim 0.4$ (glacier-dominated reach), and $\theta \sim 0.7$ (river-influenced reach) respectively. Main figure shows the longitudinal profile extracted from the digital elevation model (black) and the model fits for each section (grey). The sections are identified using the slope-area data (inset).

Fig. 7. Section along the Southern Alps (section line shown in Fig. 2c) showing S_r values for the glaciated portions (segment 2 in Figure 6) of all of the basins in this study. Black symbols highlight the larger basins that reach back to the range crest, pale grey symbols are smaller basins that do not reach the range crest. Grey, dotted line indicates uplift rate pattern (Tippett and Kamp, 1993). Notice the slight increase in S_r values for the large basins in the more rapidly uplifting, central portion of the study range, as indicated by the slight rise in the second-order polynomial fit to the large basin data (black, dotted). Grey, dashed line indicates a third-order polynomial fit to the small basin data. The two polynomial lines fit the data better than linear fits, although the improvement is not statistically significantly.

Fig. 8. (a) Distribution of S_r values for basins in the study area around Nanga Parbat, values as indicated in the key. Variations in S_r values are subtle. However, the steepest basins (highest S_r) lie within or adjacent to the rapid rock uplift zone, bounded by the white dashed lines. The largest basins within this zone have lower reference slope values, though. (b) Histogram of S_r values in the high and low uplift regions.

Fig. 9. Sections along the Southern Alps (section line shown in Fig. 2c) to illustrate variations in hillslope heights. (a) Base-of-hillslope heights and maximum elevations. Dotted line indicates uplift rate pattern (Tippett and Kamp, 1993). Triangles indicate base-of-hillslope elevation beneath the highest point on the rim of the basin, separated into basins with (light grey) and without (dark grey) an icecap near the range crest. Open (small basins not reaching the range crest) and filled (large basins reaching the range crest) triangles indicate maximum elevation within each basin. The hillslope height is the interval between the base of the hillslope and the

highest point on the basin rim. Grey line connects maximum elevations for large basins. Black, solid line is a second-order polynomial fit to the ice-cap free base-of-hillslope elevations. Base-of-hillslope elevation rises only slightly in the rapidly uplifting zone (slight steepening of the valley floor), while the highest points are significantly higher here. Thus the hillslopes are taller in the rapidly uplifting zone. The exceptions to this, where the base of the hillslope is very high, are due to the presence of a large ice cap at the range crest. The technique used here only records hillslope heights down to the uppermost surface of the ice cap, rather than the base of the hillslope beneath the ice, and so does not give a true reflection of the bedrock relief on the hillslope. (b) Distribution of headwall relief in the Southern Alps.

Fig. 10. Distribution of hillslope heights around Nanga Parbat, heights as indicated in the key. Notice that all of the tallest hillslopes are focused in or adjacent to the high uplift zone.

Fig. 11. Three-dimensional perspective view of the intersection of the modern ELA and topography in the Southern Alps. (a) Region around Mt Cook, illustrating the range-crest ice-caps discussed in the text, but otherwise only hillslopes protruding above the ELA. (b) Region to the south of Mt Cook. Now there are no range-crest ice-caps, and only hillslopes protrude above the ELA. Notice that as the rock uplift rate is lower in this region, so is the amount by which the peaks penetrate above the ELA.

Fig. 12. Cartoon sketch illustrating the key differences between glacial valley longitudinal profiles in different settings: (a) small, glaciated basin in a slowly-uplifting range (e.g., Independence/Lone Pine Creek, eastern Sierra Nevada); (b) large, glaciated basin in a slowly-uplifting range (e.g., Big Pine/Bishop Creek, eastern Sierra Nevada); (c) small, glaciated basin in a rapidly uplifting range (e.g., Patro Basin, Nanga Parbat region); (d) large, glaciated basin in a rapidly uplifting range (e.g., Diamir/Rupal Basin, Nanga Parbat region).

Table 1.

Data from the Southern Alps. Basins listed from north to south. I.q.r. is interquartile range.

Basin name	Hypsometric integral	Hypsometry i.q.r. (m)	Headwall slope (deg)	Headwall relief (m)	S_r
Styx	0.403	569	31.5	782.8	0.144
Kokatahi	0.512	679	28.1	1084	0.167
Toaroha	0.500	587	18.2	567.6	0.150
Muriel	0.431	439	27.8	423.3	0.203
Diedrich	0.532	456	27.2	851.3	0.165
Dickson	0.490	561	33.5	866	0.192
Tuke	0.475	674	24.2	777.1	0.164
Kakapotahi	0.475	523	26	853.5	0.185
MacGregor	0.508	425	33	523.5	0.188
Waitaha	0.452	661	43.3	614.1	0.123
Hendes	0.492	618	29.1	565	0.196
Amethyst	0.547	382	29.5	546	0.082
Hot Spring	0.590	447	25.8	220.6	0.141
Tribute	0.481	474	30.3	786.9	0.187
Dry	0.527	507	32.3	581.2	0.200
Wilberg	0.477	458	26.1	501.9	0.134
Rata	0.532	518	37.3	655.4	0.237
North McCulloughs	0.272	682	32.9	610.5	0.166
Littleman	0.440	679	33.3	891.5	0.184
Mcculloughs	0.468	576	34.5	501.2	0.175
Dale	0.576	699	26.1	281.8	0.386
Gaunt	0.573	447	36.2	376.8	0.286
Darnley	0.552	462	32.6	917.8	0.139
Potters	0.415	545	34.9	404.3	0.200
Tartare	0.465	649	32	673.1	0.164
Callery	0.446	852	42.2	1243	0.195
Waiho	0.518	1137	32	398.6	0.212
Docherty	0.396	573	41	426.3	0.150
Omoeroa	0.466	622	28.2	305.6	0.170
Waikukupa	0.508	578	19.4	606.5	0.221
Clearwater	0.459	525	31.6	467.2	0.144
Fox	0.455	972	43.9	737	0.174
Balfour	0.377	715	57.2	357.5	0.212
Cook	0.376	776	39.3	794.8	0.127
Havelock	0.426	525	35.4	861.8	0.200
Copland	0.404	758	41.8	1451	0.156
Architect	0.484	610	37.6	726.4	0.122
Regina	0.438	632	34.2	1107	0.201
Douglas	0.476	809	28.3	1993	0.132
Karangarua	0.440	578	51.2	998.8	0.119
Manakaiaua	0.505	446	36.1	737.8	0.140
Makawhio	0.431	623	36.4	1110	0.115
Flagstaff	0.580	486	34.8	359.2	0.162
Mahitaki	0.368	804	27.4	1466	0.137
Doughboy	0.566	418	27.5	508.5	0.471
Blackwater	0.516	394	35.7	382.8	0.154
Otoko	0.405	825	22.7	1671	0.194
Darkness	0.461	516	37.4	828.8	0.094
Tunnel	0.461	647	35.4	1114	0.199
Stew	0.573	390	26.3	444	0.159
Panel	0.550	481	25	505.6	0.196
Moeraki	0.385	615	45.5	755.5	0.154
Eggerling	0.568	507	29	711.4	0.306
Warren	0.505	555	37	686.4	0.280
Turnbull	0.454	682	29.3	558.4	0.156

Table 2. Data from the Nanga Parbat region. Lettered basins lie beyond range of topographic map coverage. Uplift rates: high signifies rapid uplift in the Nanga Parbat-Haramosh massif, medium rates of rock uplift lie to either side, and low rates lie further outboard of the NPHM.

Basin	Uplift rate	Hypsometric integral	Headwall slope (deg)	Headwall relief (m)	S_r	Basin	Uplift rate	Hypsometric integral	Headwall slope (deg)	Headwall relief (m)	S_r
a	medium	0.454	30	1158	0.25	khoto	low	0.396			
ameges	medium	0.590	25.8	545	0.17	kiner	low	0.533	24.6	180	0.13
b	medium	0.544	44.1	1639	0.15	l	high	0.390			0.11
bagrot	medium/high	0.402			0.24	lichar	high	0.583	15.8	602	
barouima	high	0.516	30.7	563	0.35	lichi	medium	0.505	38.4	1230	
basha	low	0.517	22.5	650	0.20	m	high	0.530	42.5	1378	0.19
batkor	medium	0.517	27.9	1552	0.27	manu	medium/high	0.399			0.21
bubina	medium/low	0.629	34.3	379	0.00	mayar	high	0.468	32.1	2059	0.36
bulache	high	0.570	34.6	673	0.32	minawar	medium	0.478	53.8	219	0.28
buldar	high	0.509			0.24	moster	medium/low	0.475	28.8	804	0.21
bunji	medium/high	0.505	28.5	1676	0.32	mushkin	high	0.509	35.4	1515	0.39
burji	low	0.529	24	909	0.19	n	high	0.432	54.5	1358	0.12
buto	medium/low	0.583	22.4	709	0.00	o	high	0.512	38.4	2205	0.36
c	medium	0.466	39.9	1160	0.31	p	high	0.491	41.1	1066	0.26
chhichi	high	0.443	39.5	1462	0.14	pahot	medium/low	0.598	49.1	532	
chunda	low	0.436	37.4	1062		partabpur	medium	0.552	32.5	745	0.11
ciche	low	0.421	30.6	421		patro	medium/high	0.485	42.7	1412	0.31
d	medium	0.392	41.3	1918	0.23	phuparash	high	0.449	44.7	2953	0.27
damachi	medium	0.737	34	392	0.19	q	high	0.516	41.9	1984	0.48
damot	medium	0.648	14.6	533		r	high	0.449	45.2	1967	0.39
darchan	medium/high	0.494	37.3	1547		ramghat	high	0.596	32.5	347	0.25
darel	low	0.573	26.2	1120		rondu	medium	0.547	29	459	
diamir	medium/high	0.437	36	3582	0.19	rupal	high	0.358	42.5	3111	0.13
dichil	high	0.536	39.8	1651	0.19	s	high	0.423	46.2	1335	0.36
dirkil	medium	0.366	48.2	1258	0.21	sachen	medium/high	0.412	27.8	2786	
domot	low	0.529	22.4	1144		sakwar	medium	0.458	26.9	1171	0.27
dudishal	low	0.473	21.2	1238	0.22	satpura	low	0.617	28.9	1699	
e	medium	0.472	38	2605	0.22	shaltar	high	0.662	26.7	1155	0.25
f	medium	0.508			0.21	shingan	medium	0.513	26.5	1321	0.24
g	medium	0.532	28.7	1628	0.31	shinghai	medium/low	0.702	32.5	929	
gainji	medium/high	0.587	29.8	1131	0.20	shuko	medium	0.661	28.7	523	
gashu	medium	0.627	17.4	753		skoyo	medium	0.477	39.7	1667	
gayal	low	0.655	19.8	673		stak	medium/high	0.445			0.32
gichar	low	0.547	24	612		sustung	medium	0.552	29	1688	
gine	medium	0.483	27.6	1726	0.34	susurlat	high	0.550	36.7	1485	0.26
gor	medium	0.490			0.25	t	high	0.402	42.2	1910	0.27
gunar	medium	0.448	34.6	1583	0.29	takht	medium	0.606			0.16
gurikot	medium/high	0.531	27.5	562		tato	high	0.454			0.18
h	medium	0.402			0.36	telkushi	low	0.680	26.5	259	
harban	low	0.573	29.9	578		thak	medium/low	0.544	21.7	1895	0.14
harchu	high	0.515	24.5	1052		thelichi	medium	0.468	48	1305	
hodar	low	0.477	23.2	713	0.17	thor	medium/low	0.545	20.3	1597	
hukar	low	0.502	34.9	467	0.17	tornak	medium	0.559			
hurban	high	0.548	33	2166	0.45	trik	medium	0.557	29.2	902	
i	high	0.569	34	552	0.18	tukchan	medium	0.516			0.14
ishkapal	high	0.476	29.4	2761	0.29	tulu	medium	0.596	24.5	1217	0.18
j	high	0.422	45	1672	0.20	tungas	medium/low	0.561	27.7	1091	
jalipur	medium/high	0.582	26.2	301	0.23	turmik	medium/low	0.645	33.8	981	
juche	high	0.549	32.8	2651	0.46	u	medium/high	0.454	51	1864	0.21
jutial	medium	0.642	30.4	257	0.28	urdung	medium	0.573	27	1477	
k	high	0.521	38.5	457	0.24	v	medium/high	0.422	43.9	1981	0.37
keges	medium/low	0.623	28.2	181	0.14	w	high	0.436	43.6	1799	0.17
khanbari	low	0.607	40.7	671		x	medium	0.463	37	2247	0.36

References

Adams, J., 1980, Contemporary uplift and erosion of the Southern Alps, New Zealand: Geological Society of America Bulletin, v. 91, p. 1-114.

Augustinus, P. C., 1992, The Influence of Rock Mass Strength on Glacial Valley Cross-Profile Morphometry: A Case Study from the Southern Alps, New Zealand: Earth Surface Processes and Landforms, v. 17, p. 39-51.

-, 1995, Glacial valley cross-profile development: the influence of in-situ rock stress and rock mass strength, with examples from the Southern Alps, New Zealand: Geomorphology, v. 14, p. 87-97.

Barry, R. G., 1992, Mountain Weather and Climate: London, Routledge, 402 p.

Batt, G. E., and Braun, J., 1999, The tectonic evolution of the Southern Alps, New Zealand: insights from fully thermally coupled dynamical modelling: Geophysics Journal International, v. 136, no. 2, p. 403-420.

Batt, G. E., Braun, J., Kohn, B. P., and McDougall, I., 2000, Thermochronological analysis of the dynamics of the Southern Alps, New Zealand: Geological Society of America Bulletin, v. 112, no. 2, p. 250-266.

Beaumont, C., Fullsack, P., and Hamilton, J., 1992, Erosional control of active compressional orogens, *in* McClay, K. R., ed., Thrust tectonics: London, Chapman & Hall, p. 1-18.

Beaumont, C., Jamieson, R. A., Nguyen, M. H., and Lee, B., 2001, Himalayan tectonics explained by extrusion of a low-viscosity crustal channel coupled to focused surface denudation: Nature, v. 414, p. 738-742.

Beaumont, C., Kamp, P. J. J., Hamilton, J., and Fullsack, P., 1996, The continental collision zone, South Island, New Zealand: Comparison of geodynamical models and observations: Journal of Geophysical Research, v. 101, no. B2, p. 3333-3359.

Benn, D. I., and Evans, D. J. A., 1998, Glaciers and Glaciation: London, Arnold, 734 p.

Braun, J., Zwartz, D., and Tomkin, J. H., 1999, A new surface-processes model combining glacial and fluvial erosion: Annals of Glaciology, v. 28, p. 282-290.

Brocklehurst, S. H., Granger, D. E., and Whipple, K. X., in prep., Landscape development in the Sierra Nevada: significance of 'old surfaces' at the range crest: Geology.

Brocklehurst, S. H., and Whipple, K. X., 2000, Hypsometry of Glaciated Landscapes in the western U.S. and New Zealand: EOS, v. 81, no. 48, p. F504.

-, 2001, Assessing the relative efficiency of fluvial and glacial erosion: Examples from the Sierra Nevada, California, and Sangre de Cristo Range, Colorado: GSA/GSL Earth Systems Processes Programmes with Abstracts, p. 81.

-, 2002, Glacial Erosion and Relief Production in the Eastern Sierra Nevada, California: Geomorphology, v. 42, no. 1-2, p. 1-24.

-, in prep.-a, Hypsometry of glaciated landscapes: Earth Surface Processes and Landforms.

-, in prep.-b, Rates of glacial erosion in the ablation zone: evidence from fluvial landscape simulation.

Brozovic, N., Burbank, D. W., and Meigs, A. J., 1997, Climatic Limits on Landscape Development in the Northwestern Himalaya: Science, v. 276, p. 571-574.

Burbank, D. W., Leland, J., Fielding, E., Anderson, R. S., Brozovic, N., Reid, M. R., and Duncan, C., 1996, Bedrock incision, rock uplift and threshold hillslopes in the northwestern Himalayas: Nature, v. 379, p. 505-510.

Densmore, A. L., Ellis, M. A., and Anderson, R. S., 1998, Landsliding and the evolution of normal-fault-bounded mountains: Journal of Geophysical Research, v. 103, no. B7, p. 15203-15219.

England, P., and Molnar, P., 1990, Surface uplift, uplift of rocks, and exhumation of rocks: Geology, v. 18, p. 1173-1177.

Flint, J. J., 1974, Stream gradient as a function of order, magnitude, and discharge: Water Resources Research, v. 10, p. 969-973.

Gardner, J. S., and Jones, N. K., 1993, Sediment Transport and Yield at the Raikot Glacier, Nanga Parbat, Punjab Himalaya, *in* Shroder, J. F., Jr, ed., Himalaya to the Sea: Geology, Geomorphology and the Quaternary: London, Routledge, p. 184-197.

Hallet, B., Hunter, L., and Bogen, J., 1996, Rates of erosion and sediment evacuation by glaciers: A review of field data and their implications: Global and Planetary Change, v. 12, p. 213-235.

Hewitt, K., 1993, Altitudinal Organization of Karakoram Geomorphic Processes and Depositional Environments, *in* Shroder, J. F., Jr, ed., Himalaya to the Sea: Geology, Geomorphology and the Quaternary: London, Routledge, p. 159-183.

-, 1998, Catastrophic landslides and their effects on the Upper Indus streams, Karakoram Himalaya, northern Pakistan: Geomorphology, v. 26, no. 1-3, p. 47-80.

Holmes, J. A., 1993, Present and Past Patterns of Glaciation in the Northwest Himalaya: Climatic, Tectonic and Topographic Controls, *in* Shroder, J. F., Jr, ed., Himalaya to the Sea: Geology, Geomorphology and the Quaternary: London, Routledge, p. 72-90.

Hooke, R. L., 1991, Positive feedbacks associated with erosion of glacial cirques and overdeepenings: Geological Society of America Bulletin, v. 103, p. 1104-1108.

Howard, A. D., 1997, Badland morphology and evolution: Interpretation using a simulation model: Earth Surface Processes and Landforms, v. 22, p. 211-227.

Howard, A. D., Dietrich, W. E., and Seidl, M. A., 1994, Modeling fluvial erosion on regional to continental scales: Journal of Geophysical Research, v. 99, p. 13971-13986.

Howard, A. D., and Kerby, G., 1983, Channel changes in badlands: Geological Society of America Bulletin, v. 94, p. 739-752.

Kirby, E., and Whipple, K. X., 2001, The effect of spatially variable rock uplift on river profile concavity: A new tool for neotectonic analysis of topography: Geology.

Koons, P. O., 1995, Modeling the Topographic Evolution of Collisional Belts: Annual Review of Earth and Planetary Sciences, v. 23, p. 375-408.

MacGregor, K. C., Anderson, R. S., Anderson, S. P., and Waddington, E. D., 2000, Numerical Simulations of Glacial Valley Longitudinal Profile Evolution: Geology, v. 28, no. 11, p. 1031-1034.

Mason, B., 1962, Metamorphism in the Southern Alps of New Zealand: Bulletin of the American Museum of Natural History, v. 123, p. 217-248.

Meigs, A., and Sauber, J., 2000, Southern Alaska as an example of the long-term consequences of mountain building under the influence of glaciers: Quaternary Science Reviews, v. 19, p. 1543-1562.

Merrand, Y., and Hallet, B., 2000, A physically based numerical model of orogen-scale glacial erosion: Importance of subglacial hydrology and basal stress regime: GSA Abstracts with Programs, v. 32, no. 7, p. A329.

Molnar, P., and England, P., 1990, Late Cenozoic uplift of mountain ranges and global climate change: chicken or egg?: Nature, v. 346, p. 29-34.

Montgomery, D. R., Balco, G., and Willett, S. D., 2001, Climate, tectonics and the morphology of the Andes: Geology, v. 29, no. 7, p. 579-582.

Oguchi, T., 1997, Drainage density and relative relief in humid steep mountains with frequent slope failure: Earth Surface Processes and Landforms, v. 22, p. 107-120.

Porter, S. C., 1975, Equilibrium-Line Altitudes of Late Quaternary Glaciers in the Southern Alps, New Zealand: Quaternary Research, v. 5, p. 27-47.

-, 1989, Some Geological Implications of Average Quaternary Glacial Conditions: Quaternary Research, v. 32, p. 245-261.

Raymo, M. E., and Ruddiman, W. F., 1992, Tectonic forcing of late Cenozoic climate: Nature, v. 359, p. 117-122.

Raymo, M. E., Ruddiman, W. F., and Froelich, P. N., 1988, Influence of late Cenozoic mountain building on ocean geochemical cycles: Geology, v. 16, p. 649-653.

Roe, G. H., Montgomery, D. R., and Hallet, B., 2002, Effects of orographic precipitation variations on the concavity of steady-state river profiles: Geology, v. 30, no. 2, p. 143-146.

Schneider, D. A., Edwards, M. A., Kidd, W. S. F., Khan, M. A., Seeber, L., and Zeitler, P. K., 1999, Tectonics of Nanga Parbat, western Himalaya: Synkinematic plutonism within the doubly vergent shear zones of a crustal-scale pop-up structure: Geology, v. 27, no. 11, p. 999-1002.

Sklar, L., and Dietrich, W. E., 1998, River Longitudinal Profiles and Bedrock Incision Models: Stream Power and the Influence of Sediment Supply, *in* Tinkler, K. J., and Wohl, E. E., eds., Rivers over Rock: Geophysical Monograph: Washington, DC, American Geophysical Union, p. 237-260.

Sklar, L. S., and Dietrich, W. E., 2001, Sediment and rock strength controls on river incision into bedrock: Geology, v. 29, no. 12, p. 1087-1090.

Snyder, N. P., Whipple, K. X., Tucker, G. E., and Merritts, D. J., 2000, Landscape response to tectonic forcing: DEM analysis of stream profiles in the Mendocino triple junction region, northern California: Geological Society of America Bulletin, v. 112, no. 8, p. 1250-1263.

-, in review, The importance of a stochastic distribution of floods and erosion thresholds in the bedrock river incision problem.

Strahler, A. N., 1952, Hypsometric (area-altitude) analysis of erosional topography: Geological Society of America Bulletin, v. 63, p. 1117-1141.

Stüwe, K., and Barr, T. D., 1998, On uplift and exhumation during convergence: Tectonics, v. 17, no. 1, p. 80-88.

Sugden, D. E., and John, B. S., 1976, Glaciers and Landscape: London, Arnold, 376 p.

Tippett, J. M., and Kamp, P. J. J., 1993, Fission track analysis of the late Cenozoic Vertical Kinematics of Continental Pacific Crust, South Island, New Zealand: Journal of Geophysical Research, v. 98, no. B9, p. 16119-16148.

Tomkin, J. H., and Braun, J., 2002, The influence of alpine glaciation on the relief of tectonically active mountain belts: American Journal of Science, v. 302, p. 169-190.

Tucker, G. E., and Bras, R. L., 1998, Hillslope processes, drainage density, and landscape morphology: Water Resources Research, v. 34, p. 2751-2764.

-, 2000, A Stochastic Approach to Modeling the Role of Climate Variability in Drainage Basin Evolution: Water Resources Research, v. 36, no. 7, p. 1953-1964.

Tucker, G. E., and Slingerland, R. L., 1994, Erosional dynamics, flexural isostasy, and long-lived escarpments: A numerical modeling study: Journal of Geophysical Research, v. 99, no. B6, p. 12229-12243.

Tucker, G. E., and Whipple, K. X., in press, Topographic Outcomes Predicted by Stream Erosion Models: Sensitivity Analysis and Intermodel Comparison: Journal of Geophysical Research.

Walcott, R. I., 1998, Modes of oblique compression: Late Cenozoic tectonics of the South Island of New Zealand: Reviews of Geophysics, v. 36, p. 1-26.

Whipple, K. X., and Brocklehurst, S. H., 2000, Estimating Glacial Relief Production in the Nepal Himalaya: GSA Abstracts with Programs, v. 32, p. A320.

Whipple, K. X., Kirby, E., and Brocklehurst, S. H., 1999, Geomorphic limits to climate-induced increases in topographic relief: Nature, v. 401, p. 39-43.

Whipple, K. X., and Tucker, G. E., 1999, Dynamics of the stream-power river incision model: Implications for height limits of mountain ranges, landscape response timescales, and research needs: Journal of Geophysical Research, v. 104, p. 17661-17674.

-, 2002, Implications of sediment-flux-dependent river incision models for landscape evolution: Journal of Geophysical Research, v. 107, no. B2.

Willett, S. D., 1999, Orogeny and orography: The effects of erosion on the structure of mountain belts: Journal of Geophysical Research, v. 104, no. B12, p. 28957-28981.

Willett, S. D., and Brandon, M. T., 2002, On Steady States in Mountain Belts: Geology, v. 30, no. 2, p. 175-178.

Zeitler, P. K., 1985, Cooling history of the NW Himalaya, Pakistan: Tectonics, v. 4, no. 1, p. 127-151.

Zeitler, P. K., Meltzer, A. S., Koons, P. O., Craw, D., Hallet, B., Chamberlain, C. P., Kidd, W. S. F., Park, S. K., Seeber, L., Bishop, M. P., and Shroder, J. F., 2001, Erosion, Himalayan Geodynamics, and the Geomorphology of Metamorphism: GSA Today, v. 11, no. 1, p. 4-9.

a.

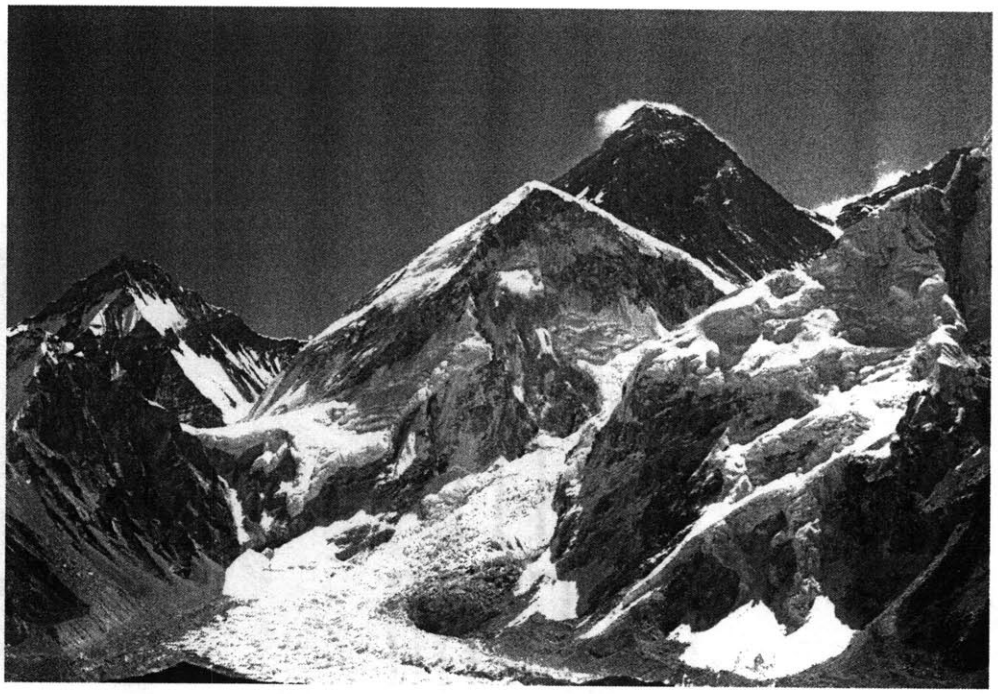

b.

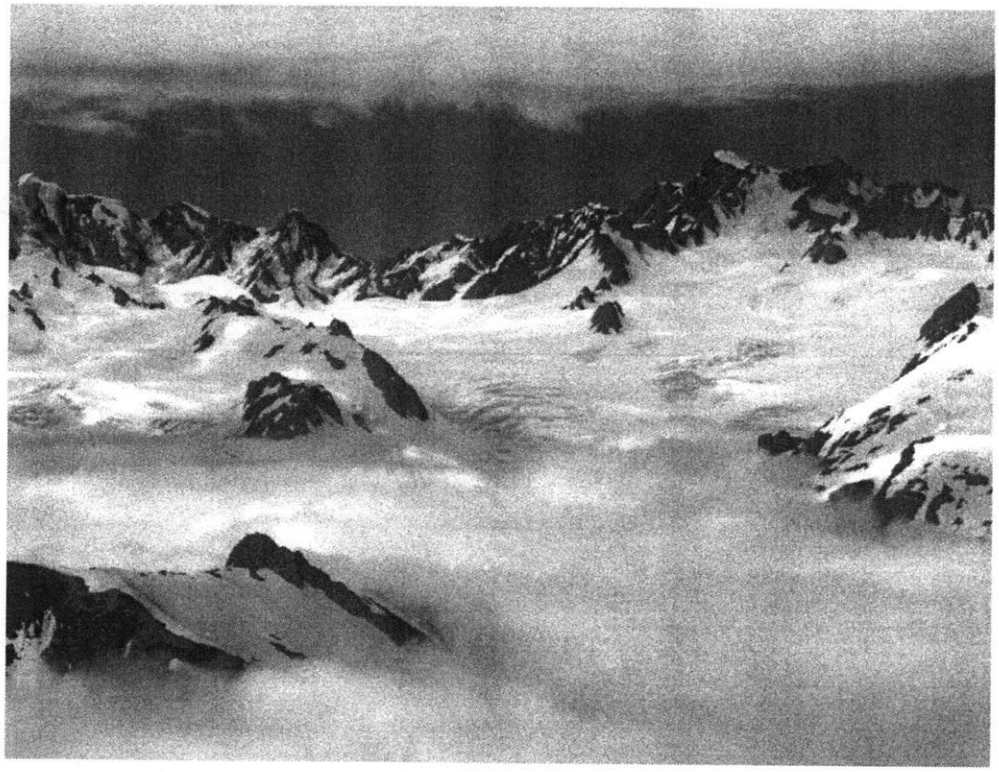

Fig. 1

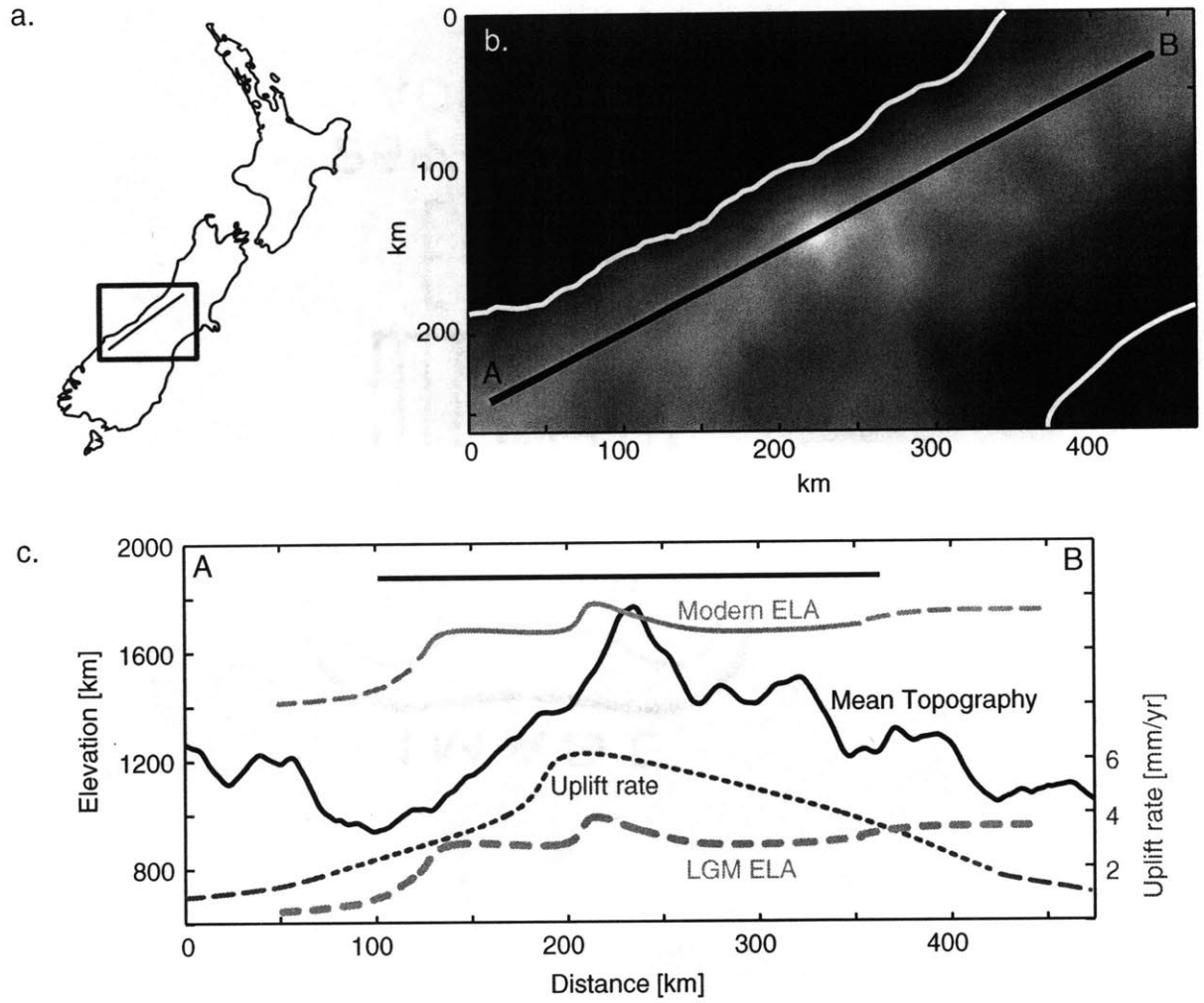
a.
b.
B
A
0
100
200
km
0
100
200
300
400
km
c.
A
B
Modern ELA
Mean Topography
Uplift rate
LGM ELA
Elevation [km]
2000
1600
1200
800
6
4
2
Uplift rate [mm/yr]
0
100
200
300
400
Distance [km]

Fig. 2

a.

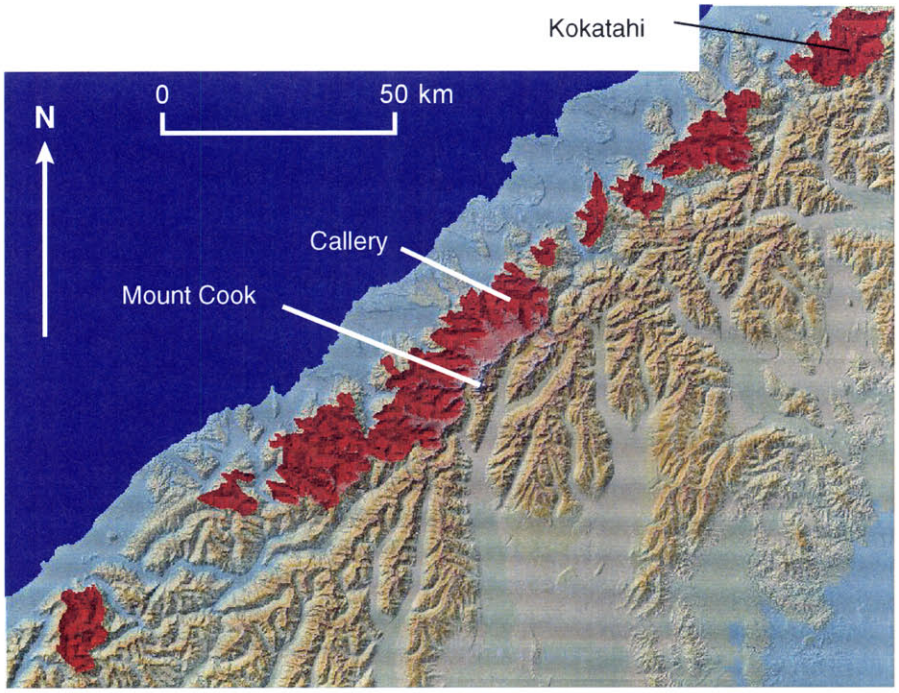
Kokatahi
0
50 km
N
Callery
Mount Cook

b.

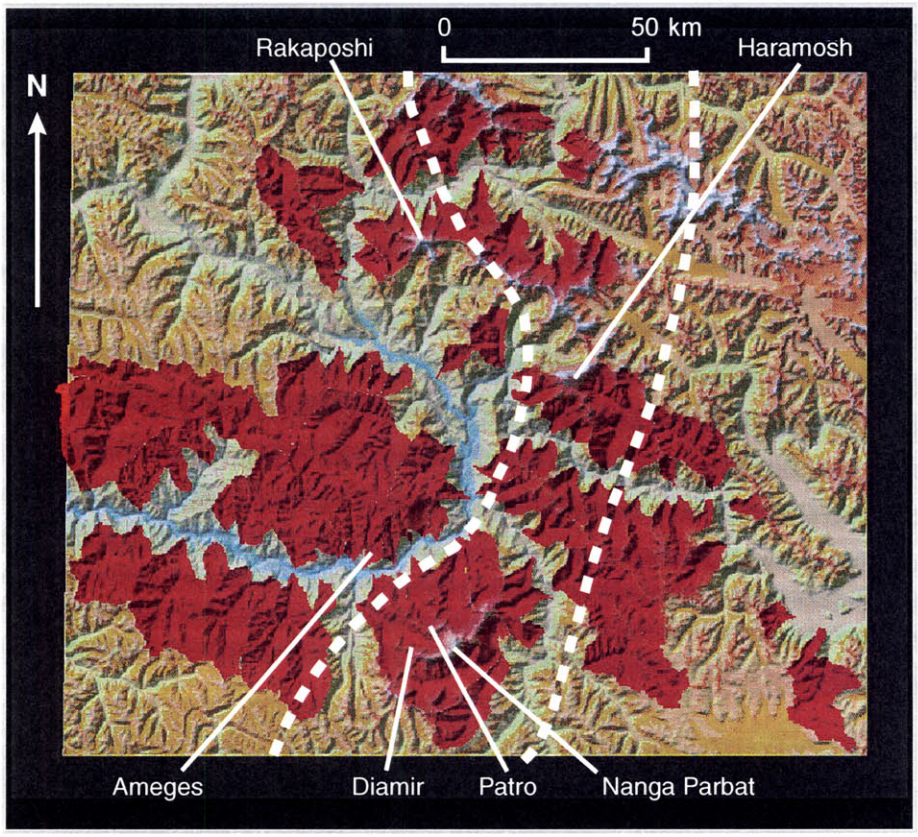
Rakaposhi
0
50 km
Haramosh
N
Ameges
Diamir
Patro
Nanga Parbat

Fig. 3

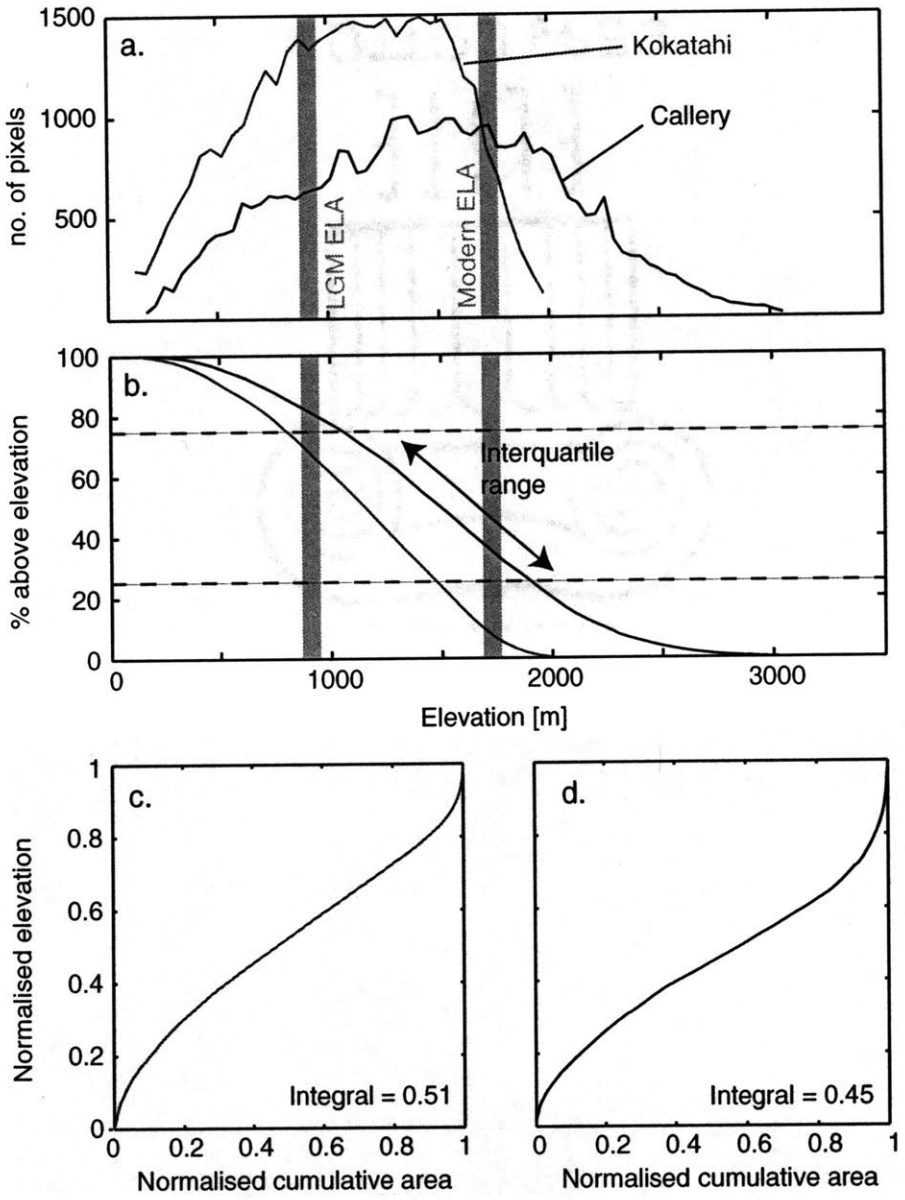
a.
Kokatahi
Callery
LGM ELA
Modern ELA
no. of pixels
1500
1000
500
b.
Interquartile range
% above elevation
100
80
60
40
20
0
0
1000
2000
3000
Elevation [m]
c.
Integral = 0.51
Normalised elevation
Normalised cumulative area
d.
Integral = 0.45
Normalised cumulative area
0
0.2
0.4
0.6
0.8
1

Fig. 4

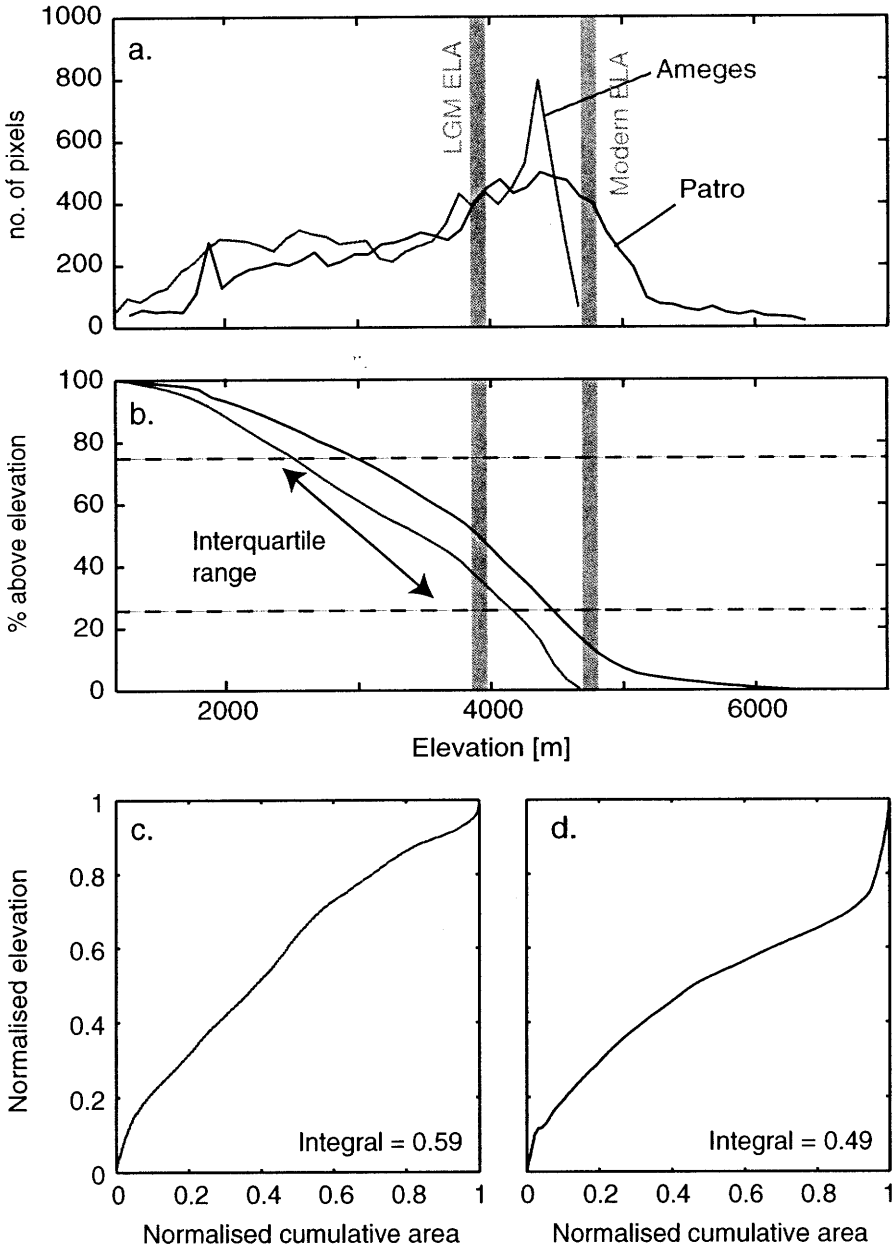
a.
no. of pixels
1000
800
600
400
200
0
LGM ELA
Modern ELA
Ameges
Patro
b.
% above elevation
100
80
60
40
20
0
Interquartile range
2000
4000
6000
Elevation [m]
c.
Normalised elevation
1
0.8
0.6
0.4
0.2
0
Integral = 0.59
0
0.2
0.4
0.6
0.8
1
Normalised cumulative area
d.
Integral = 0.49
0
0.2
0.4
0.6
0.8
1
Normalised cumulative area

Fig. 5

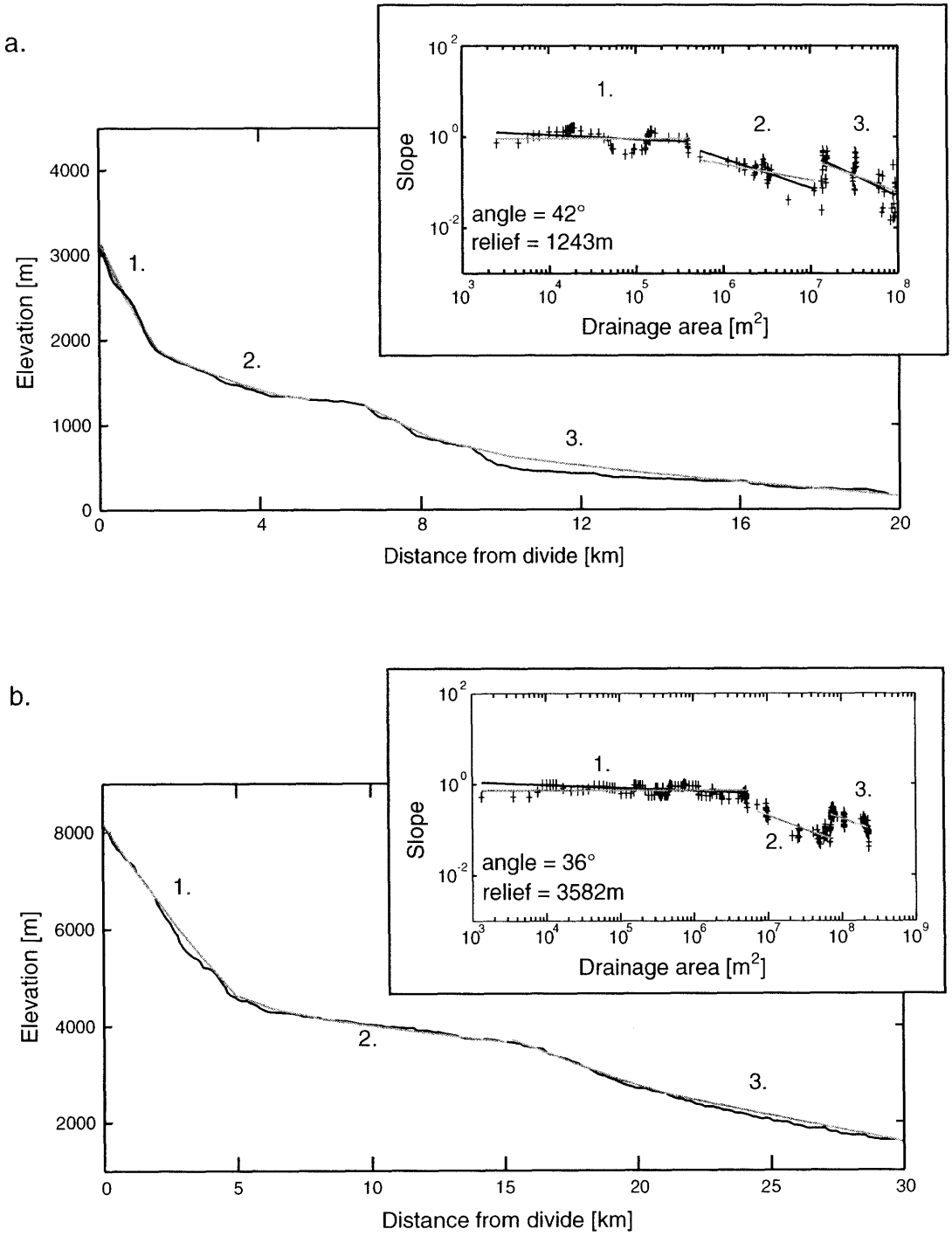
a.
Slope
Drainage area [m²]
angle = 42°
relief = 1243m
1.
2.
3.
Elevation [m]
Distance from divide [km]
b.
Slope
Drainage area [m²]
angle = 36°
relief = 3582m
1.
2.
3.
Elevation [m]
Distance from divide [km]

Fig. 6

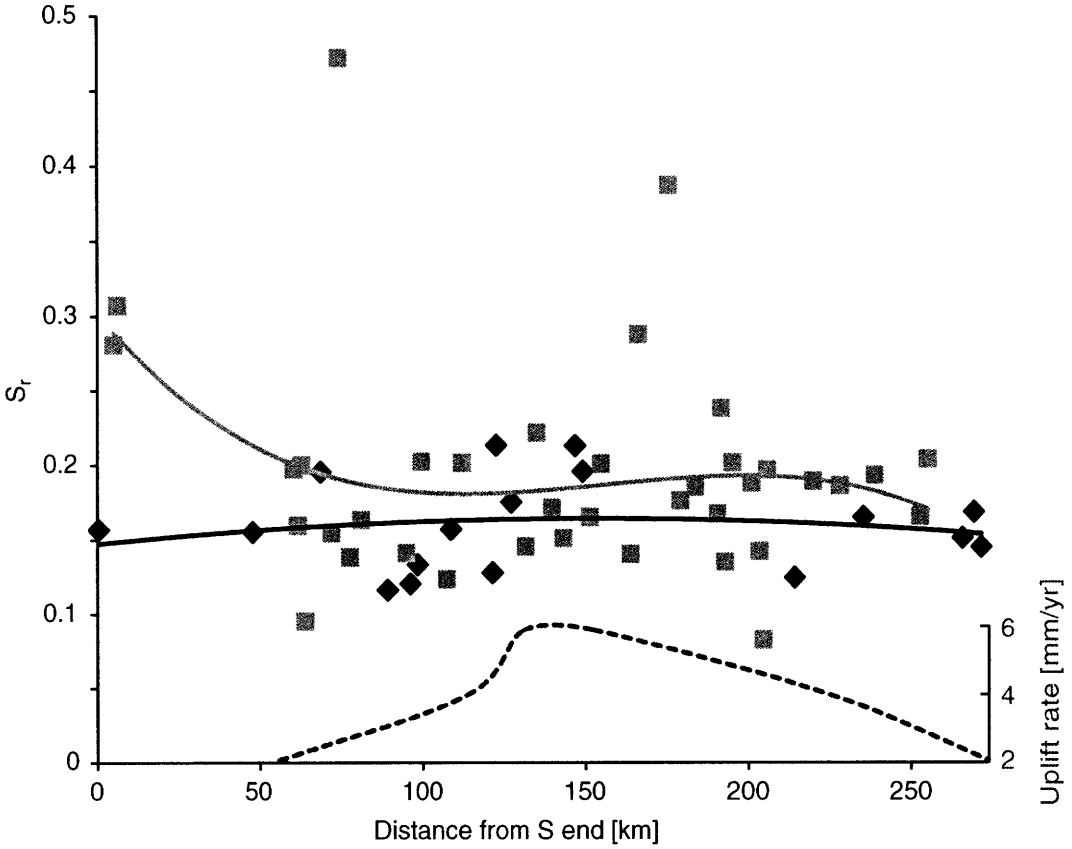
0.5
0.4
0.3
0.2
0.1
0
S_r
0
50
100
150
200
250
Distance from S end [km]
6
4
2
Uplift rate [mm/yr]

Fig. 7

a.

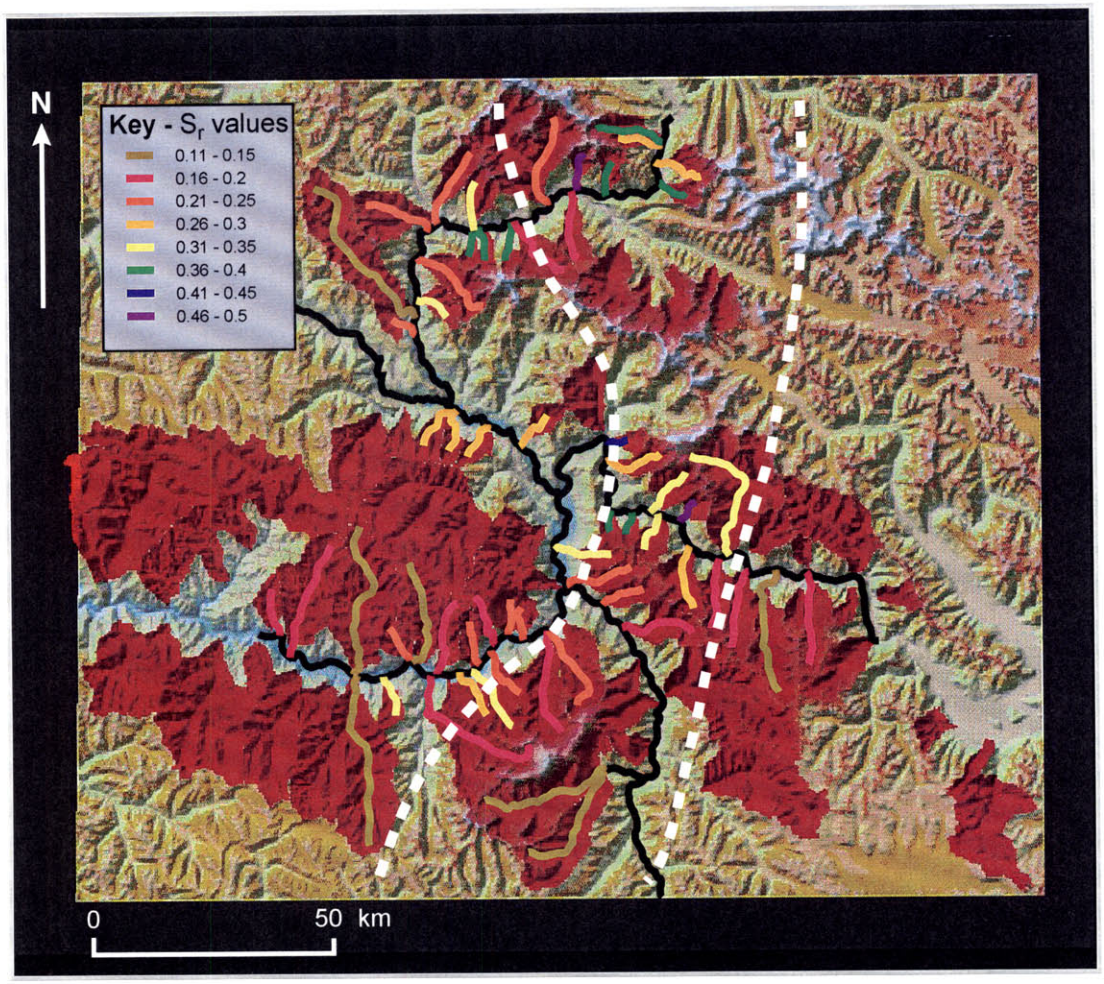
N
Key - S_r values
0.11 - 0.15
0.16 - 0.2
0.21 - 0.25
0.26 - 0.3
0.31 - 0.35
0.36 - 0.4
0.41 - 0.45
0.46 - 0.5
0
50 km

b.

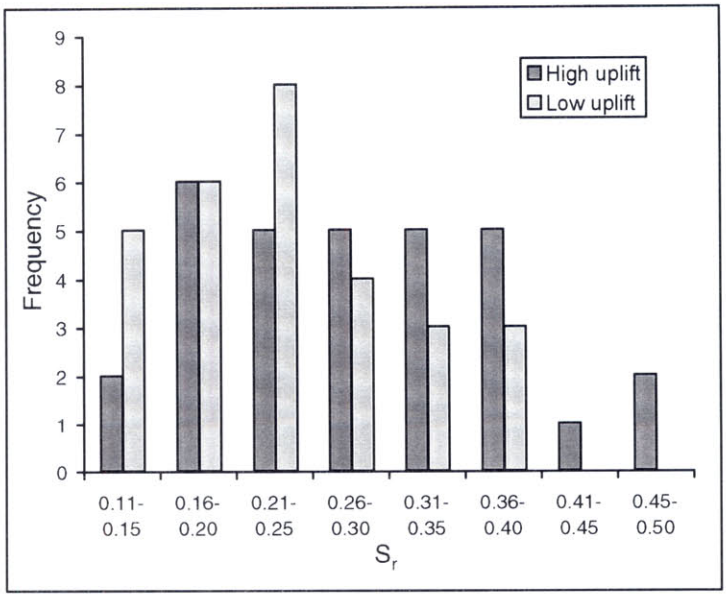
High uplift
Low uplift
Frequency
0
1
2
3
4
5
6
7
8
9
0.11-0.15
0.16-0.20
0.21-0.25
0.26-0.30
0.31-0.35
0.36-0.40
0.41-0.45
0.45-0.50
S_r

Fig. 8

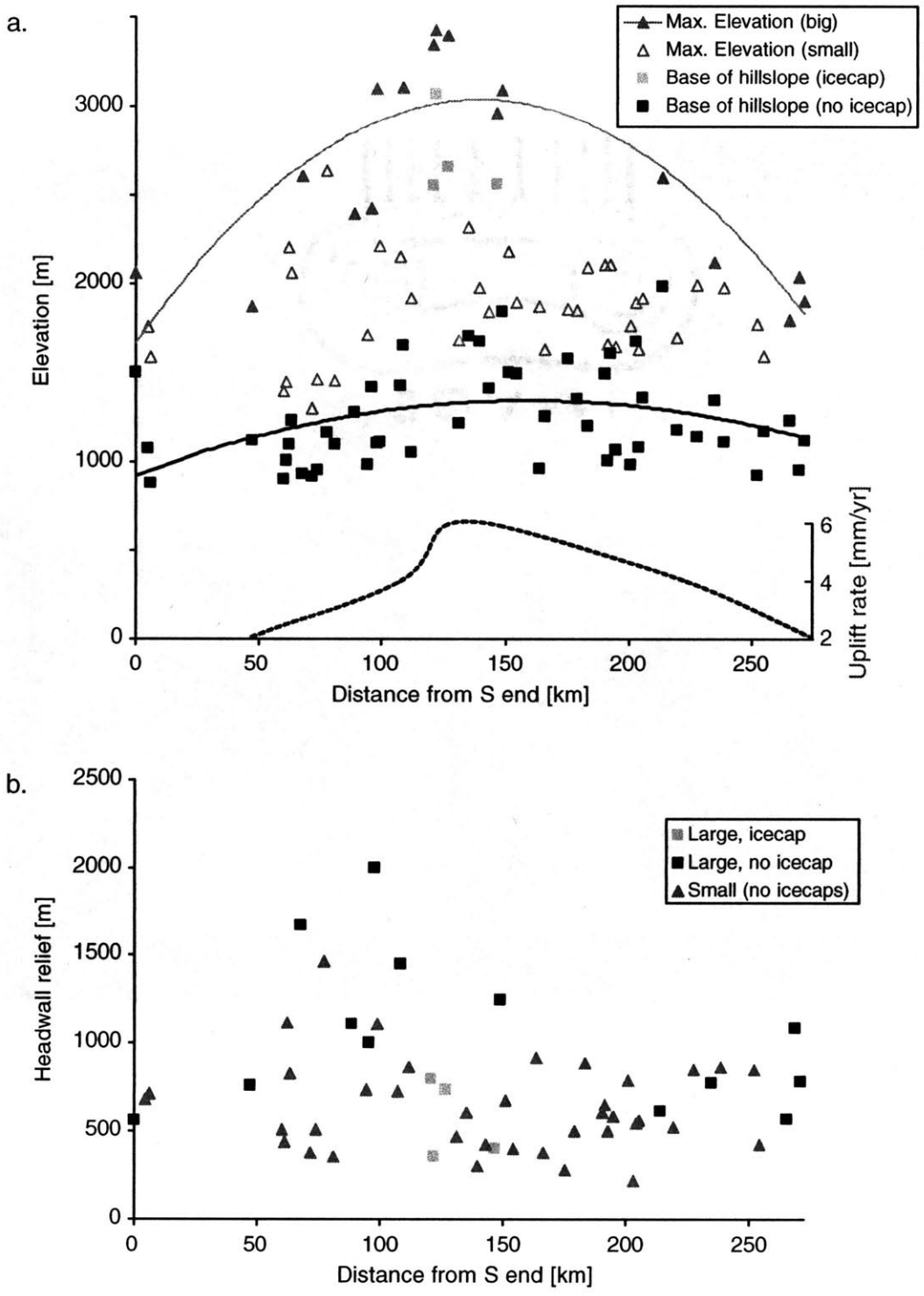
a.
Max. Elevation (big)
Max. Elevation (small)
Base of hillslope (icecap)
Base of hillslope (no icecap)
Elevation [m]
3000
2000
1000
0
0
50
100
150
200
250
Distance from S end [km]
Uplift rate [mm/yr]
6
4
2
b.
Large, icecap
Large, no icecap
Small (no icecaps)
Headwall relief [m]
2500
2000
1500
1000
500
0
0
50
100
150
200
250
Distance from S end [km]

Fig. 9

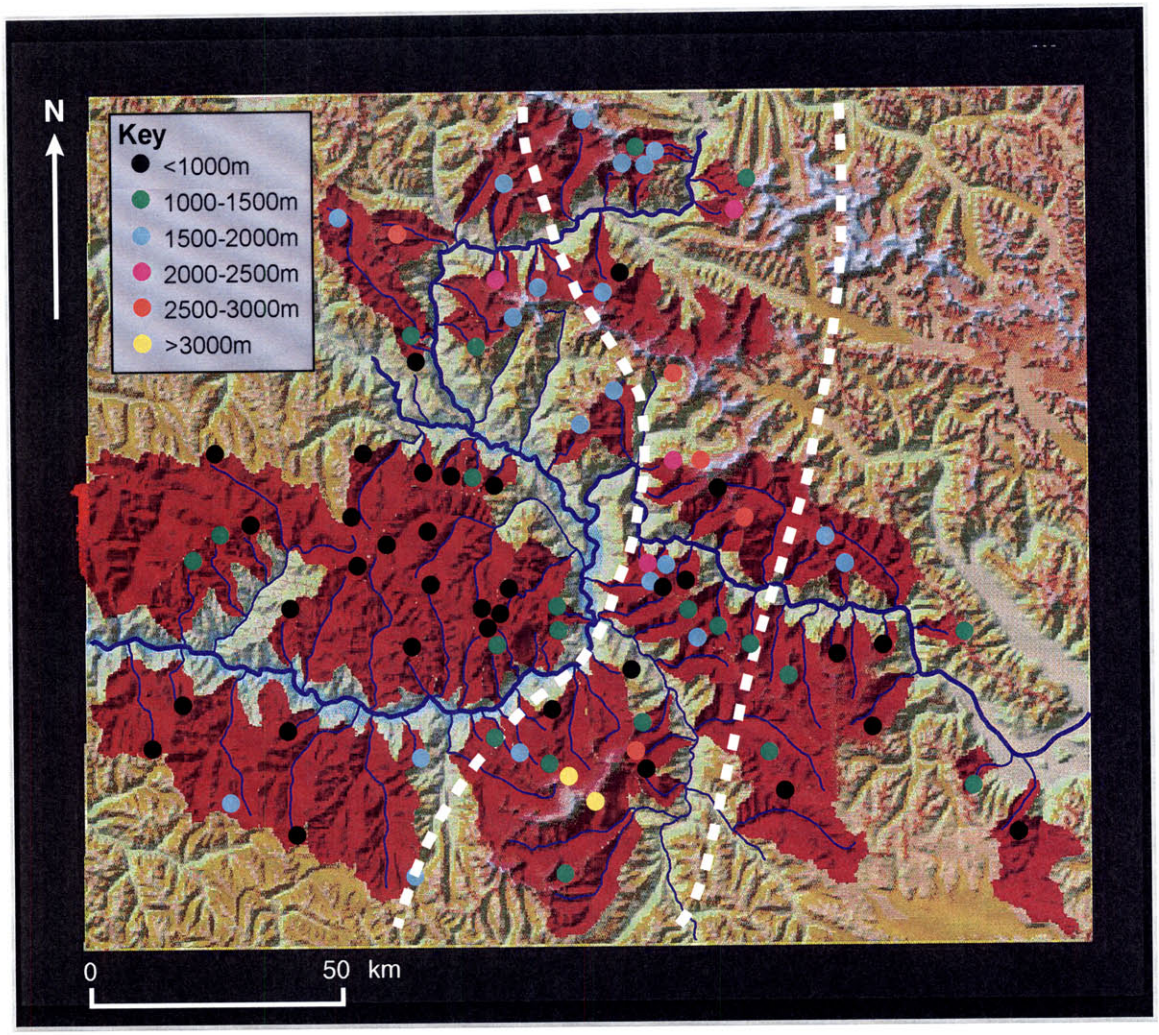
N
Key
<1000m
1000-1500m
1500-2000m
2000-2500m
2500-3000m
>3000m
0
50 km

Fig. 10

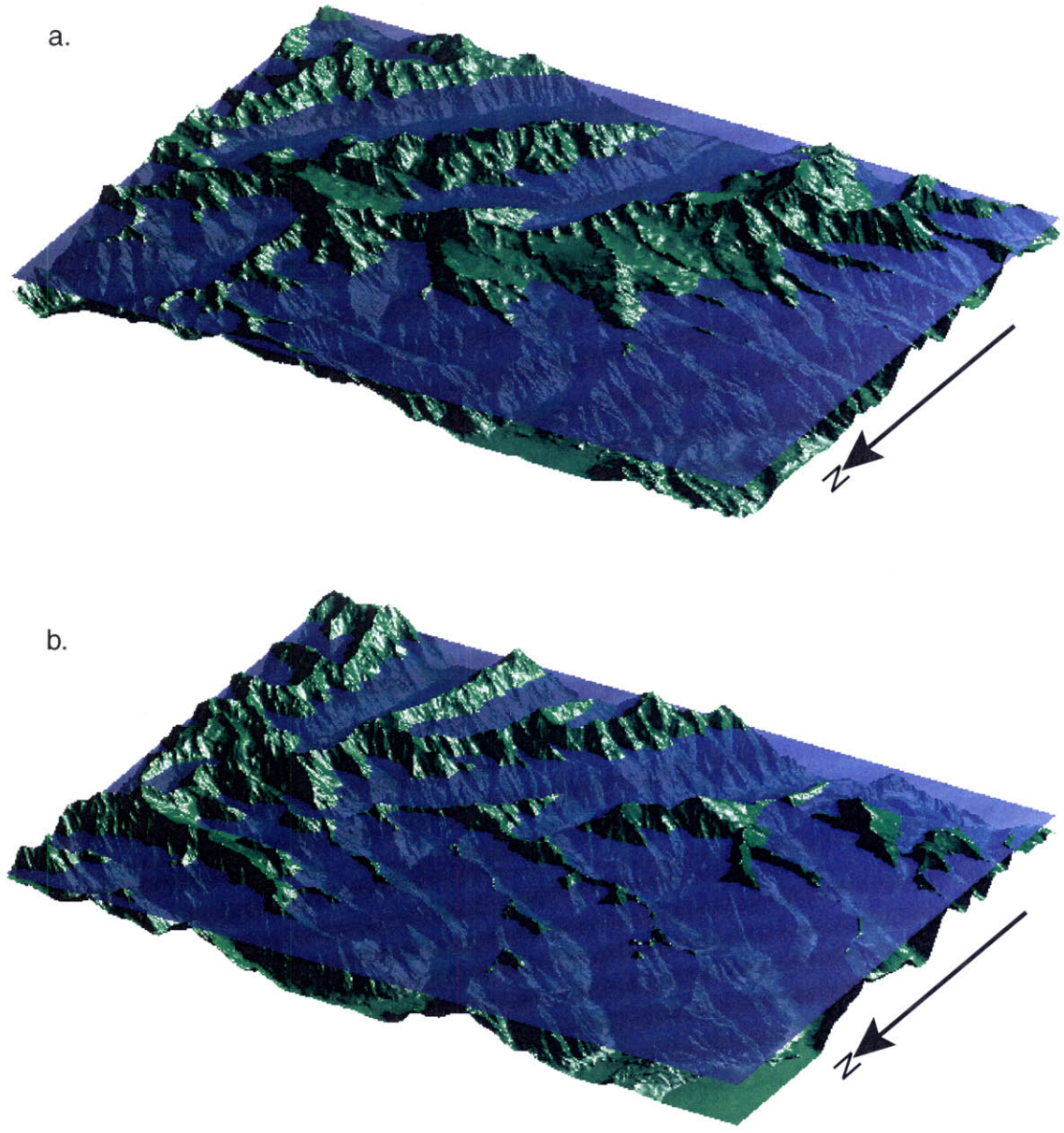

Fig. 11

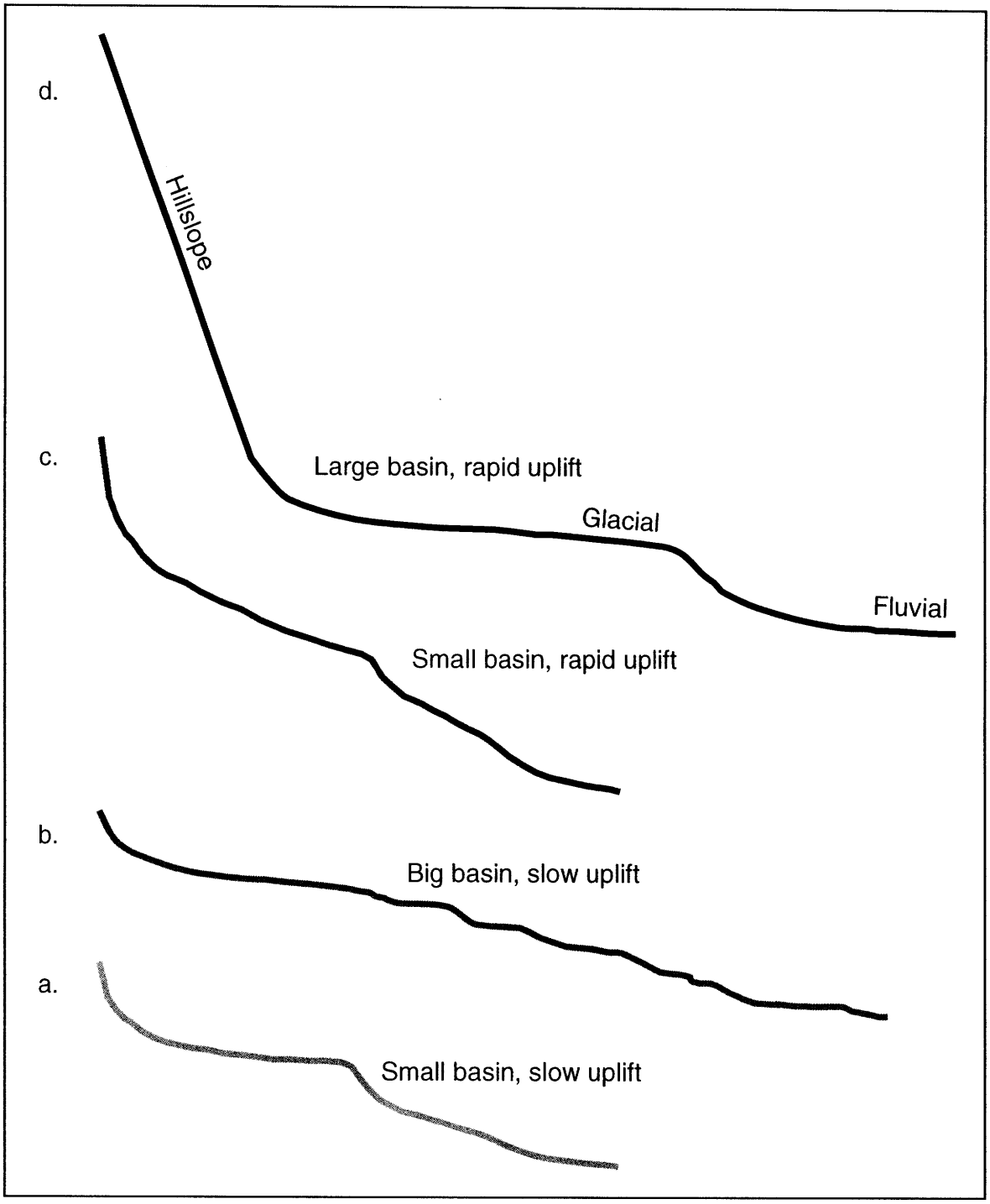
d.
Hillslope
c.
Large basin, rapid uplift
Glacial
Fluvial
Small basin, rapid uplift
b.
Big basin, slow uplift
a.
Small basin, slow uplift

Fig. 12

Chapter 9

Conclusion

The research presented in this thesis was primarily motivated by a pair of hypotheses: the "chicken-and-egg" hypothesis (Molnar and England, 1990), and the "glacial buzzsaw" hypothesis (Brozovic et al., 1997). The former suggests that relief production, principally by glacial erosion, causes a significant proportion of the current elevation of mountain peaks. The latter proposes that glaciers can erode at rates comparable to the most rapid rock uplift rates, thus limiting the majority of the landscape to elevations close to the snowline. Testing these two hypotheses involved a detailed quantitative analysis of the landscapes produced by glacial erosion, in contrast to those generated by fluvial erosion. The subsequent research on a variety of glaciated landscapes revealed a broad range of landforms, while also providing insight into the still-unresolved question of whether glaciers can erode faster than rivers, and contributing to our understanding of the development of topography in glaciated landscapes. This chapter aims to provide a succinct summary of the most pertinent conclusions from the thesis and suggest avenues of further research inspired by this work.

The chicken-and-egg hypothesis

Molnar and England (1990) noted increased sedimentation rates across the globe in the late Cenozoic, and suggested that these might reflect a change in climate (and thus erosion rates), which in turn might, through the isostatic response to relief production, lead to the apparently synchronous uplift of mountains across the globe. Zhang et al. (2001) argued that the key change in climate was the transition from long-term stability, to a period of frequent and abrupt climatic variations. The work presented here can only examine the time-integrated effects of glacial erosion, and thus cannot evaluate the question of climatic variations. However, this work does have implications for erosion rates and relief production. This study has demonstrated that glaciers can erode more rapidly than rivers (see below), but casts doubt on the subsequent claim that this can cause globally synchronous mountain uplift. In Chapter 2, a new technique for examining the distribution of relief in landscapes was used to demonstrate that small glaciers in the eastern Sierra Nevada have been responsible for a redistribution of relief, but have only

generated relief in their ability to enlarge basins at the expense of low-relief topography, and even this relief production is modest. This suggests that the case for relief production made by Molnar and England (1990) is overstated. The results presented in Chapter 3 are consistent with the hypothesis that relief production scales with ice thickness (Whipple et al., 1999). The fluvial landscape simulation technique described in Chapters 2 and 4 showed that glaciers have been responsible for bringing down both valley floors and neighbouring ridgelines above the mean Quaternary ELA in the Sangre de Cristos and the Sierra Nevada. Since the ridgelines and valley floor apparently move in concert, this limits the amounts of geophysical relief ("missing mass") that can be generated, and causes a decrease in drainage basin relief. Furthermore, the demonstration of drainage reorganisation and relief inversion by glaciers in Chapter 6 further suggests only modest potential for relief production by glaciers in the eastern Sierra Nevada. The glaciers here have, at least recently, been reworking an existing drainage network, rather than carving a new network into previously low relief topography. The development of towering headwalls above glacial cirques in the Himalaya (Chapter 8) clearly represents significant relief production, but this is in response to rapid rock uplift, rather than driving isostatic peak uplift.

The glacial buzzsaw hypothesis

Although the role of glaciers in bringing down both valley floors and ridgelines at high elevations in the Sierra Nevada and Sangre de Cristo Range was demonstrated in Chapters 2 and 4, the glacial buzzsaw hypothesis can only truly be tested in areas of more active tectonic deformation. In Chapter 8 it was demonstrated that the glacial buzzsaw hypothesis is essentially accurate in the Nanga Parbat region, in that larger glaciers in particular can maintain a low downvalley gradient even in the face of extremely rapid rock uplift. However, the rare peaks that penetrate the snowline envelope are potentially important, and the details of the landscape around Nanga Parbat contain much more diversity than Brozovic et al. (1997) suggest. The glacial buzzsaw does not describe the evolution of the Southern Alps as well, because here mean elevations rise in areas of more rapid uplift. It may be that the buzzsaw only works in the Nanga Parbat region because the zone of rapid uplift is structurally confined to a narrow region, or

alternatively that, outside the zone of most rapid uplift around Mount Cook, the Southern Alps in general have not been rising sufficiently rapidly for the glacial buzzsaw to have been imposed. In other words, other erosion processes are sufficiently rapid to keep mean elevations below the snowline-related envelope of the glacial buzzsaw. In this case the general applicability of the buzzsaw hypothesis is called into question. Other possible exceptions to the glacial buzzsaw hypothesis include the Denali massif in Alaska, and the Patagonia region of the southern Andes.

Comparing fluvial and glacial erosion at the landscape scale

The simple approach of comparing fluvial and glacial topography, both directly as observed, and by comparing observed glacial topography with locally-calibrated, simulated fluvial topography, has proven successful in elucidating the key differences between fluvial and glacial topography at scales relevant to the evolution of mountain ranges. As described in Chapter 2, glaciated valleys are characterised by stepped longitudinal profiles with lower concavities than their fluvial counterparts, although this concavity cannot be interpreted in terms of an erosion model. That glaciated profiles from both the Sierra Nevada and the Sangre de Cristos (Chapter 4) have steps indicates that steps are not merely a phenomenon associated with the weathering of Sierra Nevada granites (Wahrhaftig, 1965). Chapter 7 detailed how glacial landscapes also have hypsometries that are quite distinct from fluvial landscapes. Hypsometry can be used to indicate the degree of glacial modification of a landscape, and show a progression of modification due to lowering of the ELA similar to the classic fluvial landscape evolution sequence described by Strahler (1952).

The comparison between fluvial simulations and observed glacial topography, introduced in Chapter 2 and discussed in more detail in Chapter 4, showed that glaciers in smaller drainage basins principally modify the landscape above the mean Quaternary ELA (Porter, 1989). This contrasts with Mathes' (1930) conclusions, that the Sierra Nevada landscape is responding to pulses of uplift by being eroded around the edges, the higher regions representing a prior landscape. Meanwhile, larger glaciers are capable of generating characteristic steps and modifying the longitudinal profile to much lower elevations. Thus the condition prior to glaciation is an important influence on the

subsequent development of glaciated landscapes. This is further reflected in the results from Chapter 3, in that the shallower downvalley gradients in larger drainage basins allow thicker ice and thus the development of greater relief than in smaller, steeper basins. Fluvial simulations were also used to demonstrate that glaciers can erode headward faster than rivers (Chapters 2 & 4). Where cirques on either side of the range meet, the competing glaciers produce a horn, whereas offset valley heads allow headwall retreat. Chapter 6 built on this theme to show that drainage capture and relief inversion occur in glaciated landscapes, resulting in former valley floors now lying at the ridgeline.

Relative rates of fluvial and glacial erosion

By comparing fluvial simulations with observed glaciated landscapes (Chapters 2 & 4), it has been demonstrated that glaciers have incised the landscapes of the Sierra Nevada and the Sangre de Cristos more rapidly than rivers would have modified the landscape. In the smaller basins this occurs principally at higher elevations in the basin; for larger basins this faster modification encompasses almost the whole of the basin. However, given that at present this approach does not allow predictions of the landscape prior to the onset of glaciation (it is limited to how the landscape would look now had glaciation not occurred), it is not possible to justifiably quantify the rates of landscape modification. Horizontal headwall erosion rates attributable to glacial erosion in the Sierra Nevada and the Sangre de Cristo Range could only be constrained relative to the erosion rates that would have occurred under fluvial erosion. Glacial headwall erosion rates range from 0-1 mm/yr faster than fluvial rates over the length of the Quaternary.

The evaluation of the problem of cosmogenic isotope inheritance in temperate alpine glaciated basins described in Chapter 5 indirectly provided a lower bound on the rates of glacial incision in the eastern Sierra Nevada, in that a minimum of ~2 m of bedrock was eroded, principally by plucking, during the last glacial occupation. The assumption that glacial ice was present in the sampled area throughout the Tioga glaciation (an upper estimate for the duration of the last glacial occupation of ~11 ka) yields a minimum incision rate of ~0.2 mm/yr. Meanwhile, assuming that ice retreated prior to, and then readvanced over the sample sites during, the last recent Tioga advance, for an ice occupation of only ~2 ka, yields a minimum incision rate of ~1 mm/yr. It is

suggested that only in cases where plucking is not active will erosion rates be sufficiently slow to cause inheritance to be a problem (Briner and Swanson, 1998).

The analyses in Chapter 8 demonstrated that in some of the most rapidly uplifting regions on the planet, glaciers are capable of eroding at rates comparable to rock uplift rates (on the order of ~10 mm/yr), and furthermore are able to do so without steepening their longitudinal profile. However, glaciers in these settings are unable to prevent the development of 'runaway', towering hillslopes. Thus rates of incision on these periglacial hillslopes are significantly slower.

Further Work

This discussion of further work motivated by the research summarised in this thesis is split into two halves, firstly research motivated by and continuing very much in the style of the research presented here, and secondly some suggestions for other areas of research in light of the conclusions reached here.

Chapter 8 highlighted the importance of tall, snow-free bedrock hillslopes in alpine environments. However, little is known about these features, which undoubtedly warrant further research. Our current understanding of the evolution of these hillslopes during landscape development is limited. For example, do the hillslopes keep "running away" from the glaciers at their bases, or if not, what sets the limit to the height that they can reach? Especially when they reach several kilometers in height, these hillslopes may play a number of important roles in the interplay between glaciers and topography. Giant hillslopes are major sources of snow. Snow does not accumulate on the steepest slopes; it avalanches to the floor below. The high peaks forming the crest of these slopes influence wind patterns and thus the redistribution of wind-blown snow. Avalanches and rockslides off these hillslopes transfer considerable debris to the glaciers below. Ablation rates at the lower altitudes, where ice loss is most rapid, are reduced substantially both because debris accumulates and forms an insulating blanket on the glacier surface, and because the steep, tall hillslopes shade the glaciers below. These hillslopes form a major component of peak elevation, which is responsible for disrupting atmospheric circulation patterns and determining the effects of orographic precipitation. Thus a study of hillslope

processes in an area of rapid tectonic uplift, with the Himalaya the prime example, seems particularly important.

The drainage reorganisation and relief inversion that result in old surfaces at the crest of the Sierra Nevada (Chapter 6) require glaciers to be able to erode headward at significant rates. However, work in the Himalaya (Chapter 8) suggests that in the face of rapid rock uplift, glaciers may be unable to erode neighbouring hillslopes. Rather drainage density decreases. This would apparently prohibit drainage capture events, and thus the drainage network may be more entrenched in such environments. Instead, old surfaces observed in the Himalayas seem to reflect sudden, rapid incision within a long-lived drainage network, since they generally lie perched high on the sides of the current valleys rather than at the drainage divides (Bishop and Shroder, 2000; Shroder et al., 1993). Further study comparing and contrasting old surfaces in the two settings is desirable.

Chapters 5 and 6 presented two applications of cosmogenic isotope dating to problems of the evolution of relief in glaciated mountain belts. Both of these were focused in a small region of one mountain range, so it would be of interest to compare the results obtained in the eastern Sierra Nevada with ranges elsewhere, considering both alternative tectonic settings and differing glacial impacts. Chapter 4 hinted that conditions prior to glaciation might play a crucial role in the subsequent impact of glaciation, in particular the initial slope of the valley floor as determined by the valley size. This story remains incomplete. Similarly the test of the hypothesis that relief production scales with ice thickness (Chapter 3) is limited to a pair of mountain ranges in very similar settings; it would be valuable to extend this to other ranges, particularly those with much larger and thicker glaciers, such as the Alps.

The fluvial landscape simulation techniques described in Chapters 2 and 4 have proven very effective in allowing insight into the role of glacial erosion in modifying what would otherwise have been a fluvially-sculpted landscape. It would be illuminating to extend this approach to other ranges in other settings. Foremost amongst the possibilities would be the Southern Alps of New Zealand, where local calibration of the model would be possible, allowing further study of the response of glaciated landscapes to spatially variable rock uplift rates. Improved understanding of fluvial erosion models

would also allow the extension of this technique to ranges where local calibration is not possible, and also to justifiably predict how these landscapes might have looked prior to late Cenozoic cooling and the onset of glaciation.

Chapters 3, 4, and 8 have all drawn attention to the fact that the glaciated landscapes developed in small drainage basins are noticeably different from those developed in larger drainage basins, and provide some indication of why this might be the case. It would be highly worthwhile to test some of the hypotheses presented in these chapters, contrasting larger and smaller glaciated drainage basins in both moderately uplifting and rapidly uplifting landscapes.

At the same time as the research described here has been going on, initial efforts at incorporating glaciers into landscape evolution models have been taking place (e.g., Braun et al., 1999; MacGregor et al., 2000; Merrand and Hallet, 2000). The work presented here indicates some of the features that these models must be able to produce, namely significant downward cutting at high elevations at the same time as minor incision lower in the basin (at least in the case of smaller, steeper alpine basins), headward erosion in less rapidly uplifting settings, and the possibility for steep headwalls to "escape" glacial erosion in certain settings. Thus landscape evolution models that incorporate glacial erosion also need to include a careful treatment of the processes acting on periglacial hillslopes and the ability to erode headward (e.g., MacGregor et al., in prep.). The development of hanging valleys is also an outstanding issue. MacGregor et al. (2000) suggested that the difference in ice discharge associated with tributaries causes the development of overdeepenings and hanging valleys, while Whipple et al. (1999) imply that ice falls at hanging valleys during glacial maxima are rare. The results presented in Chapter 3 support the latter argument, and indicate that the ice thickness in the trunk stream is a major control on relief development. Current 2-D models are restricted to coarse spatial resolution so that the simplifying 'thin sheet' approximation for ice dynamics can be employed. This is probably not appropriate in steep alpine environments. Even 1-D models tend to have a wide grid spacing in comparison with the DEMs used to examine glacial topography here. With advances in computing power it will become possible to address all components of the ice dynamics, allowing a much more realistic glacier dynamics model. Carefully linked 1-D models probably represent

the first step in the process. However, other issues remain outstanding in this regard. Firstly, the role of subglacial water must still be clarified. Recent work has emphasised the complicated annual cycle in subglacial hydrology (e.g., Iken et al., 1983; MacGregor et al., in review) while there is still considerable debate over the importance of subglacial water pressure fluctuations in glacial erosion (e.g., Hallet et al., 1996; Riihimaki et al., 2000). Several chapters in this thesis have appealed to the role of water in quarrying potentially explaining, for instance, widening but not downcutting in the ablation zone of smaller glaciers, and rapid ablation zone incision in larger glaciers. Secondly, and related, is the question of how to parameterise erosion as a function of ice and water dynamics. Simple treatments of erosion as a function of sliding velocity alone may not be appropriate. The results presented in Chapter 5 suggest that the distinction between abrasion and quarrying is crucial in determining the rate of erosion. Furthermore, the large, debris-covered glaciers of the deep Himalayan cirques probably behave rather differently than the less debris-rich glaciers in other ranges. Thirdly, the role of lithology in the development of glaciated landscapes remains an exciting focus for future research. Previous work has tended to focus on the role of lithology in shaping valley cross-sectional forms (e.g., Augustinus, 1995; Harbor, 1995), while lithologic differences result in landform contrasts between the Sangre de Cristos and the Sierra Nevada (Chapter 3). A more comprehensive understanding of the response of glacial erosion to different lithologies would be valuable.

The recurring theme of the interactions between surface processes and tectonics has previously been addressed with geodynamic models incorporating only fluvial and hillslope processes. The clear distinctions between fluvial and glacial erosion rates and subsequent landscapes warrant the incorporation of glacial processes into geodynamic models. In the first instance this would be achieved most readily using some form of glacial buzzsaw, but further progress in landscape evolution modelling, as described above, would allow more accurate representations of glacial erosion to be incorporated, to gain a clearer understanding of the interactions between glacial erosion and tectonics.

Concluding remarks

The careful examination of glacial topography presented here has yielded valuable conclusions about the modification of fluvial landscapes by glaciers and thus the topographic evolution of mountain ranges in the late Cenozoic. In the broader context of the competing hypotheses relating late Cenozoic climate change and tectonic activity (Molnar and England, 1990; Raymo and Ruddiman, 1992), this work partially supports the chicken-and-egg hypothesis (Molnar and England, 1990); glacial erosion has probably increased erosion rates and thus sediment yields, but is not responsible for significantly raising mountain peaks through the generation of relief. The Raymo-Ruddiman hypothesis, that rising mountain belts caused more rapid chemical weathering, drawdown of atmospheric CO_2, and global cooling, was based on interpretations of the Cenozoic history of marine $^{87}Sr/^{86}Sr$ ratios (Raymo et al., 1988). Recent work has suggested that the strontium isotopes reflect a change in the lithologies being weathered, rather than continental weathering rates. Currently, alternative isotopes that might more accurately reflect chemical weathering rates are being sought, and the interactions between uplift, erosion, weathering and climate should still be considered. Raising mountain belts through tectonic processes such that glaciers start to develop (Raymo and Ruddiman, 1992) will generally increase erosion rates, as shown herein, although for the Raymo-Ruddiman hypothesis to be appropriate, there must be an increase in chemical weathering rates as part of the general increase in erosion rates. While the research presented here does not directly address this question, the generation of fresh rock surfaces due to glacial abrasion and quarrying is generally thought to cause more rapid chemical weathering (Anderson et al., 1997; Collins, 1999; Hallet et al., 1996). Glaciers may limit mean elevations, but the snowline at low latitudes is not low enough to prevent mountain ranges from reaching sufficient heights to influence atmospheric dynamics and cause global cooling (Ruddiman and Kutzbach, 1989). Thus the research presented here does not preclude the Raymo-Ruddiman hypothesis for late Cenozoic cooling.

References

Anderson, S. P., Drever, J. I., and Humphrey, N. F., 1997, Chemical weathering in glacial environments: Geology, v. 25, no. 5, p. 399-402.

Augustinus, P. C., 1995, Glacial valley cross-profile development: the influence of in-situ rock stress and rock mass strength, with examples from the Southern Alps, New Zealand: Geomorphology, v. 14, p. 87-97.

Bishop, M. P., and Shroder, J. F., Jr, 2000, Remote sensing and geomorphometric assessment of topographic complexity and erosion dynamics in the Nanga Parbat massif, in Khan, M. A., Treloar, P. J., Searle, M. P., and Jan, M. Q., eds., Tectonics of the Nanga Parbat Syntaxis and the Western Himalaya: Geological Society, London, Special Publications: London, The Geological Society of London, p. 181-200.

Braun, J., Zwartz, D., and Tomkin, J. H., 1999, A new surface-processes model combining glacial and fluvial erosion: Annals of Glaciology, v. 28, p. 282-290.

Briner, J. P., and Swanson, T. W., 1998, Using inherited cosmogenic 36Cl to constrain glacial erosion rates of the Cordilleran ice sheet: Geology, v. 26, p. 3-6.

Brozovic, N., Burbank, D. W., and Meigs, A. J., 1997, Climatic Limits on Landscape Development in the Northwestern Himalaya: Science, v. 276, p. 571-574.

Collins, D. N., 1999, Solute flux in meltwaters draining from a glacierized basin in the Karakoram mountains: Hydrological Processes, v. 13, p. 3001-3015.

Hallet, B., Hunter, L., and Bogen, J., 1996, Rates of erosion and sediment evacuation by glaciers: A review of field data and their implications: Global and Planetary Change, v. 12, p. 213-235.

Harbor, J., 1995, Development of glacial-valley cross sections under conditions of spatially variable resistance to erosion: Geomorphology, v. 14, no. 2, p. 99-107.

Iken, A., Flotron, A., Haeberli, W., and Rothlisberger, H., 1983, The uplift of Unteraargletscher at the beginning of the melt season: a consequence of water storage at the bed?: Journal of Glaciology, v. 29, no. 101, p. 28-47.

MacGregor, K. R., Anderson, R. S., Anderson, S. P., and Waddington, E. D., 2000, Numerical Simulations of Glacial Valley Longitudinal Profile Evolution: Geology, v. 28, no. 11, p. 1031-1034.

-, in prep., Numerical modeling of the evolution of glacial longitudinal profiles: cirque development.

MacGregor, K. R., Riihimaki, C. A., and Anderson, R. S., in review, Spatial and temporal evolution of sliding velocity on a small alpine glacier: Bench Glacier, Alaska 1999 and 2000: Journal of Glaciology.

Mathes, F. E., 1930, Geologic History of the Yosemite Valley, USGS Professional Paper.

Merrand, Y., and Hallet, B., 2000, A physically based numerical model of orogen-scale glacial erosion: Importance of subglacial hydrology and basal stress regime: GSA Abstracts with Programs, v. 32, no. 7, p. A329.

Molnar, P., and England, P., 1990, Late Cenozoic uplift of mountain ranges and global climate change: chicken or egg?: Nature, v. 346, p. 29-34.

Porter, S. C., 1989, Some Geological Implications of Average Quaternary Glacial Conditions: Quaternary Research, v. 32, p. 245-261.

Raymo, M. E., and Ruddiman, W. F., 1992, Tectonic forcing of late Cenozoic climate: Nature, v. 359, p. 117-122.

Raymo, M. E., Ruddiman, W. F., and Froelich, P. N., 1988, Influence of late Cenozoic mountain building on ocean geochemical cycles: Geology, v. 16, p. 649-653.

Riihimaki, C. A., MacGregor, K. R., Anderson, R. S., and Anderson, S. P., 2000, Fine and coarse sediment evacuation and subglacial channel network evolution at the Bench Glacier, Chugach Range, Alaska: GSA Abstracts with Programs, v. 32, no. 7, p. A-329.

Ruddiman, W. F., and Kutzbach, J. E., 1989, Forcing of Late Cenozoic Northern Hemisphere Climate by Plateau Uplift in Southern Asia and the American West: Journal of Geophysical Research, v. 94, p. 18409-18427.

Shroder, J. F., Jr, Owen, L., and Derbyshire, E., 1993, Quaternary glaciation of the Karakoram and Nanga Parbat Himalaya, in Shroder, J. F., Jr, ed., Himalaya to the Sea: Geology, Geomorphology and the Quaternary: London, Routledge, p. 132-158.

Strahler, A. N., 1952, Hypsometric (area-altitude) analysis of erosional topography: Geological Society of America Bulletin, v. 63, p. 1117-1141.

Wahrhaftig, C., 1965, Stepped topography of the Southern Sierra Nevada, California: Geological Society of America Bulletin, v. 76, p. 1165-1190.

Whipple, K. X., Kirby, E., and Brocklehurst, S. H., 1999, Geomorphic limits to climate-induced increases in topographic relief: Nature, v. 401, p. 39-43.

Zhang, P., Molnar, P., and Downs, W. R., 2001, Increased sedimentation rates and grain sizes 2-4 Myr ago due to the influence of climate change on erosion rates: Nature, v. 410.